Design, synthesis, and evaluation of bioactive molecules; Quantification of tricyclic pyrones from pharmacokinetic studies; Nanodelivery of siRNA; and Synthesis of viral protease inhibitors

by

Sahani Manjitha Weerasekara

B.Sc., University of Colombo, 2009

AN ABSTRACT OF A DISSERTATION

Submitted in partial fulfillment of the requirements for the degree

DOCTOR OF PHILOSOPHY

Department of Chemistry
College of Arts and Sciences

KANSAS STATE UNIVERSITY
Manhattan, Kansas

2016

Abstract

Four research projects were carried out and they are described in this dissertation.

Glycogen synthase kinase-3 beta (GSK3β) plays a pivotal and central role in the pathogenesis of Alzheimer's disease (AD) and protein kinase C (PKC) controls the function of other proteins via phosphorylation and involves in tumor promotion. In pursuit of identifying novel GSK3β and/or PKC inhibitors, substituted quinoline molecules were designed and synthesized based on the structure-activity-relationship studies. Synthesized molecules were evaluated for their neural protective activities and selected molecules were further tested for inhibitory activities on GSK3β and PKC enzymes. Among these compounds, compound **2** was found to have better GSK3β enzyme inhibitory and MC65 cell protection activities at low nanomolar concentrations and poor PKC inhibitory activity whereas compound **3** shows better PKC inhibitory activity. This demonstrates the potential for uses of quinoline scaffold in designing novel compounds for AD and cancer.

Pharmacokinetics and distribution profiles of two anti-Alzheimer molecules, CP2 and TP70, discovered in our laboratory were assessed using HPLC/MS. Plasma samples of mice and rats fed with TP70 via different routes over various times were analyzed to quantify the amounts of TP70 in plasma of both species. Distribution profiles of TP70 in various tissues of mice were studied and results show that TP70 penetrated the blood brain barrier and accumulated in the brain tissue in significant amounts. Similarly, the amount of CP2 in plasma of mice was analyzed. The HPLC analysis revealed that both compounds have good PK profiles and bioavailability, which would make them suitable candidates for further *in vivo* efficacy studies.

Nanodelivery of specific dsRNA for suppressing the western corn rootworm (WCR, *Diabrotica virgifera virgifera*) genes was studied using modified chitosan or modified polyvinylpyrrolidinone

(PVP) as nanocarriers. Computational simulation studies of dsRNA with these polymers revealed that nanoparticles can be formed between dsRNA and modified chitosan and PVP polymers. Nanocarriers of hydroxylated PVP (HO-PVP) and chitosan conjugated with polyethylene glycol (PEG) were synthesized, and analyzed using IR spectroscopy. Particle sizes and morphology were evaluated using AFM and encapsulation was studied using UV spectroscopy. However, the formation of stable nanoparticles with dsRNA could not be achieved with either of the polymers, and further efforts are ongoing to discover a better nanocarrier for nanodelivery of siRNA by using chitosan-galactose nanocarrier.

In our efforts to discover a novel class of tripeptidyl anti-norovirus compounds that can strongly inhibit NV3CLpro, a set of tripeptidyl molecules were synthesized by modifying the P1 - P3 of the substrate peptide including a warhead. It was found that the replacement of P1 glutamine surrogate with triazole functionality does not improve the inhibitory activities of the compounds. In addition, the synthesis of a known dipeptidyl compound (GC376) was carried out for evaluating its efficacy on feline infectious peritonitis (FIP) in cats.

Design, synthesis, and evaluation of bioactive molecules; Quantification of tricyclic pyrones from pharmacokinetic studies; Nanodelivery of siRNA; and Synthesis of viral protease inhibitors

by

Sahani Manjitha Weerasekara

B.Sc., University of Colombo, 2009

A DISSERTATION

submitted in partial fulfillment of the requirements for the degree

DOCTOR OF PHILOSOPHY

Department of Chemistry
College of Arts and Sciences

KANSAS STATE UNIVERSITY
Manhattan, Kansas

2016

Approved by:

Major Professor
Duy H. Hua

Copyright

Abstract

Four research projects were carried out and they are described in this dissertation.

Glycogen synthase kinase-3 beta (GSK3β) plays a pivotal and central role in the pathogenesis of Alzheimer's disease (AD) and protein kinase C (PKC) controls the function of other proteins via phosphorylation and involves in tumor promotion. In pursuit of identifying novel GSK3β and/or PKC inhibitors, substituted quinoline molecules were designed and synthesized based on the structure-activity-relationship studies. Synthesized molecules were evaluated for their neural protective activities and selected molecules were further tested for inhibitory activities on GSK3β and PKC enzymes. Among these compounds, compound **2** was found to have better GSK3β enzyme inhibitory and MC65 cell protection activities at low nanomolar concentrations and poor PKC inhibitory activity whereas compound **3** shows better PKC inhibitory activity. This demonstrates the potential for uses of quinoline scaffold in designing novel compounds for AD and cancer.

Pharmacokinetics and distribution profiles of two anti-Alzheimer molecules, CP2 and TP70, discovered in our laboratory were assessed using HPLC/MS. Plasma samples of mice and rats fed with TP70 via different routes over various times were analyzed to quantify the amounts of TP70 in plasma of both species. Distribution profiles of TP70 in various tissues of mice were studied and results show that TP70 penetrated the blood brain barrier and accumulated in the brain tissue in significant amounts. Similarly, the amount of CP2 in plasma of mice was analyzed. The HPLC analysis revealed that both compounds have good PK profiles and bioavailability, which would make them suitable candidates for further *in vivo* efficacy studies.

Nanodelivery of specific dsRNA for suppressing the western corn rootworm (WCR, *Diabrotica virgifera virgifera*) genes was studied using modified chitosan or modified polyvinylpyrrolidinone

(PVP) as nanocarriers. Computational simulation studies of dsRNA with these polymers revealed that nanoparticles can be formed between dsRNA and modified chitosan and PVP polymers. Nanocarriers of hydroxylated PVP (HO-PVP) and chitosan conjugated with polyethylene glycol (PEG) were synthesized, and analyzed using IR spectroscopy. Particle sizes and morphology were evaluated using AFM and encapsulation was studied using UV spectroscopy. However, the formation of stable nanoparticles with dsRNA could not be achieved with either of the polymers, and further efforts are ongoing to discover a better nanocarrier for nanodelivery of siRNA by using chitosan-galactose nanocarrrier.

In our efforts to discover a novel class of tripeptidyl anti-norovirus compounds that can strongly inhibit NV3CLpro, a set of tripeptidyl molecules were synthesized by modifying the P1 – P3 of the substrate peptide including a warhead. It was found that the replacement of P1 glutamine surrogate with triazole functionality does not improve the inhibitory activities of the compounds. In addition, the synthesis of a known dipeptidyl compound (GC376) was carried out for evaluating its efficacy on feline infectious peritonitis (FIP) in cats.

Table of Contents

List of Figures

List of Tables

List of Abbreviations

Aβ	Amyloid beta peptide
Ac	Acetate
ACAT	Acyl-CoA: cholesterol acyltransferase
Ac_2O	Acetic anhydride
AcOH	Acetic acid
AD	Alzheimer's disease
ADP	Adenosine diphosphate
AFM	Atomic force microscopy
AIBN	Azobisisobutyronitrile
AMC	Amino-4-methylcoumarin
APP	Amyloid precursor protein
ATP	Adenosine triphosphate
AUC	Area under the curve
BBr_3	Boron tribromide
BF_3.ether	Boron triflouride ethereal
BTA	1,2,4,5-benzenetetracarboxylic acid
Bu_3N	Tributylamine
Cbz	Carboxybenzyl or benzyloxycarbonyl
CBr_4	Tetrabromomethane
CDI	Carbonyl diimidazole
CH_3CN	Acetonitrile
$(Chx)_2NH$	Dicyclohexylamine

Cmax	Maximum concentration
DAG	Diacylglycerol
DCM	Dichloromethane
DIPEA	*N*, *N*-Diisopropylethylamine
DMAP	4-(dimethylamino)pyridine
DMF	*N*, *N*-dimethylformamide
DMP	Dess Martin periodinane
DMSO	Dimethyl sulfoxide
DsRNA	Double stranded RNA
DTT	Dithiothreitol
EDCI	1-Ethyl-3-(3-dimethylaminopropyl)carbodiimide
EDTA	*N*, *N*, *N*', *N* ethylenediaminetetraacetic acid
EtOAc	Ethyl acetate
EtOH	Ethanol
FECV	Feline enteric coronavirus
FIP	Feline infectious peritonitis
FRET	Fluorescence resonance energy transfer
Gln	Glutamine
Glu	Glutamic acid
GSK-3α	Glycogen synthase kinase-3 alpha
GSK-3β	Glycogen synthase kinase-3 beta
HCl	Hydrochloric acid
HEPES	2-[4-(2-hydroxyethyl)piperazin-1-yl]ethanesulfonic acid

HNO_3	Nitric acid
HMPA	Hexamethylphosphoramide
HPC	Hydroxypropyl cellulose
HPLC	High performance liquid chromatography
IP3	Inositol triphosphate-3
IP	Intraperitoneal
IV	Intravenous
LDA	Lithium diisopropylamide
LiHMDS	Lithium hexamethyldisilazane
MeOH	Methanol
MeI	Methyl Iodide
MoO_3	Molybdenum trioxide
MoO_5	Molybdenum oxide
MoOPH	Oxodiperoxymolybdlenum(pyridine) (hexamethylphosphorictriamide)
mRNA	Messenger RNA
MS	Mass spectrometry
mtDNA	Mitochondrial DNA
$NaHSO_3$	Sodium bisulfite
NaN_3	Sodium azide
NBS	*N*-bromosuccinimide
$NaBH_4$	Sodium borohydride
$NaCNBH_3$	Sodium cyanoborohydride
nBu_4NF	Tetrabutylammonium fluoride

NEt_3	Triethylamine
NFTs	Neurofibrillary tangles
NHS	*N*-hydroxysuccinimide
NPI	Noroviral protease inhibitor
NV	Norovirus
NV3Cpro	Norovirus 3C-protease
NV3CLpro	Norovirus 3C-like protease
ORFs	Open reading frames
PBS	Phosphate buffered saline
PEG	Polyethyleneglycol
PEI	Poly(ethyleneimine)
PIP_3	3-phosphoinositides
PK	Pharmacokinetics
PPh_3	Triphenylphosphine
PS	Phosphotadylserine
PS1	Presenilin 1
PS2	Presenilin 2
PKC	Protein kinase C
PVP	Polyvinylpyrrolidinone
RISC	RNA induced silencing complex
RNAi	RNA interference
SAR	Structure activity relationship
SARS	Severe acute respiratory syndrome

siRNA	Small interfering RNA
TBAF	Tetrabutylammonium fluoride
t-BuOH	Tertiary butanol
TC	Tetracycline
T2DM	Type 2 diabetes mellitus
TFA	Trifluoroacetic acid
THF	Tetrahydrofuran
TMS-N_3	Trimethylsilyl aizde
TMSCl	Trimethylsilylchloride
Tmax	Time needed to reach the maximum concentration
TP	Tricyclic pyrone
WCR	Western corn rootworm
WT	Wild type

List of Schemes

List of Structures

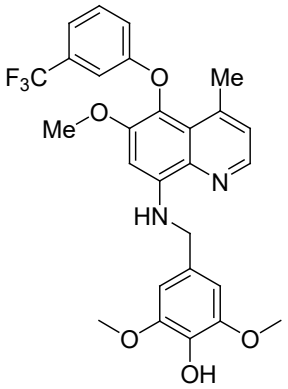

1

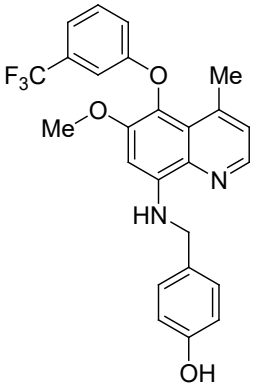

2

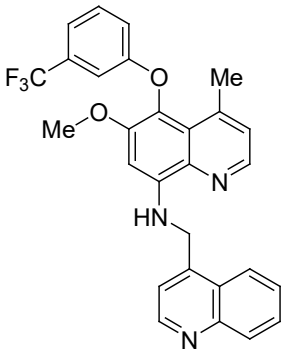

3

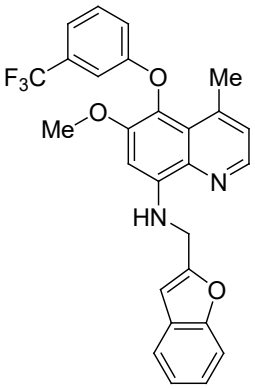

4

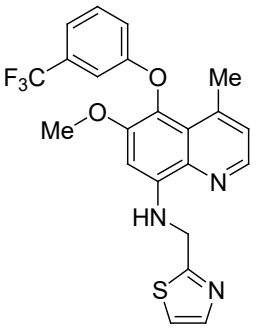

5

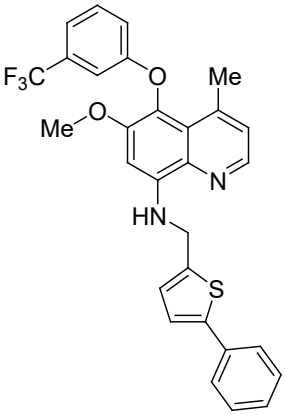

6

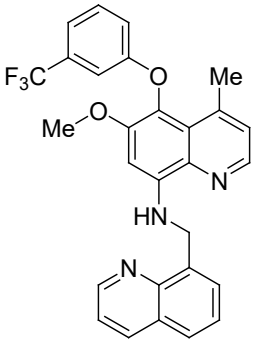

7

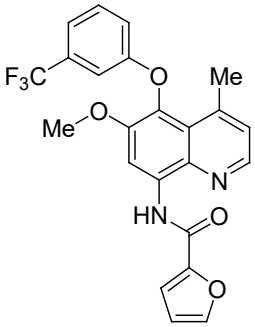

8

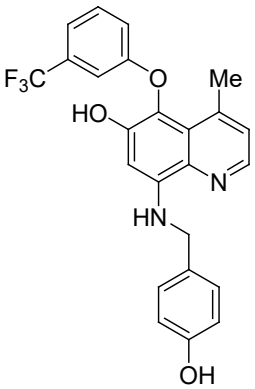

9

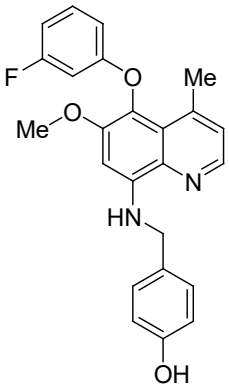

10

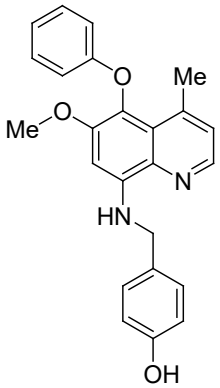

11

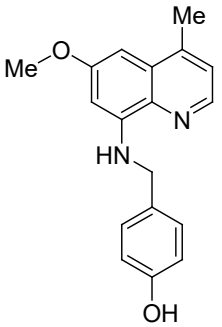

12

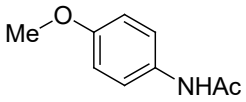

13

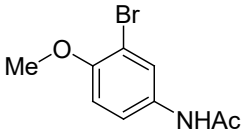

14

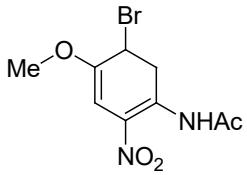

15

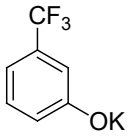

16

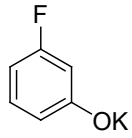

17

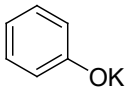

18

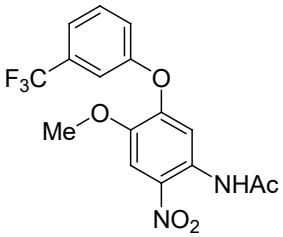

19

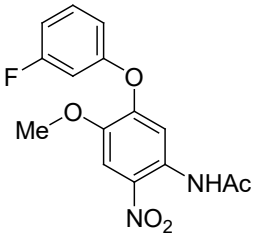

20

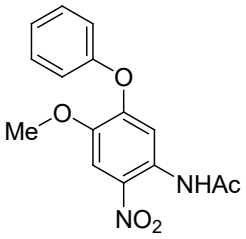

21

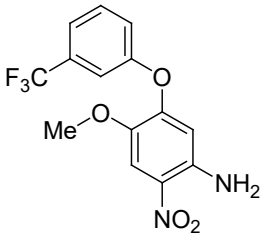

22

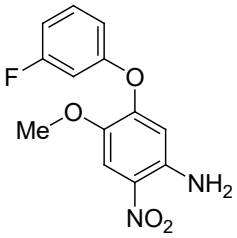

23

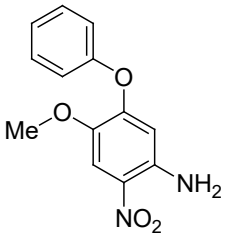

24

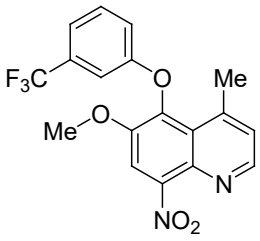

25

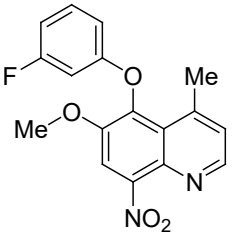

26

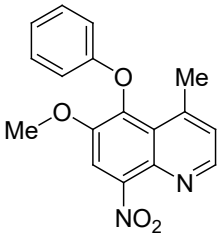

27

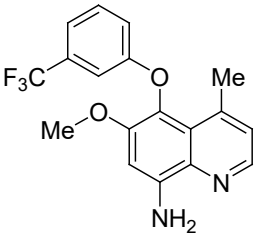

28

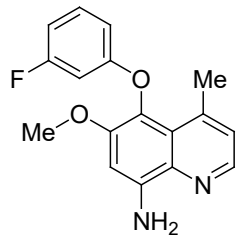

29

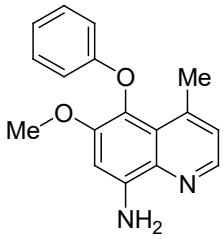

30

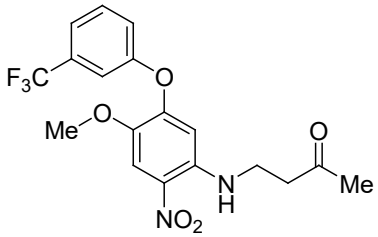

31

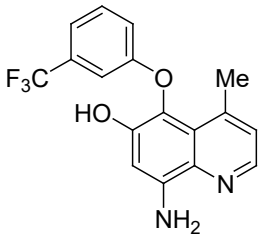

32

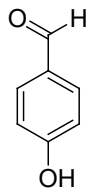

33

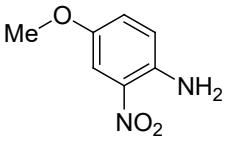

34

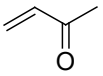

35

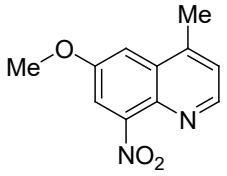

36

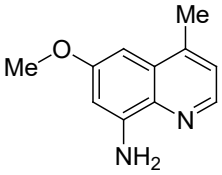

37

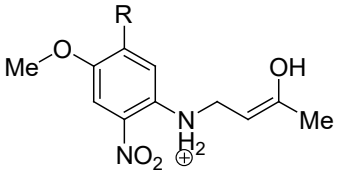

38

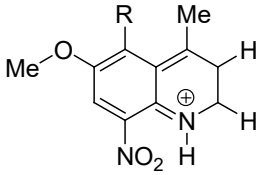

39

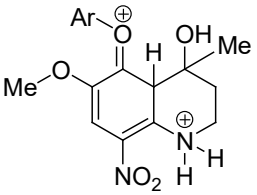

40

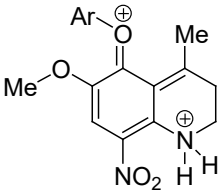

41

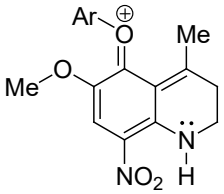

42

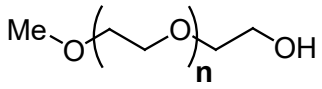

43

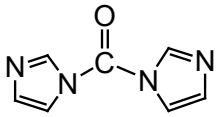

44

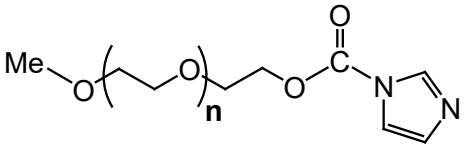

45

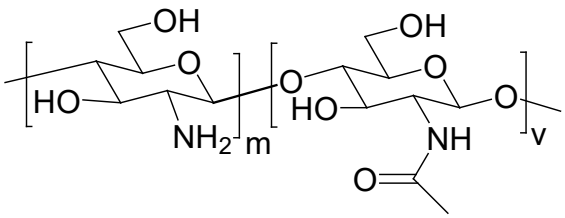

46

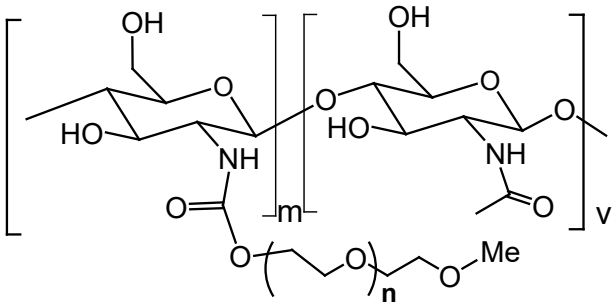

47

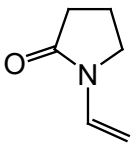

48

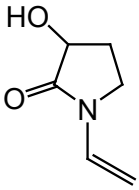

49

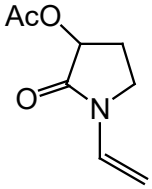

50

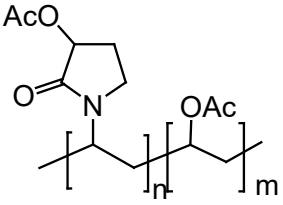

51

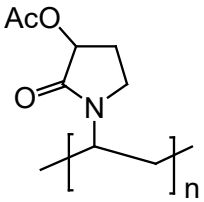

52

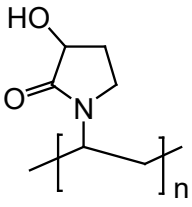

53

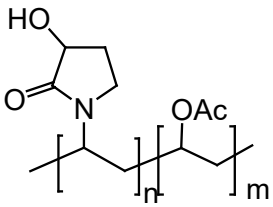

54

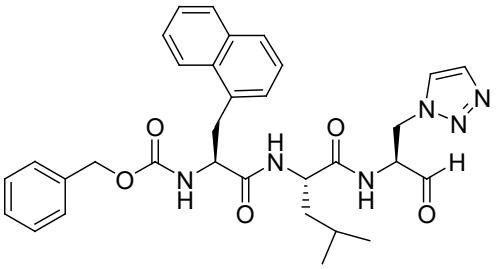

55

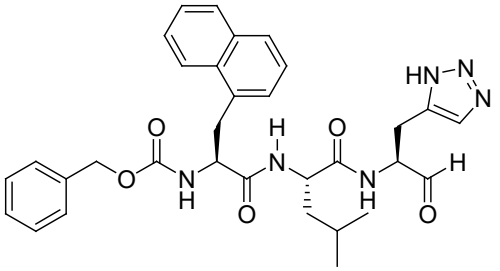

56

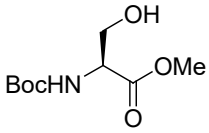

57

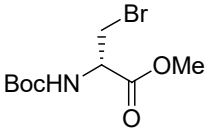

58

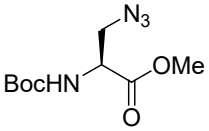

59

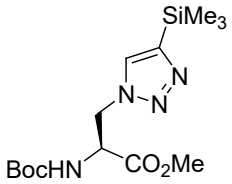

60

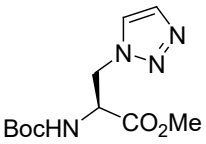

61

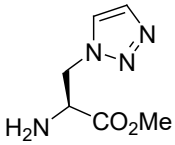

62

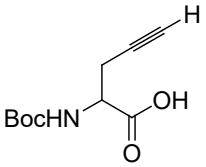

63

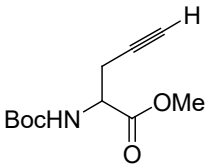

64

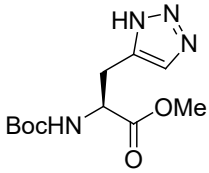

65

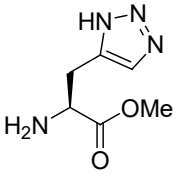

66

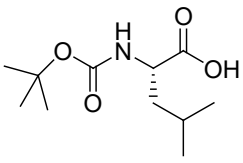

67

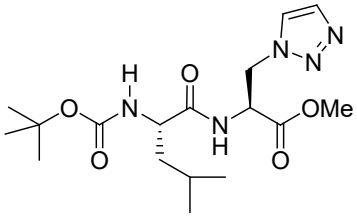

68

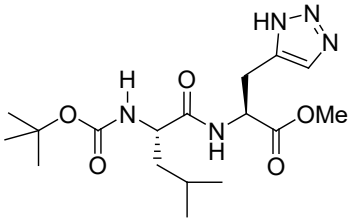

69

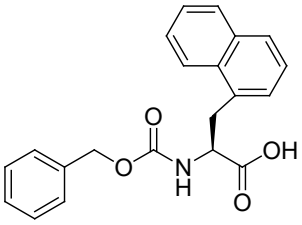

70

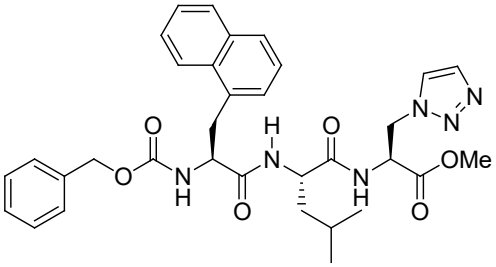

71

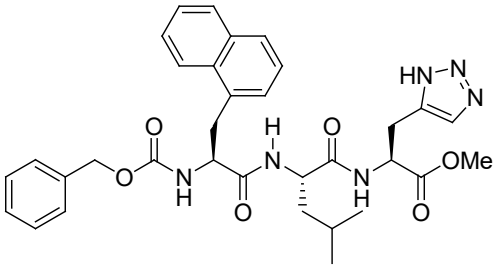

72

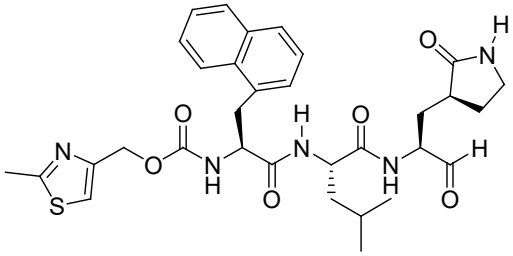

73

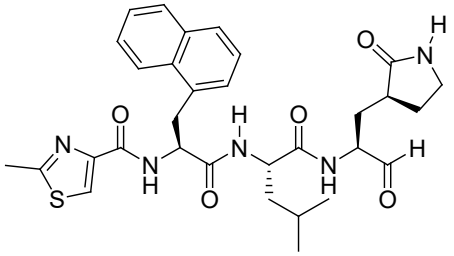

74

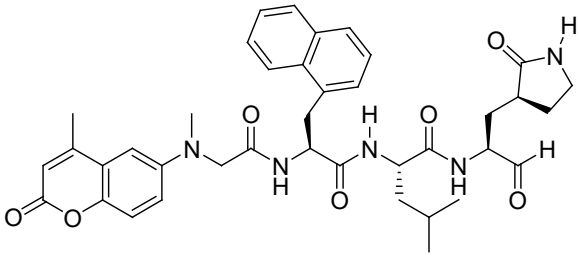

75

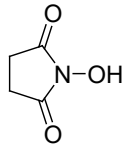

76

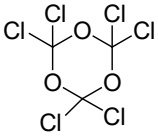

77

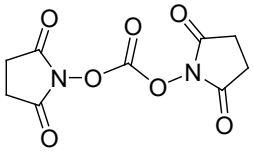

78

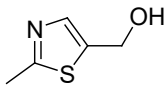

79

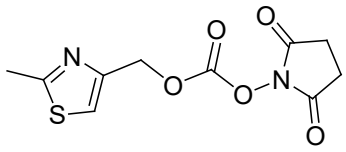

80

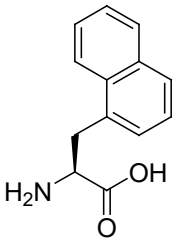

81

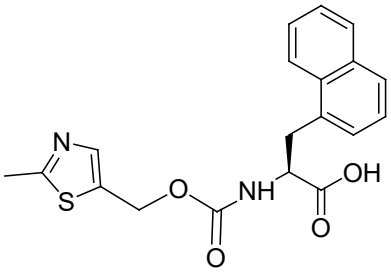

82

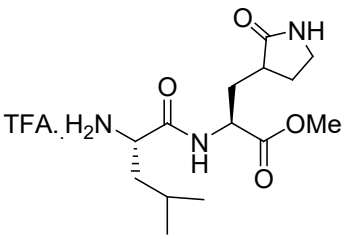

83

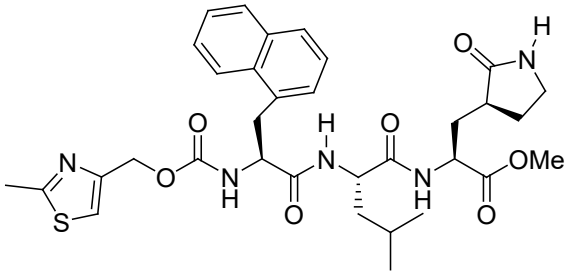

84

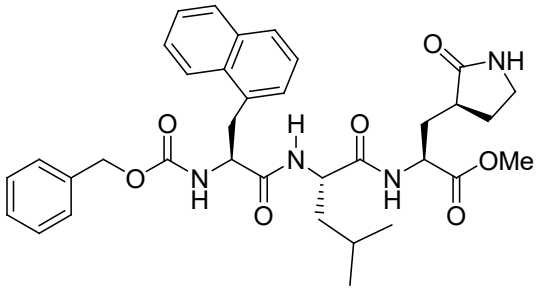

85

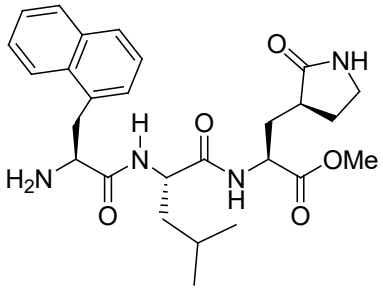

86

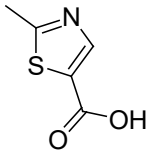

87

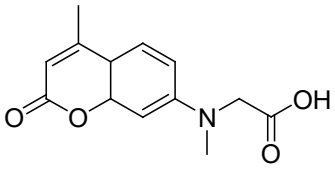

88

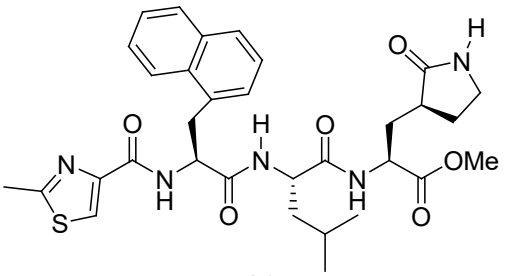

89

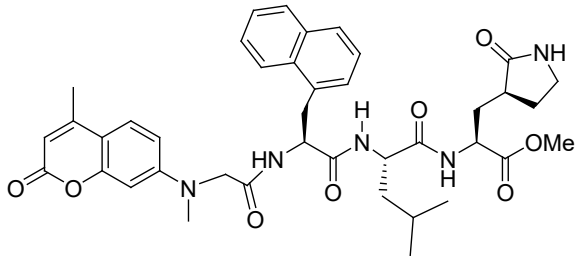

90

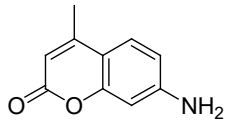

91

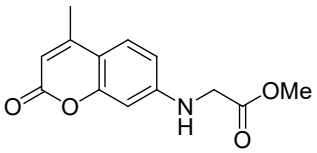

92

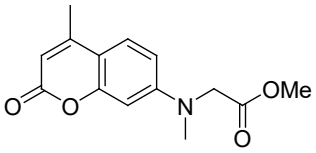

93

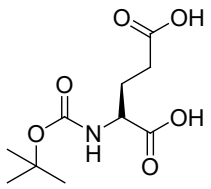

94

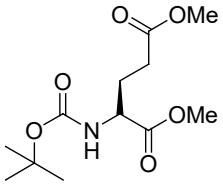

95

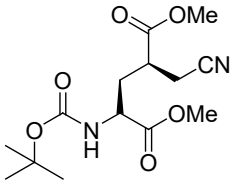

96

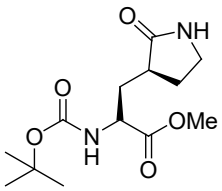

97

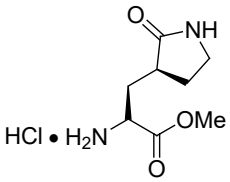

98

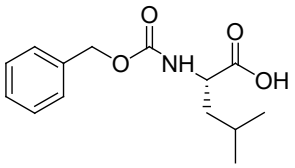

99

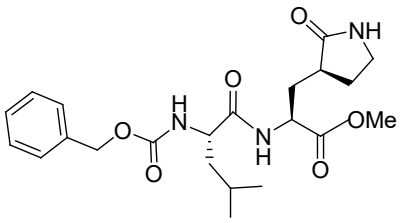

100

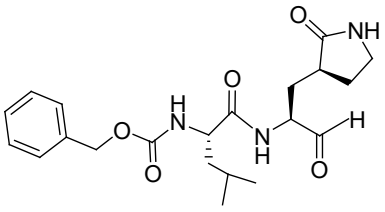

101

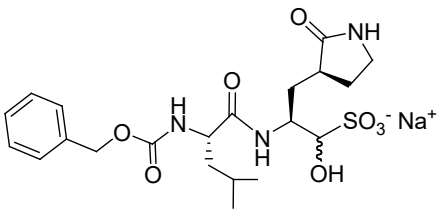

102

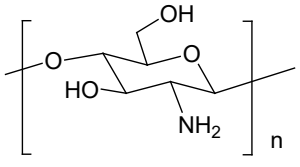

DADP-CS

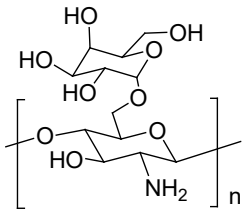

CS- galactose

List of Publications

The following publications and manuscript were achieved during the study.

(1) Design, Synthesis, and Bioevaluation of Viral 3C and 3C-Like Protease Inhibitors. Allan M. Prior, Yunjeong Kim, **Sahani Weerasekara**, Meghan Moroze, Kevin R. Alliston, Roxanne Adeline Z. Uy, William C. Groutas, Kyeong-Ok Chang, and Duy H. Hua. *Bioorganic and Medicinal Chemistry Letters* **2013**, 23, 6317-6320. PMCID: PMC 3863581; NIHMSID: NIHMS 529847

(2) Syntheses, neural protective activities, and inhibition of glycogen synthase kinase-3β of substituted quinolines. Jianyu Lu, Izumi Maezawa, **Sahani Weerasekara**, Ramazan Erenler, Tuyen D. T. Nguyen, James Nguyen, Luxi Z. Swisher, Jun Li, Lee-Way Jin, Alok Ranjan, Sanjay K. Srivastava, and Duy H. Hua. *Bioorganic and Medicinal Chemistry Letters* **2014**, 24, 3392-3397. http://dx.doi.org/10.1016/j.bmcl.2014.05.085.

(3) Broad-spectrum protease inhibitors against 3C-like proteases of feline coronaviruses and feline caliciviruses. Yunjeong Kim, Vinay Shivanna, Sanjeev Narayanan, Allan M. Prior, **Sahani Weerasekara**, Duy H. Hua, Anushka C. Galasiti Kankanamalage, William C. Groutas, and Kyeong-Ok Chang. *J. Virology*, **2015**, 89(9), 4942-49550. Doi:10.1128/JVI.03688-14.

(4) Reversal of the progression of fatal coronavirus infection in cats by a broad-spectrum coronavirus protease inhibitor. Yunjeong Kim, Hongwei Liu, Anushka C. Galasiti Kankanamalage, **Sahani Weerasekara**, Duy H. Hua, William C. Groutas, Kyeong-Ok Chang, Niels C. Pedersen. *PLOS Pathogens*, **2016** (March 30, 2016), 1-18; doi:10.1371/jouran.ppat.1005531.

(5) Current tools for norovirus drug discovery. **Sahani Weerasekara**, Allan M. Prior, and Duy H. Hua. *Expert opinion on drug discovery*, **2016**, 11(6), 529-541.

(6) Chiral Substituted Poly-N-vinylpyrrolidinones and Bimetallic Nanoclusters in Catalytic Asymmetric Oxidation Reactions. Bo Hao, Medha J. Gunaratna, Man Zhang, **Sahani Weerasekara**, Sarah N. Seiwald, Vu Nguyen, Alex Meier, and Duy H. Hua. *J. Am. Chem. Soc*. **2016**, submitted (September 10, 2016).

Acknowledgements

Foremost, I would like to express my sincere gratitude to my research advisor, Dr. Duy H. Hua, for his continuous guidance, instructions, patience, and support throughout my graduate studies at Kansas State University. Thanks for accepting me to his research group and insightful guidance for my research.

I would like to thank Dr. Takashi Ito, Dr. Yunjeong Kim, and Dr. Ping Li for being the members of my PhD advisory committee and for their valuable time and discussions. I am thankful to Dr. Timothy Rozell for his valuable time to serve as my outside chairperson for the committee. I also wish to thank all the other faculty and staff members in the Department of Chemistry and all our collaborators for their support throughout the past five years.

I would like to thank my former labmates: Dr. Keshar Prasain, Dr. Allan Prior, Dr. Jianyu Lu, Dr. Thi Nguyen, Dr. Laxman Pokhrel, Dr. Mahendra Thapa, Mr. Duy Le, and my current labmates: Ms. Medha Gunaratna, Ms. Man Zhang, and Mr. Bo Hao for their assistance, friendship, and encouragement.

My special thanks goes to department of Chemistry, Kansas State University for providing me this great opportunity to pursue my PhD degree.

I would like to acknowledge the research support staff for invaluable technical assistance.

Finally, I would like to thank my parents, my husband and my two sisters for their love and continuous encouragements.

Chapter 1 - Design, Synthesis, and Evaluation of Bioactive Molecules

1.1 Introduction

Structural modification of natural products and other widely used pharmacophores such as drug candidates is an important major field of research. The significant aspect of this approach is that it provides a way of rapidly synthesizing analogues of a common pharmacophore and therefore, would be helpful in modern drug discovery. The main objectives of these modifications are to obtain novel bioactive compounds with better pharmacological activity, physico-chemical, biochemical, pharmacokinetic and safety properties that could enhance the potency and selectivity along with better solubility, distribution and ionizability parameters. A number of research reports have aimed to design novel compounds that can function as inhibitors or enhancers through the interactions with important proteins, nucleic acids, protein-protein interacting surfaces, ion channels and signaling receptors etc. Consequently, they would have a broader therapeutic scope that could cover a wide range of diseases such as parasites, bacterial and fungal infections, allergies, cancer, cardiovascular and metabolic diseases, etc.

This chapter summarizes the work I have carried out towards the design and synthesis of a set of quinoline compounds and evaluation of these compounds to identify whether they are capable of inhibiting glycogen synthase kinase-3 beta (GSK3β) and protein kinase C (PKC) enzymes using *in vitro* enzyme assays.

Protein phosphorylation process is mainly governed by kinases and phosphatases and is one of the major post translational mechanisms used by cells to regulate enzymes and structural proteins and therefore numerous diseases are linked with abnormalities of protein phosphorylation.[1] Glycogen

synthase kinase-3 (GSK3) is one such kinases and originally identified for its regulation function of glycogen metabolism.[1] It is a proline directed serine/threonine kinase and currently a large body of evidences suggest that it is involved in variety of physiological processes such as glycogen metabolism, gene transcription, insulin action, apoptosis, microtubule stability and Wnt and Hedgehog signaling.[1,2] There are three isoforms of GSK3 exist in mammals which are called glycogen synthase kinase-3 alpha (GSK3α), glycogen synthase kinase-3 beta (GSK3β), and GSK3β2.[2] GSK3β is relatively abundant in the central nervous system and is involved in neuronal specific activities.[3] Several lines of evidences suggest that GSK3 signaling plays a significant role in neurodegeneration and is associated with neurodegenerative diseases such as Alzheimer's disease (AD).[1,2]

AD is the most common form of dementia in elderly and about 35 million people worldwide have suffered from AD.[4] AD is aggravated over time and at the early stage, it only induces a short-term memory loss; but the advanced-stage AD causes cognitive impairment, long term memory loss, and damage of motor functions as well.[4]

So far, the exact cause of AD is not known and it is believed that AD develops as a result of multiple factors rather than a single cause. Two most commonly found pathological characteristics of familial AD (from inheritance; about 5% of all AD) include the accumulation of extracellular amyloid beta (Aβ) plaques and intra-cellular neural fibrillary tangles (NFTs) in the AD patients brain.[5,6] Aβ plaques consist of beta amyloid peptides which are generated from the cleavage of amyloid precursor protein (APP), and NFTs are composed of the hyperphosphorylated tau proteins.[5,6] It has been found that GSK3β is highly expressed in AD patient's brain and involves in the hyperphosphorylation of tau protein.[2,5] Tau is a neuronal microtubule associated phosphoprotein and hyperphosphorylation of tau protein by GSK3β has found to be altering the

binding to microtubules and leads to tau degradation and aggregation.[2,5] Therefore, inhibition of GSK3β could be a potential approach to alleviate the symptoms of AD.

Previously, Hua's laboratory has synthesized a class of substituted quinolines (PQs) by derivatizing the C-8 amino function of 6-methoxy-4-methyl-5-(3-(trifluoromethyl)phenoxy)quinoline-8-amine to study their anti-cancer activities. Among the synthesized PQ compounds: *N*-(3-aminopropyl)-6-methoxy-4-methyl-5-(3-(trifluormethyl)phenoxy) quinolin-8-amine (**PQ1**), *N*-(furan-2-ylmethyl)-6-methoxy-4-methyl)-5-(3-(trifluoromethyl)phenoxy)quinolin-8-amine (**PQ7**), 6-methoxy-4-methyl-N-(quinolin-4-ylmethyl)-5-(3(trifluoromethyl)phenoxy)quinolin-8-amine (**PQ15**) were shown to have anti-breast cancer activities.[7,8] Moreover, **PQ1** also shown to possess strong MC65 neuronal cell protection activity. Notably, the structures of these compounds have a close similarity to that of known PKC inhibitors such as MT477, dequalinium, and chelerythrine chloride (these structures are shown in Figure 1.3).[9] Therefore, with known anti-cancer and strong MC65 neuronal cell protection activities, we have hypothesized that PQ compounds can function as PKC and/or GSK3β inhibitors.

In this chapter, structure guided design and synthesis of analogs of PQ molecules and evaluation of the inhibition of PKC and GSK3β enzymes are discussed.

1.2 Background

1.2.1 GSK3β and its relation with Alzheimer's disease

It is believed that oligomers of amyloid β peptide target the insulin or wnt signaling pathways and activates the GSK3β and the activated GSK3β can induce the subsequent phosphorylation of tau

protein.[10] Studies have found that tau obtained from the brains of AD patients has about 40 phosphorylation sites, 28 serines, 10 threonines and 2 tyrosines.[5] Out of that, GSK3β can phosphorylate 17 of the serine and 6 of the threonine residues.[5] Phosphorylation of tau by GSK3β predominantly occurs in the regions surrounding the microtubule binding domain, therefore, this prevents the interaction of tau with microtubules and may affects microtubule stabilization and dynamics.[5] Moreover, the hyperphosphorylated tau proteins have different structures from original tau and precipitate out as neural fibrillary tangles. As a consequence of this, the interaction between tau and microtubules weakens and tau gets detached from microtubules and may favor its self-aggregation.[5] Therefore, several GSK3β inhibitors are currently being studied as a treatment option for AD. One such compound is lithium chloride, which has been found to reduce the Aβ oligomer production in AD mouse models as well as exerting a protection effect on neuronal cells

by inhibiting the GSK3β.[11] Figure 1.1 shows the structures of some selective GSK3β inhibitors and some of those (such as tideglusib) are in clinical trial phases for AD.[12]

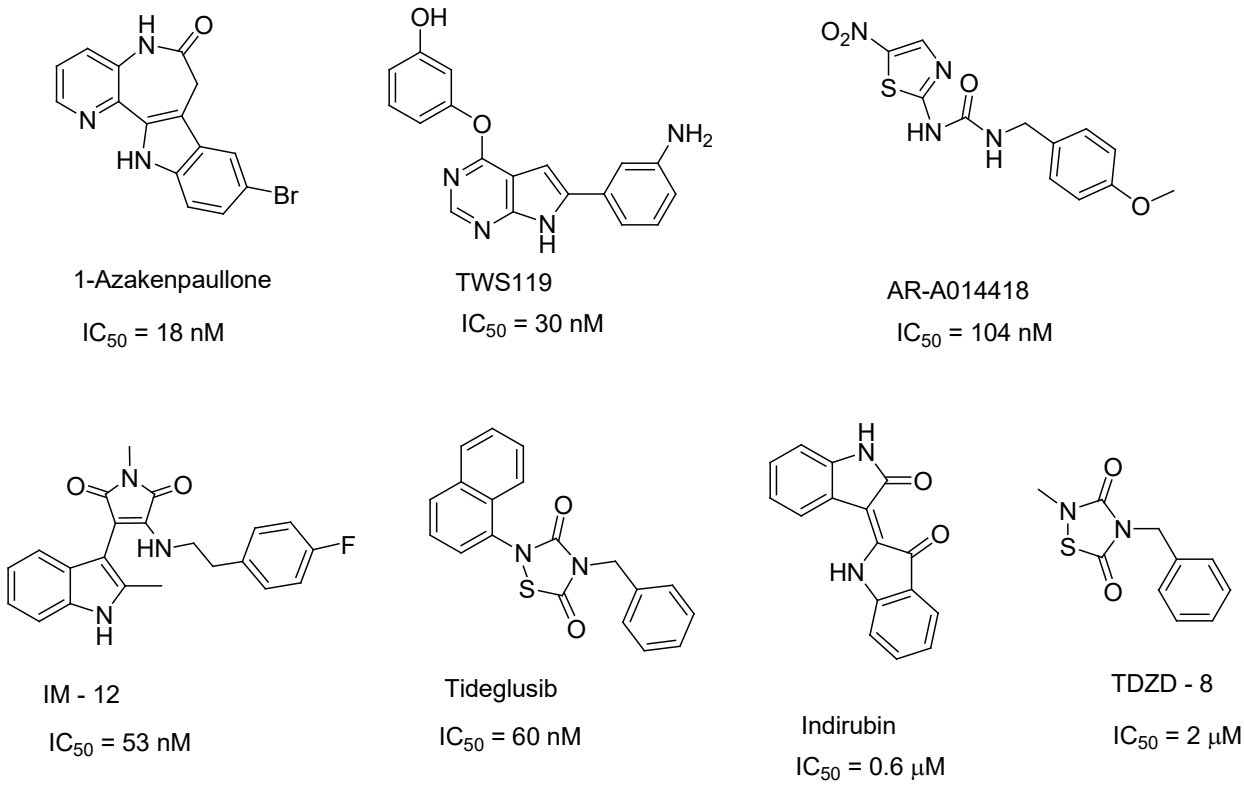

Figure 1.1: Structures of known selective GSK3β inhibitors and their inhibitory activities.[12]

By looking at the structures of reported GSK3β inhibitors, it can be seen that most of these compounds possess either pyridine, pyrimidine, pyrazole and thiazole moieties. In order to expand the structural diversity of GSK3β inhibitors, our group has focused on a library of quinoline

compounds and the structure guided design and synthesis of those compounds. Evaluation of the inhibitory properties towards GSK3β enzyme was also carried out.

1.2.2 Inhibition of PKC phosphorylation by substituted quinolines

Protein kinases are enzymes that catalyze the transfer of a γ-phosphate group from adenosine triphosphate (ATP) to serine, threonine, or tyrosine residues of specific substrate proteins.[13] This will result in the phosphorylation of proteins and affect their structures, activities, cellular location, and protein-protein interaction, since specific negatively charged phosphate group(s) was introduced.[13] There are several protein kinases. PKC is one such kinase, belongs to the family of serine/threonine protein kinases and was first reported by Yasutomi Nishizuka and coworkers in 1977.[14] There are at least 12 isozymes of PKC and they are further categorized into three sub families based on their mode of activation and similarities in amino acid sequence. These sub families include: (1) classical PKCs (cPKC: PKCα, PKCβI, PKCβII, and PKCγ) which are activated by calcium, diacylglycerol (DAG) and phosphatidylserine (PS); (2) novel PKCs (nPKC: PKCδ, PKCε, PKCη, PKCθ and PKCμ) which are activated by DAG and PS but are insensitive towards calcium; (3) atypical PKCs (aPKC; PKCζ and PKCλ) are insensitive towards both calcium and DAG but can be activated by 3-phosphoinositides (PIP_3).[15] PKC is composed of a single polypeptide chain in which the N-terminal regulatory domain (~ 20 - 40 kDa) has linked to a highly conserved C-terminal catalytic domain (~ 45 kDa) by a proteolytically labile hinge region (V3) (Figure 1.2).[16] The regulatory domain of PKC is consisted of two regions (C1 and C2) and it varies among other PKC isozymes. However, the catalytic domain that consists of two regions (C3 and C4) is highly conserved among other PKC isozymes. In classical PKCs, the C1 region functions as a DAG or PS binding site, the C2 region contains the recognition site for acidic lipids and

calcium binding, and the C3 and C4 regions function as the ATP and substrate binding sites, respectively.[14,16] The differences of novel and atypical PKCs are the absence of calcium binding site in C2 region of the novel PKC and presence of a structurally different C1 region with a lacking functional C2 region in atypical PKCs.[14-16] There is a pseudo-substrate involved in PKC enzyme activity and it binds to the substrate binding site of C4 region in the absence of activators and keeps the enzyme in inactive state.[16]

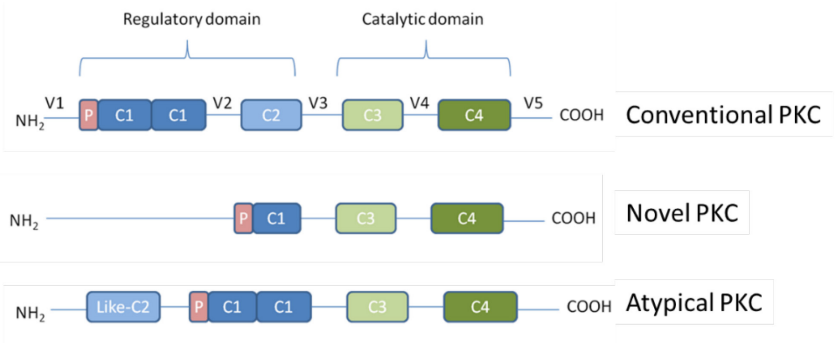

Figure 1.2: Schematic representation of the domain structure of PKC.

1.2.2.1 PKC and its relationship with cancer and other diseases

PKCs are involved in wide variety of physiological processes in mammalian cells. Short term activation of PKC leads to short term events such as secretion and ion influx whereas sustained activation is believed to cause long term effects such as proliferation, differentiation, apoptosis, migration or tumorigenesis.[17] The role of PKC as a tumor promoting agent has been recognized for decades. The finding of PKC isozymes is activated by tumor promoting agents such as phorbol esters, suggesting that PKC could be involved in tumor promotion and progression.[17,18]

It has been found out that the expression profiles of PKC isozymes are varied during cancer progression and the most common isozymes that display abnormal expression during cancer progression are α, β, and δ, but abnormal expression of other isozymes may also possible.[14,17] For

example, immunohistochemical studies have shown that there is an over expression of PKCα in urinary bladder, prostate and endometrial cancers, in contrast, downregulation of PKCα can be seen in breast, colon, hepatocellular and basal cell cancers.[14,17] In addition, PKCβ expression has been revealed to be upregulated in colon and prostate cancers and downregulated in bladder cancer. In contrast, PKCδ activity is more frequently linked to induce apoptosis.[14] However, the expression profiles of PKC isozymes have not been extensively studied yet. Some of the important downstream events following PKC activation are MEK-ERK (mitogen activated protein kinase kinase–extracellular signal-regulated kinase), and PI3K–Akt pathways.[14]

Moreover, studies have found out that increase PKC levels enhance the resistance and metastatic potential of human breast cancer cells.[19] The other notable factor of PKC is its ability to inhibit gap junctional intracellular communication (GJIC) by inhibiting gap junctional channels.[20,21] Gap junctions are formed from phosphoproteins called connexins through the process of the connexon of one cell docking with the connexon of an adjacent cell.[22] Each connexon is composed of six proteins of connexin family such as Cx43 and Cx32.[22] Except Cx26, most of the other connexins are phosphorylated by several kinases including mitogen-activated protein kinase (MAPK), protein kinase C (PKC), and protein kinase A (PKA).[22] Studies have shown that when the expression of phosphorylated form of connexin increases, it weakens the gap junctional intercellular communication (GJIC).[20-22] It is believed that restoring gap junctions by inhibiting PKC may be a treatment option for cancer since it will enhance the intercellular communication and thereby induce apoptosis.

The idea of testing PQ compounds to identify their potential as PKC inhibitors came from the fact that, some of the substituted quinolines synthesized in our laboratory were speculated to inhibit PKC phosphorylation of Cx43 by disrupting the interactions between Cx43 and Nedd4, an E3

ubiquitin ligase, resulting in the enhancement of gap junctions in breast cancer cells.[7,8,23-25] Another notable factor is the structural similarities such as having common quinoline moiety between PQs and several known PKC inhibitors like MT477, chelerythrine chloride, and dequalinium which might be linked to the PKC inhibition properties of PQs.

Several natural and synthetic PKC inhibitors have been reported. Some of the examples for natural compounds are safingol, calphostin C, miltefosine, curcumin, staurosporine and chelerythrine chloride.[26-31] Synthetic PKC inhibitors include tamoxifen, dequalinium, MT477, and analogs of staurosporine such as midostaurin (PKC412), etc.[32,33] Structures of these compounds are shown in

Figure 1.3. In most cases, these small molecules inhibit PKC by binding to either the catalytic domain (ATP binding site) or regulatory domain (diacylglycerol or calcium binding site) of PKC.

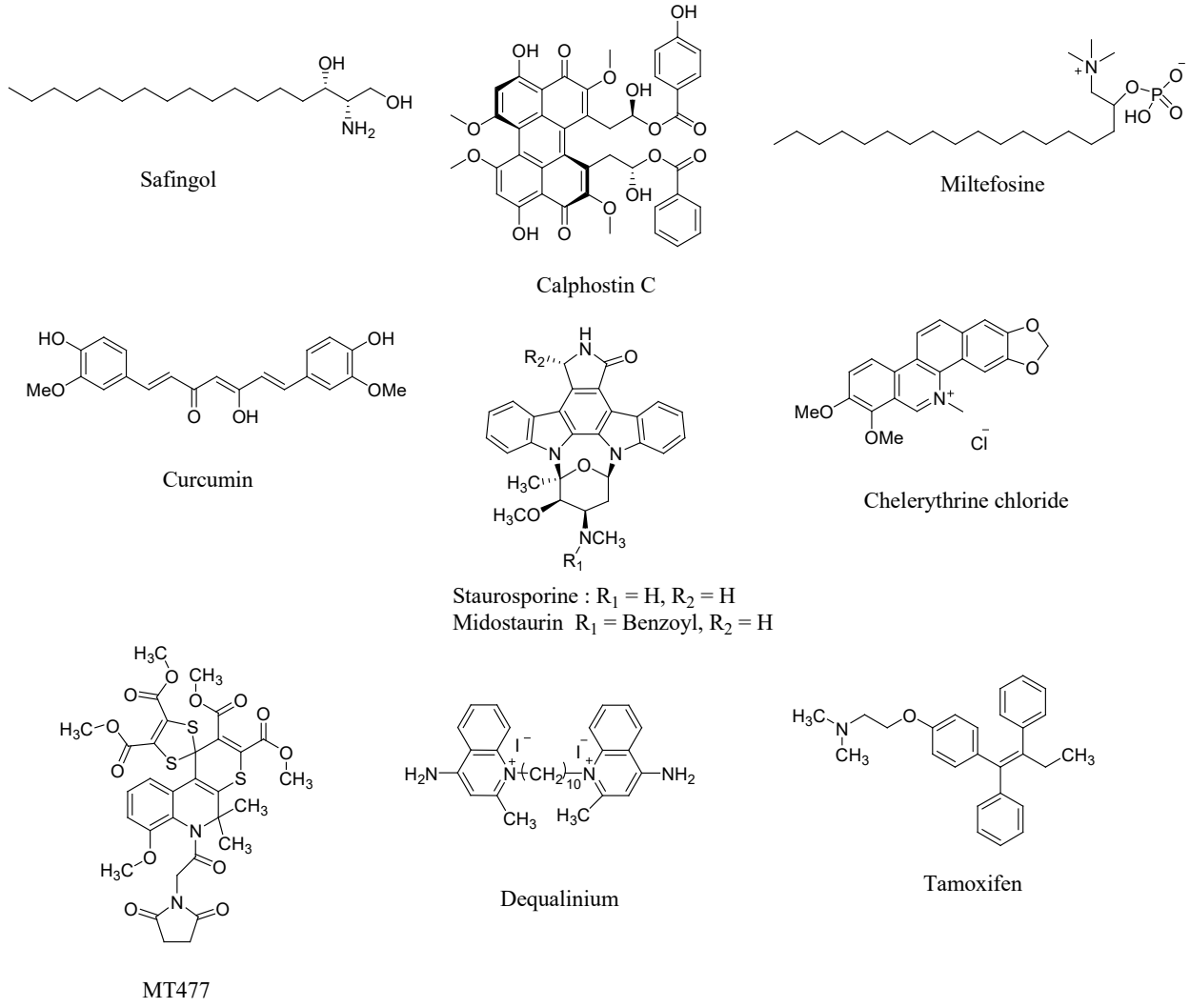

Figure 1.3: Structures of known PKC inhibitors.

1.3. Results and discussion

1.3.1 Syntheses of substituted quinoline compounds

The identification of potential GSK3β inhibitors has become an important area of research and currently more than 30 small molecule compounds have been identified as GSK3β inhibitors.[34] However, out of these molecules, only a few compounds are being evaluated in clinical trial phases.[35] Since GSK3β enzyme exhibits a broad therapeutic scope, the compounds in clinical trial phases are not only limited to Alzheimer's disease but rather testing for various other diseases such as diabetes, cancer, inflammation, epilepsy, mania and bipolar disorder etc.[34,35] Among the few compounds in advanced clinical trial phases, the compounds called "tideglusib" and "IBU-PO" are being testing for AD disease.[35] Therefore, discovery of novel compounds as GSK3β inhibitors may be highly warranted.

In related to their mechanism of action, GSK3β inhibitors can be classified as ATP competitive, non ATP competitive, and substrate competitive inhibitors.[36] These inhibitors are mainly the heterocyclic compounds and can be categorized as pyrazolopyrimidine, benzimidazole, pyridinone, pyrimidines, indolylmaleimide, imidazopyrimidines, oxadiazole and pyrazole derivatives.[34,35] Quinoline compounds are not commonly reported as GSK3β inhibitors. However, the idea behind designing a class of quinoline compounds as GSK3β inhibitors is as follows. Previously, Hua's laboratory has synthesized a number of quinoline compounds and out of those, two compounds named as **PQ1** and **PQ7** (Figure 1.4) have been tested for their potency on MC65 neural cell protection assay.[7,37] **PQ1** and **PQ7** had EC_{50} values of 147 ± 20 nM and **PQ7** 691 ± 27 nM, respectively.[7,37] MC65 cell assay can be used to identify compounds that can penetrate cells and inhibit Aβ oligomer induced neuronal toxicity. Therefore, the compounds identified from

MC65 cell assay may give a positive feedback for testing those compounds against GSK3β, because the imbalance of GSK3β is believed to promote Aβ oligomers through the elevation of enzymatic processing of APP.[37]

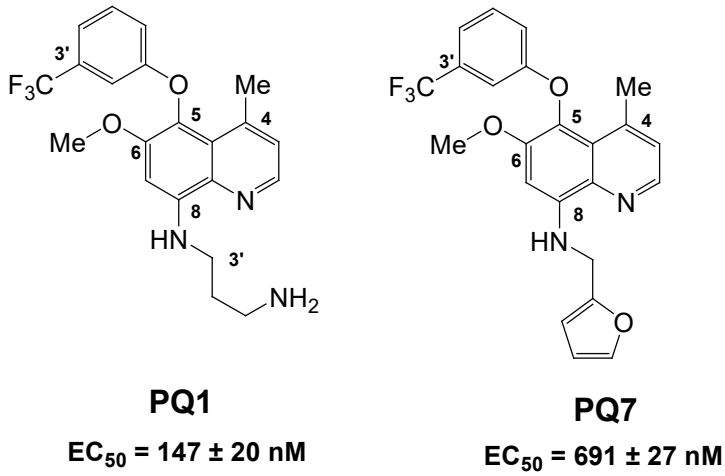

Figure 1.4: Structures and EC_{50} values for neural protection of MC65 cells of PQ1 and PQ7.[37]

As shown in Figure 1.4, structures of **PQ1** and **PQ7** possess some similarities. They both have four substituents attached to the quinoline core which are 4-methyl group, 5-(3-triflouromethylphenoxyl) group, 6-methoxyl and 8-amino group. The only structural difference of **PQ1** and **PQ7** is the substituent connected to the 8-amino group in which **PQ1** has an alkyl amino group whereas **PQ7** contains a furan moiety. However, since their EC_{50} values display a considerable difference suggesting that the substituent attached to the 8-amino group of **PQ1** and **PQ7** plays an important role in the activity of these molecules. Therefore, **PQ1** and **PQ7** were

used as models to design a new set of molecules (Figure 1.5) by altering the substituent attached to the 8-amino group of **PQ1** and **PQ7**.

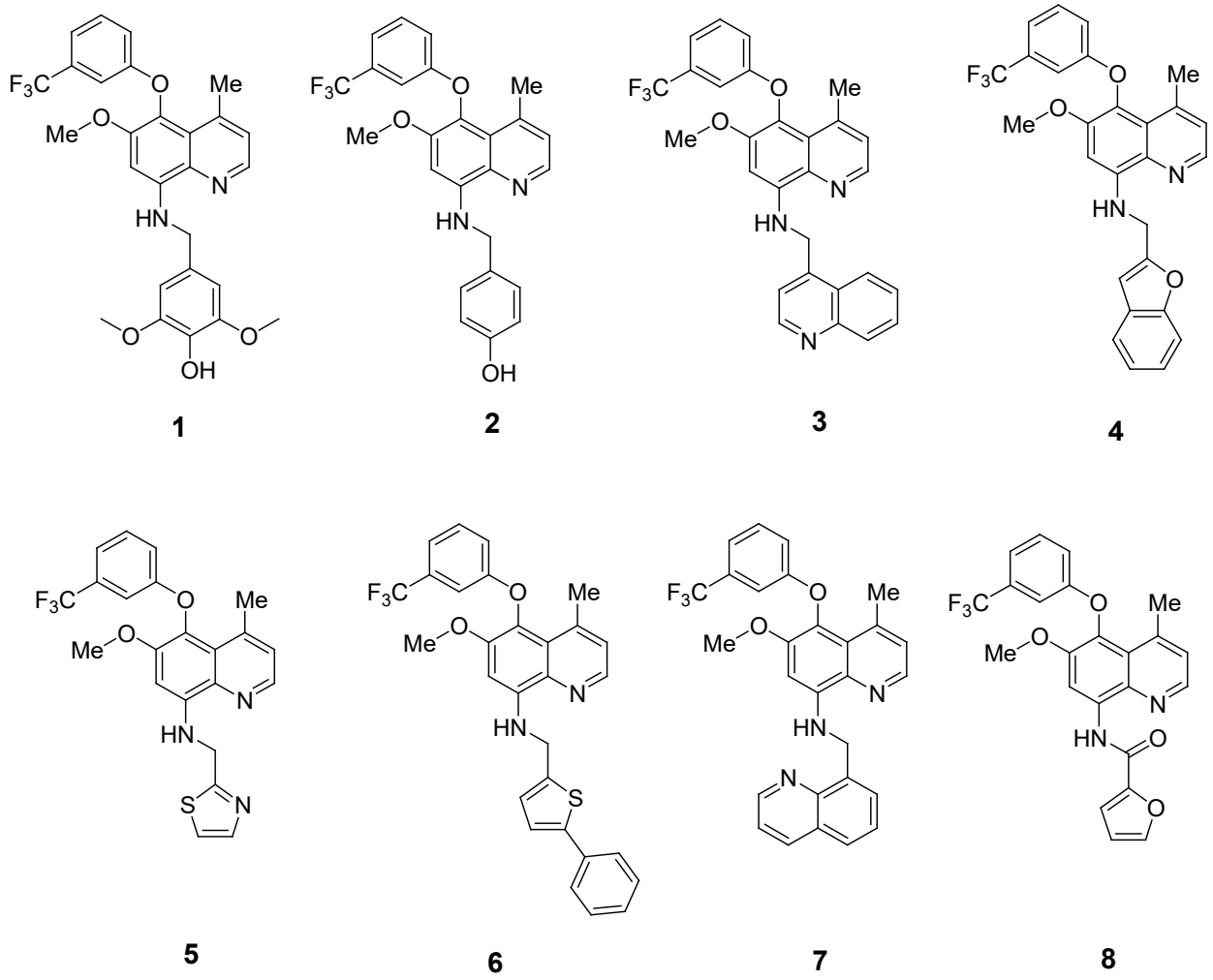

Figure 1.5: Synthesized substituted quinolines 1 – 8.[37]

Compounds **1- 8** contains various heterocycles or other aromatic structures as the substituent attached to the 8-amino group and they were synthesized by Dr. Jianyu Lu in Prof. Duy Hua's laboratory. Table 1.1 summarizes the results obtained for the MC65 neural cell protection assay for these compounds.[7,37] MC65 cells induce the cell death due to the presence of SβC gene and this gene is responsible to produce toxic amyloid beta peptides of the amyloid precursor protein

(APP). Cleavage of the fragment of APP peptide promotes the generation of toxic Aβ peptides and the accumulation of these peptides induces cell death.[38] By introducing tetracyclin (TC) in MC65 cells, the cell death can be prevented as it suppresses the expression of SβC gene. Therefore, designed quinoline compounds were incubated with MC65 cells in the absence of TC to test their cell protection activities against the Aβ peptide induced cell death.[7,37-38] This work was carried out by Dr. Izumi Maezawa in Dr. Lee-Way Jin's laboratory, M.I.N.D. Institute and Department of Pathology, UC Davis Health System, California, United States.

Table 1.1: EC_{50} (μM) and TD_{50} (μM) values of synthesized quinoline compounds on MC65 cell protection assay.[7,37]

Compound	EC_{50} (μM)	TD_{50} (μM)
PQ1	0.15 ± 0.20	2.09 ± 0.02
PQ7	0.69 ± 0.03	42.82 ± 2.43
1	0.48 ± 0.03	2.91 ± 0.15
2	0.12 ± 0.01	1.38 ± 0.08
3	0.13 ± 0.01	3.35 ± 0.36
4	0.46 ± 0.10	> 50
5	2.39 ± 0.06	20.32 ± 1.22
6	0.39 ± 0.02	14.50 ± 1.68
7	0.19 ± 0.02	> 50
8	3.47 ± 0.32	> 50

It can be seen from these results that, except compounds **2** and **3**, the rest of the compounds display higher EC_{50} and TD_{50} (toxicity dosage at 50% concentration) values suggesting that they are not strong candidates to protect cells from Aβ peptide induced cell death. However, compound **2** possesses nano-molar activity towards cell protection suggesting that the presence of 4-

hydroxybenzyl substituent attached to the 8-amino terminal may be responsible to its higher activity compared to other molecules. This compound seems to be six times more active than **PQ7**, indicates the success of structural modification. Therefore, in order to further study the structure activity relationship, compound **2** was further modified as follows to generate compounds **9** - **12** (Figure 1.6). Compound **9** was generated by replacing the 6- methoxy group of compound **2** into 6- hydroxyl group without changing the other functional groups of compound **2** whereas compounds **10** and **11** was generated by replacing the 5-(3-triflouromethylphenoxyl) group into 5-(3-fluorophenoxyl), 5-phenoxyl respectively. In the case of compound **12**, 5-(3-triflouromethylphenoxyl) group is absent.

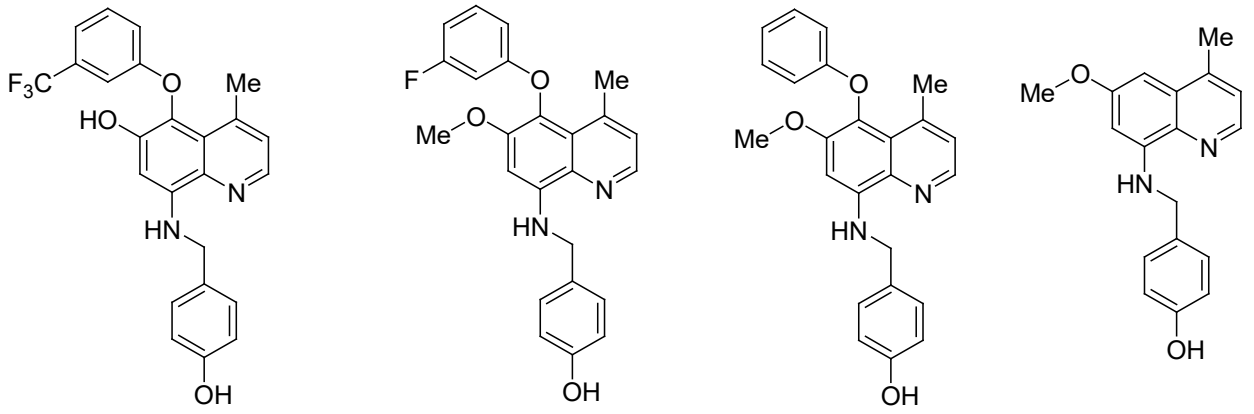

9 **10** **11** **12**

Figure 1.6: Synthesized substituted quinoline compounds 9 – 12.[37]

1.3.1.1 Syntheses of compounds 9 – 11

In order to synthesize compound **9** -**11**, first, the corresponding precursors, aminoquinolines **28**, **29** and **30**, needed to be prepared. The syntheses of compounds **28** -**30** are outlined in Scheme 1.1.

Scheme 1.1: Syntheses of compounds 28 – 30

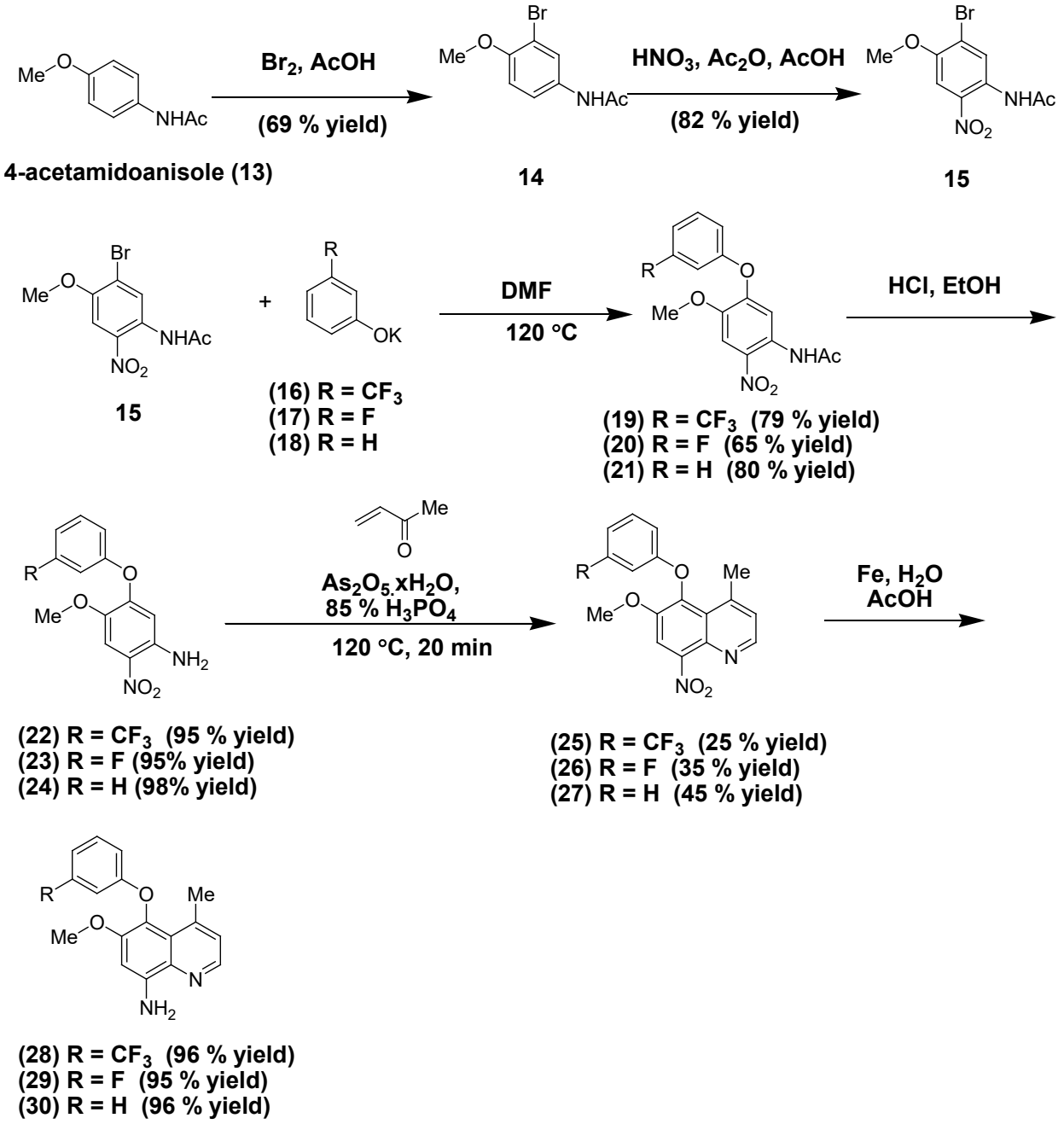

The synthesis of compound **28** was previously reported in Prof. Hua's laboratory.[7] 2-Bromo-4-acetamino-5-nitroanisole (**15**) was prepared by starting with commercially available 4-

acetamidoanisole (**13**) via sequential C2 and C5 functionalizations which was achieved via the C2 bromination of compound **13** to obtain compound **14** followed by nitration at C5 of the compound **14**.[7] Displacement of bromide **15** with potassium 3-fluorophenolate (**17**) and potassium phenolate (**18**) in DMF at 120°C gave 4-acetamino-5-nitro-2-(3-fluoromethylphenyloxy)anisole (**20**) and 4-acetamino-5-nitro-2-(phenyloxy)anisole (**21**) respectively. Since the presence of 3-fluorine moiety, an electron-withdrawing group could decrease the reactivity of the phenolate, the reaction yield for **20** was lower than that of **21**. Removal of the acetyl protecting group of compounds **20** and **21** with hydrochloric acid in ethanol afforded 4-amino-5-nitro-2-(3-fluoromethylphenyloxy)anisole (**23**) and 4-amino-5-nitro-2-(phenyloxy)anisole (**24**), respectively in quantitative yields.

Various reaction conditions have been studied in Prof. Hua's laboratory to maximize the yield of the construction of the quinoline ring from compound **22** with methyl vinyl ketone.[37,55] Treatment of **22** with vinyl methyl ketone, arsenic acid and 85% phosphoric acid at 100 °C after 20 minutes resulted a mixture of desired quinoline **25** and 1,4-adduct **31** along with starting material **22** in a ratio of 1:2:1.[7,39] However, when the reaction was carried out at 120 °C for 20 minutes, a 7:1:1 ratio of compounds **25**:**31**:**22** was achieved (Scheme 1.2).[7] In addition, the longer reaction time had decomposed the product **25** resulting in a lower yield.[7] Also the use of excess of vinyl methyl ketone did not improve the yield. It has been found that the 1,4-adduct **(31)** can be treated with arsenic acid and phosphoric acid under similar reaction conditions as that mentioned above to give quinoline **25** and amine **22** along with compound **31** in a ratio of ~7:1:1.[7] Therefore, uses of a large excess of arsenic acid and 85% phosphoric acid may minimize the formation of intermediate **31**. The results suggest that, adduct **31** is the reaction intermediate leading to quinoline **25**, but it also underwent reversed Michael addition reaction to provide amine **22** and vinyl methyl ketone. This

suggests the importance of controlling the reaction conditions in this reaction. Hence, methyl vinyl ketone was added into a mixture of compound **23**, arsenic pentoxide hydrate in 85 % phosphoric acid at 120 ˚C to give nitro quinoline **26**. Nitro quinoline **27** was synthesized in the similar manner using compound **24** as the starting material. Finally, the nitro quinolines **26** and **27** were treated with iron powder and acetic acid to afford amine quinolines **29** and **30** respectively (Scheme 1.1). Isolation of the Michael addition product from the synthesis of compound **25** has been depicted in Scheme 1.2.

Scheme 1.2: Isolation of the Michael addition product from the synthesis of compound 25

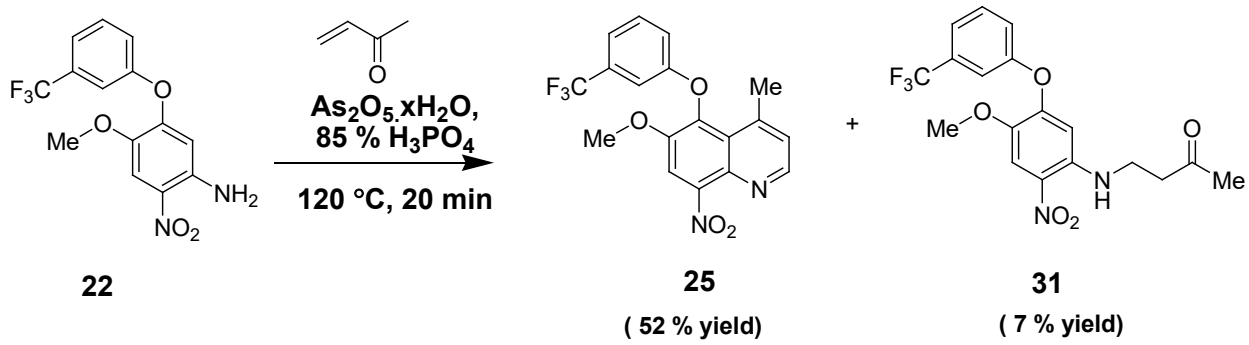

Compound **28**, **29** and **30** serve as the precursor to produce compound **9**, **10** and **11** respectively. Synthesis of compound **9** is outlined in Scheme 1.3.

Scheme 1.3: Synthesis of compound 9

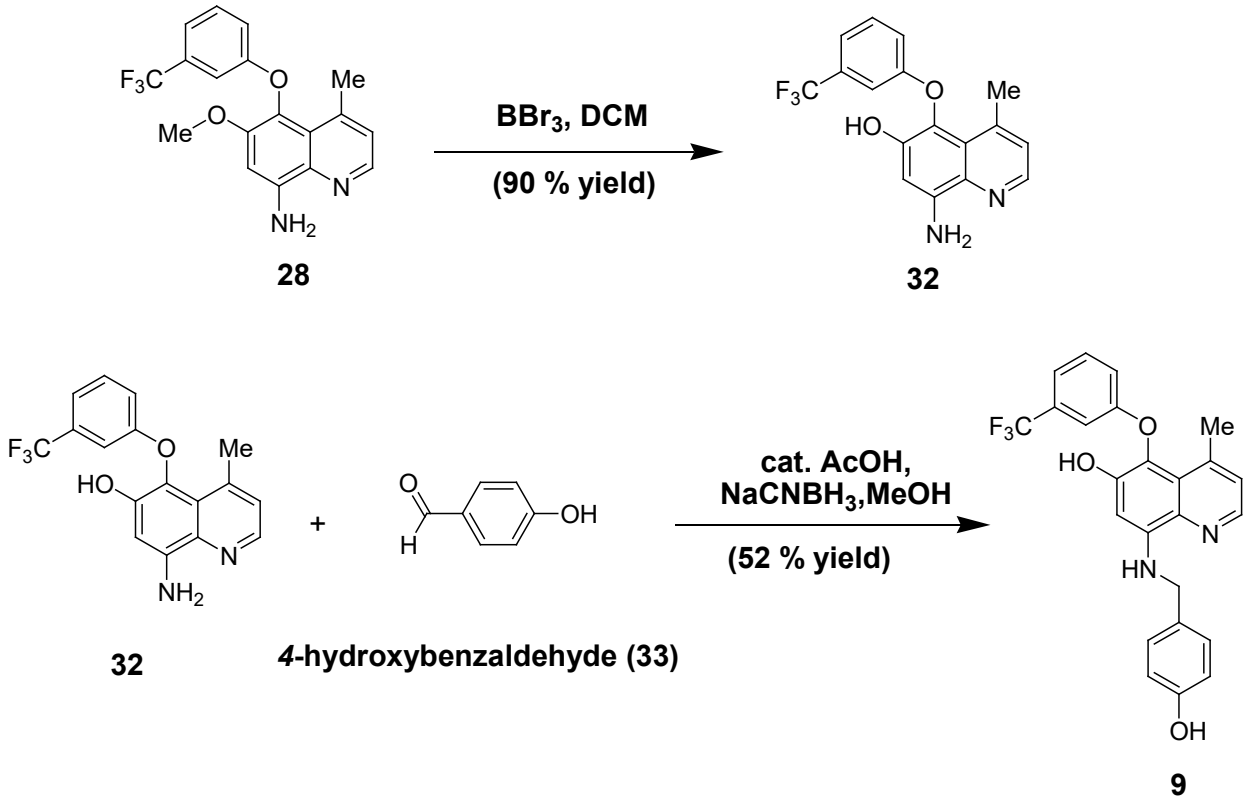

Compound **9** was prepared in two step process starting from compound **28**. In the first step, 4-methoxyl group was converted into hydroxyl by treating the compound **28** with boron tribromide (BBr_3) in dry dichloromethane at 0 °C for 30 minutes and then at room temperature for 14 hours resulting compound **32** which was then coupled with 4-hydroxybenzaldehyde (**33**). First, the compound **32** and **33** in dry methanol was stirred at 25 °C for 30 minutes followed by acetic acid and sodium cyanoborohydride were added and the mixture was stirred at 25 °C for 14 hours. This method was proven to be effective as sodium cyanoborohydide could reduce the imine intermediate formed first into the desired product and therefore, drives the equilibrium in forward direction generating more product formation. However, the yield for this reaction is moderate. It might be due to the reasons of sodium cyanoborohydride could also slowly reduce the aldehyde over long reaction period and the secondary amine functionality of the desired product could also

undergo the imine formation with aldehyde resulting a dialkylated by product, which in turn lower the yield of the reaction. Imine formation of this reaction is outlined in Scheme 1.4. The desired compound **9** was purified by column chromatography followed by recrystallization to obtain the pure product.

Scheme 1.4: Imine formation in the reaction of synthesis of compound 9

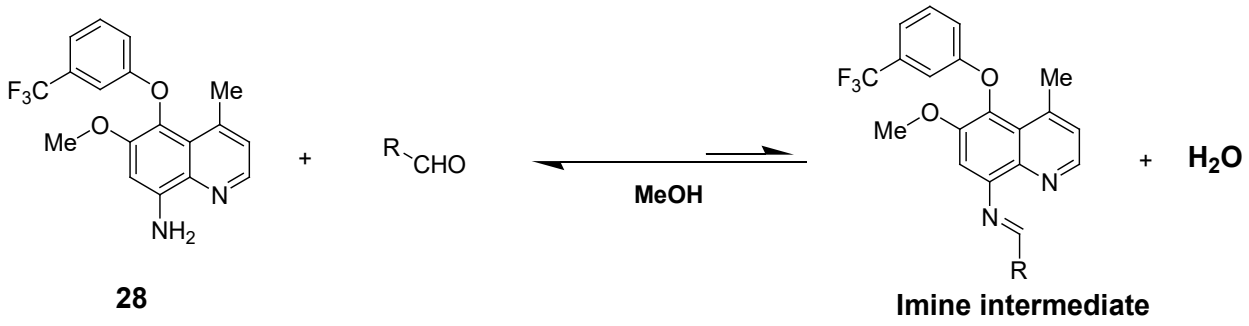

28 **Imine intermediate**

Synthesis of compounds **10**, and **11** is outlined in Scheme 1.5.

Scheme 1.5: Syntheses of compounds 10 and 11

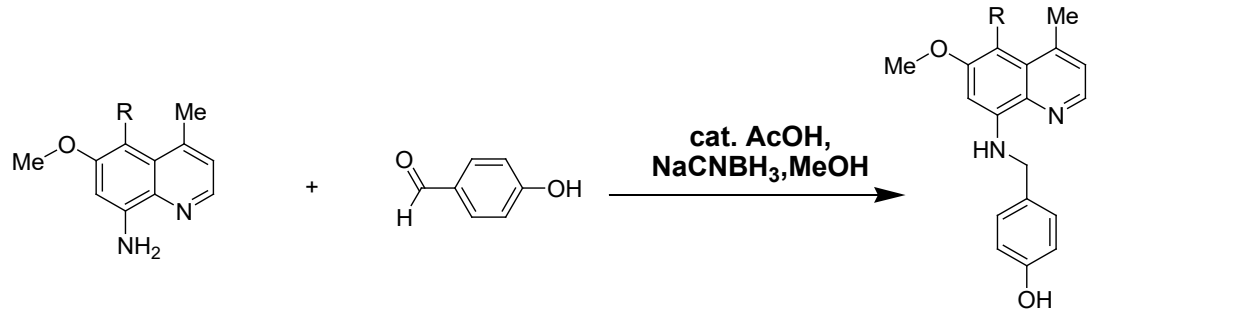

(29) R = 3-fluorphenoxyl
(30) R = Phenoxyl

(33)

(10) R = 3-Fluorphenoxyl (65 % yield)
(11) R = Phenoxyl (84 % yield)

Under similar reaction conditions as those were used to synthesize compound **9**, coupling of compounds **29** and **30** separately with 4-hydroxybenzaldehyde (**33**) gave compounds **10** and **11**, respectively, in moderate to good yields.

1.3.1.2 Synthesis of compound 12

Synthetic scheme to synthesize compound **12** was outlined in Scheme 1.6.

Scheme 1.6: Synthesis of compound 12

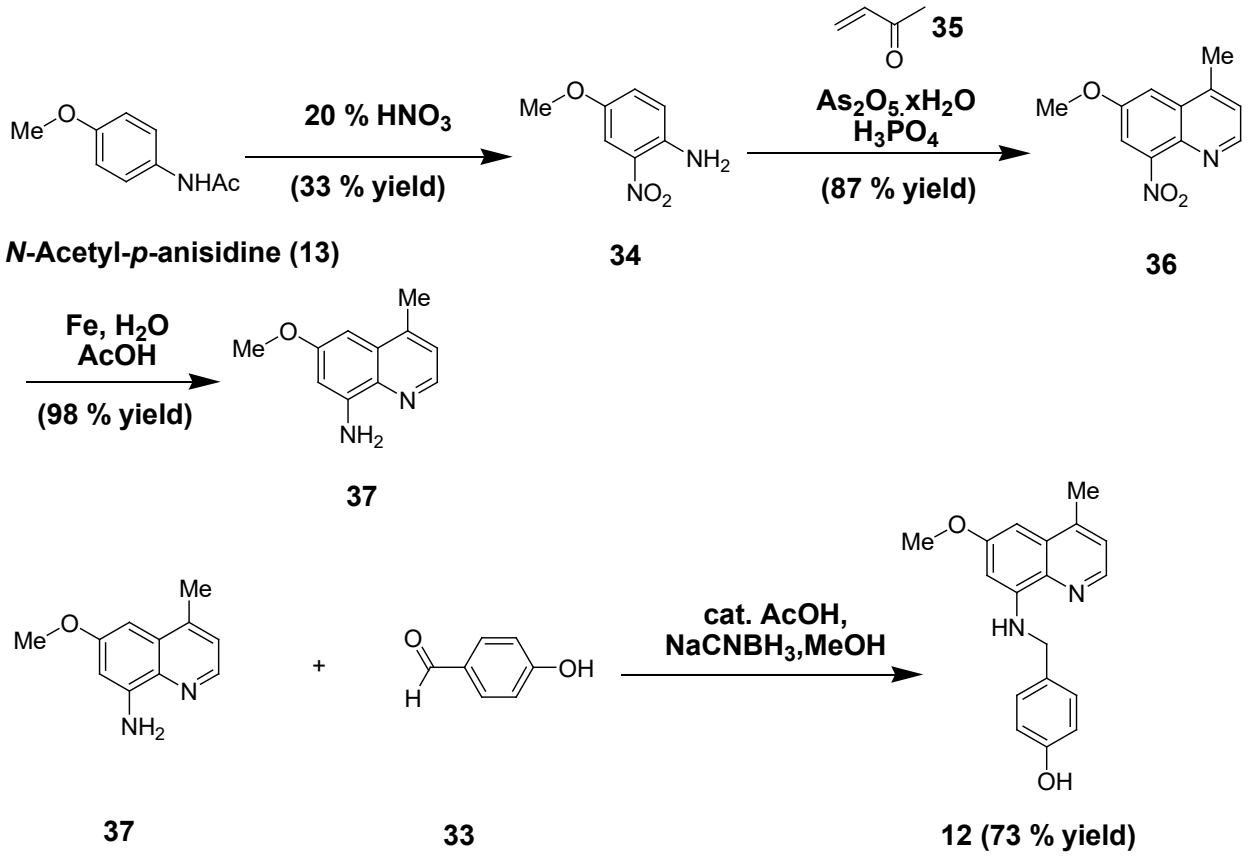

***N*-Acetyl-*p*-anisidine (13)** **34** **36**

37

37 **33** **12 (73 % yield)**

To synthesize compound **12**, amino quinoline **37** was needed. Treatment of *N*-Acetyl-*p*-anisidine (**13**) with 20 % HNO_3 yielded deacetylated nitro compound **34** in 33 % yield. Then, this compound was treated with methyl vinyl ketone (**35**), arsenic pentoxide hydrate in phosphoric acid to obtain the nitro quinoline **36**. Finally, it was reacted with iron powder in acetic acid to yield the quinoline compound **37**. Compound **37** was condensed with 4-hydroxybenzaldehyde (**33**) to obtain compound **12**.

1.3.1.3 A possible mechanism for the generation of quinoline ring structure

The formation of the quinoline ring structure is the key step of these reactions. A possible mechanism is proposed in Scheme 1.7.

Scheme 1.7: A possible mechanism for the generation of quinoline ring structure

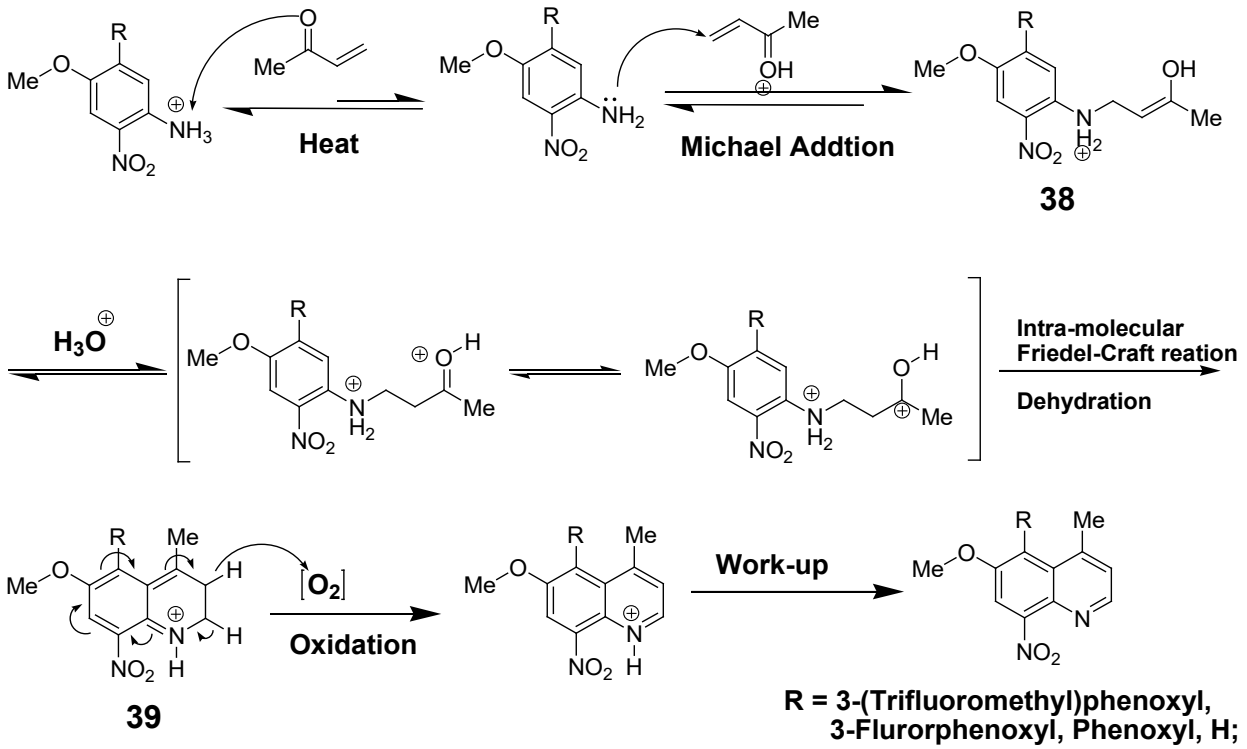

The first step of this reaction is the Michael addition between the aniline NH_2 with the methyl vinyl ketone to generate the intermediate **38**. In the case of compounds **9 -12**, these intermediates can be represented as follows (Scheme 1.8).

Scheme 1.8: Representative structures of the Michael addition intermediates of compounds 9 – 12

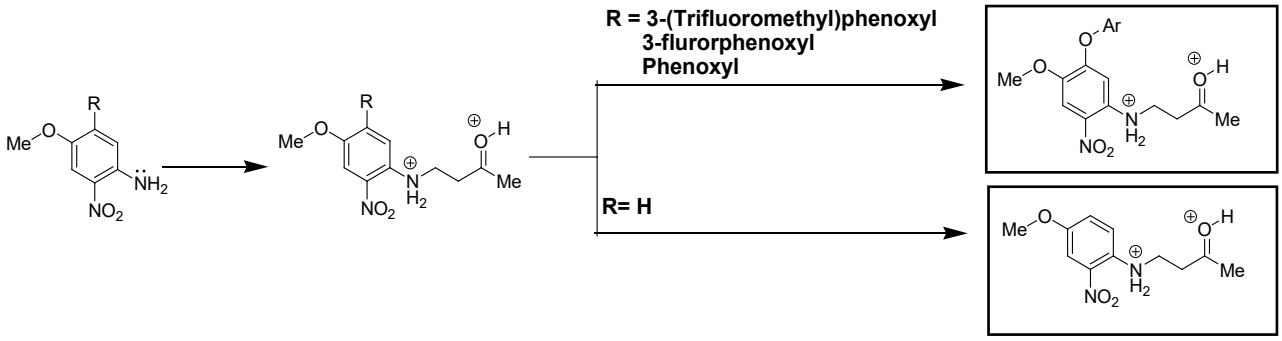

For compounds **9** – **11**, the intermediates possess an aryloxy function at 6th position. Therefore, there are two possible mechanisms (Scheme 1.9) can be predicted for the intramolecular Friedel-Craft reaction.

Scheme 1.9: Possible mechanisms for the intramolecular Friedel-Craft reaction

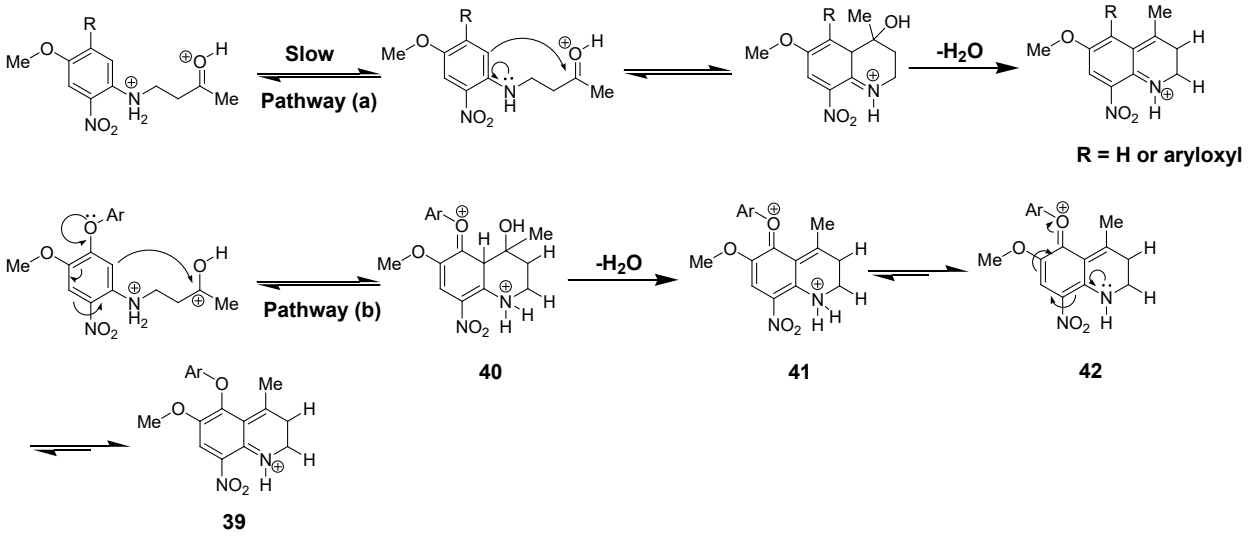

In pathway (a), protonated aniline (NH_2^+) undergoes deprotonation to generate its lone pair of electrons and then donates this lone pair of electrons to the aromatic ring to initiate the Friedel-Craft reaction process. Instead, in pathway (b), the lone pair of electrons present at oxygen at 6th position donates them to initiate the Friedel-Craft process. Since the reaction is carried out at highly acidic environment, the deprotonation of aniline nitrogen could be a slow process. Hence, the Friedel- Craft reaction can be mostly undergone via pathway (b). The di cation intermediate (**41**)

is generated after dehydration and finally the aniline nitrogen gets deprotonated to stabilize the structure and forms the intermediate **42**, which is in resonance with compound **39**.

However, for synthesizing compound **12**, the generated intermediate **38** does not possesses the aryloxy group at 6th position. Therefore, the desired product could mostly be achieved via pathway (a). In addition, due to the absent of aryloxy group at 6th position, the steric hindrance of the Friedel-Craft reaction is low. Therefore, a higher yield (87 %) could be achieved. However, for compounds **9** -**11**, the generated intermediates **28**, **29** and **30** possess 3-(trifluoromethyl) phenoxyl, 3-fluoropehnxoyl and phenoxyl groups respectively. The electron withdrawing capabilities for these groups are CF_3 > F > H. Since the presence of electron withdrawing groups can destabilize the quinoline cation intermediate, the yields can be lower. This may be the reason for observed low yields of 25 %, 35 % and 45 % for compounds **25**, **26** and **27** respectively.

In addition, to retain the aromatic ring structure of the quinoline core, an oxidation step is needed. It is possible that the As_2O_5 acts as the oxygen source of this reaction as the yield of the reaction was not affected when it is carried out in the presence of argon or not. Upon heating, As_2O_5 decomposes to As_2O_3 and molecular oxygen (Scheme 1.10), thus, As_2O_5 may provide the required oxygen *in situ* for this reaction.

Scheme 1.10: Generation of molecular oxygen from As_2O_5[40]

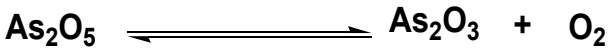

1.3.2 Evaluation of the synthesized quinoline compounds 9 – 12 on MC65 cell protection assayy

The newly synthesized compounds **9** – **12** were tested for MC65 cell protection capabilities and Table 1.3 summarizes the results. This cell based study was carried out by Dr. Izumi Maezawa in Professor Lee-Way Jin's laboratory at the University of California, Davis.[37]

Table 1.2: EC_{50} (µM) and TD_{50} (µM) values of quinoline compounds 9 - 12 on MC65 neuronal cell protection assay.[37]

Compound	EC_{50} (µM)	TD_{50} (µM)
9	0.30 ± 0.01	3.31 ± 0.30
10	0.70 ± 0.01	2.60 ± 0.20
11	0.53 ± 0.01	4.00 ± 0.38
12	2.62 ± 0.15	20.54 ± 0.21

As shown in Table 1.2, the new structural analogues of **PQ1** and **PQ7**, do not seem to be highly potent in MC65 cell protection assay. Compounds **9** - **12**, exhibit moderate EC_{50} and TD_{50} values whereas, compound **12** does not seem to protect MC65 cells. This suggests that the changes made on the **PQ1** structure, impair the bioactivity of these molecules. The detailed discussion of the

structure activity relationship with the observed bioactivities on these compounds is described in the latter part of this chapter.

1.3.3 Evaluation of the GSK3β inhibition by synthesized quinoline compounds using GSK3β assay

Synthesized quinoline compounds that showed higher MC65 cell protection activities were further assessed using GSK3β assay. Out of all twelve compounds, four of the most active compounds, **2** (EC_{50} = 0.12 ± 0.01μM), **3** (EC_{50} = 0.13 ± 0.01 μM), **7** (EC_{50} = 0.19 ± 0.02μM) and **9** (EC_{50} = 0.30 ± 0.01μM), were selected to test their enzyme inhibitory activities on GSK-3β using an ADP-Glo™ kinase assay.[41,42]

ADP-Glo™ Kinase Assay + GSK3β Kinase Enzyme System (catalog # V9371) was purchased from Promega (Madison, Wisconsin, USA) and GSK3β inhibition studies were carried out following the protocol published by Promega.[41] Detailed description of the conversion curves, kinase assays and inhibitor screening was also followed by the ADP-Glo™ kinase assay technical manual (#TM313) published by Promega.[42]

GSK3β kinase assay is a luminescent kinase assay that correlates the phosphorylation of GSK3β enzyme to the amount of ADP (adenosine diphosphate) produced from a kinase reaction.[41] During a kinase reaction, ATP (adenosine triphosphate) is converted to ADP. In the GSK3β kinase assay, the addition of the "ADP-Glo™" reagent ensures the depletion of remaining ATP and generated ADP is simultaneously convert back to ATP from a reagent called "kinase detection reagent".[41] This will allow the newly synthesized ATP to be measured using a luciferase / luciferin reaction

and the light generated is measured using a luminometer.[41] Schematic diagram of the general procedure of the GSK3β kinase assay is depicted in Figure 1.7.

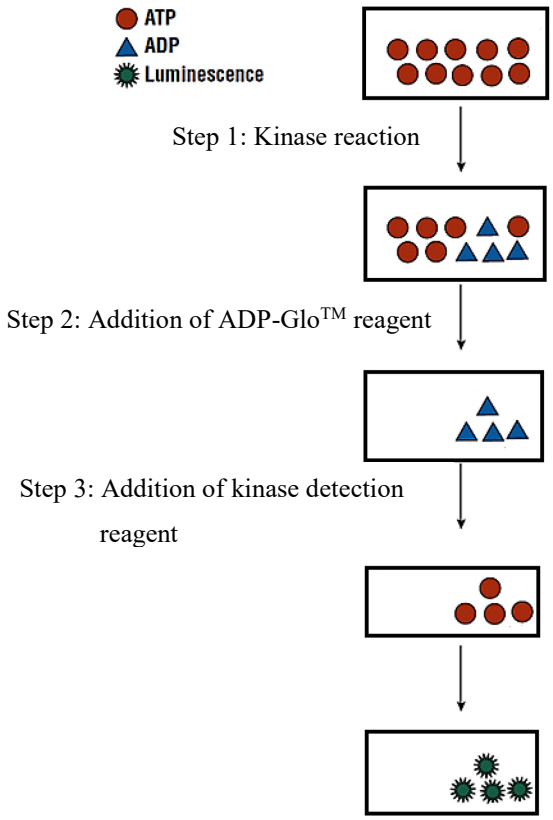

Figure 1.7: Schematic representation of the general procedure of the GSK3β assay.

The obtained luminescent signal can be positively correlated to the generated ADP concentration using an ATP- to -ADP conversion curve. Therefore, luminescent signal is also correlates with kinase activity. This assay relies on the properties of a proprietary thermostable luciferase (Ultra-Glo™ recombinant luciferase) which is formulated to generate a stable luminescent signal.[41] ADP-Glo™ Kinase Assay + GSK3β Kinase Enzyme System consists of the following: GSK3β active enzyme (0.1 µg/µL) 10 µg, GSK3β substrate (1 mg/mL) 1 mL, 5X reaction buffer A 1.5 mL, DTT (0.1 M) 25 µL. The components of the ADP-Glo™ kinase assay kit include: ADP-Glo™

reagent, kinase detection buffer, kinase detection substrate, 10 mM ultra-pure ATP, and 10 mM ADP.[42] The assay is performed in a 384 solid white multiwell plate in two steps. First, the kinase reaction is allowed to occur between the GSK3β enzyme and GSK3β substrate in the presence of ATP and inhibitor. Then ADP-Glo^{TM} reagent is added to terminate the kinase reaction and deplete the remaining ATP. Finally, the kinase detection reagent which was prepared by mixing the kinase detection buffer with kinase detection substrate is added to simultaneously convert ADP to ATP and to measure the newly synthesized ATP using a luciferase/ luciferin reaction. Luminescent signal was measured using the Glo-Max multi detection microplate luminometer in Prof. Jun Li's laboratory at Kansas State University. Detailed description of the assay protocol is mentioned in the experimental section (1.5.2) of this chapter.

1.3.3.1 Studies of the correlation between kinase activity with (1) concentration of GSK3β, and (2) incubation time

In order to find out the optimum assay conditions, first, the GSK3β kinase activity was determined. Briefly, 2 µL of different concentrations of enzyme which contain 0, 0.2, 0.39, 0.78, 1.56, 3.12, 6.25 and 12.5 ng of GSK3β was added into the wells of 384 solid white microwell plate. In a separate tube, 10 mM ATP was diluted to 100 µM ATP and the appropriate volume of this solution was mixed with an equal volume of GSK3β substrate (initial substrate concentration is 1.0 µg/µL). Then 2 µL of this ATP/substrate mixture was added into each well which has enzyme and was incubated at room temperature for 60 minutes. After 60 minutes, 5 µL of ADP-Glo^{TM} reagent was added into each well and plate was incubated at room temperature for 40 minutes. Finally, 10 µL of kinase detection reagent was added and plate was incubated at room temperature for 30 minutes.

Luminescence was recorded for each enzyme concentration using Glo-Max multi detection luminometer with 0.5 seconds integration time per well.

Table 1.3 and Figure 1.8 summarize the results and correlation of luminescence vs amount of GSK3β for the kinase activity determination.

Table 1.3: Determination of the kinase activity for GSK3β.

GSK3β, ng	0	0.2	0.39	0.78	1.56	3.12	6.25	12.5
Luminescence (RLU)	1100 ± 300	2886 ± 450	4750 ± 150	9015 ± 610	16972 ± 1400	30346 ± 2100	47000 ± 3500	49000 ± 3200

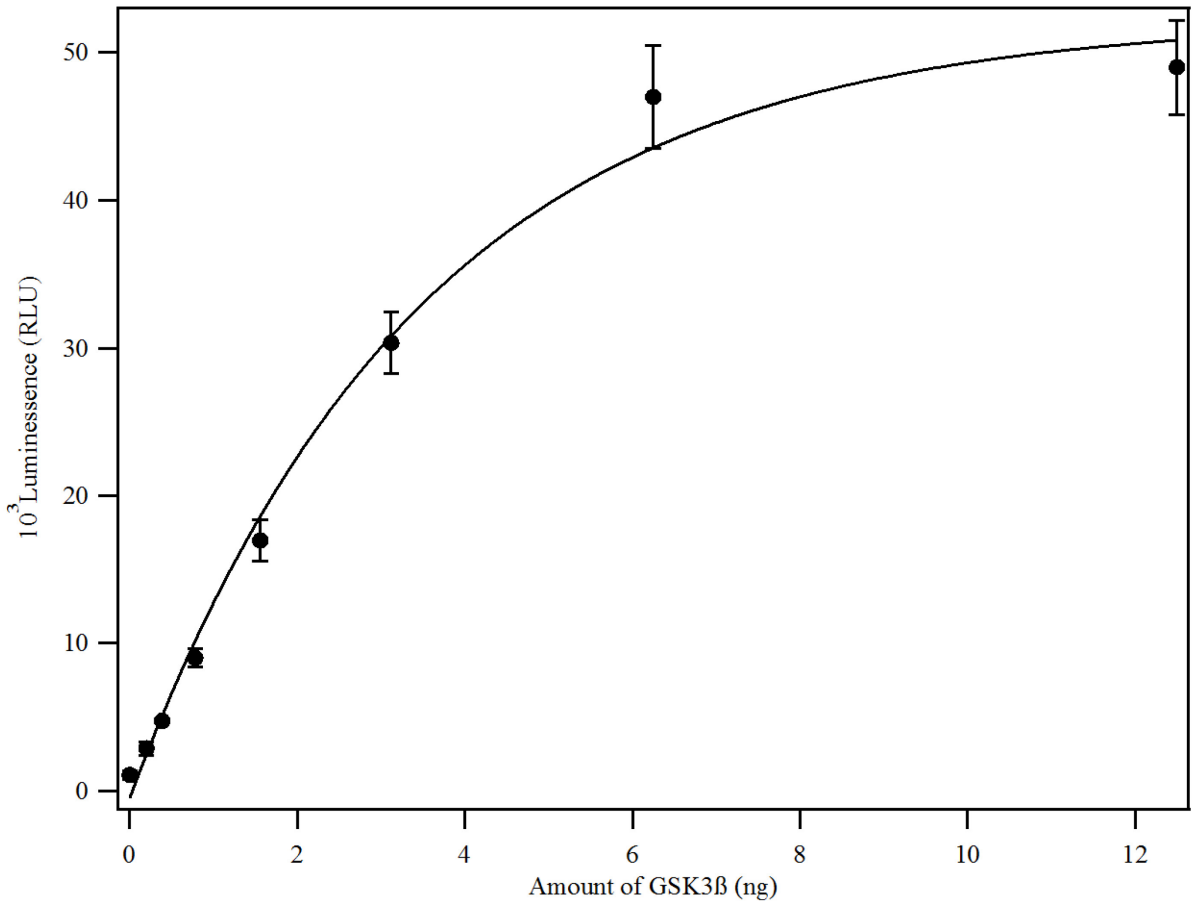

Figure 1.8: Correlation graph of the luminescence with amount of GSK3β.

It can be seen from the Figure 1.8 that luminescence values are linearly correlate with the amount of enzyme up to 3.12 ng and then mostly behave as a plateau. The middle point of the linear curve represents a luminescence value of about 15,000 (RLU) and it is relatively close to the 1 ng of enzyme. Therefore, 1 ng of enzyme was chosen as the optimal enzyme to be used in the assay.

Upon finding out the optimum enzyme concentration, next was found the best reaction time. For that 2 µL of enzyme (1 ng) was mixed with 2 µL of substrate/ATP mixed prepared same as for the kinase activity determination experiment and incubated at different time intervals such as 1, 15, 30, 45, and 60 minutes and then followed the same procedure applied to the kinase activity determination experiment. Figure 1.9 displays the correlation of luminescence with different incubation times of GSK3β enzyme.

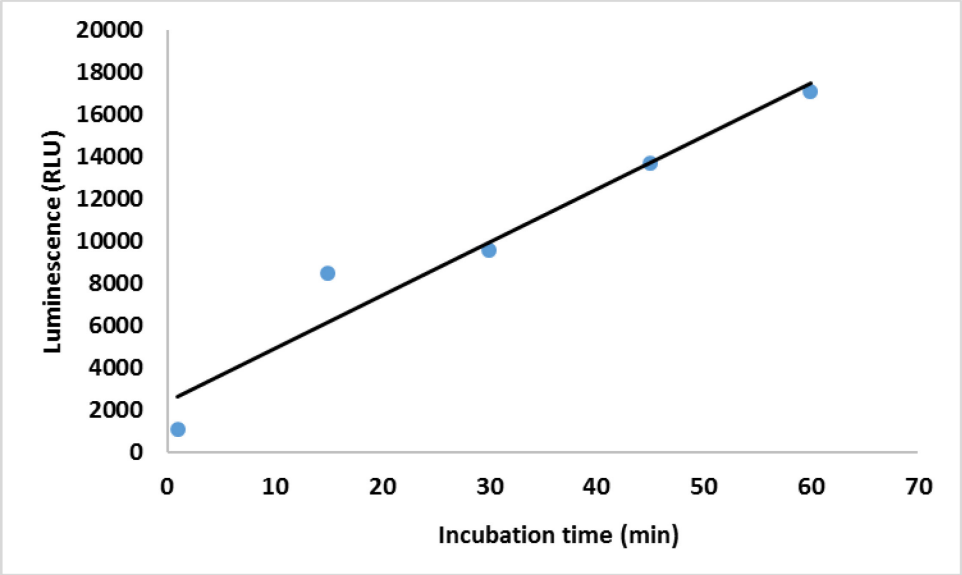

Figure 1.9: Correlation graph of the luminescence with varying incubation times of the kinase reaction.

Since 60 minutes incubation time has given the highest luminescence value it was chosen as the optimal incubation time to carry out the kinase assay.

1.3.3.2 Inhibition of GSK3β kinase activity by staurosporine

In order to validate the assay conditions, a known GSK3β enzyme inhibitor, staurosporine was used as a positive control and was analyzed for its GSK3β inhibitory activity prior to analyzing the quinoline compounds. The experiment was carried out as per the protocol supplied by Promega and as explained in section *1.5.2* of this chapter. Figure 1.10 shows the results of enzyme inhibition activities of staurosporine. The literature reported IC_{50} value of GSK3β inhibition by staurosporine was 15 nM.[43] However, it was obtained a IC_{50} value of 23 nM from the experiment.

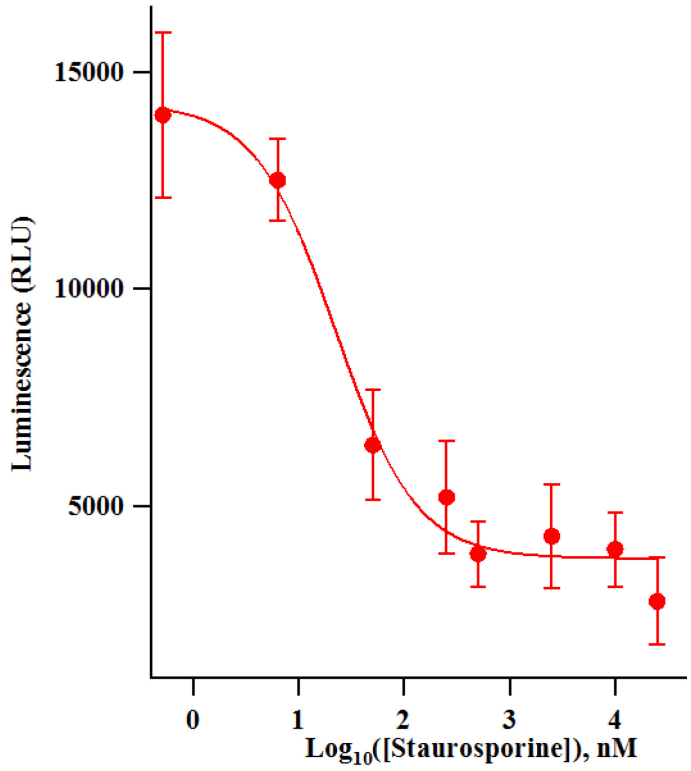

Figure 1.10: GSK3β enzyme inhibition curve for staurosporine.

1.3.3.3 GSK3β enzyme inhibition activities of synthesized quinoline compounds

The detailed procedure for GSK3β enzyme inhibition evaluation for selected quinoline compounds are listed on the experimental section of this chapter. Table 1.4 and Figures 1.11 and 1.12 display the results obtained for GSK3β assay for those compounds.

Table 1.4: Enzyme inhibition activities of synthesized quinoline compounds on GSK3β assay.[37]

Compound	GSK3β Inhibition
PQ1	> 1 mM
PQ7	> 1 mM
2 (PQ19)	35 ± 6.36 nM
3	> 1 mM
7	> 1 mM
9 (GS37)	158 ± 19.1 nM

As shown in Table 1.4, compound **2** and **9** exhibit strong GSK3β enzyme inhibition with values of 35 ± 6.36 and 158 ± 19.1 nM respectively. It suggests that compounds **2** and **9** may protect the neuronal cells by inhibiting GSK3β enzyme. This in turn proves from the observed low EC_{50} values for compounds **2** and **9** (0.12 μM and 0.3 μM respectively) from MC65 cell protection assay. However, **PQ1**, **PQ7**, compounds **3** and **7** do not seem to inhibit GSK3β enzyme suggests that, they may protect the neuronal cells through different mechanism of action. The detailed

discussion of the structure activity relationship with the observed bioactivities on these compounds will be discussed later.

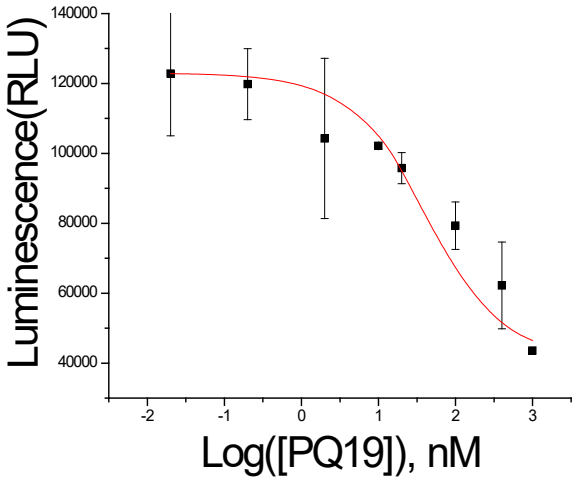

Figure 1.11: Graph of luminescence vs $\log_{10}$[concentration of PQ19] on GSK3β assay. Data points are the average of three determinations, and error bars are ± S.D.

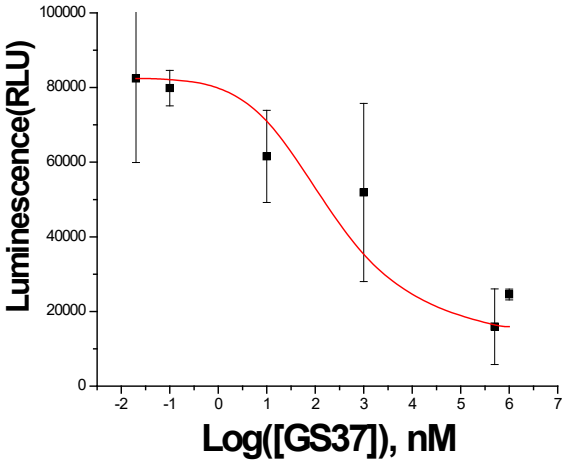

Figure 1.12: Graph of luminescence vs $\log_{10}$ [concentration of GS37] on GSK3β assay. Data points are the average of three determinations, and error bars are ± S.D.

1.3.4 Evaluation of the PKC inhibition by synthesized quinoline compounds using PepTag® non-radioactive PKC assay

PKC inhibition by substituted quinoline compounds were evaluated using the PepTag® non-radioactive PKC assay kit (catalog # V5330) purchased from Promega and PKC inhibition studies were carried out following the protocol published by Promega (technical bulletin #132) with few modifications.[44]

PepTag® non-radioactive protein kinase C assay kit consists of the following: PepTag® C1 peptide (0.4 µg/µL in water) conjugated to a fluorescent dye molecule; PKC enzyme (25 µg/mL) with 20 mM tris(hydroxymethyl)aminomethane hydrochloride ($C(CH_2OH)_3NH_2$. HCl; Tris-HCl), pH 7.4, 2 mM ethylenediaminetetraacetic acid (EDTA), 1 mM DTT, 10 mM K_3PO_4, 0.05 % Triton® X-100 and 50 % glycerol; PepTag® PKC reaction buffer (pH 7.4) having 100 mM 4-(2-hydroxyethyl)-1-piperazineethanesulfonic acid (HEPES), 6.5 mM $CaCl_2$, 5 mM dithiothreitol (DTT), 50 mM $MgCl_2$, and 5 mM adenosine triphosphate (ATP); gel solubilization solution; PKC activator solution having 1 mg/mL of phosphatidylserine (PS) in water; and peptide protection solution.[44]

C1 peptide substrate of the PepTag® assay kit consists of eleven amino acid residues (amino acids sequence of C1 peptide: proline – leucine – serine – arginine – threonine – leucine – serine – valine

– alanine – alanine – lysine) and it is attached to a dye molecule which imparts a bright pink fluorescence to the C1 peptide (Figure 1:13).

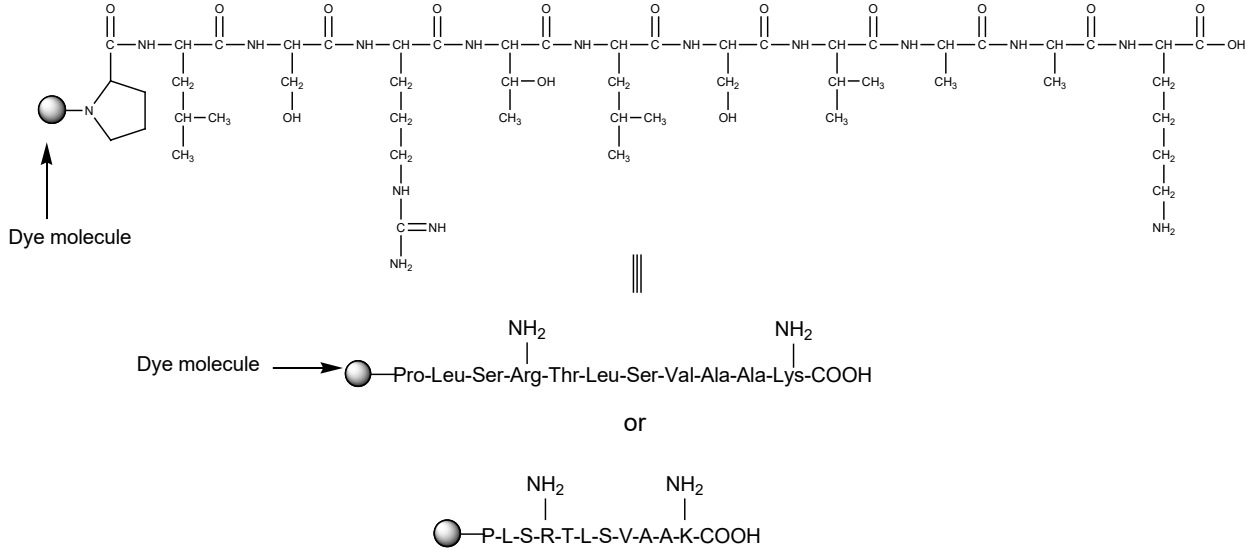

Figure 1.13: Amino acid sequence of C1 peptide substrate.

The PKC assay is performed at pH = 7.4, in which C1 peptide exists in its nonphosphorylated form with a net +1 charge. When the PKC enzyme is phosphorylated by its substrate, it changes from net +1 charge to net -1 charge as illustrated in Figure 1.14. During the phosphorylation, only Ser -7 residue is phosphorylated whereas Ser-3 and Thr-5 will not be phosphorylated due to steric hindrance. The phosphorylated and nonphosphorylated C1 peptides are then separated using agarose gel electrophoresis (Figure 1.14). During the electrophoresis the nonphosphorylated peptide (positively charged) moves towards the negatively charged anode whereas the phosphorylated peptide (negatively charged) moves toward the positively charged cathode and will be separated as shown in Figure 1.14.[44] The phosphorylated and nonphosphorylated bands were visualized under UV light and the fluorescence intensities (pixel intensities) of the bands were quantified using Kodak Gel Logic 1500 Digital Imaging System and Imagequant 5.2 software; in Dr. Govindsamy Vediyappan laboratory, in the Department of Biology, Kansas State

University. The percentage phosphorylation of the C1 peptide was quantified by means of the ratio of the phosphorylated band intensity to the sum of the phosphorylated and nonphosphorylated band intensities obtained from the Kodak Gel Logic 1500 Digital Imaging System and Imagequant 5.2 software. Since this assay is a non-radioactive, it is more convenient than that of radioactive

assays that are used to determine the enzyme activity by measuring the transfer of radioactive phosphate ($^{32}PO_4^{2-}$) group from the enzyme to the substrate peptides or proteins.

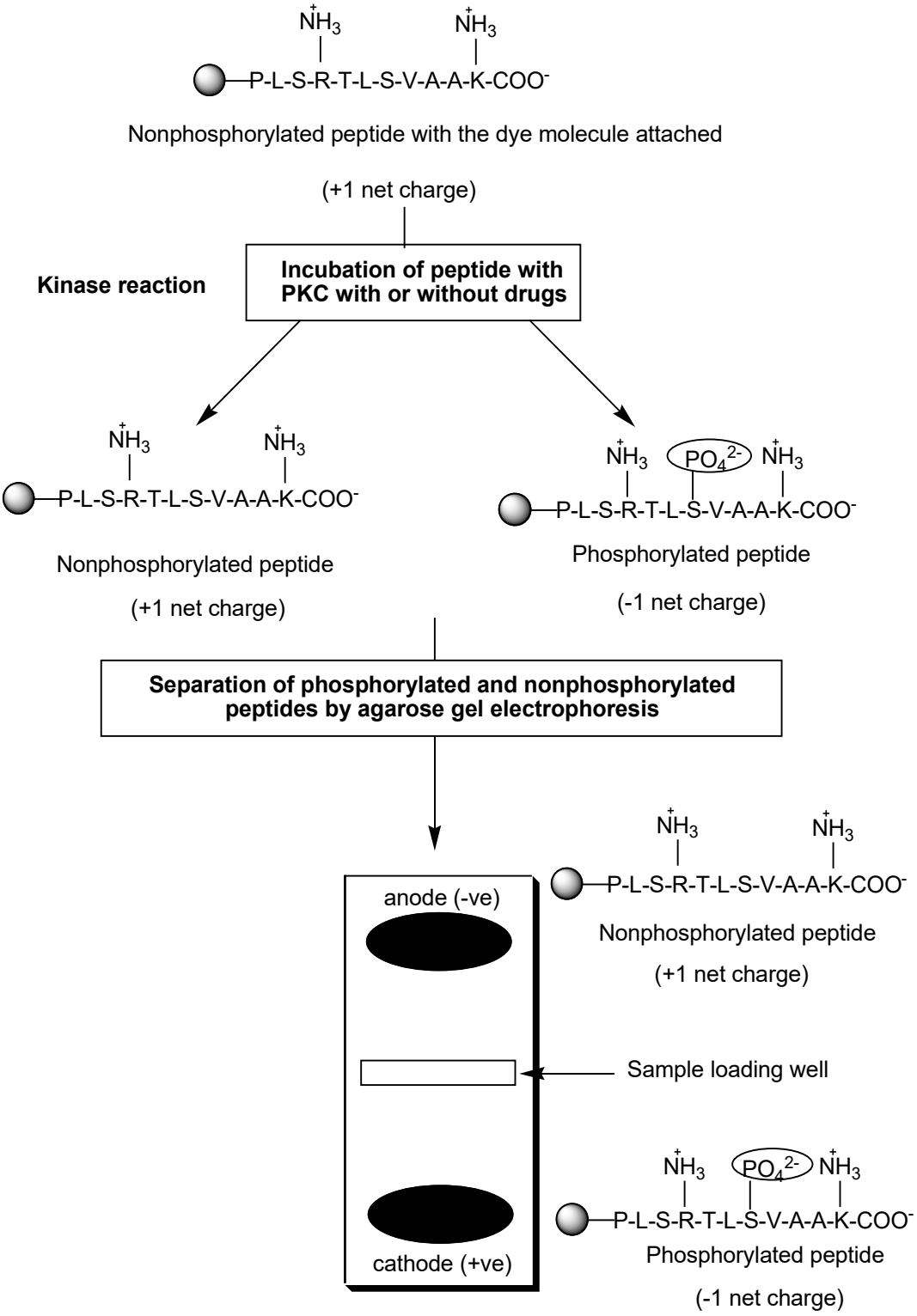

Figure 1.14: Schematic representation of the phosphorylation of C1 peptide by PKC and the separation of phosphorylated and nonphosphorylated C1 peptides by agarose gel electrophoresis.

1.3.4.1 Correlation of peptide phosphorylation with different concentrations of PKC

Table 1.5 and Figures 1.15 and 1.16 indicate the results of percentage phosphorylation of C1 peptide with different amounts of PKC (0, 5, 15, 20, 30, and 40 ng) as determined by photoimaging analysis.

Table 1.5: Percentages phosphorylation of C1 peptide with different amounts of PKC (0, 5, 15, 20, 30, and 40 ng) determined by photo imaging analysis.

Amount of PKC (ng)	Volume (Pixel Intensity)		A+B (Intensity due to 0.8 µg of C1 peptide)	Corrected amount of peptide phosphorylated (A', µg) (0.8× A/(A+B)	% Peptide phosphorylation (A' × 100/ 0.8) %
	Phosphorylated peptide (A)	Non phosphorylated peptide (B)			
0	0	129513	129513	0	0
5	17595	133628	151223	0.093	11.63
15	80358	148940	229298	0.280	35
20	91876	134506	226382	0.325	40.58
30	110573	104745	215318	0.411	51.35
40	140443	94755	235198	0.478	60

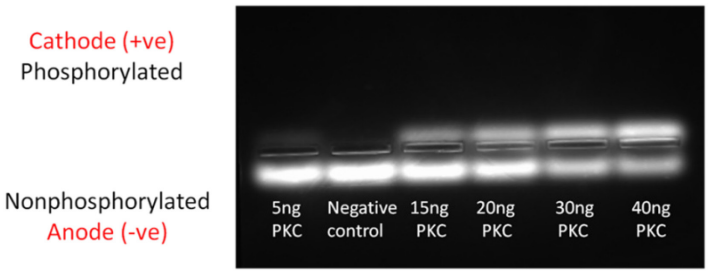

Figure 1.15: Gel image of C1 peptide phosphorylation with various amounts of PKC.

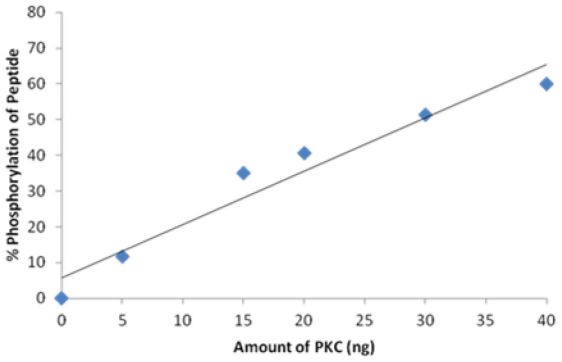

Figure 1.16: Correlation graph of % phosphorylation of C1 peptide with various amounts of PKC (ng).

A correlation graph from the percentages of phosphorylation of C1 peptide and varying amounts of PKC enzyme was established using photo imaging analyses prior to the analysis of the quinoline compounds. As shown in Figure 1.16, phosphorylation of the substrate peptide increased linearly with the increased amount of PKC enzyme with the range of 0 – 40 ng. Negative control represents the experiment with 0 ng PKC enzyme. The amount of PKC required to phosphorylate 50% of the C1 peptide was found to be 30 ng from photo-imaging analysis (Table 1.5). PKC inhibition studies

of the quinoline compounds were carried out using 15 ng of PKC enzyme which produces about 35% of C1 peptide phosphorylation.

1.3.4.2 Inhibition of PKC phosphorylation by synthesized quinoline compounds

Inhibition of PKC phosphorylation was assessed for compounds **2**, **3**, **7** and **9**. Compounds **PQ1** and **PQ7** were analyzed by Dr. Keshar Prasain in Dr. Hua's laboratory. Previously reported PKC inhibitor, staurosporine was used as the positive control to study the assay conditions and to examine whether it produced a similar range of IC_{50} value as that of reported value.

The PKC assay was performed according to the protocol published by Promega and detailed description about the experimental procedures are mentioned in experimental section of this chapter.

Figures 1.17, and 1.18 demonstrate the results for the staurosporine obtained from PKC assay.

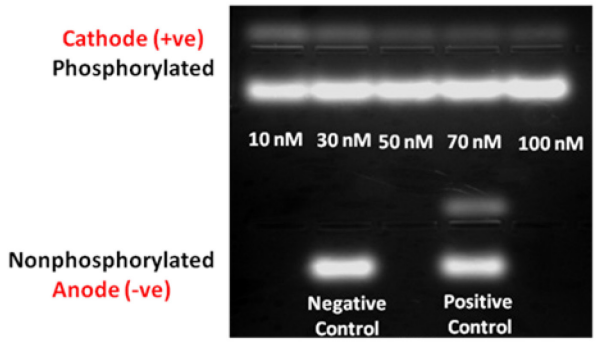

Figure 1.17: Gel images of C1 peptide phosphorylation with different concentrations of staurosporine.

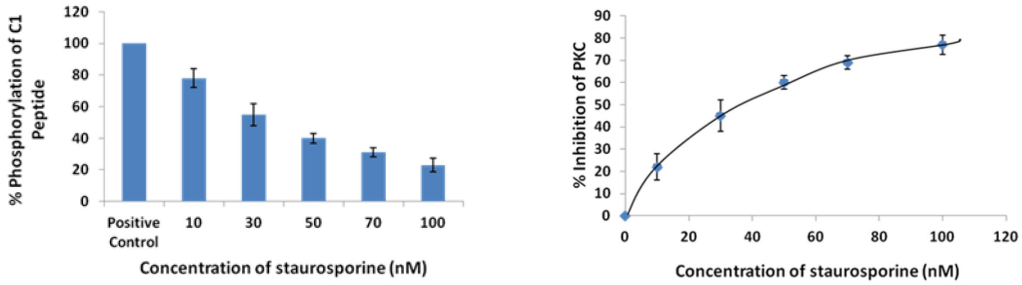

Figure 1.18: Correlation graphs for % phosphorylation of C1 peptide (left) and % inhibition of C1 peptide (right) with different concentrations of staurosporine. The graphs are provided with (±) standard errors (± 2 - ± 8) obtained from three separate experiments.

As shown in Figure 1.17, staurosporine seems to behave as a potent PKC inhibitor. The phosphorylated peptide band was appeared to be very faint with different concentrations of staurosporine suggesting that it strongly inhibited the PKC enzyme. The IC_{50} value for the inhibition of PKC phosphorylation by staurosporine was found to be 33 nM and an IC_{50} value of

22 nM has been previously reported.[45] These two values are nearly close, hence the PKC assay conditions of the experiment can be assumed to be behaved properly.

After studying the assay parameters, quinoline compounds **2**, **3**, **7** and **9** was studied for the PKC inhibition.

Figures 1.19 and 1.20 demonstrate the results for the PKC inhibition by quinoline compound **2** (**PQ19**).

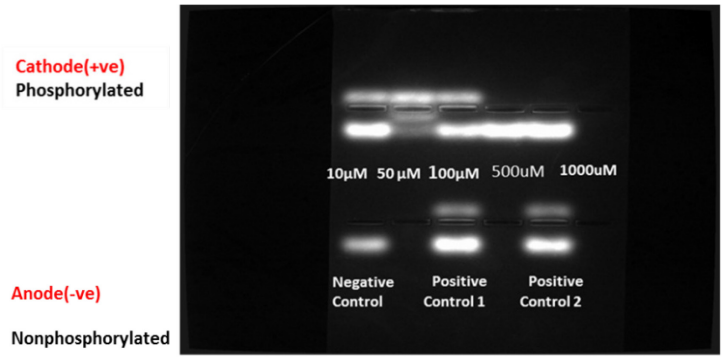

Figure 1.19: Gel image of C1 peptide phosphorylation with different concentrations of compound 2 (PQ19).

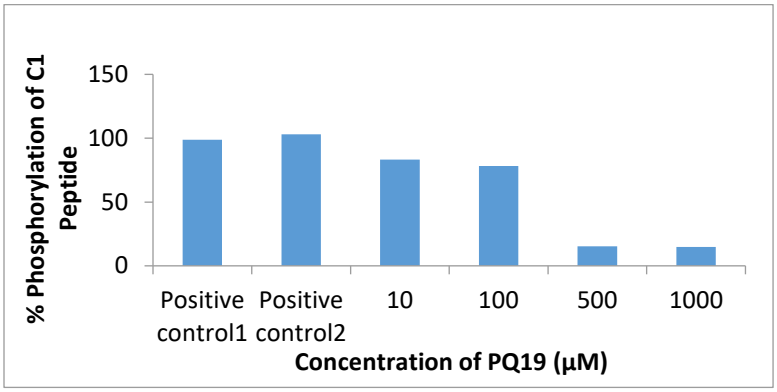

Figure 1.20: Correlation graph of % phosphorylation of C1 peptide with different concentrations of compound 2 (PQ19).

Nano-molar concentrations of compound **2** was chosen for the initial screening. However, it did not result any inhibition of PKC phosphorylation up to 1,000 nM concentration. Therefore, micro molar concentrations were chosen. From the data on Figures 1.19 and 1.20, it can be concluded that compound **2** (**PQ19**) did not behave as a potent PKC inhibitor. However, it was the most potent compound from MC65 cell protection assay, and has a very good GSK3β enzyme inhibition. The resulted higher IC_{50} value (240 ± 21.2 μM) of compound **2** (**PQ19**) indicates that it is not selective for PKC enzyme. This in turn proves that compound **2** may be a selective inhibitor for GSK3β. However, in order to make a clear decision, compound must be tested with other kinases such as CDK1, CDK2, CDK5 as well.

Figures 1.21 and 1.22 demonstrate the results for the PKC inhibition by quinoline compound **3** (**PQ15**).

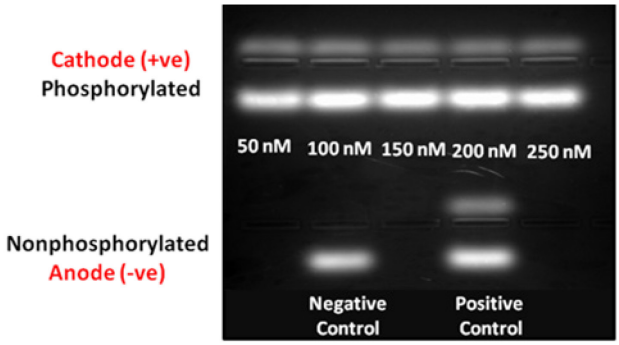

Figure 1.21: Gel image of C1 peptide phosphorylation with different concentrations of compound 3 (PQ15).

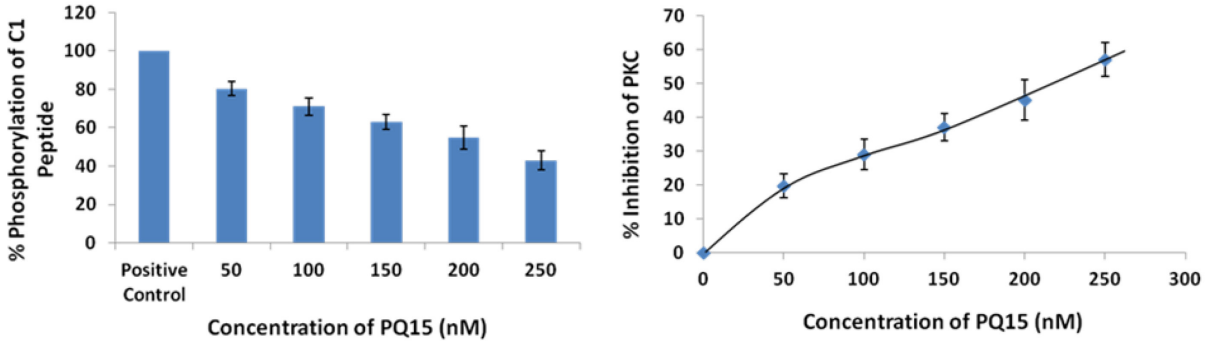

Figure 1.22: Correlation graphs for % phosphorylation of C1 peptide (left) and % inhibition of C1 peptide (right) with different concentrations of compound 3 (PQ15). The graphs are provided with (±) standard errors (± 4 - ± 8) obtained from three separate experiments.

As shown in Figures 1.21 and 1.22, the IC_{50} value for the inhibition of PKC phosphorylation by compound **3** (**PQ15**) was found to be 216.3 nM. Though, it is not a very potent PKC inhibitor, the

nanomolar concentration of IC_{50} value suggests that it can also inhibit PKC phosphorylation somewhat strongly compared to compound **2**.

Figures 1.23 and 1.24 demonstrate the results for the PKC inhibition by quinoline compound **7** (**PQ25**).

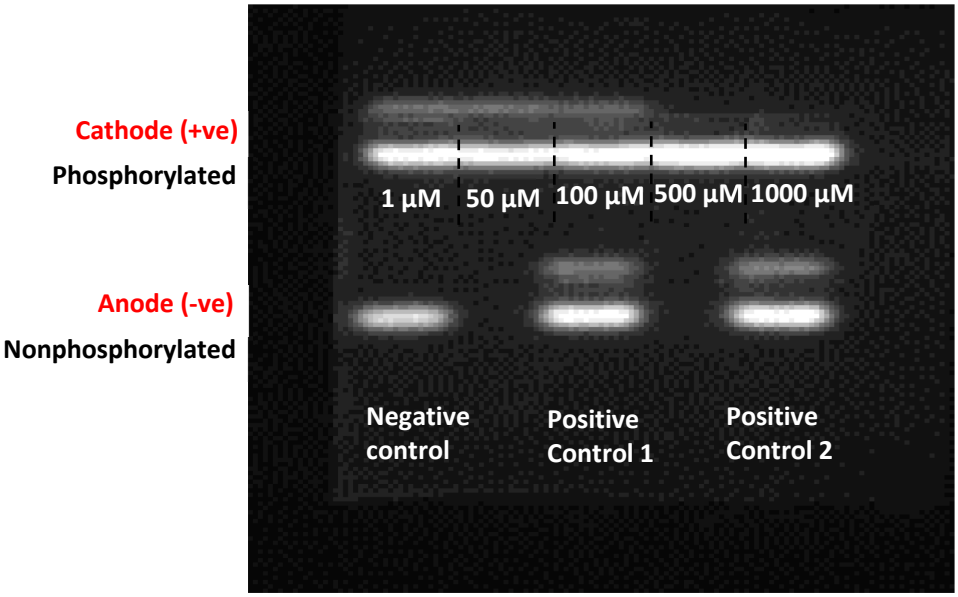

Figure 1.23: Gel image of C1 peptide phosphorylation with different concentrations of compound 7 (PQ25).

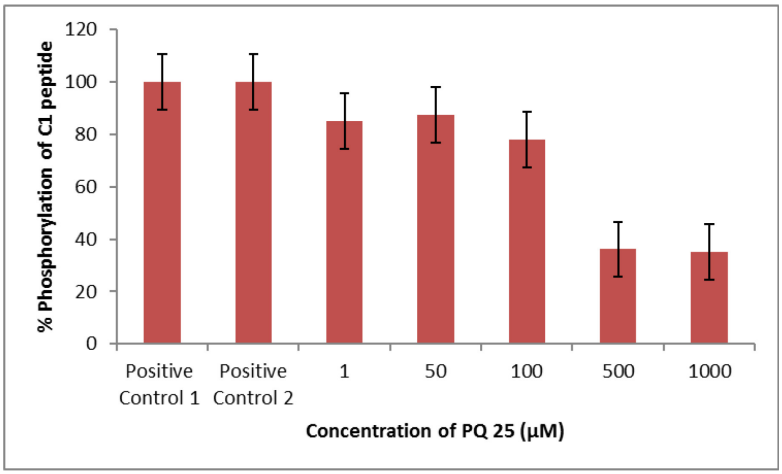

Figure 1.24: Correlation graph of % phosphorylation of C1 peptide with different concentrations of compound 7 (PQ25).

Figures 1.25 and 1.26 demonstrate the results for the PKC inhibition by quinoline compound **9** (**GS37**).

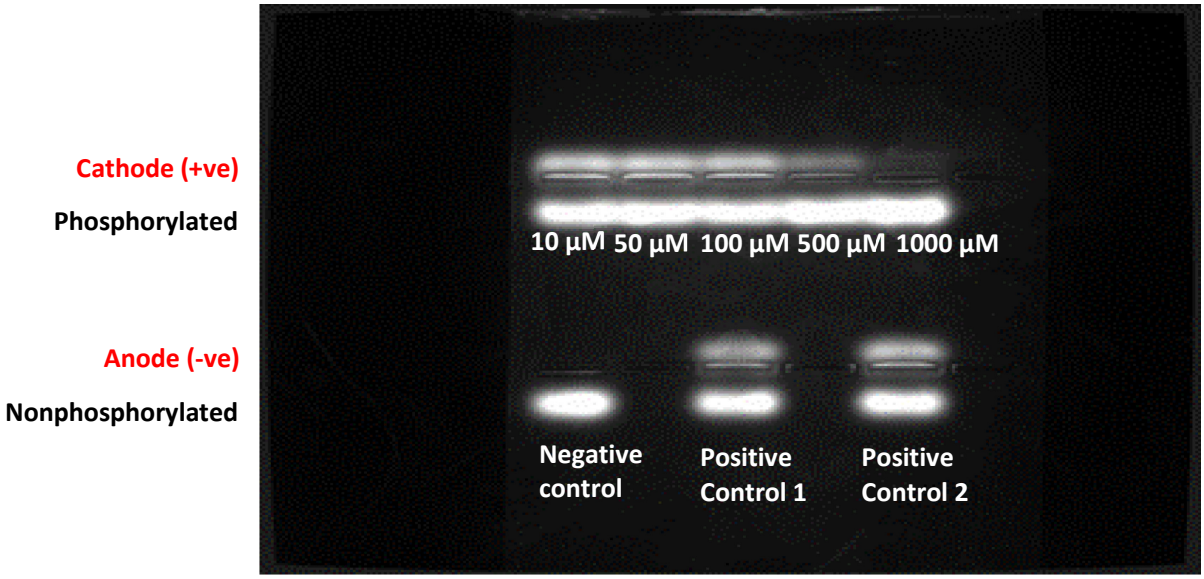

Figure 1.25: Gel image of C1 peptide phosphorylation with different concentrations of compound 9 (GS37).

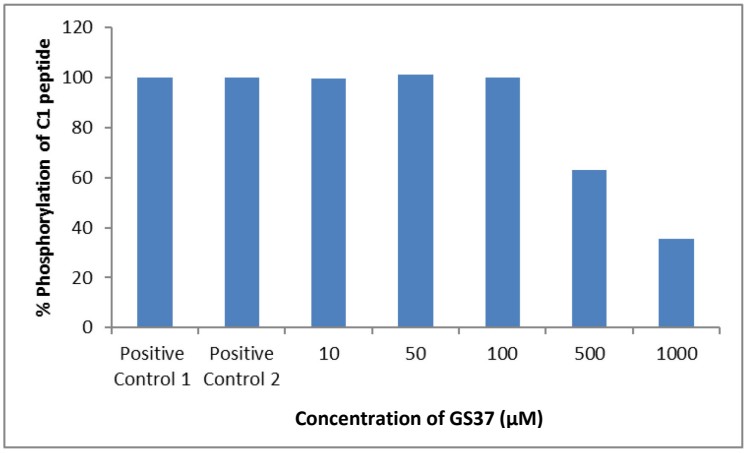

Figure 1.26: Correlation graph of % phosphorylation of C1 peptide with different concentrations of compound 9 (GS37).

According to the results shown above, both compounds **7** and **9** do not show good inhibition against PKC enzyme. However, compound **9** was found as a strong GSK3β inhibitor. Therefore, compound **9** is a selective inhibitor for GSK3β and a weak inhibitor for PKC.

Table 1.6: Summary of the results of the PKC inhibition activities and GSK3β activities of the synthesized quinoline compounds.[37]

Compound	PKC inhibition	GSK3β inhibition
PQ1	35 ± 8 nM	> 1 mM
PQ7	42.3 nM	> 1 mM
2 (PQ19)	240 ± 21.2 μM	35 ± 6.36 nM
3 (PQ15)	216.3 nM	> 1 mM
7 (PQ25)	400 ± 13.7 μM	> 1 mM
9 (GS37)	750 ± 9.3 μM	158 ± 19.1 nM

From the data summarized in Table 1.3, a structure activity relationship (SAR) could be derived and it will be helpful for the development of more potent and less toxic compounds for the AD therapy in future.

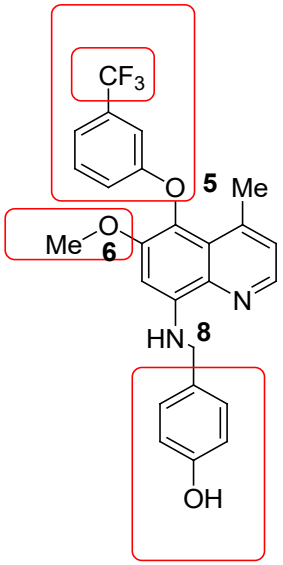

Figure 1.27: Important functionalities for the overall activity of quinoline compounds.

The replacement of the trifluoromethyl (CF_3) group on the 5-aryloxy ring might not be a good idea as the newly designed compounds **10**, **11** and **12** did not show better cell protection activities. In addition, **PQ1** seems to be a better inhibitor for PKC instead of GSK3β enzyme.

Among all the compounds tested, compound **2** (**PQ19**) shows the highest cell protection activity (EC_{50} = 120 ± 10 nM) and the GSK3β inhibition activity. By comparing the structures **1** and **2**, the only difference present is the group which is attached to 8- amino group. The changes made on the 8-amino group seem not good as when the 4-hydroxybenzyl group is replaced with other moieties, the cell protection capability of the molecule seem to be lost. In addition, 5-aryloxy group also seem to be important for the better cell protection activities of these molecules. Both compounds **2** and **9** inhibits the GSK3β enzyme suggests that the replacement of the methoxy group with

hydroxyl group does not alter the SAR. However, by looking at the PKC and GSK3β inhibition results, it can be seen that there's no clear relationship on the inhibitory activities of these molecules. For example, **PQ1**, **PQ7** and **PQ15** seem to have better inhibition against PKC, but they are almost not capable to inhibit GSK3β enzyme. Moreover, compound **2** and **9** were found to be strong GSK3β inhibitors, but they are not behaving as PKC inhibitors. This suggests that these molecules have separate mechanism of action towards these two enzymes. In summary it can be concluded that 3-trifluoromethylphenoxyl at 5- position, methoxyl at 6- position and 4-hydroxybenzyl at 8-amino position are all important features to the overall activities of the designed quinoline compounds.

1.3.5 Future perspectives

In our initial efforts on identifying a new set of substituted quinolines as novel GSK3β inhibitors, compounds **PQ1** (EC_{50} = 0.15 ± 0.20 μM, TD_{50} = 2.09 ± 0.02 μM) and **2** (EC_{50} = 0.12 ± 0.01 μM, TD_{50} = 1.38 ± 0.08 μM) were chosen as the lead compounds to design a new set of molecules. If we further expand this project to discover more potent as well as less toxic GSK3β inhibitors, it can be seen that compound **7** also a good candidate to generate novel analogues as GSK3β inhibitors due to its strong MC65 cell protection activities (EC_{50} = 0.19 ± 0.02 μM) along with a very low toxicity profile (TD_{50} = > 50 μM). Therefore, following analogues derived from compound **7** are proposed herein as a future approach of this project.

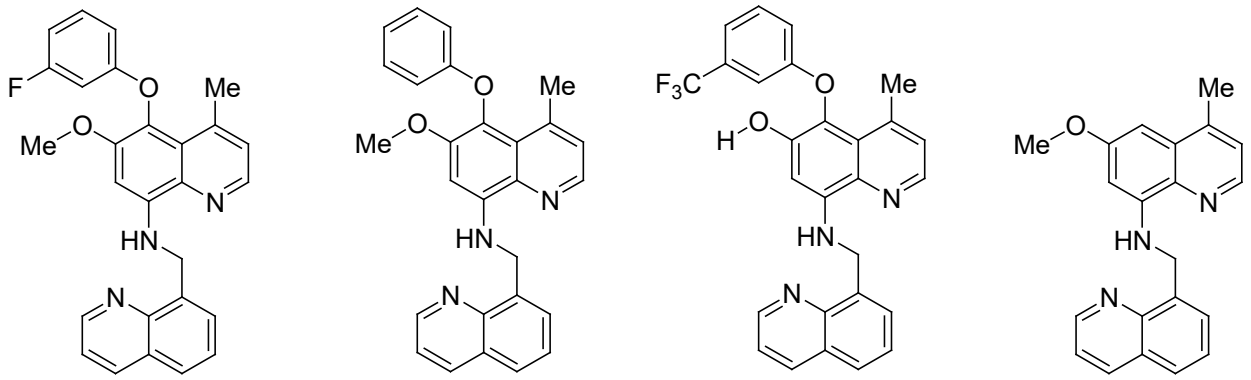

Figure 1.28: Analogues of compound 7 to be prepared in future.

1.4 Conclusion

A library of substituted quinoline compounds were designed, synthesized and evaluated to study their inhibitory activities towards GSK3β enzyme and PKC phosphorylation. Synthesized quinoline compounds **2** and **3** showed strong MC65 cell protection activities. Except compounds **5**, **8**, and **12**, the rest of the compounds too displayed low micro molar efficacies towards neuronal cell protection. Synthesized quinolines, which showed higher potency towards MC65 cell assays were further evaluated to test the selectivity and inhibitory activities towards GSK3β and PKC enzymes. Compounds **2** and **9** were found to be strong inhibitors towards GSK3β enzyme with IC_{50} values of 35 ± 6.36 nM and 158 ± 19.1 nM, respectively. In addition, these two compounds only showed weak inhibitory activities towards PKC enzymes, suggesting they are selective GSK3β inhibitors. From the PKC assay, it was found that **PQ1**, **PQ7** and compound **3** showed better inhibitory activities in nanomolar range towards PKC enzyme. Moreover, they are not GSK3β inhibitors. SAR studies revealed that the importance of having 3-trifluoromethylphenoxyl at C5- position, methoxyl at C6- position and 4-hydroxybenzyl at 8-amino position for the better

inhibitory activities of the quinoline compounds towards GSK3β inhibition. In future, the potent compounds can be further evaluated for their specificities towards other enzymes such as CDK1, CDK2, etc. and can be tested in animal models to study whether they can reduce the level of hyperphosphorylated tau or neurofibrillary tangles and thereby lead to develop new AD drug candidates.

1.5 Experimental Section

The structures, and syntheses of compounds described in this section have been reported recently.[37] (Syntheses, neural protective activities, and inhibition of glycogen synthase kinase-3β of substituted quinolines. Jianyu Lu, Izumi Maezawa, Sahani Weerasekara, Ramazan Erenler, Tuyen D. T. Nguyen, James Nguyen, Luxi Z. Swisher, Jun Li, Lee-Way Jin, Alok Ranjan, Sanjay K. Srivastava, and Duy H. Hua. *Bioorganic and Medicinal Chemistry Letters* 24, **2014**, 3392-3397. Copyright (2014), Elsevier.

1.5.1 General Methods

Nuclear magnetic resonance (NMR) spectra were recorded on a Varian Unity plus 400 MHz or 200 MHz spectrometer for ^{1}H and ^{13}C in deuterated chloroform ($CDCl_3$), unless otherwise indicated. Tetramethylsilane was used as the internal reference and the data reported in ppm. Low-resolution mass spectra were taken from an API 2000-triple quadrupole ESI-MS/MS mass spectrometer (from Applied Biosystems). Tetrahydrofuran (THF) and diethyl ether were dried and distilled over sodium and benzophenone. Methylene chloride was dried and distilled over calcium hydride (CaH_2). Chemicals were purchased from Fisher Scientific Co., Aldrich Chemical Co.,

Chem-Impex International, and VWR. Melting points were tested on Thomas Hoover capillary melting point apparatus.

4-Acetamino-5-nitro-2-(3-fluorophenyloxy) anisole (**20**)

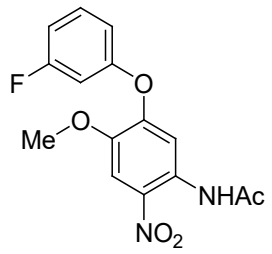

20

3-fluorophenol (300.0 mg, 2.678 mmol) and potassium t-butoxide (300.5 mg, 2.678 mmol) was dissolved in 10 mL dry t-butanol (distilled over sodium) and was stirred at 25 ºC for 12 hours under argon atmosphere. Then, this mixture was concentrated and vacuum dried to obtain potassium 3-fluorophenolate (**17**) as a yellow solid. The 3-fluorophenolate (**17**) was dissolved in 4 mL dry DMF (distilled over calcium hydride) and was added into *N*-(5-bromo-4-methoxy-2-nitrophenyl) acetamide (**15**) (722.5 mg, 2.500 mmol) in 4 mL dry DMF at 60 ºC under argon. This solution was stirred at 120 ºC for 24 hours. The cooled solution was poured into ice-water with vigorous stirring. The solid precipitated was collected by filtration and recrystallized using ethanol to give 520.5 mg (65% yield) of compound **20** as a light yellow solid. Melting point: 125 – 126 ºC; ^{1}H NMR δ 10.46 (s, 1H, NH), 8.37 (s, 1H), 7.78 (s, 1H), 7.37 (td, J = 8.4, 6.4 Hz, 1H), 6.94 (td, J = 7.6, 2.4 Hz, 1H), 6.89 (dd, J = 8.0, 2.0 Hz, 1H), 6.81 (dt, J = 9.6, 2.4 Hz, 1H), 3.95 (s, 3H, OMe), 2.23 (s, 3H, Me); ^{13}C NMR δ 169.2 (C=O), 164.7 (d, $^{1}J_{CF}$ = 247 Hz, CF), 156.2 (d, $^{3}J_{CF}$ = 11 Hz), 152.9, 145.7, 131.141 (d, $^{3}J_{CF}$ = 10 Hz), 131.137, 115.4 (d, $^{4}J_{CF}$ = 3.6 Hz), 112.3 (d, $^{2}J_{CF}$

= 21 Hz), 110.7, 108.7, 107.8, 107.5, 56.7 (OMe), 25.8 (Me); MS (electrospray), m/z 343.3 $(M+Na)^+$.

4-Acetamino-5-nitro-2-phenyloxyanisole (**21**)

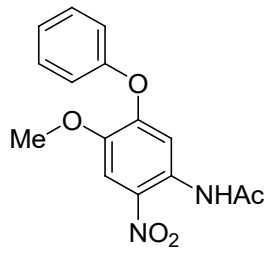

21

Compound **21** was prepared following the same procedure used for synthesizing compound **20**. Potassium phenolate (**18**) was synthesized from the reaction of phenol (360 mg, 3.825 mmol) with potassium t-butoxide (429.3 mg, 3.825 mmol). The reaction of the potassium phenolate (**18**) with compound **15** (982 mg, 3.400 mmol) gave 821 mg (yield 80%) of compound **21** as yellow solid. Melting point: 124 – 126 ºC; ^{1}H NMR δ 10.46 (s, 1H, NH), 8.25 (s, 1H), 7.80 (s, 1H), 7.49 - 7.39 (m, 2H), 7.29 - 7.22 (m, 1H), 7.12 - 7.09 (m, 2H), 3.96 (s, 3H, OMe), 2.23 (s, 3H, Me); ^{13}C NMR

δ 169.2, 154.7, 154.3, 145.4, 131.4, 130.4, 125.8, 120.4, 109.20, 109.18, 108.48, 108.47, 56.7 (OMe), 25.7 (Me); MS (electrospray), m/z 325.3 $(M+Na)^+$.

4-Amino-5-nitro-2-(3-fluorophenyloxy) anisole (**23**)

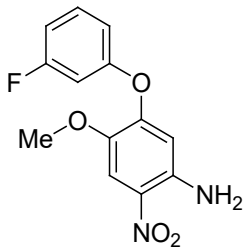

23

A solution of compound **20** (310.0 mg, 0.968 mmol) in 35 mL of conc. HCl and ethanol (1:7) was stirred under reflux for 2 hours. After 2 hours, the reaction was cooled to room temperature and was poured onto ice-water mixture, and stirred for 30 minutes. The resulted solid was collected by filtration, washed with water, and vacuum dried to give 240 mg of **23** (95 %, yield) as orange solid which is sufficiently pure for carried out in the next step. Melting point: 120 - 121°C; ^{1}H NMR δ 7.70 (s, 1 H), 7.34 (td, J = 8.4, 6.4 Hz, 1H), 6.92 (td, J = 7.6, 2.4 Hz, 1H), 6.87 (dd, J = 8.0, 2.0 Hz, 1H), 6.81 (dt, J = 9.6, 2.4 Hz, 1H), 6.13 (s, 1H), 5.96 (s, 2H, NH_2), 3.90 (s, 3H, OMe); ^{13}C NMR δ 163.6 (d, $^1J_{CF}$ = 247 Hz, CF), 156.2 (d, $^3J_{CF}$ = 10 Hz), 154.4, 142.2, 141.9, 131.1 (d, $^3J_{CF}$ = 10

Hz), 126.7, 115.7 (d, $^4J_{CF}$ = 3 Hz), 112.2 (d, $^2J_{CF}$ = 20.6 Hz), 108.3, 107.9 (d, $^2J_{CF}$ = 24 Hz), 106.1, 56.6 (OMe); MS (electrospray), m/z 279.2 $(M+H)^+$.

4-Amino-5-nitro-2-phenyloxyanisole (**24**)

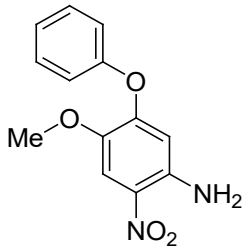

24

Compound **24** was prepared via the same procedure as that of compound **23**. Deprotection of compound **21** (260.0 mg, 0.839 mmol) gave 214 mg (98 % yield) of **24** as yellow solid. Melting point: 162 – 163 ºC; ^{1}H NMR δ 7.65 (s, 1H), 7.44 - 7.40 (m, 2H), 7.27 - 7.23 (m, 1H), 7.12 - 7.09 (m, 2H), 6.01 (s, 1H), 6.10 – 5.3 (bs, 2 H, NH2), 3.92 (s, 3H, OMe); ^{13}C NMR δ 155.8, 154.7, 142.1, 142.0, 130.4, 125.6, 120.8, 108.0, 104.6, 56.6 (OMe); MS (electrospray), m/z 261.2 $(M+H)^+$.

6-Methoxy-4-methyl-8-nitro-5-(3-fluorophenyloxy)quinoline (**26**)

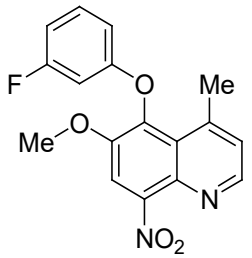

26

A mixture of compound **23** (240.0 mg, 0.863 mmol) and H_3AsO_4 (395.2 mg; 1.736 mmol) in 3 mL 85% H_3PO_4 was heated to 120 ºC. Methyl vinyl ketone (90.8 mg; 1.290 mmol) was added

dropwise into this mixture and stirred for 30 minutes. The dark solution was quickly poured onto ice-water solution and was basified to pH = ~ 10 with 2N NaOH, extracted 3 times with methylene chloride. The combined organic layers were washed with water, brine, dried ($MgSO_4$), concentrated, and column chromatographed on silica gel using a mixture of hexane and ethyl acetate (2:1) as the eluent to give 99 mg (35% yield) of compound **26** as brown solid. Melting point: 167 – 169 ºC; ^{1}H NMR δ 8.76 (d, J = 4.3 Hz, 1H), 7.88 (s, 1H), 7.28 - 7.21, (m, 2H), 6.78 (td, J = 2.4, 0.16 Hz, 1H), 6.76 - 6.56 (m, 2H), 3.89 (s, 3H, OMe), 2.73 (s, 3H, Me); ^{13}C NMR δ 163.9 (d, $^1J_{CF}$ = 246 Hz, CF), 159.1 (d, $^3J_{CF}$ =10 Hz), 150.9, 148.4, 146.9, 143.9, 140.1, 136.2, 130.8 (d, $^3J_{CF}$ = 10 Hz), 125.9, 125.3, 111.9, 110.9 (d, $^4J_{CF}$ = 3 Hz), 109.7 (d, $^2J_{CF}$ = 21 Hz), 103.3 (d, $^2J_{CF}$ = 25 Hz), 57.4 (OMe), 23.4 (Me); MS (electrospray), m/z 329.3 $(M+H)^+$.

6-Methoxy-4-methyl-8-nitro-5-phenyloxyquinoline (**27**)

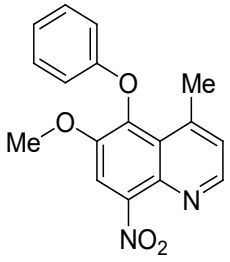

27

Compound **27** was prepared using the same procedure as that of compound **26**. Reaction of methyl vinyl ketone (89.8 mg, 1.275 mmol), **24** (220 mg, 0.846 mmol), H_3AsO_4 (387.0 mg, 1.689 mmol) and 3 mL of 85% H_3PO_4 gave 118 mg (45 % yield) of compound **27** as brown solid. Melting point: 170 – 172 ºC; ^{1}H NMR δ 8.76 (d, J = 4.3 Hz, 1H), 7.88 (s, 1H), 7.28 - 7.21 (m, 2H), 7.22 (d, J = 2.0 Hz, 1H), 7.05 (t, J = 6.0 Hz, 1H), 6.81 - 6.78 (m, 2H), 3.89 (s, 3H, OMe), 2.73 (s, 3H, Me);

^{13}C NMR δ 158.0, 150.9, 148.6, 146.5, 144.3, 140.8, 136.4, 130.4, 130.0, 125.8, 125.5, 122.7, 120.8, 115.2, 112.2, 57.4 (OMe), 23.5 (Me); MS (electrospray), m/z 311.2 $(M+H)^+$.

8-Amino-6-methoxy-4-methyl-5-(3-fluorophenyloxy)quinoline (**29**)

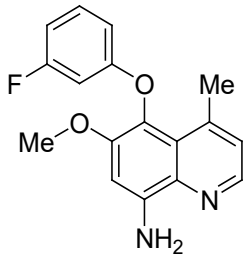

29

Compound **26** (35.0 mg, 0.106 mmol) and iron powder (33.6 mg, 0.636 mmol) was mixed with 5 mL of aqueous 10% acetic acid solution and heated under reflux for 2 hours. The mixture was cooled to room temperature, diluted with water, extracted with 25 mL THF first, and followed by diethyl ether 2 times. The combined organic layers were washed with water and brine, dried ($MgSO_4$), concentrated, and column chromatographed on silica gel using a mixture of hexane and diethyl ether (1:1) as an eluent to give 29 mg (92% yield) of compound **29** as yellow solid. Melting point: 146 - 147 ºC; ^{1}H NMR δ 8.45 (d, J = 4.3 Hz, 1H), 7.19 (dd, J = 8.2, 6.6 Hz, 1H), 7.08 (d, J = 4 Hz, 1H), 6.8 (s, 1H), 6.67 (td, J = 8.2, 2.3 Hz, 1H), 6.60 (dd, J = 8.2, 2.3 Hz, 1H), 6.48 (dt, J = 10.9, 2.0 Hz, 1H), 5.15 (bs, 2H, NH_2), 3.85 (s, 3H, OMe), 2.62 (s, 3H, Me); ^{13}C NMR δ 164.0 (d, $^1J_{CF}$ = 244 Hz), 161.0 (d, $^3J_{CF}$ = 10 Hz), 150.7, 145.6, 143.6, 143.0, 134.0, 130.4 (d, $^3J_{CF}$ = 9 Hz),

127.6, 125.1, 124.7, 111.0 (d, $^4J_{CF}$ = 3 Hz), 108.4 (d, $^2J_{CF}$ = 21 Hz), 102.9 (d, $^2J_{CF}$ = 25 Hz), 98.0, 56.4 (OMe), 22.9 (Me); MS (electrospray), m/z 299.3 $(M+H)^+$.

8-Amino-6-methoxy-4-methyl-5-phenyloxyquinoline (**30**)

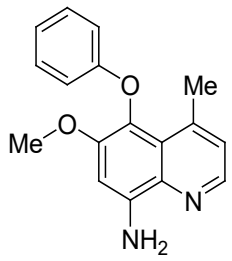

30

Compound **30** was prepared using the same procedure as that of compound **29**. Reaction of compound **27** (57 mg, 0.184 mmol), iron powder (62.0 mg, 1.100 mmol) and 10 mL aqueous 10% acetic acid solution gave 47 mg (92% yield) of compound **30** as brown solid. Melting point: 145 - 146 ^oC; ^1H NMR δ 8.44 (d, J = 4.3 Hz, 1H), 7.26 - 7.20 (m, 2H), 7.03 (dd, J = 4.4, 0.8 Hz, 1H), 6.97 (t, J = 3.6 Hz, 1H), 6.79 - 6.76 (m, 3H), 5.15 (bs, 2H, NH_2), 3.78 (s, 3H, OMe), 2.63 (s, 3H,

CH_3); ^{13}C NMR δ 159.7, 150.8, 145.5, 143.3, 143.26, 134.1, 129.7, 128.0, 125.0, 124.9, 121.5, 115.0, 98.4, 56.8 (OMe), 23.4 (Me); MS (electrospray), m/z 281.4 $(M+H)^+$.

8-Amino-4-methyl-5-(3-(trifluoromethyl)phenoxy)quinolin-6-ol (**32**)

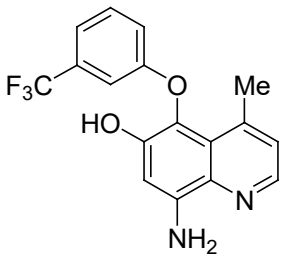

32

To a solution of compound **28** (98.2 mg, 0.282 mmol) in 2 ml dry dichloromethane (distilled over calcium hydride) was added 1 mL of 1.0 M BBr_3 in dichloromethane (4.0 eq) 0°C. This mixture was warmed to 25 °C and stirred overnight, diluted with aqueous sodium bicarbonate solution, and extracted three times with dichloromethane. The combined extract was washed with water, brine, dried ($MgSO_4$), and concentrated to give 78 mg (83% yield) of compound **32** as brown solid which is sufficiently pure for carried out in the next step. Melting point: 133 – 135 °C; ^1H NMR δ 8.46 (d, J = 4.4 Hz, 1H), 7.38 (t, J = 8.0 Hz, 1H), 7.29 (d, J = 7.2 Hz, 1H), 7.14 (s, 1H), 7.08 (d, J = 3.6 Hz, 1H), 6.93 (d, J = 7.6 Hz, 1H), 6.73 (s, 1H), 5.40 (bs, 1H, OH), 5.30 – 5.10 (bs, 2H, NH_2), 2.55 (s, 3H); ^{13}C NMR δ 159.1, 147.8, 145.4, 144.2, 141.8, 134.9, 133.1 (q, $^2J_{CF}$ = 37 Hz, C-CF_3) 130.9,

125.1, 124.5, 124.2, 123.0 (q, $^{1}J_{CF}$ = 270 Hz, CF_3), 119.5, 118.2 (q, $^{3}J_{CF}$ = 4 Hz), 112.5 (q, $^{3}J_{CF}$ = 4 Hz), 100.5, 22.7 (Me); MS (electrospray), m/z 335.1 $(M+H)^+$.

4-Methoxy-2-nitrobenzenamine (**34**)

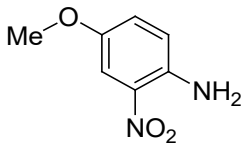

34

N-Acetyl-*p*-anisidine (2.0 g, 12.0 mmol) was mixed with 20% aqueous nitric acid, and this mixture was heated under reflux for 1 hour. After 1 hour, it was poured onto the ice-water mixture and stirred vigorously for 10 minutes. The solid precipitated was collected by filtration to give crude product of **34**, which was purified by recrystallization in ethanol to give 413 mg (33% yield) of compound **34** as brown solid. ^{1}H NMR δ 7.54 (d, J = 3.2 Hz, 1H), 7.08 (dd, J = 9.3, 4.3 Hz, 1H), 6.76 (d, J = 9.3 Hz, 1H), 3.79 (s, 3H); MS, m/z 169.0 $(M+H)^+$.

6-Methoxy-4-methyl-8-nitroquinoline (**36**)

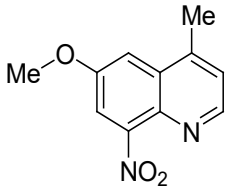

36

Compound **36** was prepared using the same procedure as that of compound **26**. Reaction of methyl vinyl ketone (275 mg, 3.93 mmol), **35** (440.0 mg, 2.62 mmol), H_3AsO_4 (1.20 g, 5.24 mmol) and 12 mL of 85% H_3PO_4 gave 500.0 mg (87% yield) of compound **36** as brown solid. Melting point: 159 - 162 °C; ^{1}H NMR ($CDCl_3$) δ 8.77 (d, J = 4 Hz, 1H), 7.67 (d, J = 2.8 Hz, 1H), 7.40 (d, J = 2.8

Hz, 1H), 7.33 - 7.34 (m, 1H), 4.00 (s, 3H, OMe), 2.70 (s, 3H, CH_3). ^{13}C NMR δ 156.1, 149.9, 143.4, 135.3, 130.3, 123.8, 115.6, 106.2, 56.4 (OMe), 19.4 (Me); MS (electrospray), m/z 241.0 $[M+Na]^+$, 219.1 $[M+H]^+$.

8-Amino-6-methoxy-4-methylquinoline (**37**)

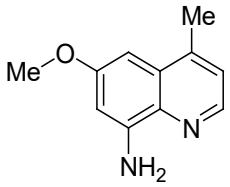

37

Compound **37** was prepared using the same procedure as that of compound **29.** Reaction of compound **36** (250 mg, 1.15 mmol) with iron powder (385.0 mg, 6.88 mmol) in 60 mL of aqueous 10% acetic acid solution gave 212 mg (98% yield) of compound **37** as brown solid. Melting point: 88 - 91 °C; ^1H NMR δ 8.48 (d, J = 4.4 Hz, 1H), 7.17 (dd, J = 4.4, 0.8 Hz, 1H), 6.59 (d, J = 2.4 Hz, 1H), 6.55 (d, J = 2.4 Hz, 1H), 5.13 (bs, 2H, NH_2), 3.80 (s, 3H, OMe), 2.61 (s, 3H, CH_3); ^{13}C NMR

δ 158.8, 145.8, 144.8, 142.9, 135.1, 129.9, 122.8, 101.2, 91.5, 55.4 (OMe), 19.4 (Me); MS (electrospray), m/z 189.3 [M+H].

8-(4-Hydroxybenzylamino)-4-methyl-5-(3-(trifluoromethyl)phenoxy)quinolin-6-ol (**9**)

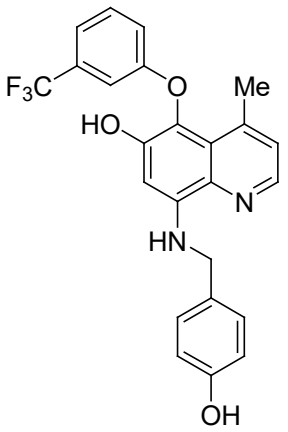

9

A solution of 50 mg (0.149 mmol) of compound **32** and 20 mg (0.163 mmol) of 4-hydroxybenzaldehyde in 2 mL dry methanol was stirred for 30 minutes under argon atmosphere until the solid dissolved. 3 drops of acetic acid were added, and the brown mixture was stirred for 30 minutes at room temperature. In to this mixture, 28 mg (0.450 mmol) of sodium cyanoborohydride was added, and the solution was stirred for 12 hours. Yellow solids precipitated out from the solution. This mixture was diluted with 30 mL of aqueous NH_4Cl solution, and extracted three times with ethyl acetate. The combined organic layers were washed with water, brine, dried ($MgSO_4$), concentrated, and column chromatographed on silica gel using a mixture of hexane and diethyl ether (1:1) as an eluent; the obtained product was recrystallized with 2 mL of hexane and diethyl ether (1:1) to give 34 mg (52% yield) of compound **9** as yellow solid; Melting point: 194 – 195 ^oC; ^1H NMR (DMSO-d6) δ 9.64 (bs, 1H, NH), 9.28 (s, 1H, OH), 8.37 (d, J = 4.0 Hz, 1H), 7.47 (t, J = 8.4 Hz, 1H), 7.28 (d, J = 7.6 Hz, 1H), 7.20 (d, J = 8.4 Hz, 2H), 7.15 (d, J =

4.4 Hz, 1H), 7.01 (s, 1H), 6.97 – 6.93 (m, 2H), 6.72 (d, J = 8.4 Hz, 2H), 6.36 (s, 1H), 4.32 (d, J = 6 Hz, 2H), 2.51 (s, 3H, Ar-Me; overlap with DMSO-d6 signal); ^{13}C NMR (DMSO-d6) δ 160.2, 157.1, 149.5, 144.4, 144.37, 141.3, 133.6, 131.6, 130.9 (q, $^{2}J_{CF}$ = 31 Hz, -C-CF_3), 130.1, 129.1 125.5, 124.6, 124.5 (q, $^{1}J_{CF}$ = 270 Hz, CF_3), 123.1, 119.5, 118.3 (q, $^{3}J_{CF}$ = 4 Hz), 115.9, 112.0 (q, $^{3}J_{CF}$ = 4 Hz), 97.2, 46.7 (CH_2N), 23.1 (Me); MS (electrospray), m/z 441.5 $(M+H)^+$.

4-((5-(3-Fluorophenoxy)-6-methoxy-4-methylquinolin-8-ylamino)methyl)phenol (**10**)

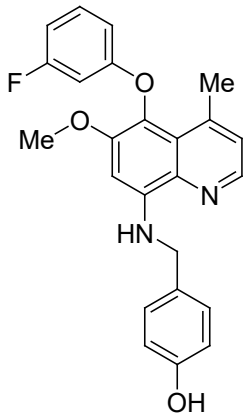

10

A solution of 34 mg (0.114 mmol) of compound **29** and 15 mg (0.125 mmol) 4-hydoxybenzaldehyde in 1 mL of dry methanol was stirred under argon atmosphere at 25 °C for 30 minutes. To it, 2 drops of acetic acid were added. The mixture was stirred at 25 °C for 1 hour. Then, 21 mg (0.342 mmol) of sodium cyanoborohydride was added, and the solution was stirred for 12 hours, diluted with 30 mL of aqueous NH_4Cl solution, and extracted three times with ethyl acetate. The combined organic layers were washed with water, brine, dried ($MgSO_4$), concentrated, and column chromatographed on silica gel using a mixture of hexane and diethyl ether (1:1). The product was washed with 3 mL of hexane: diethyl ether (1:1) to obtain pure product of **10** 29 mg (65%) as yellow solid. Melting point: 168 - 169 °C; ^{1}H NMR δ 8.41 (d, J = 4.8 Hz, 1H), 7.28 (d, J

= 8.0 Hz, 2H), 7.19 (dt, J = 8.4, 6.8 Hz, 1H), 7.10 (dd, J = 4.4, 0.8 Hz, 1H), 6.79 (d, J = 8.0 Hz, 2H), 6.66 (td, J = 6, 0.4 Hz, 1H), 6.62 (dd, J = 8.4, 0.4 Hz, 1H), 6.51 - 6.49 (m, 3H), 5.02 (s, 1H, OH), 4.44 (s, 2H, CH_2N), 3.79 (s, 3H, OMe), 2.65 (s, 3H, Me); ^{13}C NMR δ 164.0 (d, $^1J_{CF}$ = 247 Hz), 161.2 (d, $^3J_{CF}$ = 10 Hz), 155.4, 151.2, 145.0, 144.3, 143.4, 133.7, 130.7, 130.4 (d, $^3J_{CF}$ = 10 Hz), 129.4, 126.4, 125.2, 124.7, 115.8, 111.0 (d, $^4J_{CF}$ = 3 Hz), 108.3 (d, $^2J_{CF}$ = 21 Hz), 103.0 (d, $^2J_{CF}$ = 21 Hz), 93.9, 56.8 (OMe), 47.8 (CH_2N), 23.4 (Me); MS (electrospray), m/z 427.1 $(M+Na)^+$. Succinic salt of **10** was prepared using 20 mg (0.047 mmol) of **10** and 5.5 mg (0.047 mmol) of succinic acid.

4-((6-Methoxy-4-methyl-5-phenoxyquinolin-8-ylamino)methyl)phenol (**11**)

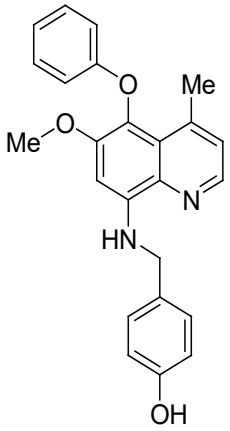

11

Compound **11** was prepared following the same procedure as that of compound **10**. Reaction of compound **30** (58 mg, 0.207 mmol) with 4-hydroxbenzaldehyde (28 mg, 0.228 mmol) gave 74 mg (84%) of compound **11** as a yellow solid. Melting point: 181 - 182 ºC; ^1H NMR δ 8.41 (d, J = 4.0 Hz, 1H), 7.31 – 7.23 (m, 4H), 7.08 (d, J = 4.4 Hz, 1H), 6.95 (t, J =7.2 Hz, 1H), 6.81 - 6.79 (m, 4H), 6.54 (s, 1H), 6.53 (bs, 1H, OH), 6.08 (bs, 1H, NH), 4.45 (s, 2H, CH_2N), 3.79 (s, 3H, OMe), 2.67 (s, 3H, Me); ^{13}C NMR δ 159.8, 155.4, 151.3, 144.9, 144.0, 143.7, 133.8, 130.7, 129.7, 129.4,

126.8, 125.04, 125.0, 121.4, 115.7, 115.1, 94.32, 94.30, 56.9 (OMe), 47.8 (CH_2N), 23.5 (Me); MS (electrospray), m/z 409.2 $(M+Na)^+$, 387.1 $(M+H)^+$. Succinic salt of **11** was prepared in the same way as that of compound **10** by starting with 20 mg (0.052 mmol) of **11** and 6.1 mg (0.052 mmol) of succinic acid.

8-Amino-6-methoxy-4-methylquinoline (**12**)

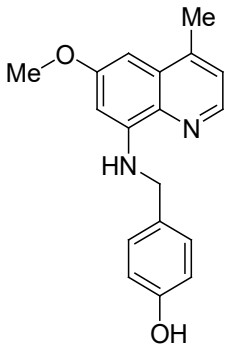

12

Compound **12** was prepared following the same procedure as that of compound **10**. Reaction of compound **37** (100 mg, 0.532 mmol) with 4-hydroxbenzaldehyde (71 mg, 0.585 mmol) gave 114 mg (73%) of compound **12** as a yellow solid. Melting point: 164 ºC; ^{1}H NMR δ 8.43 (d, J = 4.4 Hz, 1H), 7.24 (d, J = 8.0 Hz, 2H), 7.20 (d, J = 4.0 Hz, 1H), 6.76 (d, J = 8.4 Hz, 2H), 6.46 (d, J = 2.8 Hz, 1H), 6.43 (bs, 1H, -OH), 6.34 (d, J = 1.6 Hz, 1H), 6.07 (bs, 1H, -NH), 4.38 (d, J = 4.8 Hz, 2H), 3.90 (s, 3H, -OMe), 2.62 (s, 3H, Ar-Me); ^{13}C NMR δ 159.4, 155.4, 146.2, 144.2, 143.4, 134.8, 130.8, 129.9, 129.3, 122.9, 115.6, 97.2, 89.3, 55.4, 47.5, 19.5; MS, m/z 295.2 $(M+H)^+$. Succinic

salt of **12** was prepared in the same way as compound **10** by starting with 20 mg (0.068 mmol) of **12** and 8.1 mg (0.068 mmol) of succinic acid.

1.5.2 GSK3β inhibition studies of substituted quinolines using GSK3β kinase assay

GSK3β inhibition studies were carried out following the protocols based on Promega technical manual (TM313) and GSK-3β kinase assay manual published by Promega.[41,42]

GSK3β kinase enzyme portion of the kit is consisted of following: GSK3β, 10 µg (Human, recombinant full-length), GSK3β Substrate which has the amino acid sequence of YRRAAVPPSPSLSRHSSPHQ(pS)EDEEE derived from human muscle glycogen synthase 1 and 5X Reaction Buffer A consisted of 200 mM Tris, 7.5, 100 mM $MgCl_2$, 0.5 mg/ml BSA and 0.1M DTT. ADP-Glo portion is consisted of following: ADP-Glo reagent, kinase detection buffer, kinase detection substrate, 10 mM ultra-pure ATP and 10 mM ADP.

1.5.2.1 Experimental procedure for the kinase activity determination

Prior to analyzing the quinoline compounds, the optimal conditions to run the assay was determined.

First, the concentration of GSK3β which gives optimal enzyme activity was found out.

Different concentrations of GSK3β which contain 0, 0.2, 0.39, 0.78, 1.56, 3.12, 6.25, 12.5 and 25 ng in 2 µL were prepared by using a stock solution of the enzyme in 1X kinase buffer (composition was listed previously). A 10 mM ATP and GSK3 substrate was diluted with 1X buffer to obtain

100 µM ATP and 0.8 µg/µL substrate respectively. Then 2 µL from each different concentration of the enzyme, 2 µL of substrate/ATP mix was added into the separate wells of 384 low volume plate and incubated at room temperature for 60 minutes in a low speed plate shaker. After 60 minutes, 5 µL of ADP-Glo reagent was added into each well and further incubated at room temperature for 40 minutes. Then 10 µL of kinase detection reagent was added into each well and incubated at room temperature for 30 minutes. Finally, the luminescence was measured in a Glo-Max multi detection luminometer within 0.5 seconds integration time.

Next, the best reaction time was found out. The optimum concentration of the enzyme was found to be 1 ng from the previous experiment. Therefore, 2 µL of the enzyme which contains 1 ng of enzyme was mixed with 1 µL of 100 µM ATP and 1 µL of 0.8 µg/µL substrate in a 384 low volume plates. The plates were incubated at 1,15, 30, 45, 60 minutes at room temperature separately in a low speed shaker. After the desired time, similar procedure mentioned above (*1.5.2.1*) was followed to add ADP-Glo reagent and kinase detection reagent and the luminescence values were obtained in Glo-Max multi detection luminometer within 0.5 seconds integration time.

1.5.2.2 Experimental procedure for the GSK3β inhibition by staurosporine

After finding out the optimum enzyme concentration and best time for the inhibition studies, a known inhibitor staurosporine was analyzed to compare the IC_{50} values. In which case, 1 µL of different concentrations of staurosporine prepared in 5% DMSO were added into the separate wells of 384 low volume plate first followed by 2 µL of the enzyme which contains 1 ng of enzyme was added. Then it was added 2 µL of substrate/ATP mix (1 µL of 100 µM ATP and 1 µL of 0.8 µg/µL substrate). The similar procedure mentioned above (1.5.2.1) was followed to add ADP-Glo reagent

and kinase detection reagent and the luminescence values were obtained from the luminometer. Finally, luminescence vs Log concentration of staurosporine was plotted and the IC_{50} value of staurosporine was calculated from the inhibition curve.

1.5.2.3 General procedure for the GSK3β inhibition studies of quinoline compounds

Enzyme, substrate and ATP was diluted to obtain 0.5 ng/µL, 0.8 µg/µL, and 100 µM respectively in 1X kinase buffer.

Then to the wells of the 384 low volume plate, they were added in the following order

1 µL of inhibitor of various concentrations dissolved in either 5% DMSO or 1X buffer (based on the solubility of these compounds) were added into separate wells of 384 micro-well plate and into each well 2 µL of enzyme which contains 1 ng of enzyme was added followed by 2 µL of ATP/substrate mix (contains 1 µL from 0.8 µg/µL substrate and 1 µL of 100 µM ATP). As a control, 1 µL of 5% DMSO or 1X buffer was added without any inhibitors and the other components were added accordingly. Plate was incubated at room temperature for 60 minutes in a low speed plate shaker. After 60 minutes, 5 µL of ADP-Glo reagent was added into each well and further incubated at room temperature for 40 minutes. Then 10 µL of kinase detection reagent was added into each well and incubated at room temperature for 30 minutes. Finally, the luminescence was measured in a Glo-Max multi detection luminometer within 0.5 seconds integration time.

1.5.3 PKC inhibition studies of substituted quinolines using Pep Tag non-radioactive PKC assay

PKC inhibition studies of substituted quinolines were carried out following the protocol supplied by Promega (technical bulletin #132).[44] The negative control of the experiments was consisted of C1 peptide without PKC enzyme and PKC inhibitor (staurosporine or PQs) and the positive control was consisted of both C1 peptide and PKC enzyme but without PKC inhibitor. The inhibition of phosphorylation of PKC by staurosporine or tested quinoline compounds with various concentrations was determined by the decrease in the intensities of their respective phosphorylated bands as compared to the phosphorylated bands of the positive controls.

1.5.3.1 Preparation of different reaction solutions

Each experiment was consisted of 7 or 8 reactions namely one negative control, one or two positive controls, and five of the different concentrations of PKC inhibitor (staurosporine or PQs). The procedure was followed based on Promega technical bulletin (#132) and is described below:

1. Eight 1-mL micro centrifuge tubes were labeled as mixture, negative control, positive control, and the remaining five with different PKC inhibitor concentrations.
2. A 6 µL of deionized water was added to negative control, whereas to positive control 3 µL (15 ng) of diluted PKC (PKC dilution solution comprises of 100 µg/mL of bovine serum albumin (BSA) and 0.05% of Triton® X-100) and 3 µL of deionized water or 1:2 mixtures of DMSO and deionized water (based on the solvent used for dissolving PKC inhibitors) was added.
3. Different concentrations of PKC inhibitors (5 tubes) were prepared by adding 3 µL (15 ng) of diluted PKC and 3 µL of solution of required concentration from the testing compound (each tube

had a different concentration of testing compound) in deionized water or 1:2 mixtures of DMSO and deionized water.

4. For the tube labeled as mixture was added 17.5 µL of PKC reaction buffer, 17.5 µL of PKC activator solution, 3.5 µL peptide protection solution, and 14 µL (5.6 µg) of C1 peptide at 0 °C and incubated for 2 minutes in water bath maintained at 30 °C. Then 7.5 µL of this solution was added to each tube labeled as negative control, positive control, and five reactions with varying drug concentrations. Each tube had 0.8 µg of C1 peptide in the total volume of 13.5 µL.

5. Negative control, positive control, and five tubes with different concentrations of testing compound were incubated in a water bath maintained at 30 °C for 45 minutes.

6. The PKC enzyme in each tube was deactivated by placing the tubes in boiling water for 10 minutes.

7. The tubes were allowed to cool to room temperature and 0.5 µL of 80% glycerol was added to each tubes. At this point, the samples were ready to be loaded into the agarose gel for carrying out the horizontal gel electrophoresis. Agarose gel plate need to prepared and ready prior to load the samples into the gel.

1.5.3.2 Preparation of agarose gel for electrophoresis

Agarose (0.4 g) was added to a solution of 50 mL of 50 mM Tris-HCl (pH 8.0) buffer, heated to boiling in a microwave till all of the agarose was dissolved. It was cooled to about 60 °C, and was slowly added into a gel tray having required number of comb(s) placed in a mini horizontal electrophoresis apparatus. If there were any bubbles in the solution, they were carefully removed with a pipette tip. The agarose solution was solidified to a gel after about 20 minutes. The comb(s)

were removed carefully to obtain the desired number of wells for sample loading. Finally, the gel was covered with 50 mM Tris-HCl solution (pH 8.0) as a running buffer.

1.5.3.3 Separation of phosphorylated and nonphosphorylated peptides by electrophoresis

The samples from each tube (as described in section *1.5.3.1*) were loaded into the separate wells of the agarose gel placed in a horizontal gel electrophoresis chamber and electrophoresis was carried out at 100 V for 30 minutes. During the electrophoresis, the nonphosphorylated peptides (+Ve charged) move towards the negatively charged electrode (anode) and the phosphorylated peptides (-Ve charged) move towards the positively charged electrode (cathode) as they get a net -1 charge after phosphorylation, and separate from each other.

1.5.3.4 Quantification of phosphorylated and nonphosphorylated peptides by photo imaging technique

After the electrophoresis, gel was removed from the electrophoresis chamber and was quickly photographed under UV by Kodak Gel Logic 1500 Digital Imaging System. Quantification of both phosphorylated and nonphosphorylated bands were carried out by Imagequant 5.2 software (Molecular Dynamics/Amersham Biosciences). Quantification of the bands using Imagequant 5.2 software is referred as photo imaging. During the quantification, the tiff image file of the gel was inverted which results black colour bands with a white background, (opposite to the normal picture) and background correction was done to minimize noise. The obtained volumes of the bands (pixel intensities) were then used to determine the amounts of phosphorylated and non-phosphorylated C1 peptide which is discussed in detailed in section *1.3.4.1*. To minimize the

effects result from diffusion and overflowing of the lanes during the sample loading, the sum of intensities or volumes of both phosphorylated and nonphosphorylated bands of each reaction were considered to be the contribution of 0.8 μg of peptide which was present in each reaction. The correlation studies between the peptide phosphorylation with different concentration of PKC (0 - 40 ng) were carried out before testing the synthesized compounds.

1.6 References

1. Kaytor, M. D.; Orr, H. T., The GSK3β signaling cascade and neurodegenerative disease. *Current opinion in neurobiology* **2002**, *12* (3), 275-278.

2. Hooper, C.; Killick, R.; Lovestone, S., The GSK3 hypothesis of Alzheimer's disease. *Journal of neurochemistry* **2008**, *104* (6), 1433-1439.

3. Luo, J., The role of GSK3beta in the development of the central nervous system. *Frontiers in biology* **2012**, *7* (3), 212-220.

4. Isik, A. T., Late onset Alzheimer's disease in older people. *Clinical interventions in aging* **2010**, *5*, 307.

5. Hernández, F.; de Barreda, E. G.; Fuster-Matanzo, A.; Lucas, J. J.; Avila, J., GSK3: a possible link between beta amyloid peptide and tau protein. *Experimental neurology* **2010**, *223* (2), 322-325.

6. Mokhtar, S. H.; Bakhuraysah, M. M.; Cram, D. S.; Petratos, S., The beta-amyloid protein of alzheimer's disease: communication breakdown by modifying the neuronal cytoskeleton. *International Journal of Alzheimer's Disease* **2013**.

7. Shi, A.; Nguyen, T. A.; Battina, S. K.; Rana, S.; Takemoto, D. J.; Chiang, P. K.; Hua, D. H., Synthesis and anti-breast cancer activities of substituted quinolines. *Bioorganic & medicinal chemistry letters* **2008**, *18* (11), 3364-3368.

8. Gakhar, G.; Ohira, T.; Shi, A.; Hua, D. H.; Nguyen, T. A., Antitumor effect of substituted quinolines in breast cancer cells. *Drug Development Research* **2008**, *69* (8), 526-534.

9. Da Rocha, A.; Mans, D. R. A.; Regner, A.; Schwartsmann, G., Targeting protein kinase C: new therapeutic opportunities against high-grade malignant gliomas? *The oncologist* **2002***, 7* (1), 17-33.

10. Iqbal, K.; Alonso, A. d. C.; Chen, S.; Chohan, M. O.; El-Akkad, E.; Gong, C.-X.; Khatoon, S.; Li, B.; Liu, F.; Rahman, A., Tau pathology in Alzheimer disease and other tauopathies. Biochimica et Biophysica Acta (BBA)-*Molecular Basis of Disease* **2005***, 1739* (2), 198-210.

11. Sofola, O.; Kerr, F.; Rogers, I.; Killick, R.; Augustin, H.; Gandy, C.; Allen, M. J.; Hardy, J.; Lovestone, S.; Partridge, L., Correction: Inhibition of GSK-3 Ameliorates Aβ Pathology in an Adult-Onset Drosophila Model of Alzheimer's Disease. *PLoS genetics* **2012***, 8* (1).

12. http://www.selleckchem.com/subunits/GSK-3beta_GSK-3_selpan.html?gclid=COTunofc0M8CFYNGXgodYVgJIg

13. Wang, Z.; Cole, P. A., Catalytic mechanisms and regulation of protein kinases. *Methods in enzymology* **2014***, 548*, 1-21.

14. Koivunen, J.; Aaltonen, V.; Peltonen, J., Protein kinase C (PKC) family in cancer progression. *Cancer letters* **2006***, 235* (1), 1-10.

15. Schenk, P. W.; Snaar-Jagalska, B. E., Signal perception and transduction: the role of protein kinases. Biochimica et Biophysica Acta (BBA)-*Molecular Cell Research* **1999***, 1449* (1), 1-24.

16. Newton, A. C., Protein kinase C: structure, function, and regulation. *Journal of Biological Chemistry* **1995***, 270* (48), 28495-28498.

17. Mackay, H. J.; Twelves, C. J., Targeting the protein kinase C family: are we there yet? *Nature Reviews Cancer* **2007***, 7* (7), 554-562.

18. Castagna, M.; Takai, Y.; Kaibuchi, K.; Sano, K.; Kikkawa, U.; Nishizuka, Y., Direct activation of calcium-activated, phospholipid-dependent protein kinase by tumor-promoting phorbol esters. *Journal of Biological Chemistry* **1982**, *257* (13), 7847-7851.

19. Blobe, G. C.; Obeid, L. M.; Hannun, Y. A., Regulation of protein kinase C and role in cancer biology. *Cancer and Metastasis Reviews* **1994**, *13* (3-4), 411-431.

20. Giepmans, B. N., Gap junctions and connexin-interacting proteins. *Cardiovascular research* **2004**, *62* (2), 233-245.

21. Bao, X.; Altenberg, G. A.; Reuss, L., Mechanism of regulation of the gap junction protein connexin 43 by protein kinase C-mediated phosphorylation. *American Journal of Physiology-Cell Physiology* **2004**, *286* (3), C647-C654.

22. Goodenough, D. A.; Goliger, J. A.; Paul, D. L., Connexins, connexons, and intercellular communication. *Annual review of biochemistry* **1996**, *65* (1), 475-502.

23. Bernzweig, J.; Heiniger, B.; Prasain, K.; Lu, J.; H Hua, D.; A Nguyen, T., Anti-breast cancer agents, quinolines, targeting gap junction. *Medicinal Chemistry* **2011**, *7* (5), 448-453.

24. Heiniger, B.; Gakhar, G.; Prasain, K.; Hua, D. H.; Nguyen, T. A., Second-generation substituted quinolines as anticancer drugs for breast cancer. *Anticancer research* **2010**, *30* (10), 3927-3932.

25. Ding, Y.; Prasain, K.; Nguyen, T. D.; Hua, D. H.; Nguyen, T. A., The effect of the PQ1 anti-breast cancer agent on normal tissues. *Anti-cancer drugs* **2012**, *23* (9), 897-905.

26. Schwartz, G. K.; Ward, D.; Saltz, L.; Casper, E. S.; Spiess, T.; Mullen, E.; Woodworth, J.; Venuti, R.; Zervos, P.; Storniolo, A., A pilot clinical/pharmacological study of the protein

kinase C-specific inhibitor safingol alone and in combination with doxorubicin. *Clinical cancer research* **1997***, 3* (4), 537-543.

27. Kobayashi, E.; Nakano, H.; Morimoto, M.; Tamaoki, T.; Calphostin, C., a novel microbial compound, is a highly potent and specific inhibitor of phospholipid/Ca 2+ dependent protein kinase. *Biochem Biophys Res Commun* **1989***, 135*, 397-402.

28. Smorenburg, C.; Seynaeve, C.; Bontenbal, M.; Planting, A. S.; Sindermann, H.; Verweij, J., Phase II study of miltefosine 6% solution as topical treatment of skin metastases in breast cancer patients. *Anti-cancer drugs* **2000***, 11* (10), 825-828.

29. Liu, J.-Y.; Lin, S.-J.; Lin, J.-K., Inhibitory effects of curcumin on protein kinase C activity induced by 12-O-tetradecanoyl-phorbol-13-acetate in NIH 3T3 cells. *Carcinogenesis* **1993***, 14* (5), 857-861.

30. Omura, S.; Iwai, Y.; Hirano, A.; Nakagawa, A.; Awaya, J.; Tsuchiya, H.; Takahashi, Y.; Asuma, R., A new alkaloid AM-2282 of Streptomyces origin taxonomy, fermentation, isolation and preliminary characterization. *The Journal of antibiotics* **1977***, 30* (4), 275-282.

31. Chan, S.-L.; Lee, M. C.; Tan, K. O.; Yang, L.-K.; Lee, A. S.; Flotow, H.; Fu, N. Y.; Butler, M. S.; Soejarto, D. D.; Buss, A. D., Identification of chelerythrine as an inhibitor of BclXL function. *Journal of Biological Chemistry* **2003***, 278* (23), 20453-20456.

32. Jasinski, P.; Zwolak, P.; Terai, K.; Borja-Cacho, D.; Dudek, A. Z., PKC-alpha inhibitor MT477 slows tumor growth with minimal toxicity in in vivo model of non-Ras-mutated cancer via induction of apoptosis. *Investigational new drugs* **2011***, 29* (1), 33-40.

33. Swannie, H. C.; Kaye, S. B., Protein kinase C inhibitors. *Current oncology reports* **2002***, 4* (1), 37-46.

34. Meijer, L.; Flajolet, M.; Greengard, P., Pharmacological inhibitors of glycogen synthase kinase 3. *Trends in pharmacological sciences* **2004**, *25* (9), 471-480.

35. Pandey, M. K.;DeGrado, T. R., Glycogen Synthase Kinase-3 (GSK-3)-Targeted Therapy and Imaging. *Theranostics* **2016**, *6* (4), 571-593.

36. Eldar-Finkelman, H.; Martinez, A., GSK-3 inhibitors: preclinical and clinical focus on CNS. *Front. Mol. Neurosci* **2011**, *4* (32), 1-18.

37. Lu, J.; Maezawa, I.; Weerasekara, S.; Erenler, R.; Nguyen, T. D.; Nguyen, J.; Swisher, L. Z.; Li, J.; Jin, L.-W.; Ranjan, A., Hua, D.H., Syntheses, neural protective activities, and inhibition of glycogen synthase kinase-3β of substituted quinolines. *Bioorganic & medicinal chemistry letters* **2014**, *24* (15), 3392-3397.

38. Pokhrel, L.; Maezawa, I.; Nguyen, T. D.; Chang, K.-O.; Jin, L.-W.; Hua, D. H., Inhibition of Acyl-CoA: cholesterol acyltransferase (ACAT), overexpression of cholesterol transporter gene, and protection of amyloid β (Aβ) oligomers-induced neuronal cell death by tricyclic pyrone molecules. *Journal of medicinal chemistry* **2012**, *55* (20), 8969-8973.

39. LaMontagne, M. P.; Blumbergs, P.; Strube, R. E., Antimalarials. 14. 5-(Aryloxy)-4-methylprimaquine analogs. A highly effective series of blood and tissue schizonticidal agents. *Journal of medicinal chemistry* **1982**, *25* (9), 1094-1097.

40. Jansen, M., Crystal structure of As_2O_5. *Angewandte Chemie International Edition in English* **1977**, *16* (5), 314-315.

41. GSK-3β Kinase assay protocol: https://www.promega.com/-/media/files/resources/protocols/kinase-enzyme-appnotes/gsk3b-kinase-assay-protocol.pdf?la=en

42. ADP-GloTM Kinase assay protocol: https://www.promega.com/-/media/files/resources/protocols/technical-bulletins/kinase-enzyme-system-protocol.pdf

43. Bertrand, J.; Thieffine, S.; Vulpetti, A.; Cristiani, C.; Valsasina, B.; Knapp, S.; Kalisz, H.; Flocco, M., Structural characterization of the GSK-3β active site using selective and non-selective ATP-mimetic inhibitors. *Journal of molecular biology* **2003***, 333* (2), 393-407.

44. PepTag® Assay for non-radioactive detection of PKC: https://www.promega.com/-/media/files/resources/protocols/technical-bulletins/0/peptag-assay-for-non-radioactive-detection-of-protein-kinase-c-protocol.pdf

45. Meggio, F.; Deana, A. D.; Ruzzene, M.; Brunati, A. M.; Cesaro, L.; Guerra, B.; Meyer, T.; Mett, H.; Fabbro, D.; Furet, P., Different susceptibility of protein kinases to staurosporine inhibition. *European Journal of Biochemistry* **1995***, 234* (1), 317-322.

Chapter 2 - Quantification of Tricyclic Pyrones From Pharmacokinetic Studies

2.1 Introduction

Alzheimer's disease (AD) was described by Alois Alzheimer, a German neurologist in 1906. AD features by lifelong progressive deterioration of cognitive function, most commonly of the memory, and motor functions. It affects patients' daily activities ultimately leading to loss of independence. When the disease progresses, severe cognitive impairment will result in patients, who become susceptible to infections and pneumonia. To date, no specific drug has been approved by the Food and drug administration (FDA) that can prevent the progression of AD.[1,2]

AD is the most common cause of dementia in the elderly and about 35 million people worldwide have been suffered from AD.[3-4] In the United States, it is now considered as the fifth-leading cause of death for individuals at age 65 and older accounting for about 5.5 million US population.[3,4] Currently, only four medications are approved by the FDA that can temporarily relieve symptoms and these include Donepezil (Aricept®), rivastigmine (Exelon®), galantamine (Razadyne®) and memantine (Namenda®).[5] Therefore, new AD therapeutic development is highly beneficial.

It has been hypothesized that the accumulation of extracellular amyloid plaques generated from amyloid-beta (Abeta or Aβ) protein aggregation and the accumulation of intracellular neurofibrillary tangles (NFTs) formed from the aggregation of hyperphosphorylated tau proteins initiate a cascade of molecular events leading to synaptic dysfunction, inflammation and neuronal death observed in AD brains.[6,7,8] It has also been hypothesized that intracellular Aβ induces a

higher toxicity, being at least 10,000 times more toxic than extracellular Aβ oligomers.[6] Therefore, it is suggested that the intraneuronal accumulation of Aβ is the primary toxic species and might be the first step of amyloid cascade leading to the AD. Therefore, key designing strategies for AD therapeutics are the targeting methods to reduce the level of Aβ peptide, inhibition its further aggregation, and eliminate existing Aβ aggregates.[9,10]

Drugs targeting Aβ and downstream events could be one of the primary therapeutic targets in AD. Previously, our laboratory has synthesized a class of tricyclic pyrone compounds (TPs).[11] The lead compound, CP2 (code name; Figure 2.1) was found to prevent cell death associated with Aβ oligomers and inhibited Aβ aggregation *in vitro* and Aβ-induced cell death using MC65 cell assays.[12] Moreover, it has been shown to reduce the level of amyloid plaques and soluble Aβ amyloids *in vivo* and disaggregate Aβ42 oligomers and protofibrils *in vitro*.[12,13] In addition, it was found that long-term CP2 treatment not only restored memory but also improved motor functions in AD mouse models.[14] CP2 was further modified at position C-13 to obtain similar analogues and one such compound called TP70 (code name; Figure 2.1) was found to possess strong cell protective properties against intracellularly induced Aβ toxicity, inhibitory activities against acyl-CoA: cholesterol acyltransferase (ACAT), and enhancing properties of ATP-binding cassette subfamily A member 1 (ABCA1) cholesterol transporter gene with nanomolar efficacy.[15]

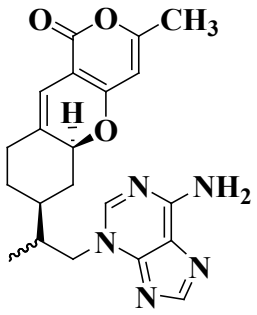

CP2

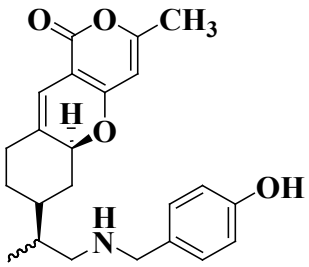

TP70

Figure 2.1: Chemical structures of CP2 and TP70.

In this chapter, I summarized the work that I have carried out in analyzing pharmacokinetic properties of CP2 and TP70 via quantification of CP2 and TP70 in various tissues and plasma samples of mice (wild type and transgenic) using high performance liquid chromatography (HPLC).

Oral feeding via drinking water or intravenous (iv) administration of CP2 were conducted by Dr. Liang Zhang in Dr. Eugenia Trushina's laboratory at Mayo Clinic, Rochester, MN and Dr. Simon Xie at AfaSci Research Laboratory, Redwood City, CA. Oral (po) or intravenous (iv) route administration of TP70 and tissues collection were done by Dr. Ximin Simon Xie group. In this chapter, the data of the distributions of CP2 and TP70 in different tissues and plasma of mice are described and discussed.

2.2 Background

There are two major types of AD, termed as early onset or familial AD and late onset or sporadic AD.[16] Patients who display the first symptoms of AD before the age of 65 are classified under early onset and this category of AD accounts for about 5% of all AD cases worldwide and is

believed to be occurred by genetic mutations.[17] The remaining 95% of AD incidence are categorized under late onset of AD and still the exact cause for this category remains to be elucidated.[17]

2.2.1 AD hypothesis and Aβ generation

Even though, the exact causes of AD are unknown, it is believed that, multiple factors such as genetic, environmental, and life style factors likely contribute to the late onset of AD patients. In early onset, several mutations related to amyloid precursor protein (APP) on chromosome 21, and presenilin 1 (PS1), and presenilin 2 (PS2) on chromosome 12 and chromosome 1, respectively, have shown to be involved under genetic factors.[18-20] APP is a transmembrane glycoprotein and is found in many tissues and organs, including the brain and spinal cord (central nervous system). Though its primary function remains unknown, it has been implicated as a regulator of synapse formation, neural plasticity and iron export. Presenilins are a family of related multi-pass transmembrane proteins that function as a part of the gamma-secretase intramembrane protease complex. Vertebrates have two presenilin genes, called PSEN1 (located on chromosome 14 in humans) that encodes presenilin 1 (PS1) and PSEN2 (on chromosome 1 in humans) that codes for presenilin 2 (PS-2). These proteases have shown to increase the production of amyloid-β 40 ($A\beta_{40}$) or amyloid-β 42 ($A\beta_{42}$) through cleavage of the APP protein at position 711 and 713 via elevating the activity of γ secretase enzyme.[20-22] $A\beta_{42}$ is considered more toxic than $A\beta_{40}$ and aggregates readily resulting most abundant isoform in amyloid plaques.[1,23,24] These amyloid deposits are found in certain parts such as arterioles of the pia mater that surrounds the cerebrum, cortical arterioles, capillaries and vessels in other brain areas.[1,25] It is believed that, vascular Aβ accumulation leads to a damage of the vascular wall, endothelial dysfunction, and vessel reactivity

etc. This will eventually lead to cerebrovascular dysfunction, subsequent neuronal loss and dysfunction resulting symptoms of AD.[26] However, the afore mentioned mutations have been found to cause about less than 30% of the early onset of AD and majority of the disease origins still remain to be discovered. The "amyloid cascade hypothesis" proposed by Hardy and Allsop suggests that the accumulation and aggregation of Aβ would hamper the events like formation of neural fibrillary tangles (NFTs), lowering the neurotransmitters release, disruption of synaptic connections, lead to initiate neuronal loss and dementia.[27] However, recent studies demonstrate that nonfibrillar oligomeric Aβ species are more toxic and better correlate with the severity of the disease and synaptic loss than the fibrillary Aβ deposits in AD brain.[27]

2.2.2 Tau protein aggregation in AD

The presence of tau protein aggregates is another feature found in brains of AD patients. Tau is a microtubule stabilizing protein in axons, which binds with microtubules and favors its polymerization. Tau is more abundant in axons and the size of the tau oligomers can be varying between 94 - 1800 kDa with 3 - 10 monomers in a multimeric structure. It has been found that a tau protein in normal brain consists of 2 - 3 phosphates per mole of protein, whereas in AD condition, this could rise up to 3 - 4 fold hyperphosphorylation compared to that in normal brain. Phosphorylation takes place at serine and threonine residues. When tau protein undergoes hyperphosphorylation, its conformation changes and tends to detach from the microtubules, and accumulates in the cell soma. These insoluble aggregates form prefibrillar oligomeric and fibrillary aggregates such as paired helical filaments (PHFs) and neurofibrillary tangles (NFTs).[23,28-32] Some recent studies show that, isolated oligomers have the potential to induce memory impairments and synaptic dysfunction than monomers or NFTs.[33] However, neurofibrillary tangles truncated at

positions Glu 391 and Ser 421 has resulted apoptosis in cultured cells.[34] When tau gets deviated from its native form, it can self-aggregate and causes a self-propagation of taupathy. Another factor responsible to AD in related to tau proteins is the impairment of the protein clearance mechanisms such as the chaperone/ubiquitin proteasomal and authophagy-lysosomal pathways.[35,36]

2.2.2.1 Kinases in tau hyperphosphorylation

Since hyperphosphorylated tau is associated with AD, the attention has also been given to the kinases that are involved in the phosphorylation of tau proteins.[34] The abnormally phosphorylated tau at over 30 serine/threonine residues and proline directed sites have found to be substrates for several protein kinases.[34] These kinases include glycogen synthase kinase-3 (GSK-3), cyclin dependent protein kinase-5(cdk5), protein kinase A (PKA), calcium and calmodulin-dependent protein kinase-II (CaMKII), mitogen activated protein (MAP) kinase ERK 1/2, and stress-activated protein kinases.[37-41] Among all these kinases, the expression of GSK-3β and cdk5 are higher in brain and these two enzymes have been found to involve in phosphorylation of tau in a larger number of sites. In addition, the kinases belong to MAP kinase family such as ERK1, ERK2, p70S6 and the stress activated kinases (JNK and p38) have been associated with neurofibrillary degeneration in AD by phosphorylating tau at several different sites.[42] Tau protein is also associated with abnormal glycosylation. It is implicated that abnormal glycosylation promotes the phosphorylation of tau by kinases such as PKA, GSK3β and cdk5.[37,38]

2.2.3 Diabetes mellitus and the risks of AD

In addition to the above facts, some researchers showed evidences that diabetes mellitus may also contribute to AD. Generally, diabetic people have higher incidence of cognitive impairment and

therefore, they are at about 50 - 60% of increased risk for AD.[43-45] However, there's a complex mechanism associated with these two diseases and the exact relationship is not known yet. Studies have been done so far illustrate that key components which link these two diseases are insulin resistance and inflammatory signaling pathways which have close relationship with hyperphosphorylation of tau protein and abnormal regulation in the clearance process of amyloid beta in comparison to the non-diabetic AD cases.[46,47] Deposition of Aβ plaques, mitochondrial dysfunction and inflammatory stress in peripheral tissues are common features between AD and type 2 diabetic mellitus (T2DM) patients.[43-45] However, the underlying factors that governed those conditions in T2DM are remain unknown yet.

T2DM is caused by selective destruction of pancreatic β cells and associated neuropathy as a result of the aggregation of neuroendocrine hormone called amylin. It is the most common form of diabetes and more than 95% of the patients show local amyloid deposits which is mainly composed of amylin. Amylin is an amyloid polypeptide with 37 amino acids and derived from proteolytic cleavage of 89-amino acid islet amyloid precursor protein or proamylin.[46,47] In diabetic patients it has been found that amylin is deposited in temporal lobe gray matter which represent a major part of the central nervous system. In addition, these amylin aggregates can be co-localized with Aβ aggregates to form amylin-Aβ plaques. Previously, it was believed that glucose uptake into the brain was insulin independent and mediated only by GLUT-1 and GLUT-3 transporters. However, later scientists have found out that, there are insulin sensitive insulin transporters present both in the brain and the blood brain barrier and they are significantly decreases in AD. Moreover, the substrate for insulin receptor, which is insulin receptor substrate-1 also binds to the amyloid precursor protein (APP). In addition, insulin degrading enzyme not only degrades insulin but also

degrades APP, Aβ and amylin and presence of insulin and insulin like growth factor (IGF-1) have found to prevent amyloid formation by decreasing APP in AD.[46,47] Recent studies also proposed that the sequences of $A\beta_{1-42}$ and $amylin_{1-37}$ have about 25% identity and 50% similarity and therefore, some domains in Aβ and amylin participate in the co-assembly of Aβ-amylin. It is believed that, chemical depletion of insulin and insulin like growth factor (IGF) signaling mechanism and oxidative injury can lead to cause AD-type neurodegeneration.

2.2.4 Mitochondrial dysfunction and the risks of AD

In addition to amyloid and tau associated mechanisms, other factors such as mitochondrial dysfunction and oxidative stress have also connected with AD.[48-50] Mitochondria are involved in critically regulating cell death, a key feature of neurodegeneration. Since the major risk factors for AD is aging, studies have indicated that increased disorganization of the mitochondrial structure, damage to the components of the mitochondria, decline in mitochondrial oxidative phosphorylation, mutations in mitochondrial DNA such as large scale deletions and point mutations, accumulation of mitochondrial DNA mutations, and oxidative stress significantly contribute to aging and therefore there could be some associations of mitochondria for AD.[48-50] Mitochondria are one of the most metabolically active organelles in the cell. It has been found that several key mitochondrial components such as key enzymes of oxidative metabolism, including α-ketoglutarate dehydrogenase complex (KGDHC), pyruvate dehydrogenase complex (PDHC), cytochrome oxidase (COX) have been reduced in AD. Notably, the degree of dementia has been found to correlate well with the reductions in KGDHC activity than with the amount of senile plaques and neurofibrillary tangles (NFTs) in experiments performed with the brains of ApoE4-positive AD patients.[48-50]

Recent studies hypothesize that there is a relationship between Aβ with the mitochondrial dysfunction. It has been proposed that mitochondria associated and/or intra-mitochondrial Aβ may directly cause neurotoxicity.[51] However, the origin of mitochondrial Aβ is not well understood. The fact that, so far researchers were not able to find the beta-secretase activity inside the mitochondrial membrane, suggests two alternatives: (1) the products of beta-secretases are transported to the mitochondria; and (2) Aβ peptide is generated completely on a separated site and then moved inside the mitochondria.[52] Some of the studies suggest that Aβ enters the mitochondria by binding with some proteins such as alcohol dehydrogenase. Recently, it was found out that Aβ moves inside the mitochondria using the mitochondrial outer-membrane translocase (TOM) and predominantly located in the inner membrane's cristae.[53] In vitro studies have shown that the interaction of Aβ with mitochondria induces a decrease in the respiratory states 3 and 4, and decrease in the activity of cytochrome c oxidase and some other Kreb's cycles enzymes.[52-55] Moreover, recent studies show that Aβ can inhibit the generation of mitochondrial ATP and alter the correct functioning of alpha-subunit of ATP synthase.[52] Moreover, studies performed via chronic administration of subtoxic doses of Aβ have revealed that it can inhibit the transportation of nuclear proteins to the mitochondria and results the impairment of its membrane potential and increase the production of reactive oxygen species (ROS) via activating the enzymes such as NADPH oxidase, xanthine oxidase and the A2 phospholipases.[52] All of these effects contribute to mitochondrial dysfunction and to the loss of synaptic function and plasticity which are highly believed as major mechanisms for memory loss in AD.[56-58] Therefore, understanding the role of mitochondrial dysfunction in the pathogenesis of AD could be highly relevant for the early diagnosis of AD.

2.2.5 The altered cholesterol metabolism in the pathogenesis of AD

New findings also demonstrate the involvement of cholesterol metabolism in the control of both the generation and/or accumulation of Aβ.[59] Moreover, the neurons with tangles were found to have higher levels of cholesterol compared to the healthy neurons.[60,61] Cholesterol is transported through the cell membrane via ATP-binding cassette subfamily A member 1 (ABCA1), cholesterol transporters and they are also shown to mediate the secretion of Aβ from the cells.[62] Acetyl-coenzyme A acetyltransferases (ACAT) is essential for the regulation of intracellular cholesterol homeostasis and distribution of cholesterol throughout the body by converting free cholesterol to neutral cholesteryl ester for storage.[63] Therefore, the inhibition of ACAT will reduce the formation of cholesterol ester and increasing the level of free cholesterol inside the cells, which then induce cholesterol efflux by increasing the cholesterol transporter gene ABCA1. Thus, ACAT inhibitors are good candidates for regulating of amyloid pathology by regulating cholesterol homeostasis.[64-66]

The lead compounds CP2 and TP70 possess inhibitory activity against ACAT along with the upregulation of ABCA1 gene promoting the efflux of cholesterol, increasing the efficiency of cholesterol transporters, restoring axonal trafficking, and enhancing hippocampal synaptic activity.[15] TP70 also protects the neuronal cell death. In addition, both CP2 and TP70 were found to have high oral bioavailability, excellent blood brain barrier permeability and low toxicity. These synergistic cellular actions could be potential mechanisms underlying the protective effects *in vivo*.

2.3 Pharmacokinetic analysis using HPLC

High performance liquid chromatography (HPLC) is one of the most widely used analytical techniques for quantifying and analyze compounds administered via various methods. The

technique of HPLC separates the compounds through the mass transfer of analytes between stationary and mobile phases. HPLC is divided into two categories such as normal and reverse phase. In the normal phase chromatography, a polar stationary phase is used to separate polar analytes such as amines, anilines, nitroaromatics, phenols and pesticides, etc., whereas in reverse phase, non-polar stationary phase (long chain alkyls such as C-18 or C8) used along with the isocratic elution of a mobile phase mixture of two solvents such as water and another solvent of lower eluting strength (methanol, acetonitrile) to separate moderately polar to non-polar compounds. Mobile phase composition plays an important role in reverse phase HPLC (RP-HPLC). Most commonly used RP-HPLC solvents are water, acetonitrile (ACN), methanol (MeOH) and tetrahydrofuran (THF) and have a low UV cut-off of 200, 210, 280 nm respectively. HPLC method can be set up for either isocratic or gradient elution. In isocratic elution the mobile phase composition remains constant throughout the analysis. In gradient elution, the mobile phase composition varies during the analysis and provides better resolution and decrease analysis time. The development of a proper chromatography method for the analysis is a major criteria when carrying out HPLC analysis. The most important parameters to consider during method development are resolution, sensitivity, precision, accuracy, limit of detection, limit of quantitation, linearity, reproducibility, time of analysis and robustness of the method.[67-69]

Pharmacokinetics is the study of drug disposition in the body and it provides a mathematical basis to study the time course of drugs and their effects in the body (or their disappearance or metabolism in the body). The pharmacokinetics processes such as absorption, distribution, metabolism and elimination are the major factors need to be considered and the plasma concentration of the drug will rise and fall according to the rates of these processes. These pharmacokinetics processes

usually referred as ADME (absorption, distribution, metabolism and elimination) and a fundamental understanding of these parameters is required to understand the concentration of the drug in the body when administered.[69,70]

Absorption of a drug refers to the movement of the drug into the blood stream, with the rate dependent on the physical characteristics of the drug and its formulation. A drug which is not given directly into the blood stream via intravenous administration, the drug need to be transported from the site of administration into the systemic circulation in order for it to be considered as absorbed. Distribution of a drug refers to the movement of a drug to and from the blood and various tissues of the body such as fat, muscle and brain tissues. Drug distribution is determined by the blood flow to the tissues and the ability of the drug to enter the vasculature system. The distribution of the drug across the membranes involves one or more of the several processes such as passive diffusion, filtration, bulk flow, active transport, filtrated transport, ion-pair transport, endocytosis and exocytosis. Elimination of a drug from the body is depend on two processes: biotransformation or metabolism of the drug to one or more metabolites mainly in the liver and the excretion of the parent drug or its metabolites which is mainly occurred in the kidney.[71,72]

Once the drug is absorbed into the blood stream, the drug then distributes through the body. As the blood recirculates, the drug moves from bloodstream into the body's tissues. The different organs and tissues can receive varying amount of doses of the drugs and the drug can remain for a varying amount of time in each organ and tissue. The distribution of drug among tissues of various organs depend on several parameters such as vascular permeability, regional blood flow, cardiac output, perfusion rate of the tissue, ability of the drug to bind to plasma proteins and the

lipophilicity and the solubility of the drugs. The drug can be easily distributed in highly perfused organs such as the liver, kidney and heart, whereas it distributed in small quantities through less perfused tissues such as muscles, fat and peripheral organs. The unbound drug present in plasma is moved from plasma to the tissues until the equilibrium is established. Understanding the distribution of a compound or its metabolites in biological fluids, primarily blood, plasma, serum, urine or tissue extracts is a major aspect of bioanalysis and is a subject of prime importance in the treatment of various diseases. The determination of the drug concentration in biological fluids in animals and man is vital to understand the time course of drug action and it is an essential part of the drug discovery and development process. Currently, the main technique used in quantitative bioanalysis is HPLC which is coupled with tandem mass spectrometry (HPLC-MS/MS) of electron spray ionization (ESI) or atmospheric pressure chemical ionization techniques (APCI).[70-72]

A compound is considered to have a good pharmacokinetics (PK) profile if it contains following properties: (1) acceptable solubility, (2) completely absorbed with high bioavailability (F > 50 % for oral drug), (3) a low plasma clearance (<30% blood flow), long half-life ($t_{1/2}$ > 6 hours) and acceptable distribution of volume, (4) have linear kinetics and eliminates by renal excretion and hepatic metabolism pathways, and (5) a sufficient or at least acceptable safety margin (safety margin >10x, depending on different therapeutic targets).[70-73]

For studying the pharmacokinetic and bioavailability parameters for *in vivo* applications, the drugs are mainly administered through three main routes that include oral (po), intravenous (iv) and intraperitoneal (ip). A key factor that determines the desired route is whether the compound is intended for a local or systemic or parenteral effect. However, it is also necessary to administer

the compound to selected animal by the intended route of administration as well as the intravenously as parenteral administration usually produce the highest bioavailability of the substances due to the avoidance of the first pass effect of hepatic metabolism. In oral route of administration, the drug in the form of solution is administered directly into the lower esophagus or stomach by the use of a feeding needle or through drinking water, which what we used in our drug treatment. The maximum volume that can be fed by oral route is 10 mL/kg body weight of mice. In intravenous administration, substances are administered as a bolus or infusion directly into blood vessels on either an acute or chronic basis. Intraperitoneal route (IP) is also commonly used to administer substances into mice in which the drug in the form of a solution is injected into the peritoneal cavity (a space that surrounds the abdominal organs). The volume of the solution that can be administered depends on species, strain, route and frequency of administration, and composition of the solution. Generally, for IP injections, the maximum volume of drug solution is 2 mL in an adult mouse. [73]

There are some of the basic parameters that governs the effectiveness of the separation.[73-76]

2.3.1 Pharmacokinetics parameters

2.3.1.1 The retention factor (k)

This is used to describe the migration rate of the analyte on the column and defined as follows. Generally, components display an ideal separation under the conditions in which k is between 1 - 5. For the components which take a longer time to elute from the column compared to the mobile phase, will have a larger retention factor ($k > 20$). k can be manipulated by varying the composition of the mobile and stationary phases. [74-76]

$k = t_R - t_M / t_M$

t_R = retention time of a component

t_M = dead time (time required for the mobile phase to pass through the column)

When a drug is administered intravenously, the amount of drug in the body immediately after the injection is equal to the dose that applied, D_o. Due to the elimination processes such as metabolism and excretion, the amount of intact drug in the body is declined exponentially according to the following equation. [74-76]

$D = D_0 e^{-kt}$

D = the amount of drug in the body at time t

D_0 = the intravenous dose

k = elimination rate constant

2.3.1.2 Elimination half-life ($t_{1/2}$)

A more frequently used term to describe the rate at which a drug is removed from the body is the half-life. It is the time required for the amount of the drug in the body (plasma drug concentration) to decline to half of its value. Since k is inversely proportional to half-life, when the half-life is short, k is high and plasma concentration decline rapidly. This term can be calculated from elimination rate constant as well as the plasma drug concentration curve. The half-life and elimination rate constant are related by the equation as shown below

$t_{1/2} = 0.693/k$

2.3.1.3 Bioavailability (absorption)

This value is also called the absorption and it is the ratio of concentrations of a compound in blood following intravenous and oral administration. This value is usually expressed as a percentage and is defined as the fraction (F) of the administered dose of a drug that reaches the systemic circulation in an active form.

$$Absorption = D_{oral} / D_i * 100$$

D_{oral} = the distribution of a compound after oral administration

D_i = the distribution of the compound after intravenous administration

The bioavailability of orally administered drugs can be reduced by many biological and pharmaceutical factors. Biological factors include the effects of gut and liver enzymes, which can metabolize a drug during the course of its absorption and first pass through liver, effects of food and gastric acid, which can sequester or inactivate a drug. Pharmaceutical factors include the rate and extent of tablet disintegration and dissolution. A compound will have a low bioavailability if it is associated with high metabolic clearance which results from an extensive first-pass effect.

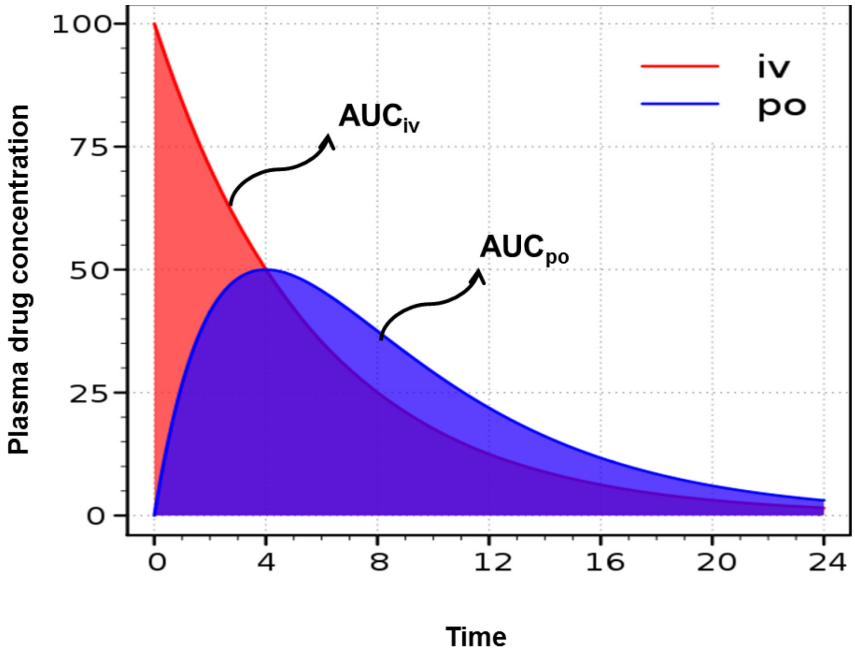

Figure 2.2: A standardized plasma drug concentration curve with different time intervals after oral or intravenous administration of a drug.[75]

The oral bioavailability of a drug is determined by dividing the area under the curve (AUC) of an orally administered dose of the drug by the AUC of an intravenously administered dose of the same drug. Figure 2.2 shows an example[75] of the standardized plasma drug concentration after oral and iv administration of a particular drug over the times. Y axis represents the plasma drug concentration and it is often denoted in µg/mL or mg/L. The X-axis represents the time scale usually in hours. The main parameters of the plasma drug concentration curve are the maximum plasma concentration (C_{max}), and the time required to reach C_{max} which is denoted by T_{max}. AUC represents the measure of the total amount of drug during the time course for a particular administration method.[74,75] The bioavailability (F) can be defined as follows.

$$\text{Bioavailability } (F) = AUC_{po} \big/ AUC_{iv}$$

AUC_{po} = the AUC of the oral administration

AUC_{iv} = the AUC of the intravenous administered drug

In order to calculate the AUC from the Figure 2.2, first, the area of each trapezoid need to be calculated. Finally, the addition of all trapezoid areas will represents the AUC.

If the curve represents an increasing trend

$$Area_{trapezoid} = 1/2(C_1 + C_2)\ (t_2 - t_1)$$

If the curve represents a decreasing trend

$$Area_{log} = (C_1 - C_2)\ (t_2 - t_1)/(lnC_1 - lnC_2)$$

C = drug concentration

t = time

The bioavailability of the drugs administered via other routes can also be determined in the same manner as the bioavailability of drugs administered orally. [74-76]

2.3.1.4 Clearance

Clearance is the ratio of the dose to the AUC. Therefore, higher the AUC for a given dose, the lower the clearance. Clearance is also a function of the distribution and elimination. It can also be defined as follows.[74-76]

$$Clearance = dose / AUC$$

$$Clearance = Vk$$

V = volume of distribution (volume of the fluid in which the dose is initially diluted)

k = elimination constant

2.4 Results and discussion

2.4.1 Distribution of TP70 in various organs of mice

Pharmacokinetic and bioavailability studies of TP70 was carried out by quantifying the amount of TP70 in plasma and other vital organs such as brain, heart, liver, lungs, spleen and kidney. The purpose of these studies is to determine the optimal dosage of TP70 prior to carry out the efficacy studies of TP70 in AD mice. A dose of 25 mg/kg of TP70 in 2% DMSO in 0.5% HPC (based on *in vitro* studies) was administered to the male, 3 months old WT C57BL/6NHsd (Harlan) mice by intraperitoneal route (ip route). A detailed description about the administration of TP70 into mice and analytical procedures are provided in the experimental section of this chapter. After carrying out the HPLC analysis for plasma and each organ, the distribution of TP70 in plasma and other organs were determined by plotting a calibration graph with the ratios of peak areas of TP70 to 4-methoxyphenol (as an internal standard in the HPLC measurement) vs. molar ratios of TP70 to 4-methoxyphenol as mentioned in the experimental section of this chapter. The calibration graph for TP70 is shown in Figure 2.3.

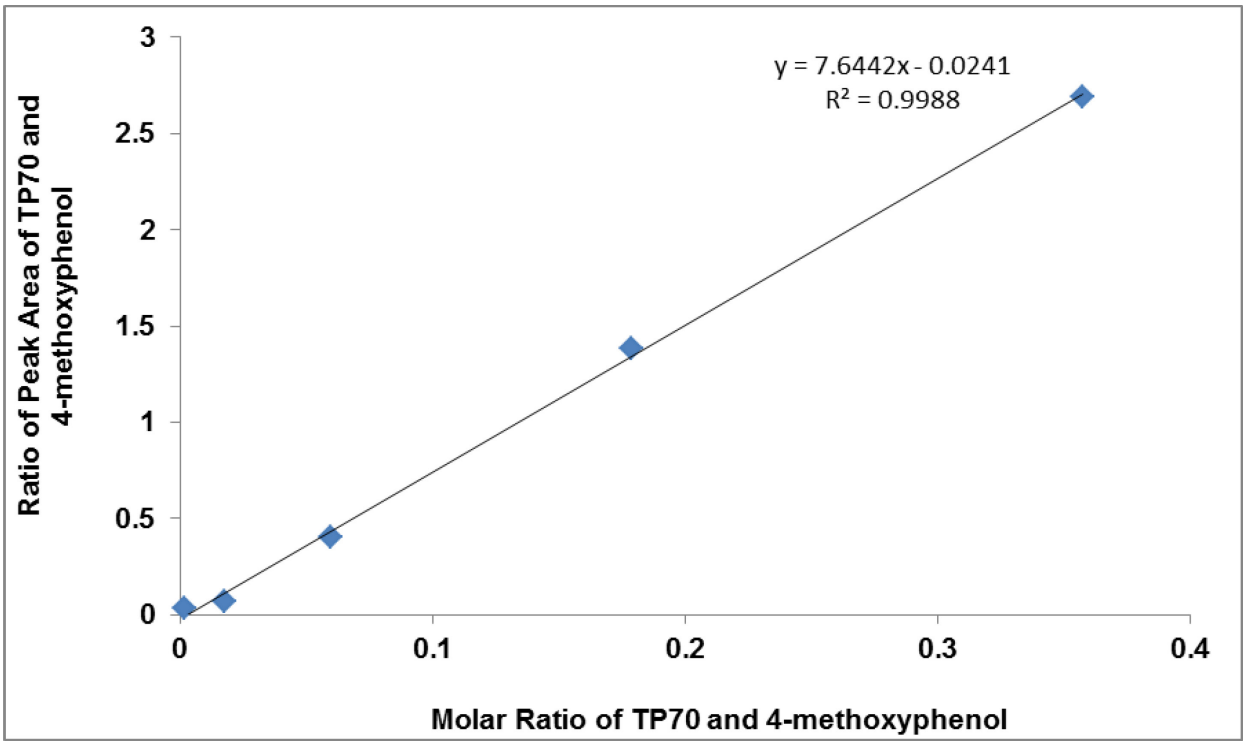

Figure 2.3: Correlation of ratios peak areas of authentic 4-methoxyphenol and pure TP70 from HPLC chromatogram and molar ratios of TP70 and 4-methoxyphenol injected.

The calibration graph was obtained by injecting a volume of 100 µL of solutions of different concentrations of authentic TP70 and pure 4-methoxyphenol into the HPLC. The peak areas corresponding to TP70 and 4-methoxyphenol was integrated from HPLC chromatogram, and the ratios of peaks were obtained. The results of the ratios of HPLC peak areas and the ratios from TP70 and pure 4-methoxyphenol concentrations were plotted, and a linear correlation line was obtained from the graph.

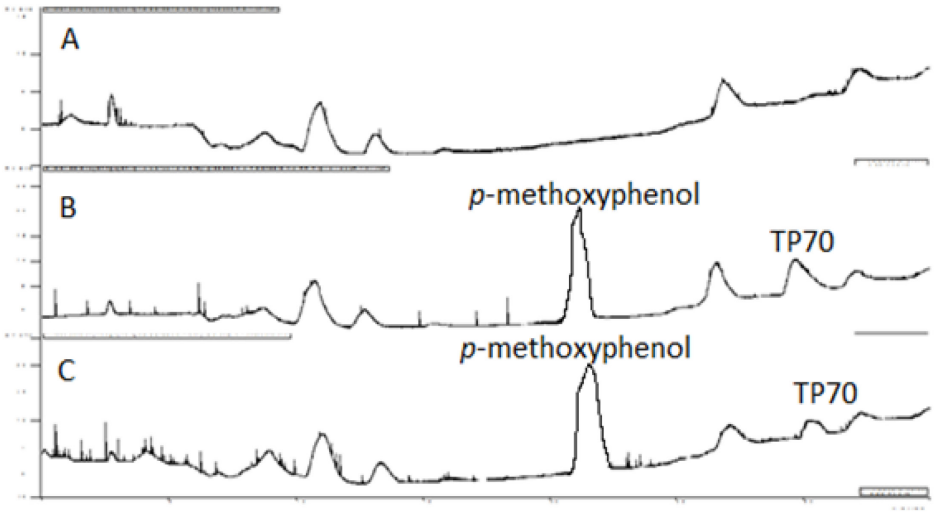

Figure 2.4: Representative HPLC chromatograms. A is the HPLC chromatogram of the control (kidney without TP70). B is the HPLC chromatogram of 1:1 mol ratio of 4-methoxyphenol and pure TP70. C is the HPLC chromatogram of the kidney extract with a known amount of 4-methoxyphenol. The peak at 30 minutes retention time in C has the same mass as pure TP70 which was confirmed by mass spectrometry.

The amount of TP70 in tissue extracts were determined by calculating the peak areas ratios of TP70 to 4-methoxyphenol from the HPLC chromatogram. Figure 2.4.C represents the HPLC chromatogram of the tissue (kidney) extract injected with the known amount of 4-methoxyphenol and the peak at 30 minute corresponds to the amount of TP70 in the tissue extract and had the same retention time as that of authentic TP70. The representative mass spectrum of the eluent corresponding to the peak at 30 minute is highlighted in Figure 2.5.

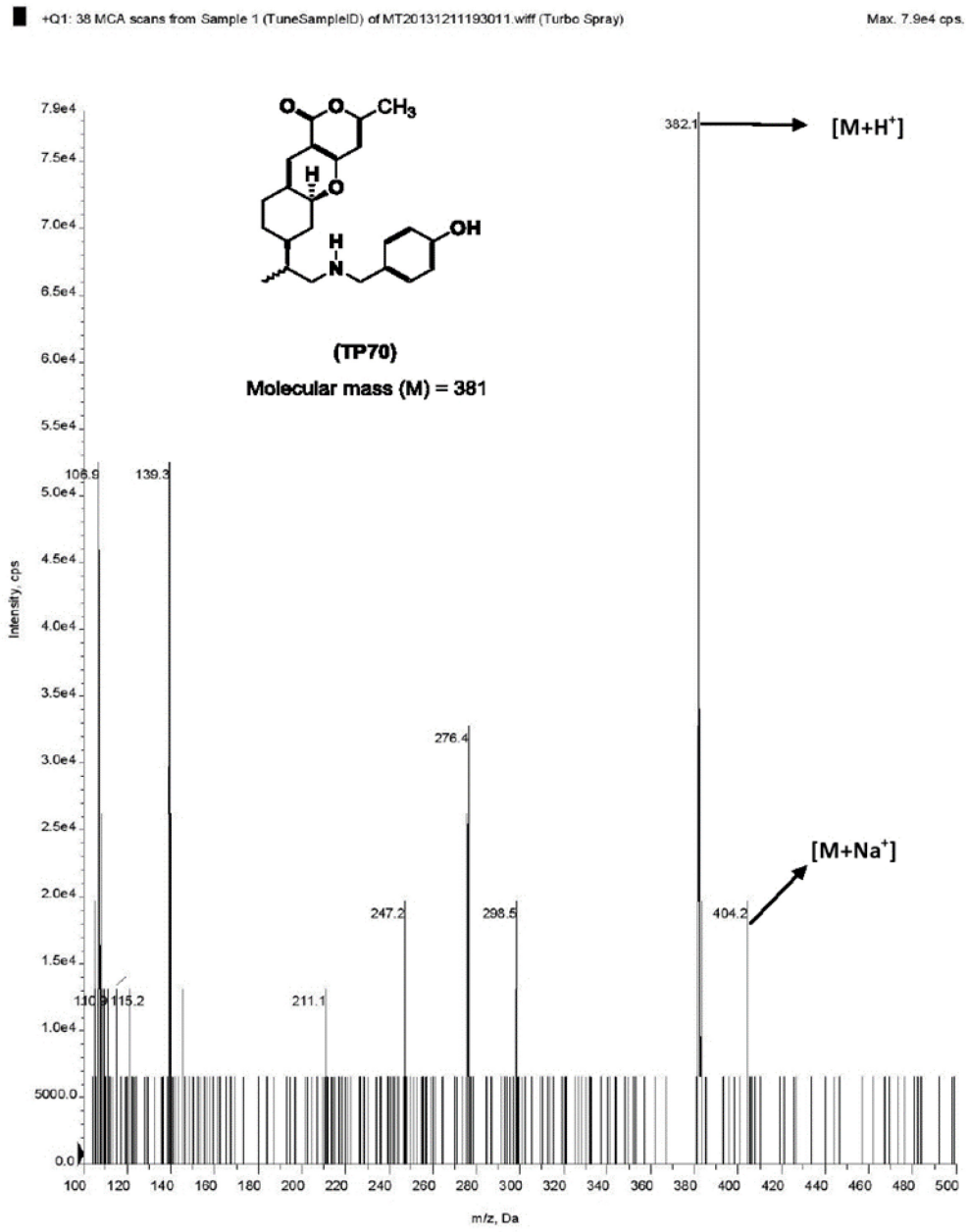

Figure 2.5: Mass spectrum of the eluant corresponding to the peak at 30 minutes (of Figure 2.4.C) which is identical to pure TP70.

The summary of the results of the amounts of TP70 in various organs and the half-life values are shown in Table 2.1 and Figure 2.6.

Table 2.1: Results of PK study of TP70 (25 mg/kg body weight; ip route; n = 3) and distribution in various organs of mice.

Time (hr)	Average concentrations of TP70 (mg/L)							
	Plasma	Brain	Heart	Liver	Lung	Kidney	Intestine	Spleen
0.5	5.6 ± 0.5	18.6 ± 1.9	10.9 ± 0.65	13.4 ± 2.8	11.8 ± 1	16.7 ± 1.4	12.3 ± 3.3	11.3 ± 0.4
1	3.7 ± 0.03	12.5 ± 1	0.9 ± 0.38	18.4 ± 4.9	5.3 ± 2.3	11.2 ± 1.3	8.8 ± 1.9	7.8 ± 1.6
2	0.6 ± 0.07	8.5 ± 0.2	0.2 ± 0.04	5.7 ± 1.8	3.8 ± 1.3	9.9 ± 2	3.5 ± 2.2	2.5 ± 1.98
4	0.2 ± 0.13	3.6 ± 0.4	0.03	4.9 ± 1.4	2.8 ± 0.7	7.2 ± 3.7	2.4 ± 0.28	0.8 ± 0.43
6	0.02	2.5 ± 0.4	0.01	2 ± 0.8	0.6 ± 0.5	6 ± 1.4	0.2 ± 0.25	0.15
24	0	1.12 ± 0.08	0	0	0	0.8 ± 0.6	0	0
$t_{1/2}$ (hr)	1.06	1.36	0.6	2	1.57	4.2	1.5	1.3

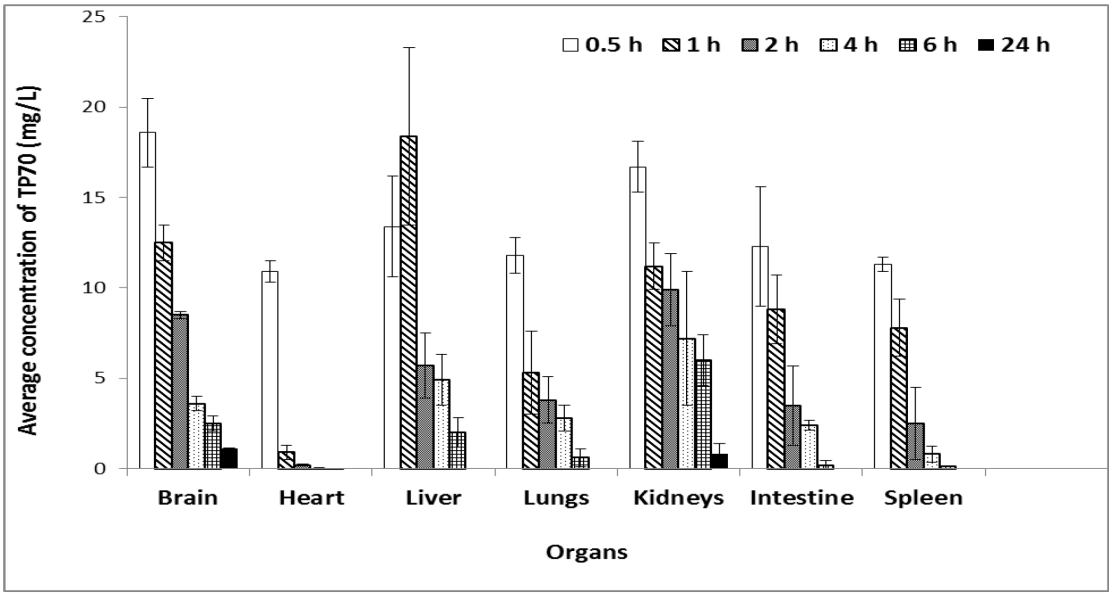

Figure 2.6: Results of PK study of TP70 (25 mg/kg body weight; ip route; n = 3) and distribution in various organs of mice. Each bar represents the average concentration of TP70 measured from 3 mice and is provided with (±) standard error.

The distribution of TP70 was analyzed in 0.5, 1, 2, 4, 6 and 24 hours intervals for each organ. The TP70 was detected in major organs such as brain, heart, liver, lungs, spleen and kidney in 0.5 hours from the ip administration. Out of these organs, liver had the highest distribution of TP70 with the respective amount of 65 μg when considering the total amount of drug over 24 hours and brain had the next higher level of drug which implies the good penetration of the drug through the blood brain barrier. It can be seen that, the amount of TP70 gradually decreases from 0.5 hour to 6 hours in most of the organs. However, in the heart, the concentration of TP70, seems to be dramatically changes from 0.5 hour to 1 hour. Moreover, the amount of TP70 was decreased to 1.12 mg/L in brain and 0.8 mg/L in kidney after 24 hours from the administration and there had no detectable amount in other organs such as heart, lungs, intestine, spleen and liver. Notably, TP70 accumulates in the brain in effective quantity. These results indicate that TP70 can be absorbed, distributed and metabolized in various tissues successfully and able to excrete from the body of mice.

2.4.2 Pharmacokinetics (PK) and bioavailability of TP70 in plasma of mice/rats from the intravenous (iv) and oral gavage (po) administration

The quantification of TP70 in plasma samples were carried out for mice samples. A dose of 25 mg/kg of TP70 dissolved in 2% DMSO in 0.5% HPC was administered to the male, 4 – 6 months old WT C57BL/6 mice (~ 25 g) either intravenously (iv) or orally (po). The distribution of TP70 in plasma samples were analyzed by withdrawing blood from tail vein at 5, 15, 30, 60, 120, 240, and 360 minutes' intervals.

To further examine the pharmacokinetics of TP70 in relatively larger species, rat models were used. A dose of 25 mg/kg of TP70 was administered to the male, 3-months old WT Sprague-

Dawley rats (175 – 235 g) by iv and po routes. TP70 in plasma samples were determined by plotting a calibration graph with the ratios of peak areas of TP70 to 4-methoxyphenol vs. molar ratios of TP70 to 4-methoxyphenol as mentioned in the experimental section of this chapter.

Tables 2.2, 2.3 and Figures 2.7, 2.8 summarize results of PK and bioavailability of TP70 in plasma from the iv and po administration for mice and rats.

Table 2.2: Results of PK study of TP70 (25 mg/kg body weight; oral and iv routes; n = 3) in plasma for mice samples.

	Average concentration of TP70 in plasma (mg/L)	
	po route	**iv route**
5		16.6 ± 6.1
15	2.8 ± 0.09	10.2 ± 4
30	3.9 ± 0.14	8.2 ± 3.5
60	6.9 ± 0.17	3.7 ± 0.8
120	4.2 ± 0.19	2.02 ± 0.6
240	2.4 ± 1.37	1.8 ± 0.5
360	1.2 ± 0.23	0.9 ± 0.3
AUC (mg.min/L)	678	989
F	0.68	1
$t_{1/2}$ (hours)	2.05	1.06

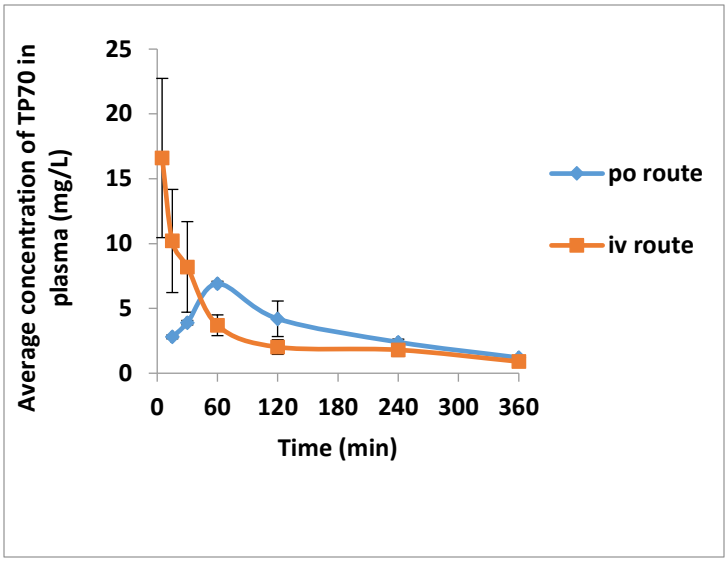

Figure 2.7: Results of PK study of TP70 (25 mg/kg body weight; oral and iv routes; n = 3) in plasma of mice. Each bar represents the average concentration of TP70 measured from 3 mice and is provided with (±) standard error.

Table 2.3: Results of PK study of TP70 (25 mg/kg body weight; oral and iv routes; n = 3) in plasma for rat samples.

Time (min)	**Average concentration of TP70 in plasma (mg/L)**	
	po route	**iv route**
5	0	39.4 ± 6.86
15	7.9 ± 3.4	34.9 ± 2.13
60	19.2 ± 0.62	18.2 ± 1.56
120	13.6 ± 2.63	15.4 ± 3.12
240	9.2 ± 2.71	12.4 ± 2.33
360	5.6 ± 0.95	5.5 ± 1.82
AUC	3330	5221
F	0.64	1
$t_{1/2}$ (hours)	2.98	2.3

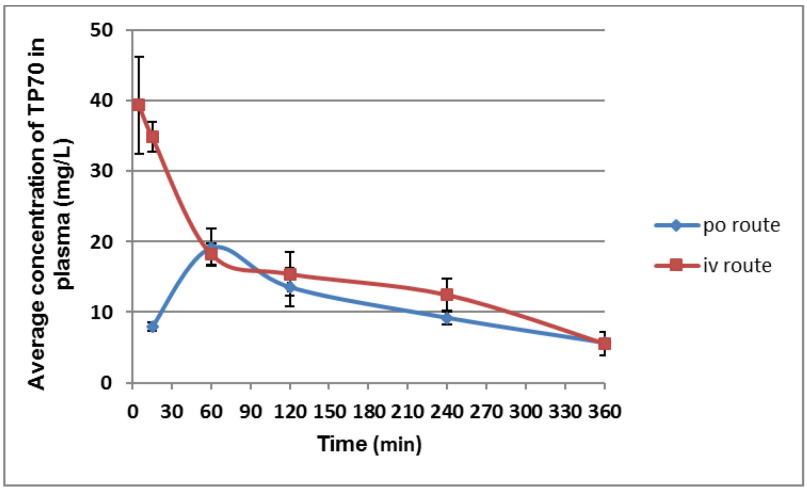

Figure 2.8: Results of PK study of TP70 (25 mg/kg body weight; oral gavage and iv routes; n = 3) in plasma for rats. Each bar represents the average concentration of TP70 measured from 3 mice and is provided with (±) standard error.

As shown from Table 2.2 and Table 2.3, the highest amount of TP70 can be detected in plasma after 5 minutes from the iv administration for both mice and rat species with a concentration of 16.6 mg/L and 39.4 mg/L respectively. The time required to detect TP70 in plasma was higher when the drug was administered via po route and the highest concentration of TP70 can be seen after 1 hour for both mice and rat species with a concentration of 6.9 mg/L and 19.2 mg/L respectively. For the iv route in mice, at first the drug concentration reduces quickly from 16.6 (mg/L) at 5 minutes to 3.7 (mg/L) at 1hour; then, it slowly decreases to 0.9 mg/L within 6 hours of the drug administration. In contrast, there is a quick increase from 15 minutes to 1 hour for TP70 with a concentration of 2.8 (mg/L) and 6.9 (mg/L) respectively, when po administration in mice. After reaching the highest concentration of TP70 at 1 h, TP70 was found decrease steadily from 1 hour to 6 hours. A similar pattern can be seen for rat samples for both iv and po route administration. Moreover, there's a higher amount of TP70 can be seen in rat samples than that of mice samples at 6 hours for both iv and po route administration. Bioavailability (*F*) and elimination

half-life ($t_{1/2}$) for po route is nearly similar for both species, whereas, $t_{1/2}$ values for iv route is relatively higher for rat samples compared to that of mice. Overall, these results indicate that TP70 has good clearance property and the values of area under the curve (*AUC*) and bioavailability (*F*) point out that the drug can be administered for efficacy evaluation *in vivo*.

2.4.3 Pharmacokinetic (PK) and bioavailability of TP70 in plasma and brain of the AD mice administered with TP70 in drinking water

Apart from the studies carried out for wild type mice (WT mice), we further examined the pharmacokinetics and bioavailability of TP70 in AD mouse transgenic models. Since, WT mice may not completely represent the PK profile of AD mouse models, the following experiment was conducted using APP/PS1 AD mouse models. APP/PS1 (amyloid precursor protein/presenilin 1 hybrid) mouse contains human transgenes for both APP bearing the Swedish mutation and PSEN1 containing an L166P mutation, therefore good candidates for represent AD mouse models. A dose of 25 mg/kg (mice body weight) of TP70 in 6 ml of drinking water per mouse was administered for male, 10-12 month-old APP/PS1 mice housed in cages consisting of 3 - 4 mice per cage. Each group cage was supplied with a bottle of water with dissolved TP70 (70.7 mg TP70 per 504 mL of water) and mice were allowed to drink the TP70 water freely. Blood samples were collected from each mouse on day 7, day 14 and 4 months after the initial introduction of TP70 water and analyzed for quantifying the amount of TP70 on day 7, day 14 and 4 months.

Table 2.4: Results of PK study of TP70 (25 mg/kg body weight; drinking water) in plasma samples of APP/PS1 mice.

Mouse ID	Concentration of TP70 in plasma (mg/L)		
	Day 7	**Day 14**	**4 months**
P1- 1	1.96	0.94	2.55
P1- 2	1.26	2.29	1.92
P1- 3	1.29	5.18	5.46
P1- 4	2.25	3.99	-
Average concentration of TP70 in plasma- **cage 1** (mg/ L)	**1.69 ± 0.5**	**3.08 ± 1.86**	**3.31 ± 1.89**
P5 - 4	1.17	3.86	0.83
P7 - 5	1.70	2.64	1.42
P7 – 6	4.40	5.03	2.29
P7- 7	1.15	1.99	0.90
Average concentration of TP70 in plasma- **cage 2** (mg/ L)	**2.11 ± 1.56**	**3.38 ± 1.35**	**1.36 ± 0.67**
P8 - 1	3.23	3.02	3.13
P8 – 7	1.35	1.39	2.00
P9- 11	1.76	1.23	3.64
Average concentration of TP70 in plasma- **cage 3** (mg/ L)	**2.11 ± 0.99**	**1.88 ± 0.99**	**2.92 ± 0.84**
Average concentration (mg/L)	**1.97 ± 0.24**	**2.78 ± 0.8**	**2.53 ± 1.03**

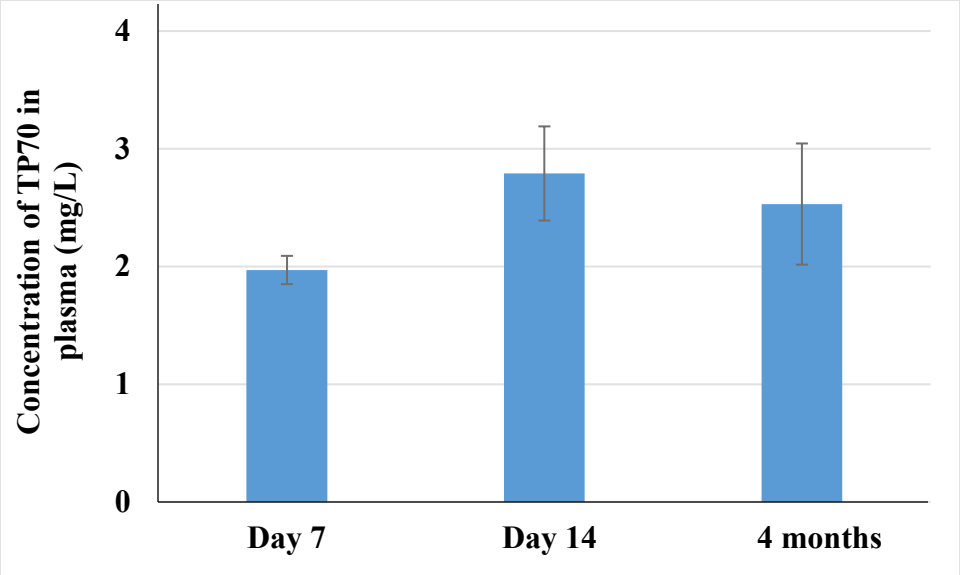

Figure 2.9: Results of PK study of TP70 (25 mg/kg body weight; drinking water) in plasma for AD mice following TP70 in drinking. Each bar represents the average concentration of TP70 measured from 11 mice and is provided with (±) standard error.

As depicted in Table 2.4 and Figure 2.9, treatment of TP70 for longer period of time seems to be well tolerated in AD mice. Concentration of TP70 seems to be gradually increasing from day 7 to day 14 with a concentration of 1.97 mg/L and 2.78 mg/L respectively. However, TP70 concentration in plasma is not significantly change from day 7 to 4 months. This indicates that, once it reached a particular range of concentration, plasma concentration remains nearly constant and TP70 may be distribute through the major organs of AD mice upon administrating for certain period of time. Therefore, TP70 seems to have a good clearance property.

To further study the cytotoxicity of TP70 for WT and AD mouse models over long period of time, a dose of 50 mg/kg of TP70 was administered via ip to wide type (WT) C57BL/6 and 5xFAD mice for 2 months. 5xFAD mice contains five familial mutations of human APP and PSEN1 genes to generate a large amount of Aβ42, thus represents a suitable AD mouse model. After 2 months,

animals were assessed for cognitive and motor function and sacrificed to quantify the amount of TP70 in plasma and brain tissues after 2 months.

Table 2.5: Results of PK study of TP70 (50 mg/kg) in plasma and brain of WT type and 5xFAD mice.

Mouse ID	Concentration of TP70 in plasma (mg/L)	Concentration of TP70 in brain (mg/L)
WT mice		
2B	4.92	2.44
3N	2.92	2.24
3B	2.51	2.46
Average concentration of TP70 in WT type mice (mg/L)	**3.45 ± 1.3**	**2.38 ± 0.12**
5XFAD mice		
2L	2.33	1.22
3R	4.91	1.58
3L	6.93	2.03
3R	11.93	1.73
Average concentration of TP70 in 5XFAD mice type mice (mg/ L)	**6.52 ± 4.1**	**1.64 ± 0.34**

There's a higher concentration of TP70 present in plasma at 2 months for AD mice compared to WT mice. When compared to plasma, brain has low concentration of TP70 in both WT and 5XFAD mice. Moreover, AD mice brain have relatively lower concentration of TP70 (1.64 mg/L)

compared to that of WT mice (2.38 mg/L). However, when considering the total concentrations of TP70 in both plasma and brain, AD mice have about 8.06 mg/L and WT mice have about 5.83 mg/L. Therefore, it seems that TP70 tolerates well in AD mice. Moreover, behavioral assessment of the mice suggests that high dose treatment of TP70 doesn't cause any adverse effects.

2.4.4 Distribution of CP2 in plasma of rats

Distribution of CP2 in the plasma were quantified for rat samples. A calibration graph was plot with the ratios of CP2 to 4-methoxyphenol vs. molar ratios of CP2 to 4-methoxyphenol as mentioned in the experimental section of this chapter. The calibration graph for CP2 is shown in Figure 2.10.

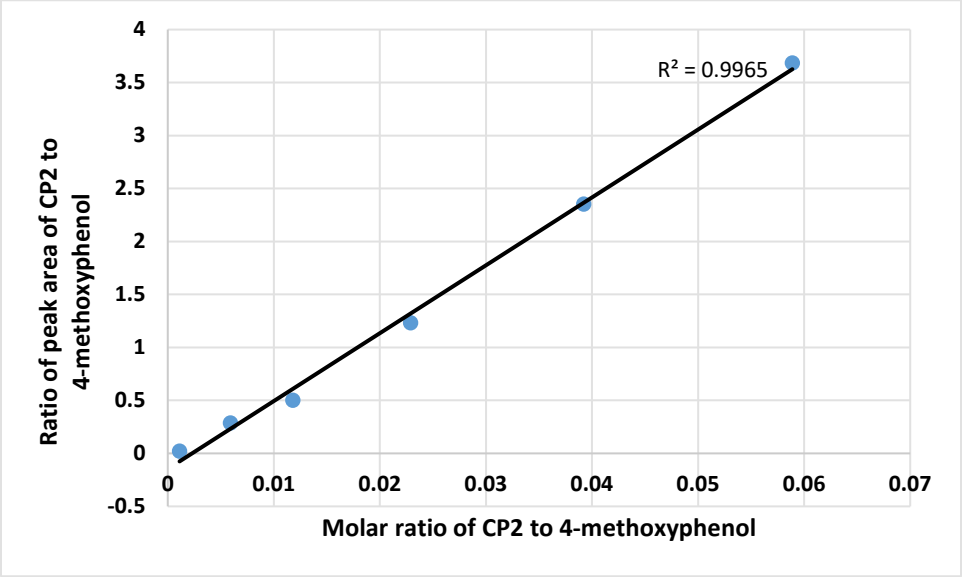

Figure 2.10: Correlation of ratios peak areas of pure CP2 and authentic 4-methoxyphenol from HPLC chromatogram and molar ratios of pure CP2 and authentic 4-methoxyphenol injected.

Solutions of 100 μL of various concentrations of pure CP2 and authentic 4-methoxyphenol (as an internal standard for measurement in HPLC) were injected into an HPLC, the peak areas corresponding to CP2 and 4-methoxyphenol were integrated from the HPLC chromatogram, and the ratios of the peaks were obtained. These results of the ratios of HPLC peak areas and the ratios from CP2 and 4-methoxyphenol concentrations were plotted, and a linear correlation line was obtained from the graph.

The amount of CP2 in the cell or tissues extract was calculated by determining the peak areas ratio of CP2 to 4-methoxyphenol and determining the number of moles of CP2 from the correlation graphs, as the number of moles of 4-methoxyphenol added to the cell and tissue extract was known. HPLC chromatograms of the plasma extract injected with a known amount of 4-methoxyphenol showed a peak at 14 minutes which had the same retention time compared to the authentic CP2 as shown in Figure 2.11.

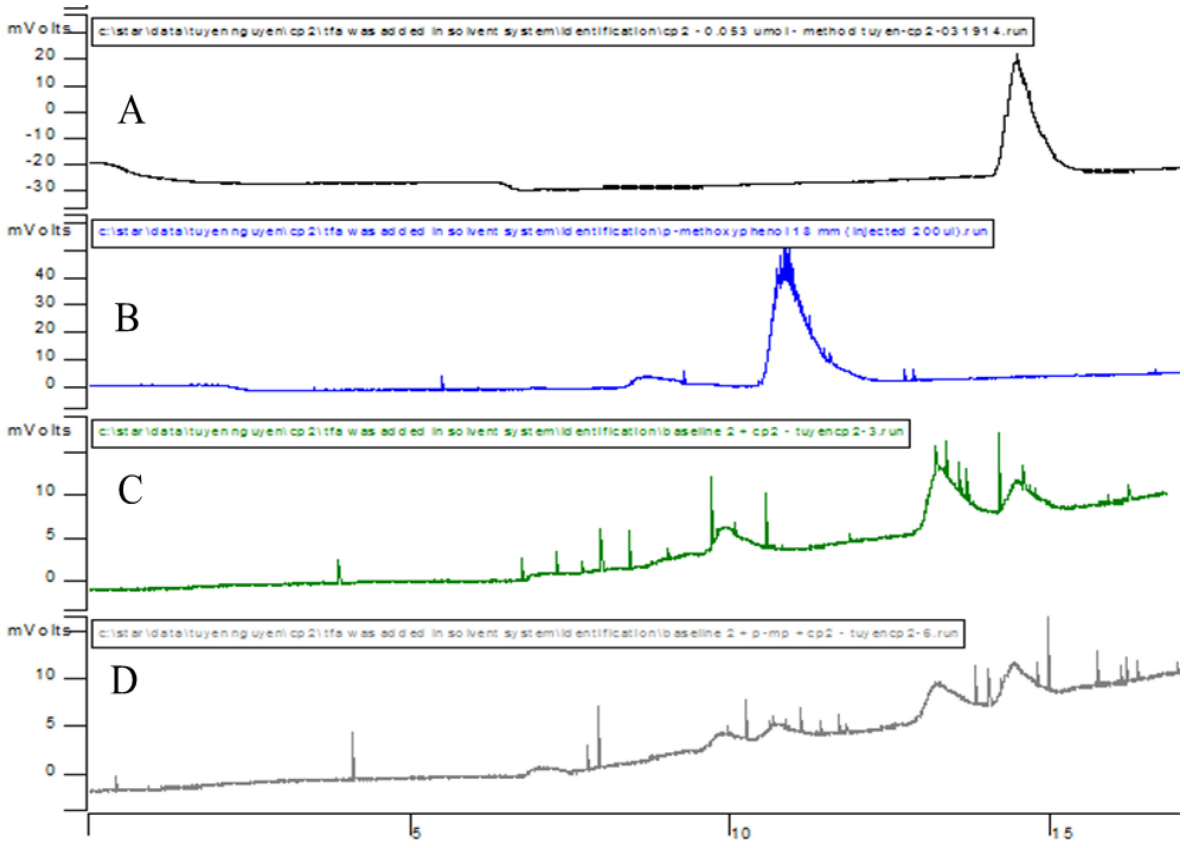

Figure 2.11: Representative HPLC chromatograms. A is the HPLC chromatogram of the pure CP2. B is the HPLC chromatogram of pure 4-methoxyphenol. C is the HPLC chromatogram of the control (plasma without CP2) with a known amount of CP2. D is the HPLC chromatogram of the plasma with a known amount of 4-methoxyphenol. The peak at 14 minutes retention time in D has the same mass as pure CP2 which was confirmed by mass spectrometry.

The representative mass spectrum of eluant corresponding to the peak at 14 minutes is highlighted in Figure 2.12.

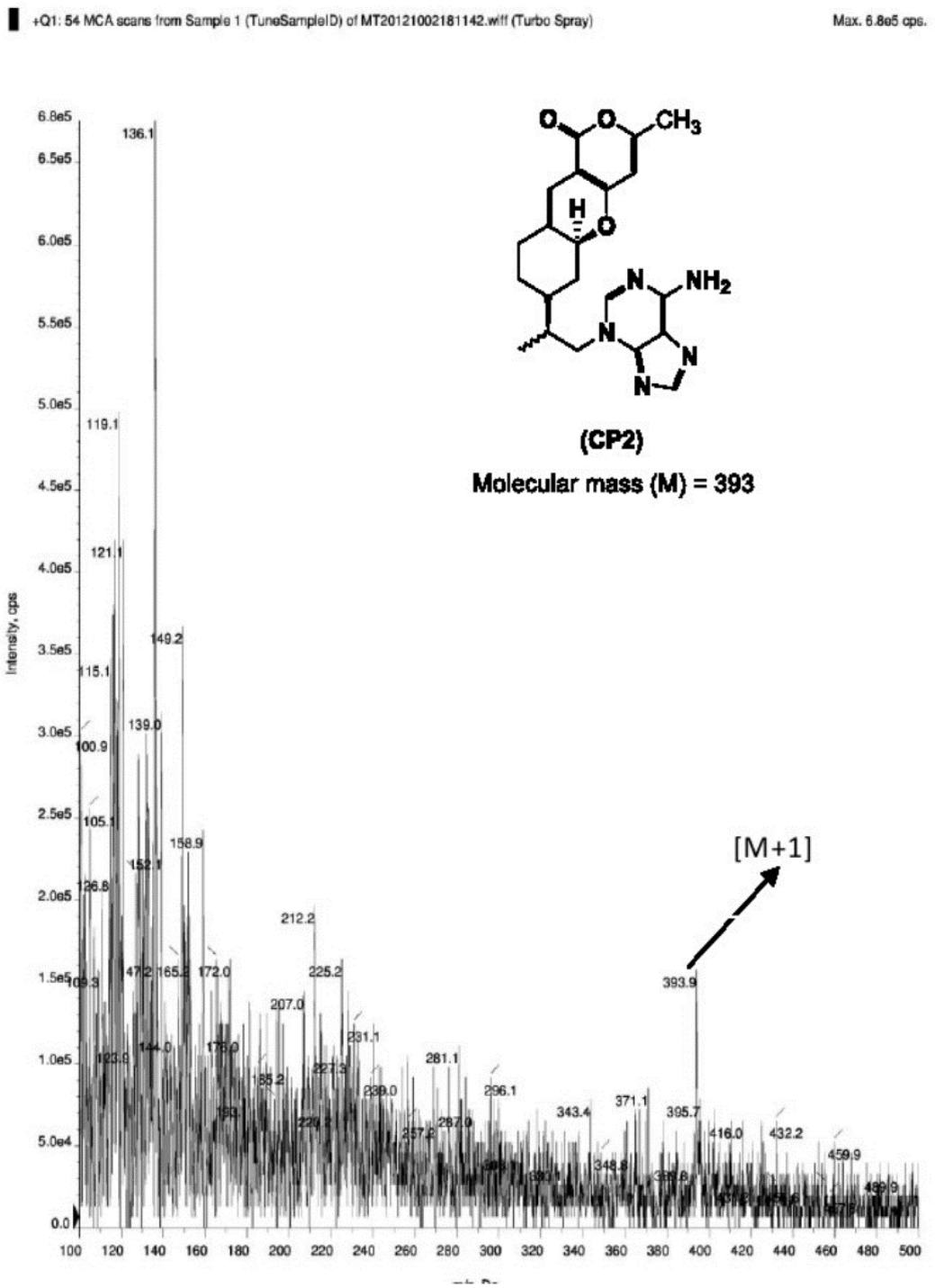

Figure 2.12: Mass spectrum of the eluant corresponding to the peak at 14 minutes (of Figure 2.11.D) which is identical to pure CP2.

2.4.5 Pharmacokinetic (PK) and bioavailability of CP2 in plasma of rats from the intravenous (iv) and oral gavage (po) administration

The quantification of CP2 in plasma samples were carried out for rats samples. A dose of 25 mg/kg (rat body weight) of CP2 dissolved in 2% DMSO was administered to the male, 3-month old WT Sprague-Dawley rats (175 g – 235 g) either intravenously (iv) or orally (po). The distribution of CP2 in plasma samples were analyzed by withdrawing blood from tail vein at 5, 15, 30, 60, 120, 240, and 360 minutes' intervals. CP2 in plasma samples were determined by plotting a calibration graph with the ratios of peak areas of CP2 to 4-methoxyphenol vs. molar ratios of CP2 to 4-methoxyphenol as mentioned in the experimental section of this chapter.

Table 2.6: Results of PK study of CP2 (25 mg/kg body weight) in rats; n =3.

Time (min)	Average concentration of CP2 in plasma (mg/L)	
	IV route	**po route**
5	24.84 ± 0.62	
15	9.86 ± 0.61	4.71 ± 0.4
60	6.57 ± 0.41	14.0 ± 1.7
120	3.99 ± 0.22	7.02 ± 0.63
240	1.24 ± 0.23	2.46 ± 0.83
360	0.32 ± 0.3	1.4 ± 0.37
AUC (mg.min/L)	1248.69	935.58
F	1	0.75

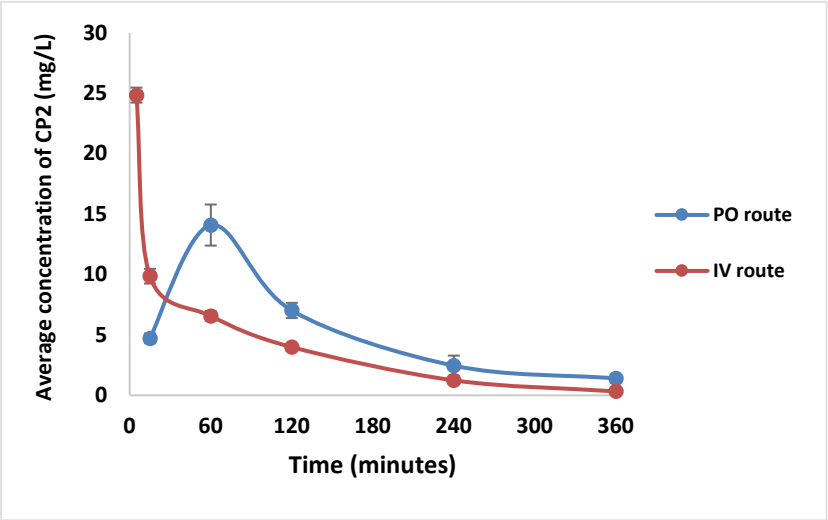

Figure 2.13: Results of PK study of CP2 (25 mg/kg body weight; oral gavage and iv routes; n = 3) in plasma for rats. Each bar represents the average concentration of CP2 measured from 3 mice and is provided with (±) standard error.

As shown from Table 2.6, the highest amount of CP2 can be detected in plasma after 5 minutes from the iv administration for rat species with a concentration of 24.8 mg/L. The time required to detect the CP2 in plasma was higher when the drug was administered via po route and the highest concentration of CP2 can be seen after 1hour with a concentration of 14.0 mg/L. For the iv route in rats, at first the drug concentration reduces quickly from 24.8 (mg/L) at 5 minutes to 6.6 (mg/L) at 1 hour; then, it is slowly decreasing to 0.3 mg/L within 6 hours of the drug administration. In contrast, there is a quick increase from 15 minutes to 1 hour with the CP2 concentration of 4.7 (mg/L) and 14.0 (mg/L) when po administration in rats. After reaching the highest concentration of CP2 at 1 h, CP2 was found decreasing steadily from 1 hour to 6 hours. Overall, these results indicate that CP2 has good clearance property and the values of area under the curve (AUC) and bioavailability (F) point out that the drug can be administered for efficacy evaluation *in vivo*.

2.5 Conclusion

Pharmacokinetics and bioavailability of compounds TP70 and CP2 were determined in mice and rat species. When IV administration of both compounds, considerable plasma concentration can be detected in both mice and rat species after 5 minutes. In PO route, for both compounds, the peak plasma concentration was reached after 60 minutes for both species. When considering about the distribution of TP70 in organs, the highest amount of TP70 was detected in brain after 30 minutes from ip route administration. Since AD drugs are targeting the brain region, the distribution of TP70 in the highest amount in brain region suggests that it can be a good candidate to proceed further. In addition, the clearance profile of TP70 suggests that it is not accumulated in any of the vital organs in relatively higher amounts for longer period of time. Moreover, the experiments performed with AD mice suggest that the administration of TP70 via drinking over longer period of time (4 months) did not cause significant accumulation of the drug in brain or plasma tissues. Therefore, it provides advantages when considering the toxicity and adverse effects of TP70. Area under the curve and bioavailability value *F* were calculated, and data show that both TP70 and CP2 has a good PK profile and bioavailability. Overall, these data will be helpful in estimating the optimum dose for efficacy studies in future.

2.6 Experimental Section

2.6.1 TP70 administration in mice and plasma/ tissue collection

A dose of 25 mg/kg (mice body weight) of TP70 as trifluoroacetic acid (TFA) salt was dissolved in 2% DMSO in 0.5% hydroxypropyl-cellulose (HPC) was administered to the male, 3 months old

WT C57BL/6 (Harlan) mice (n = 3) via ip route and organ was collected in pre chilled (dry ice) tube and stored at –20 °C.

A dose of 25 mg/kg (mice body weight) of TP70 as trifluoroacetic acid (TFA) salt was dissolved in 2% DMSO in 0.5% hydroxypropyl-cellulose (HPC) was administered to the male, 3 months old WT C57BL/6 (Harlan) mice (n = 3) and WT Sprague-Dawley rats (n = 3) by oral (po) or intravenous injection (iv). Cardiac blood collection was withdrawn from tail vein at 5, 15, 30, 60, 120, 240, and 360 minutes' intervals and treated with ethylenediamine tetraacetic acid (EDTA). About 250 µL plasma was collected from each mouse. All the plasma samples collected were stored at -78 ^{0}C until further analysis was carried.

2.6.2 TP70 treatments in mouse via drinking water and plasma samples collection

A dose of 25 mg/kg (mice body weight) of TP70 in 6 ml of drinking water per mouse was administered for male, 10 - 12 months' old APP/PS1 mice housed in cages consisting of 3 - 4 mice per cage. Each group cage was supplied with a bottle of water with dissolved TP70 (70.7 mg TP70 per 504 ml of water) and mice were allowed to drink the TP70 water freely. Blood samples were collected from each mouse on day 7, day 14 and 4 months after the initial introduction of TP70 water and was treated with ethylenediamine tetraacetic acid (EDTA). About 250 µL plasma was collected from each mouse. All the plasma samples collected were stored at -78 ^{0}C until further analysis was carried.

2.6.3 TP70 treatments in mouse brain and plasma samples

A dose of 50 mg/kg (mice body weight) of TP70 in 6 ml of drinking water per mouse was administered for male 4 months old, C57BL/6 and 5xFAD mice for 2 months. Mice were sacrificed by cervical dislocation. The isolated brain tissues and plasma were stored at -78 ^{0}C until further analysis was carried.

2.6.4 Extraction of TP70 from the cells and the tissues of mice

Plasma samples were added 3 mL of deionized water and 10 mL of 9:1 mixture of ethyl acetate and 1-propanol. This solution was sonicated for 6 minutes. The organic layer was separated from a separatory funnel. The aqueous layer was extracted twice with 10 mL of a 9:1 mixture of ethyl acetate and 1-propanol. The organic layers were combined, washed with 10 mL of brine, dried over anhydrous $MgSO_4$, and concentrated to dryness on a rotary evaporator. The residue was diluted with 1 mL of 1-propanol and filtered through a 0.2 μm filter disc (PTFE 0.2 μm, Fisherbrand). The propanol solution was concentrated to dryness on a rotary evaporator. The residue was added 300 μL of methanol and 100 μL of this solution was analyzed using HPLC and mass spectrometry as described below.

In the case of organs, they were weighed first and cut into small pieces. The same procedure above mentioned was then conducted.

2.6.5 Quantification of TP70 using HPLC

HPLC analysis of TP70 was carried out on a Varian Prostar 210 with a UV-Vis detector. A C18 reverse phase column from Xper-chrom Aegis (S. No: 104117, 250 x 10 mm, 10 micron) was used for analysis of TP-70. A flow rate of 10 mL/min and detection wavelength of 254 nm were used. A gradient elution of solvent A, containing deionized water and solvent B, containing methanol was applied for the analysis of TP70. 4-methoxyphenol was used as the internal standard.

Solutions of 100 µL of various concentrations of TP70 with 4-methoxyphenol were injected into the HPLC instrument and the peak areas corresponding to TP70 and 4-methoxyphenol were integrated from the HPLC chromatogram, and the ratios of the peaks were obtained. The results of the ratios of the HPLC peak areas and the ratios from TP70 and 4-methoxyphenol concentrations were plotted, and a linear correlation line was obtained from the graph (Figure 2.3). With the use of this correlation diagram and the ratio of HPLC peak areas of TP70 and 4-methoxyphenol obtained by injecting cells or tissue extract with known amount of 4-methoxyphenol, the amount of TP70 in the cells or tissue extract was determined.

Moreover, the peak resulted from the eluant of the injection of the cells or tissue extract which corresponds to the peak that has the same retention time as that of authentic TP70 was collected, concentrated on rotary evaporator and their mass spectrum were determined using mass spectrometer. The mass spectrum acquired from the collected peak of TP70 from the cells or tissue extract were identical to that of TP70 mass spectrum and a mass of 382 and 404 corresponding to

[$M+H^+$] and [$M+Na^+$] of TP70 were found in their mass spectra which is identical to that of pure TP70 verifying the identity of TP70.

The concentration of TP70 in the organs was obtained by finding the number of moles of TP70 in the given volume of the organs (assuming that mass of organs = volume of organs ~ 1).

2.6.6 CP2 administration and plasma collection of rats

A dose of 25 mg/kg (rats body weight) of CP2 dissolved in 4% DMSO was administered to the male, WT Sprague-Dawley rats (n=3) by oral (po) or intravenous injection (iv). Oral dosing was performed with an oral feeding gavage in which a bolus deposit (1 mL) of CP2 was transferred directly to the stomach. Intravenous dosing was performed using the left catheters on the rats. While anesthetized in 3% isoflurane, the rat received a 0.5 ml bolus iv injection through the left catheter. Cardiac blood collection was withdrawn from tail vein at 5, 15, 30, 60, 120, 240, and 360 minutes' intervals and treated with ethylenediamine tetraacetic acid (EDTA). About 250 μL plasma was collected from each mouse. All the plasma samples collected were stored at -78 ^{0}C until further analysis was carried.

2.6.7 Extraction of CP2 from the plasma of rats

Plasma samples were added 3 mL of deionized water and 10 mL of 9:1 mixture of ethyl acetate and 1-propanol. This solution was sonicated for 6 minutes. The organic layer was separated from

a separator funnel. The aqueous layer was extracted twice with 10 mL of a 9:1 mixture of ethyl acetate and 1-propanol. The organic layers were combined, washed with 10 mL of brine, dried over anhydrous $MgSO_4$, and concentrated to dryness on a rotary evaporator. The residue was diluted with 1 mL of 1-propanol and filtered through a 0.2 µm filter disc (PTFE 0.2 µm, Fisherbrand). The propanol solution was concentrated to dryness on a rotary evaporator. The residue was added 300 µL of methanol and 100 µL of this solution was analyzed using HPLC and mass spectrometry as described below.

2.6.8 Quantification of CP2 using HPLC

HPLC analysis of CP2 was carried out on a Varian Prostar 210 with a UV-Vis detector. A C18 reverse phase column from Xper-chrom Aegis (S. No: 104117, 250 x 10 mm, 10 micron) was used for CP2. A flow rate of 10 mL/min and detection wavelength of 254 nm were used. A gradient elution of solvent A, containing deionized water with 0.1% trifluoroacetic acid and solvent B, containing methanol with 0.1% trifluoroacetic acid was applied for the analysis of CP2. 4-Methoxyphenol was used as the internal standard.

Solutions of 100 µL of various concentrations of CP2 with 4-Methoxyphenol were injected into the HPLC instrument and the peak areas corresponding to CP2 and 4-Methoxyphenol were integrated from the HPLC chromatogram, and the ratios of the peaks were obtained. The results of the ratios of the HPLC peak areas and the ratios from CP2 and 4-Methoxyphenol concentrations were plotted, and a linear correlation line was obtained from the graph (Figure 2.10). With the use of this correlation diagram and the ratio of HPLC peak areas of CP2 and 4-Methoxyphenol

obtained by injecting cells or tissue extract with known amount of 4-Methoxyphenol, the amount of CP2 in the cells was determined.

Moreover, the peak resulted from the eluant of the injection of the cells or tissue extract which corresponds to the peak that has the same retention time as that of authentic CP2 was collected, concentrated on rotary evaporator and their mass spectrum were determined using mass spectrometer. The mass spectrum acquired from the collected peak of CP2 from the cells or tissue extract were identical to that of CP2 mass spectrum and a mass of 394 corresponding to $[M+H^+]$ of CP2 were found in their mass spectra which is identical to that of pure CP2 verifying the identity of CP2.

2.6 References

1. Amiri, H.; Saeidi, K.; Borhani, P.; Manafirad, A.; Ghavami, M.; Zerbi, V., Alzheimer's disease: pathophysiology and applications of magnetic nanoparticles as MRI theranostic agents. *ACS chemical neuroscience* **2013,** *4* (11), 1417-1429.

2. Wolfe, M. S., Introduction to special issue on Alzheimer's disease. *Journal of medicinal chemistry* **2012,** *55* (21), 8977-8978.

3. Friedland, R.; Hall, K.; Kalaria, R.; Ndetei, D. M.; Galasko, D.; Ogunniyi, A.; Arizaga, R.; Luchsinger, J.; Maestre, G.; Prince, M., Alzheimer's disease and vascular dementia in developing countries: prevalence, management, and risk factors. **2008**.

4. Duthey, B., Background paper 6.11: Alzheimer disease and other dementias. *A Public Health Approach to Innovation* **2013**, 1-74.

5. Ryan, L., Update on Alzheimer's disease clinical trials. *National institutes on aging (NIA), national institutes of health (NIH), on national Alzheimer's coordinating center (NACC). Available online at: https://www. alz. washington. edu/NONMEMBER/SPR12/Ryan. pdf. Acc essed February 17th* **2014**.

6. Cárdenas-Aguayo, M. a. d. C.; Gómez-Virgilio, L.; DeRosa, S.; Meraz-Ríos, M. A., The role of tau oligomers in the onset of Alzheimer's disease neuropathology. *ACS chemical neuroscience* **2014,** *5* (12), 1178-1191.

7. Hardy, J.; Selkoe, D. J., The amyloid hypothesis of Alzheimer's disease: progress and problems on the road to therapeutics. *Science* **2002,** *297* (5580), 353-356.

8. LEE, V. Y., Regulation of tau phosphorylation in Alzheimer's disease. *Annals of the New York Academy of Sciences* **1996,** *777* (1), 107-113.

9. B Martin, S.; LS Dowling, A.; Head, E., Therapeutic interventions targeting Beta amyloid pathogenesis in an aging dog model. *Current neuropharmacology* **2011,** *9* (4), 651-661.

10. Lemere, C. A.; Masliah, E., Can Alzheimer disease be prevented by amyloid-β immunotherapy? *Nature Reviews Neurology* **2010,** *6* (2), 108-119.

11. Maezawa, I.; Hong, H. S.; Wu, H. C.; Battina, S. K.; Rana, S.; Iwamoto, T.; Radke, G. A.; Pettersson, E.; Martin, G. M.; Hua, D. H., A novel tricyclic pyrone compound ameliorates cell death associated with intracellular amyloid-β oligomeric complexes. *Journal of neurochemistry* **2006,** *98* (1), 57-67.

12. Rana, S.; Hong, H.-S.; Barrigan, L.; Jin, L.-W.; Hua, D. H., Syntheses of tricyclic pyrones and pyridinones and protection of Aβ-peptide induced MC65 neuronal cell death. *Bioorganic & medicinal chemistry letters* **2009,** *19* (3), 670-674.

13. Hong, H. S.; Rana, S.; Barrigan, L.; Shi, A.; Zhang, Y.; Zhou, F.; Jin, L. W.; Hua, D. H., Inhibition of Alzheimer's amyloid toxicity with a tricyclic pyrone molecule in vitro and in vivo. *Journal of neurochemistry* **2009,** *108* (4), 1097-1108.

14. Zhang, L.; Zhang, S.; Maezawa, I.; Trushin, S.; Minhas, P.; Pinto, M.; Jin, L.-W.; Prasain, K.; Nguyen, T. D.; Yamazaki, Y., Kanekiyo, T.; Bu, Guojun.; Gateno, B.; Chang, Kyenong-OK.; Nath, K. A.; Nemutlu, E.; Dzeja, P.; Pang, Y.; Hua, D. H.; Trushina, E.; Modulation of mitochondrial complex I activity averts cognitive decline in multiple animal models of familial Alzheimer's disease. *EBioMedicine* **2015,** *2* (4), 294-305.

15. Pokhrel, L.; Maezawa, I.; Nguyen, T. D.; Chang, K.-O.; Jin, L.-W.; Hua, D. H., Inhibition of Acyl-CoA: cholesterol acyltransferase (ACAT), overexpression of cholesterol transporter gene, and protection of amyloid β (Aβ) oligomers-induced neuronal cell death by tricyclic pyrone molecules. *Journal of medicinal chemistry* **2012,** *55* (20), 8969-8973.

16. Tellechea, P.; Pujol, N.; Esteve-Belloch, P.; Echeveste, B.; Garcia-Eulate, M. R.; Arbizu, J.; Riverol, M., Early- and late-onset Alzheimer disease: Are they the same entity? *Neurologia* **2015**.

17. Zou, Z.; Liu, C.; Che, C.; Huang, H., Clinical genetics of Alzheimer's disease. *BioMed research international* **2014,** *2014*.

18. Tang, Y.-P.; Gershon, E. S., Genetic studies in Alzheimer's disease. *Dialogues in clinical neuroscience* **2003,** *5*, 17-26.

19. Ryan, N. S.; Rossor, M. N., Correlating familial Alzheimer's disease gene mutations with clinical phenotype. *Biomarkers in medicine* **2010,** *4* (1), 99-112.

20. Cai, Y.; An, S. S. A.; Kim, S., Mutations in presenilin 2 and its implications in Alzheimer's disease and other dementia-associated disorders. *Clinical interventions in aging* **2015,** *10*, 1163-1172.

21. Zhang, C.; Browne, A.; DiVito, J. R.; Stevenson, J. A.; Romano, D.; Dong, Y.; Xie, Z.; Tanzi, R. E., Amyloid-β production via cleavage of amyloid-β protein precursor is modulated by cell density. *Journal of Alzheimer's Disease* **2010,** *22* (2), 683-694.

22. Cole, S. L.; Vassar, R., The Alzheimer's disease β-secretase enzyme, BACE1. *Molecular neurodegeneration* **2007,** *2* (1), 1-25.

23. Serrano-Pozo, A.; Frosch, M. P.; Masliah, E.; Hyman, B. T., Neuropathological alterations in Alzheimer disease. *Cold Spring Harbor perspectives in medicine* **2011,** *1* (1), a006189.

24. Murphy, M. P.; LeVine III, H., Alzheimer's disease and the amyloid-β peptide. *Journal of Alzheimer's Disease* **2010,** *19* (1), 311-323.

25. Poduslo, J. F.; Hultman, K. L.; Curran, G. L.; Preboske, G. M.; Chamberlain, R.; Marjańska, M.; Garwood, M.; Jack, C. R.; Wengenack, T. M., Targeting vascular amyloid in arterioles of Alzheimer disease transgenic mice with amyloid β protein antibody-coated nanoparticles. *Journal of Neuropathology & Experimental Neurology* **2011,** *70* (8), 653-661.

26. Kelleher, R. J.; Soiza, R. L., Evidence of endothelial dysfunction in the development of Alzheimer's disease: is Alzheimer'sa vascular disorder. *Am J Cardiovasc Dis* **2013,** *3* (4), 197-226.

27. Hubin, E. S., *Influence of Genetic Variability and External Regulating Factors on Amyloid-beta Peptide Aggregation*. University of Twente: 2014.

28. De Felice, F. G.; Wu, D.; Lambert, M. P.; Fernandez, S. J.; Velasco, P. T.; Lacor, P. N.; Bigio, E. H.; Jerecic, J.; Acton, P. J.; Shughrue, P. J., Alzheimer's disease-type neuronal tau hyperphosphorylation induced by Aβ oligomers. *Neurobiology of aging* **2008,** *29* (9), 1334-1347.

29. Iqbal, K.; Alonso, A. d. C.; Chen, S.; Chohan, M. O.; El-Akkad, E.; Gong, C.-X.; Khatoon, S.; Li, B.; Liu, F.; Rahman, A., Tau pathology in Alzheimer disease and other tauopathies. *Biochimica et Biophysica Acta (BBA)-Molecular Basis of Disease* **2005,** *1739* (2), 198-210.

30. Wolfe, M. S., The role of tau in neurodegenerative diseases and its potential as a therapeutic target. *Scientifica* **2012,** *2012, 1-22*.

31. Avila, J., Tau phosphorylation and aggregation in Alzheimer's disease pathology. *FEBS letters* **2006,** *580* (12), 2922-2927.

32. Kolarova, M.; García-Sierra, F.; Bartos, A.; Ricny, J.; Ripova, D., Structure and pathology of tau protein in Alzheimer disease. *International journal of Alzheimer's disease* **2012,** *2012, 1-14*.

33. Lasagna-Reeves, C. A.; Castillo-Carranza, D. L.; Sengupta, U.; Clos, A. L.; Jackson, G. R.; Kayed, R., Tau oligomers impair memory and induce synaptic and mitochondrial dysfunction in wild-type mice. *Molecular neurodegeneration* **2011,** *6* (1), 1-14.

34. Wang, J. Z.; Grundke-Iqbal, I.; Iqbal, K., Kinases and phosphatases and tau sites involved in Alzheimer neurofibrillary degeneration. *European Journal of Neuroscience* **2007,** *25* (1), 59-68.

35. Ciechanover, A.; Kwon, Y. T., Degradation of misfolded proteins in neurodegenerative diseases: therapeutic targets and strategies. *Experimental & molecular medicine* **2015,** *47* (3), e147.

36. Saez, I.; Vilchez, D., The Mechanistic Links Between Proteasome Activity, Aging and Agerelated Diseases. *Current genomics* **2014,** *15* (1), 38-51.

37. Planel, E.; Bretteville, A.; Liu, L.; Virag, L.; Du, A. L.; Yu, W. H.; Dickson, D. W.; Whittington, R. A.; Duff, K. E., Acceleration and persistence of neurofibrillary pathology in a mouse model of tauopathy following anesthesia. *The FASEB Journal* **2009,** *23* (8), 2595-2604.

38. Mendoza, J.; Sekiya, M.; Taniguchi, T.; Iijima, K. M.; Wang, R.; Ando, K., Global analysis of phosphorylation of tau by the checkpoint kinases Chk1 and Chk2 in vitro. *Journal of proteome research* **2013,** *12* (6), 2654-2665.

39. Iqbal, K.; Gong, C.-X.; Liu, F., Hyperphosphorylation-induced tau oligomers. *Tau oligomers* **2014**, 105-113.

40. Metcalfe, M. J.; Figueiredo-Pereira, M. E., Relationship between tau pathology and neuroinflammation in Alzheimer's disease. *Mount Sinai Journal of Medicine: A Journal of Translational and Personalized Medicine* **2010,** *77* (1), 50-58.

41. Cowan, C. M.; Mudher, A., Are tau aggregates toxic or protective in tauopathies? *Tau oligomers* **2014**, 6-18.

42. Ferrer, I.; Gomez-Isla, T.; Puig, B.; Freixes, M.; Ribe, E.; Dalfo, E.; Avila, J., Current advances on different kinases involved in tau phosphorylation, and implications in Alzheimer's disease and tauopathies. *Current Alzheimer Research* **2005,** *2* (1), 3-18.

43. Kawamura, T.; Umemura, T.; Hotta, N., Cognitive impairment in diabetic patients: Can diabetic control prevent cognitive decline? *Journal of diabetes investigation* **2012,** *3* (5), 413-423.

44. Akter, K.; Lanza, E. A.; Martin, S. A.; Myronyuk, N.; Rua, M.; Raffa, R. B., Diabetes mellitus and Alzheimer's disease: shared pathology and treatment? *British journal of clinical pharmacology* **2011,** *71* (3), 365-376.

45. Feinkohl, I.; Price, J. F.; Strachan, M. W.; Frier, B. M., The impact of diabetes on cognitive decline: potential vascular, metabolic, and psychosocial risk factors. *Alzheimer's research & therapy* **2015,** *7* (1), 1-21.

46. Mittal, K.; Katare, D. P., Shared links between type 2 diabetes mellitus and Alzheimer's disease: A review. *Diabetes & Metabolic Syndrome: Clinical Research & Reviews* **2016**.

47. Messier, C.; Gagnon, M., Glucose regulation and cognitive functions: relation to Alzheimer's disease and diabetes. *Behavioural brain research* **1996,** *75* (1), 1-11.

48. Zhu, X.; Smith, M. A.; Perry, G.; Aliev, G., Mitochondrial failures in Alzheimer's disease. *American journal of Alzheimer's disease and other dementias* **2004,** *19* (6), 345-352.

49. Reddy, P. H.; Beal, M. F., Are mitochondria critical in the pathogenesis of Alzheimer's disease? *Brain Research Reviews* **2005,** *49* (3), 618-632.

50. Lin, M. T.; Beal, M. F., Mitochondrial dysfunction and oxidative stress in neurodegenerative diseases. *Nature* **2006,** *443* (7113), 787-795.

51. Pagani, L.; Eckert, A., Amyloid-Beta interaction with mitochondria. *International Journal of Alzheimer's Disease* **2011,** *2011,* 1-12.

52. Carrillo-Mora, P.; Luna, R.; Colín-Barenque, L., Amyloid beta: multiple mechanisms of toxicity and only some protective effects? *Oxidative medicine and cellular longevity* **2014,** *2014*.

53. Alberts, B.; Johnson, A.; Lewis, J.; Raff, M.; Roberts, K.; Walter, P., The Transport of Proteins into Mitochondria and Chloroplasts. **2002**.

54. Yan, S. D.; Stern, D. M., Mitochondrial dysfunction and Alzheimer's disease: role of amyloid-β peptide alcohol dehydrogenase (ABAD). *International journal of experimental pathology* **2005,** *86* (3), 161-171.

55. Reddy, P. H.; Beal, M. F., Amyloid beta, mitochondrial dysfunction and synaptic damage: implications for cognitive decline in aging and Alzheimer's disease. *Trends in molecular medicine* **2008,** *14* (2), 45-53.

56. Manczak, M.; Park, B. S.; Jung, Y.; Reddy, P. H., Differential expression of oxidative phosphorylation genes in patients with Alzheimer's disease. *Neuromolecular medicine* **2004,** *5* (2), 147-162.

57. Spuch, C.; Ortolano, S.; Navarro, C., New insights in the amyloid-Beta interaction with mitochondria. *Journal of aging research* **2012,** *2012,* 1-10.

58. Moreira, P. I.; Carvalho, C.; Zhu, X.; Smith, M. A.; Perry, G., Mitochondrial dysfunction is a trigger of Alzheimer's disease pathophysiology. *Biochimica et Biophysica Acta (BBA)-Molecular Basis of Disease* **2010,** *1802* (1), 2-10.

59. Wolozin, B., Cholesterol and the biology of Alzheimer's disease. *Neuron* **2004,** *41* (1), 7-10.

60. Distl, R.; Meske, V.; Ohm, T. G., Tangle-bearing neurons contain more free cholesterol than adjacent tangle-free neurons. *Acta neuropathologica* **2001,** *101* (6), 547-554.

61. Fukumoto, H.; Deng, A.; Irizarry, M. C.; Fitzgerald, M. L.; Rebeck, G. W., Induction of the cholesterol transporter ABCA1 in central nervous system cells by liver X receptor agonists increases secreted Aβ levels. *Journal of Biological Chemistry* **2002,** *277* (50), 48508-48513.

62. Mayeux, R.; Sano, M.; Chen, J.; Tatemichi, T.; Stern, Y., Risk of dementia in first-degree relatives of patients with Alzheimer's disease and related disorders. *Archives of Neurology* **1991,** *48* (3), 269-273.

63. Schmitz, G.; Robenek, H.; Beuck, M.; Krause, R.; Schurek, A.; Niemann, R., Ca++ antagonists and ACAT inhibitors promote cholesterol efflux from macrophages by different

mechanisms. I. Characterization of cellular lipid metabolism. *Arteriosclerosis, Thrombosis, and Vascular Biology* **1988,** *8* (1), 46-56.

64. Puglielli, L.; Tanzi, R. E.; Kovacs, D. M., Alzheimer's disease: the cholesterol connection. *Nature neuroscience* **2003,** *6* (4), 345-351.

65. Huttunen, H. J.; Kovacs, D. M., ACAT as a drug target for Alzheimer's disease. *Neurodegenerative Diseases* **2008,** *5* (3-4), 212-214.

66. Hutter-Paier, B.; Huttunen, H. J.; Puglielli, L.; Eckman, C. B.; Kim, D. Y.; Hofmeister, A.; Moir, R. D.; Domnitz, S. B.; Frosch, M. P.; Windisch, M., The ACAT inhibitor CP-113,818 markedly reduces amyloid pathology in a mouse model of Alzheimer's disease. *Neuron* **2004,** *44* (2), 227-238.

67. Singh, R., HPLC method development and validation-an overview. *Journal of Pharmaceutical Education and Research* **2013,** *4* (1), 26.

68. Swartz, M. E.; Krull, I. S., *Analytical method development and validation*. CRC Press: 1997.

69. Bansal, S.; DeStefano, A., Key elements of bioanalytical method validation for small molecules. *The AAPS journal* **2007,** *9* (1), E109-E114.

70. Pandey, S.; Pandey, P.; Tiwari, G.; Tiwari, R., Bioanalysis in drug discovery and development. *Pharmaceutical methods* **2010,** *1* (1), 14-24.

71. Tucker, G. T., Principles of pharmacokinetics. *Drug concentrations in neuropsychiatry* **1980**, 13-26.

72. Wan, H., What ADME tests should be conducted for preclinical studies? *ADMET and DMPK* **2013,** *1* (3), 19-28.

73. Turner, P. V.; Brabb, T.; Pekow, C.; Vasbinder, M. A., Administration of substances to laboratory animals: routes of administration and factors to consider. *Journal of the American Association for Laboratory Animal Science* **2011,** *50* (5), 600-613.

74. Caldwell, G. W., Compound optimization in early-and late-phase drug discovery: acceptable pharmacokinetic properties utilizing combined physicochemical, in vitro and in vivo screens. *Current Opinion in Drug Discovery and Development* **2000,** *3* (1), 30-41.

75. Howland, R. D.; Mycek, M. J.; Harvey, R. A.; Champe, P. C., *Lippincott's illustrated reviews: Pharmacology*. Lippincott Williams & Wilkins Philadelphia: 2006.

76. Gibaldi, M., *Biopharmaceutics and Clinical Pharmacokinetics*. Lea and Febiger: 1977; p 181 pp.

Chapter 3 - Nanodelivery of siRNA Using Polymer Based Nanomaterials

3.1 Introduction

Since its initial discovery by Mello, Fire and coworkers in 1903, RNA interference (RNAi) has achieved a greater therapeutic potential in the treatment of various diseases such as cancer, genetic disorders, autoimmune diseases and viral infections.[1,2] In recent years, RNAi has been broadened to another major field, which is the genetic control of insect pests. Due to the availability of genomic sequences of insects of various groups, this technology has been achieved a significant advance in recent years and several studies have shown the potential use of RNAi to control agriculturally important insect pests.[3-7] However, several obstacles and challenges are associated with genetic control of insect pests such as effective delivery of double stranded RNA (dsRNA) in insects, preventing its degradation by nucleases, enhancing its cellular uptake and endosomal release into insect cells etc.[8-11] In addition, there's a significant variation of RNAi efficiency present in different taxonomic group of insects.[5] Therefore, the development of effective dsRNA delivery methods is highly warranted.

Nanomaterials are found to be promising tools to enhance the delivery efficiency of small interfering RNA (siRNA) or dsRNA recently. Several nanocarriers such as polymeric nanoparticles, cationic lipids, dendrimers, proteins, peptides and polyamino acids have been introduced by several research groups that can encapsulate desired RNA molecules and thereby facilitate uptake into cell.[12] Among them, polymeric nanoparticles have been widely exploited for use as a delivery method for nucleic acids in RNAi based gene therapeutics.

In this chapter, I summarized the work that I have carried out to investigate the nanodelivery of specific dsRNA with the use of polymer based nanomatrials for suppressing the western corn

rootworm (WCR, *Diabrotica virgifera virgifera*) genes. Two nanoparticles (NPs) were synthesized as the delivery aids for dsRNA, namely chitosan: PEG, and α-OH -PVP polymer conjugates. They were encapsulated with specific dsRNA molecules and encapsulation of nanoparticles with dsRNA was studied from various techniques and finally observed the RNAi efficacy for the encapsulated materials. This research was done in collaboration with Dr. Kun Yan Zhu in the department of Entomology at Kansas State University. All dsRNA's provided and RNAi efficiency testing was performed by Dr. Young Ho Kim, in Dr. Kun Yan Zhu's laboratory, Kansas State University. Preliminary results from Dr. Zhu's laboratory have shown that dsRNA was effective in gene suppression in WCR. In order to address the problems associated with delivery of dsRNA into WCR, two different polymer-based nanomaterials have been synthesized and evaluated their encapsulation efficiency with different dsRNA molecules to investigate the nanodelivery of dsRNA for suppressing the WCR. In this chapter, the synthesis of the polymers encapsulation of dsRNA in forming nanomaterials, and the testing of their encapsulation efficiencies are discussed.

3.2 Background

3.2.1 RNAi technology in insect pests management

Agricultural production of food needs to be continuously adapt to increasing consumers´ demand in conjunction with rising environmental concerns. Insect pests are one of the major causes for losses in agricultural production, and therefore results significant economic losses each year.[12] Currently, the crop damage caused by various insect pests species is managed by the application of pesticides or the use of transgenic crops expressing *Bacillus thuringiensis* (*Bt*) toxin proteins.[11]

When considering about pesticides, in the United States alone, it costs about $ 10 billion for the use of about 600 different pesticides to protect crop plants annually.[13] Besides, they have now caused several escalating problems such as the evolution of insect resistance to the pesticides, the appearance of secondary pest outbreaks, and the potential hazards on environment etc.[11,14] Though the use of *Bacillus thuringiensis* (*Bt*) toxin has shown considerable success over chemical insecticides in a range of crops, many important insect species are not controlled by *Bt* protection.[14] Therefore, the development of novel approaches to control agricultural pests are highly warranted. Recently, RNAi technology has been widely exploited for use in insect pest management. RNAi is a sequence specific post transcriptional gene silencing mechanism which is widely expressed in animals, plants, and microorganisms and act as a defense mechanism against abnormal DNA.[16] There are some reported studies, in which the successful delivery of double stranded RNA (dsRNA) to insects by ingestion resulted the expected gene target silencing and therefore, have caused death or affected the viability of the target insect, resulting in control of the pest.[5,15] The major advantage of RNAi technology in insects pest management is it has low off target effects, thus significantly increases the safety of non-target organisms and the environment.[5,15]

3.2.2 siRNA mediated gene silencing mechanism

In insects, it has been found that, dsRNA is more effective at producing RNAi than sense or anti sense RNA.[16] The RNAi process occurred in insects can be divided into three main steps. First, a long endogenous or exogenous dsRNA molecule, that is either expressed in, or introduced into the cell binds to a RNase iii type enzyme called “Dicer” and the enzyme digest dsRNA into small interfering RNAs which are also called siRNA, short interfering RNA, or silencing RNA.[16,17] siRNAs are double stranded and contains 20 – 25 base pairs. In the second step, a multi-functional

protein called Argonaute 2, unwinds siRNA and sense strand of siRNA is cleaved and the guide stand is incorporated into the RNA induced silencing complex (RISC) in the cytosol.[2,18,19] In the third step, guide strand in RISC cleaves the target messenger RNA (mRNA) that shares complete or partial sequence homology of the dsRNA using an endonuclease enzyme called "slicer". The cleavage site of specific mRNA is at a position between nucleotides 10 and 11 relative to the 5′-end on the complementary antisense strand.[2,18,19] The inhibition of sequence specific mRNA will result the inhibition of targeted gene expression and therefore inhibit the protein production and protein function in a sequence specific manner.

3.2.3 Delivery of dsRNA into insects through the use of nanomaterials

There are several challenges associated with delivering dsRNA into insects. Naked dsRNA alone cannot be administered into insects as they are not stable under environmental conditions, have poor penetration abilities into the cells, and readily cleave by nucleases.[9] In order to result a successful RNAi machinery in insects, dsRNA needs to be directed into the cells of insects and thus there needs to be a system that can effectively deliver the dsRNA into target cells.

Recently, nanomaterials have been considered as a method to incorporate dsRNA molecules. A successful nanodelivery platform must have certain advantages that include: (1) protect dsRNA from harmful effects from environment such as temperature, (2) successful delivery of dsRNA into target cells through the penetration of insect's membranes (3) prevention the degradation of dsRNA by nucleases in insect's body (4) maximize the cellular uptake of dsRNA by the target tissues.

Nanomaterials have a particle size of 1 - 1,000 nm, and it should contain important characteristics properties to be used as a delivery vehicle.[20-22] Surface properties of the nanomaterials play an

important role in terms of uptake and complex formation with polyanionic nucleic acids of dsRNA.[21] Studies conducted *in vitro* have indicated that positively charged nanomaterials can interact with negatively charged cellular membranes and thereby promote uptake into the cell. Moreover, they can involve in the complex formation with polyanionic nucleic acids as well.[22] It has been discovered several natural and synthetic polymer based nanomaterials for siRNA/dsRNA delivery over the past years and some of them demonstrate a great promise to be used as successful delivery agents.[13] Most of the natural polymers offer nontoxic, biodegradable and biocompatible properties and some of the examples for natural polymers include chitosan, cationic polypeptides, cyclodextrin, and atelocollagen etc.[23] Most commonly used synthetic polymers for siRNA administration includes linear and branched polymers of poly(ethyleneimine) (PEI) or conjugation of PEG chains with PEI, dimethylaminoethyl methacrylate, polyfluorene, and cyclodextrin based polycations` etc.[23,24]

Members in Dr. Kun Yan Zhu's laboratory have investigated different nanoparticles complexed with dsRNA for studying RNAi efficiency in different organisms.[25] For example, they have studied the repression of two chitin synthase genes, *AgCHS1* and *AgCHS2*, present in *Anopheles gambiae* using chitosan/*AgCHS* dsRNA-based nanoparticles and found that *AgCHS1* transcript level and chitin content were reduced by 62.8 and 33.8%, respectively, in the larvae fed on chitosan/*AgCHS1* dsRNA nanoparticles compared with those of the control larvae fed on chitosan/GFP dsRNA nanoparticles.[25]

3.3 Results and discussion

To study the RNAi based strategy for the control of insect pests, we have investigated the nanodelivery of specific dsRNA for suppressing the western corn rootworm (WCR, *Diabrotica*

virgifera virgifera) genes. Among the several insect pests that cause significant economic losses in agricultural sector in US, the WCR, is one of the country's most devastating corn pests and causes about $1 billion losses annually in US.[26] Corn rootworms are widely spread throughout US corn growing regions and cause their damage as a larva – the immature stage of the insect.[26] Previous results of Dr. Zhu's laboratory suggested that dsRNA was effective in gene suppression in WCR. Therefore, to address the challenges associated with the delivery of dsRNA into insects, we studied the nanodelivery of dsRNA using modified chitosan and modified polyvinylpyrrolidinone (PVP) as nanocarriers.

3.3.1 Chitosan: PEG/dsRNA nanoparticles

Chitosan which is derived from the alkaline deacetylation of chitin, is a linear polymer of an aminosaccharide (D-glucosamine). Chitosan based nanoparticles are preferably used worldwide for various applications due to their biodegradability, high permeability, non-toxicity to human and cost effectiveness.[27] For example, chitosan/alginate, chitosan/tripolyphosphate nanoparticles have been reported as carrier systems for the herbicide paraquat.[28,29] However, chitosan alone has been known to have relatively low transfection efficiency. This could be due the inefficient release of endosomally trapped nucleic acid (e.g., dsRNA) into the cytosol as chitosan can form electrostatic interactions with amino groups of chitosan with phosphate groups of nucleic acids (Figure 3.1). This will make chitosan to tightly bound to nucleic acids and creates low solubility of the complex in water.

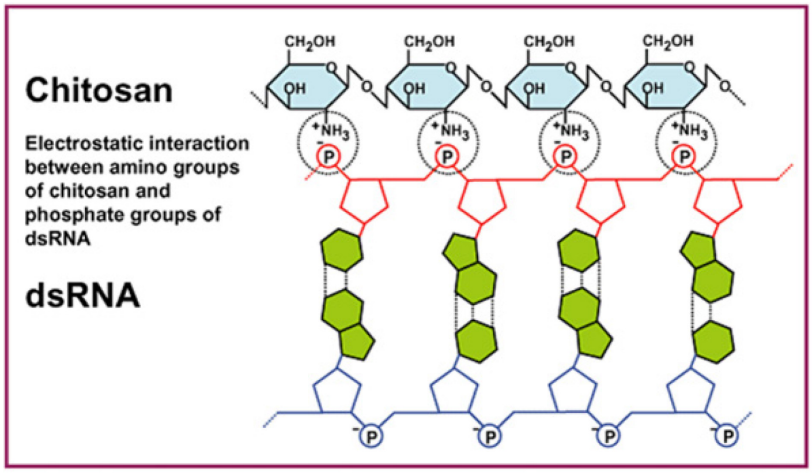

Figure 3.1: Interactions between chitosan and dsRNA[25]. Figure adapted from Zhang, X. *Insect molecular biology*. 2010, 19, 683-693 with permission from John Wiley and Sons (copyright © 2010).

Therefore, to enhance the efficacy of nanoparticle based RNAi, polyethylene glycol (PEG) was incorporated and nanoparticle was formed as chitosan: PEG conjugates (Figure 3.2).

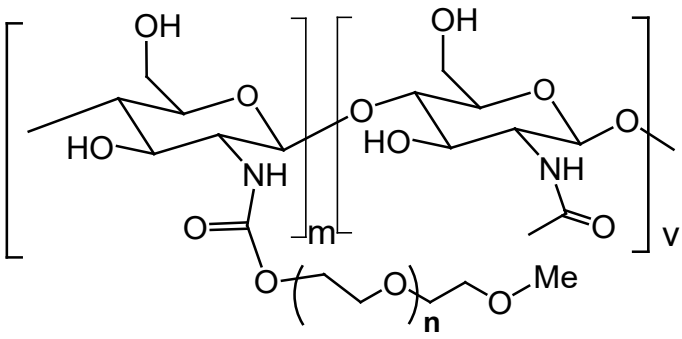

Figure 3.2: Structure of chitosan: PEG polymer.

In order to gain insight into whether chitosan: PEG nanocarriers are capable of forming complexes with nucleotides, a simulation of chitosan: PEG copolymer with dsRNA was performed. This was done by Dr. Jeffrey Comer in Nanotechnology Innovation Center of Kansas State Institute of Computational Comparative Medicine, Department of Anatomy and Physiology, College of

Veterinary Medicine, Kansas State University. Figure 3.3 indicates the simulation results of chitosan: PEG nanocarriers with dsRNA.

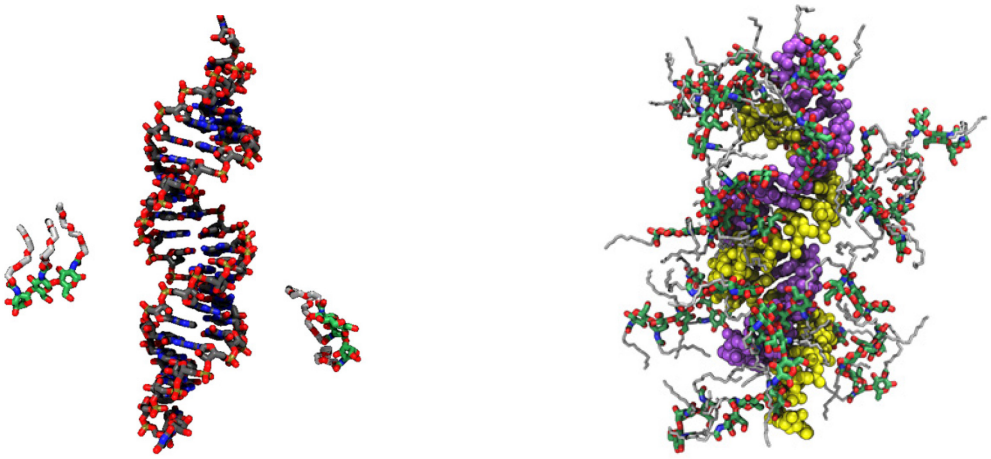

Figure 3.3: Simulation diagram of chitosan: PEG nanocarriers with dsRNA.

It can be seen from Figure 3.3 that chitosan: PEG polymer conjugates are observed to physisorption to the surface of the RNA helix due to strong ionic interactions. With these ideas in hand, chitosan: PEG conjugates in which a PEGylation density of PEG's (500 MW) groups per 5 chitosan monomers were synthesized to incorporate into dsRNA.

3.3.1.1 Synthesis of chitosan: PEG polymer conjugate and its characterization

Synthetic scheme for the synthesis of chitosan: PEG (5:1) polymer conjugates is shown in Scheme 3.1.

Scheme 3.1: Synthesis of chitosan: PEG polymer nanocarrier

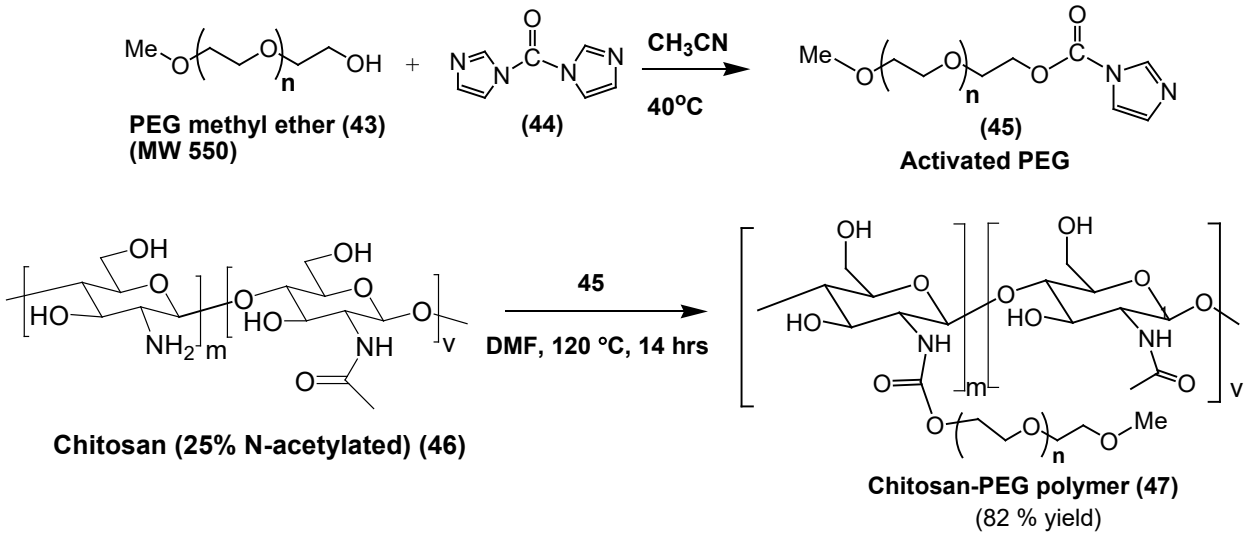

Synthesis of chitosan: PEG polymer (**47**) was achieved in two step process as outlined in Scheme 3.1. PEG methyl ester (**43**) was dissolved in acetonitrile and it was added carbonyl diimidazole (CDI) (**44**) and heated to 40 °C to obtain the activated PEG (**45**) in 80 % yield. Then it was reacted with commercially available 75% deacetylated chitosan (**46**) in DMF at 120 °C for 14 hours to obtain chitosan: PEG polymer (**47**) in 70% yield. Detailed experimental procedure is written in the experimental section of this chapter.

The synthesized chitosan: PEG polymer (**47**) was characterized by IR spectroscopy. The molecular weight of polymer **47** was found to be 120,558 Da as determined by gel permeation chromatography using TSKgel GMHxl column and THF as eluent. It has been found that the C-2-amino functions of chitosan, in which amino moieties have been acetylated by 25%, were covalently linked with polyethylene glycol (PEG) through carbamate function by ~30% thereby reducing the cationic character of the polymer. A total of 55% of the amino groups have been transformed into carbamates.

3.3.1.2 Encapsulation of chitosan: PEG nanocarrier with adenine

Ability of chitosan: PEG nanocarrier to encapsulate small molecules like adenine and adenosine monophosphate was evaluated before testing the encapsulation ability of chitosan: PEG nanocarriers with specific dsRNA. Hence, a 5% by weight of adenine (MW 135.13 g/mol) was encapsulated by chitosan: PEG nanocarrier (95% by weight) in water, and the resulting solution was lyophilized to give a solid. The detailed procedure of encapsulation will be discussed in experimental section of this chapter.

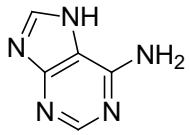

Adenine

Figure 3.4: Structure of adenine.

Figure 3.5 shows the computer simulation image of the chitosan: PEG nanocarrier with adenine. There are 2.2Å and 2.13 Å contacts between two chitosan hydroxyl groups and an adenine nitrogen suggest the possibility of interaction of nanocarrier with adenine.

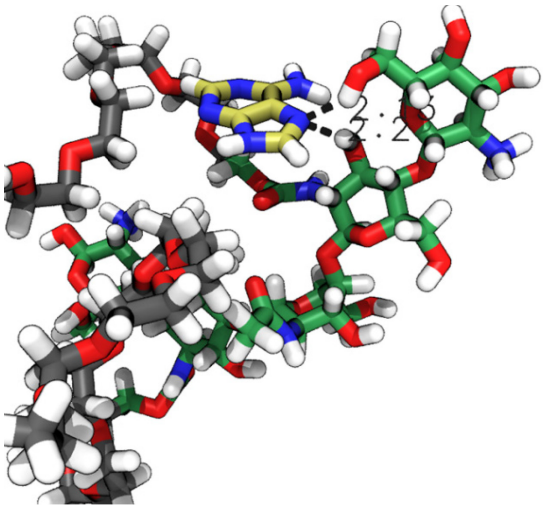

Figure 3.5: Computer simulation image of the chitosan: PEG nanocarrier with adenine.

Encapsulation of chitosan: PEG nanocarrier with adenine was studied using UV visible spectrometry over different time intervals. Chitosan: PEG/adenine nanoparticles were dissolved in deionized water to obtain 0. 0172 mM concentration. This solution was tested for UV absorbance over 0, 2, 4, 6, and 60 hours in the presence of deionized water as the blank. In addition, adenine powder was dissolved in deionized water to obtain 0.0172 mM concentration and the UV absorbance of this solution was taken in the presence of deionized water as the blank. Figure 3.7 indicates the corresponding UV spectrum.

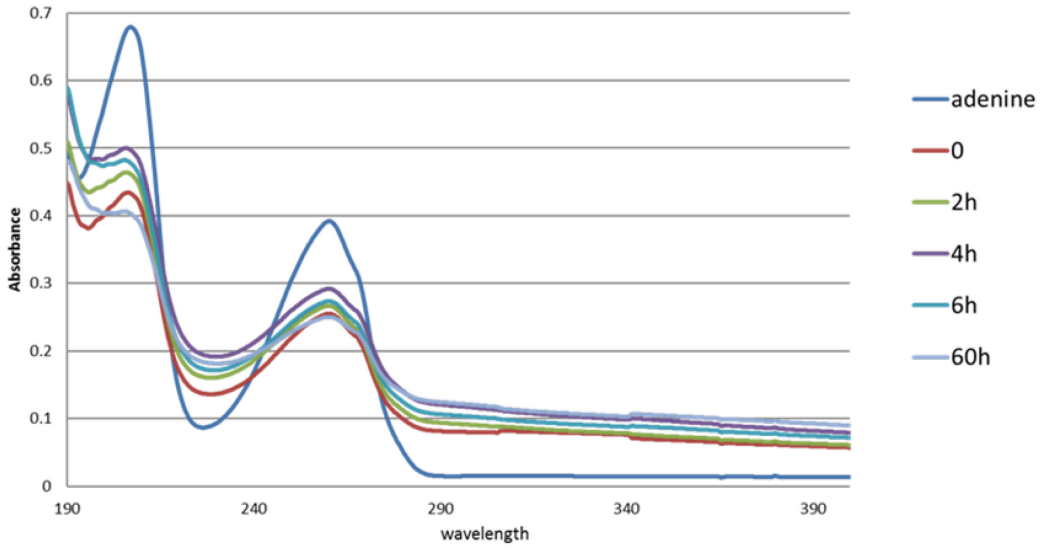

Figure 3.6: UV visible spectrum of the encapsulated chitosan: PEG/ adenine nanocarrier solution over different time intervals.

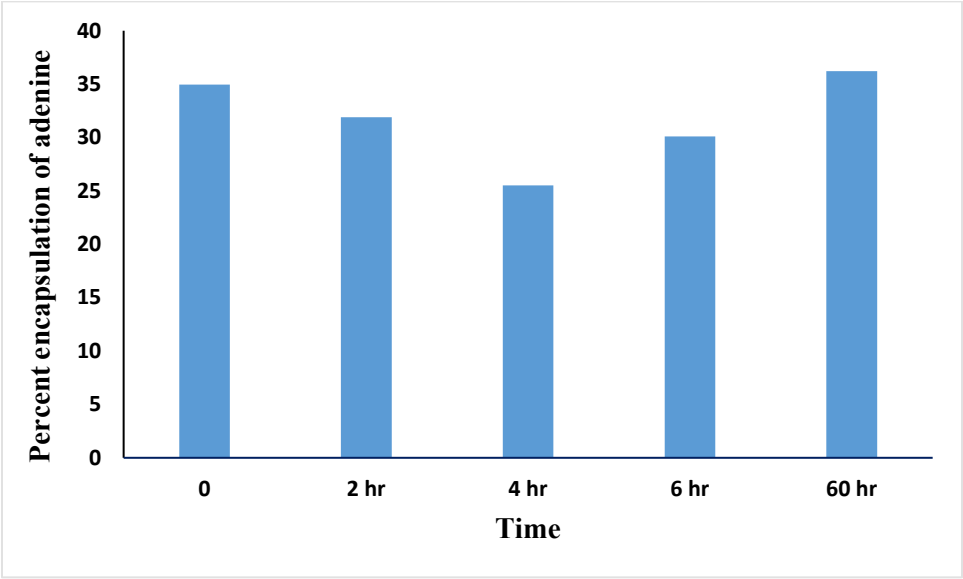

Figure 3.7: Correlation graph of percent encapsulation of adenine over different time intervals.

As shown in Figure 3.6, UV absorbance for the adenine alone is higher compared to that of the adenine/nanocarrier solution, suggesting the possibility of the encapsulation of adenine in to

chitosan: PEG nanocarriers to form chitosan: PEG/adenine nanoparticles. The lowest absorbance was resulted in 0 minute and it was gradually increased up to 4 hours indicates that adenine gradually comes off from the nanocarrier. As shown in Figure 3.7, the highest percent encapsulation of adenine into nanocarrier can be seen at 0 minute and the lowest percent encapsulation was at 4 hours. When comparing the UV absorbance curves for 6 hours and 60 hours, it seems that UV absorbance are smaller than that of 4 hours. This suggests that some of the released adenine gets re-encapsulated with nanocarrier to form adenine/polymer nanoparticles and this in turn can be proved from the higher percent encapsulation of adenine into nanocarrier at 6 hours and 60 hours than that of 4 hours.

3.3.1.3 Encapsulation of chitosan: PEG nanocarrier with dsDNA

We further tested the ability of chitosan: PEG nanocarrier to encapsulate relatively large dsDNA molecules. Clathrin heavy chain (CHC) ds DNA sample (523 base pairs; MW 509,402 Da) was provided by Dr. Kun Yan Zhu's laboratory and 5 % by weight of dsDNA was encapsulated with chitosan: PEG nanocarrier (95 % by weight) in water, following the same procedure used for the encapsulation of adenine with chitosan: PEG polymer.

Encapsulation ability of dsDNA with chitosan: PEG nanocarrier was studied using agarose gel electrophoresis by Dr. Youngho Kim in Dr. Kun Yan Zhu's laboratory. A 10 µl of each of the 2.1 µg/µl (left panel; two left lanes) and 21 µg/µl (right panel; left lane) nanoparticle solutions (chitosan: PEG /dsDNA) was loaded to each lane of the agarose gel. The amounts of dsDNA were approximately 0.1 (left panel) and 1.0 µg (right panel) respectively, based on the 5 % encapsulation of dsDNA into nanocarrier. Figure 3.8 shows the electrophoresis result.

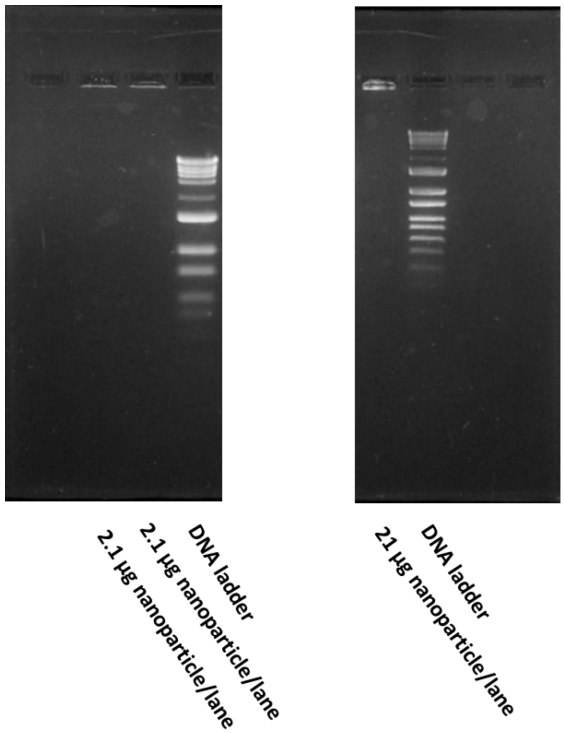

Figure 3.8: Gel image of the encapsulated chitosan: PEG/dsDNA nanoparticles.

As shown in Figure 3.7, the dsDNA is not moved in the nanoparticle lane suggests that dsRNA is successfully encapsulated by chitosan: PEG polymer conjugates.

The particle sizes and morphology of the chitosan: PEG nanocarriers and encapsulated dsDNA/polymer nanoparticles were measured using atomic force microscopy (AFM) using a tapping mode with a high aspect ratio tip. Figure 3.8 shows the representative AFM images of chitosan: PEG nanocarriers and encapsulated chitosan-PEG/dsDNA nanoparticles.

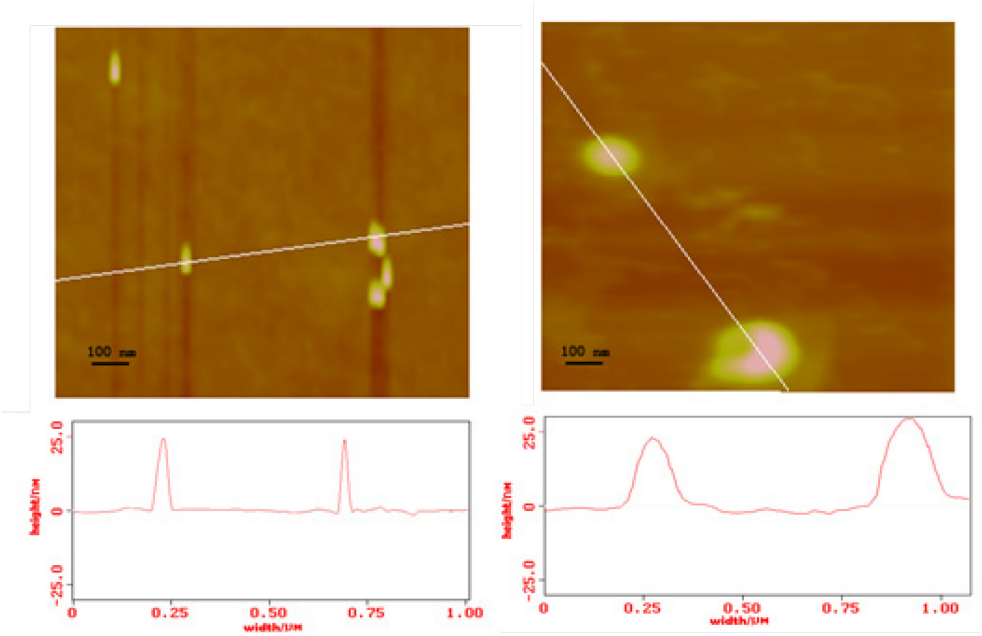

Figure 3.9: Representative AFM images of chitosan: PEG nanocarrier (left panel - top), the width (40 nm) and height (25 nm) (bottom) of the nanocarriers and encapsulated chitosan: PEG/dsDNA nanoparticles (right panel- top), and the width (160 nm) and height (25 nm) (bottom) of the nanoparticles. Scale bar is 100 nm.

As shown in Figure 3.8, AFM images of the chitosan-PEG/dsDNA nanoparticle complex has a spherical shape. The average diameters of the spherical chitosan: PEG and incorporated chitosan: PEG/dsDNA are 40 nm and 160 nm, respectively.

3.3.2 Poly(N-vinyl-α-hydroxypyrrolidone)/dsRNA nanoparticles

To further understanding the encapsulation of dsRNA with different nanocarriers, we modified PVP, an FDA approved polymer with the introduction of an α-hydroxy (α-OH) functional group to form poly(*N*-vinyl-α-hydroxypyrrolidone) or α-OH-PVP. We hypothesized that the presence of the α-OH group attached to PVP polymer can form hydrogen bonding with RNA and therefore incorporates RNA into α-OH-PVP. However, the affinity of α-OH-PVP to RNA may be smaller than that of positively charged chitosan conjugates. Figure 3.9 shows the computer simulation

image of RNA backbone with the α-OH-PVP, and it illustrates the hydrogen bonding between the α-OH group and RNA phosphodiester backbone.

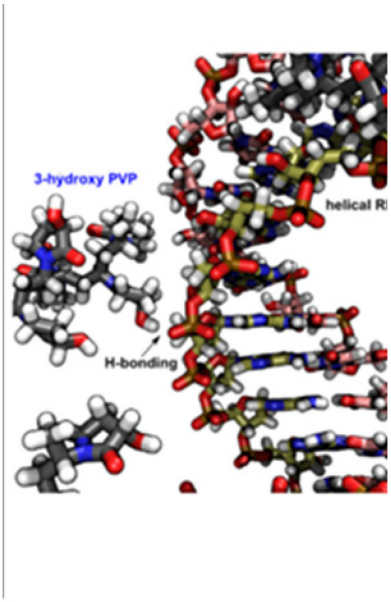

Figure 3.10: Computer simulation image of α-OH-PVP with dsRNA.

3.3.2.1 Synthesis of poly(N-vinyl-α-hydroxypyrrolidone)

Synthetic scheme for the synthesis of poly(*N*-vinyl-α-hydroxypyrrolidone) polymer is shown in Scheme 3.2.

Scheme 3.2: Synthesis of α-OH-PVP

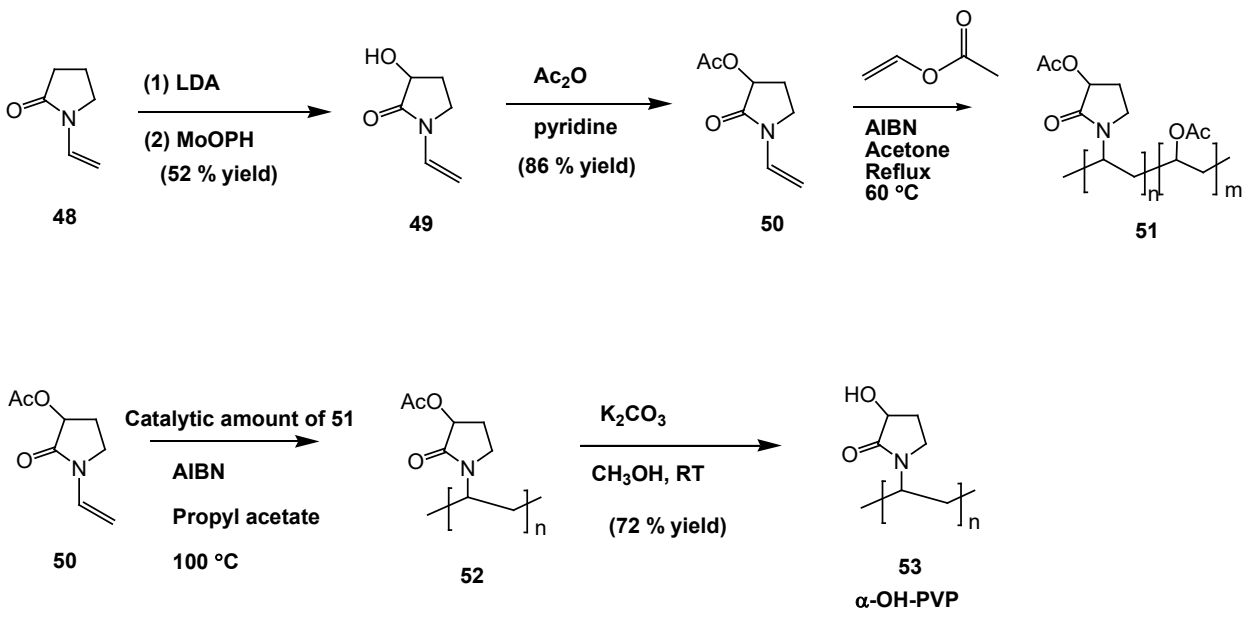

Synthesis of α-OH-PVP was achieved as outlined in the Scheme 3.2. Commercially available *N*-vinylpyrrolidone (**48**) was hydroxylated at C-3 position following the reported method in which the conversion of compound **48** to **49** was performed using the inverse addition procedure for MoOPH oxidation.[30]

Scheme 3.3: Preparation of oxodiperoxymolybdlenum(pyridine) (hexamethylphosphoric triamide) (MoOPH) [30]

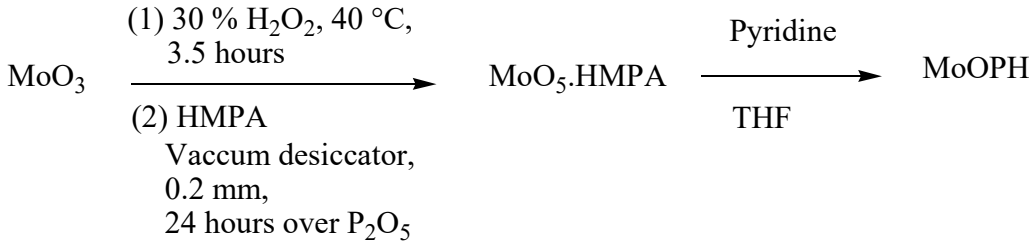

Briefly, the enolate of compound **48** was prepared using dropwise addition of titrated LDA solution in to a solution of **48** in dry THF at -78 °C. In a separate flask, MoOPH crystals were added dry

THF and it was cooled to -22 °C. Then the enolate of the compound **48** was introduced dropwise to the stirred MoOPH suspension at -22 °C and stirred for 15 minutes.

Scheme 3.4: Synthesis of α-OH-PVP copolymer from 3-hydroxy- *N*-vinylpyrrolidone

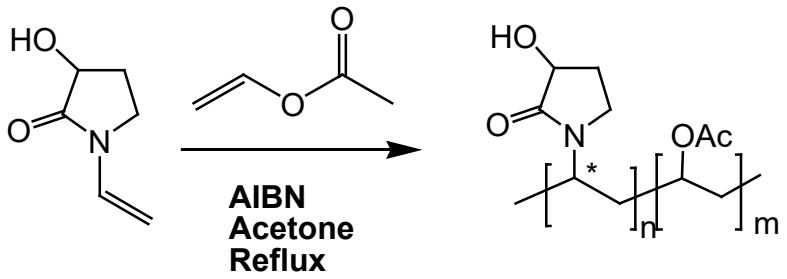

49 **54**

The conversion of **49** to **54** was studied in the presence of vinyl acetate, catalytic amount of AIBN in acetone under reflux conditions. However, this reaction did not result the desired product. Therefore, compound **49** was acetylated using acetic anhydride under pyridine to obtain compound **50**. Copolymerization of compound **50** using vinyl acetate, catalytic amount of AIBN in acetone under reflux conditions yielded the copolymer **51**. Reaction of compound **50** with catalytic amounts of compound **51**, AIBN, in propyl acetate as the solvent at 100 °C resulted the polymer **52**. This reaction was initially tried using ethyl acetate as the solvent at 70 – 80 °C. However, the polymerization reaction did not take place under this condition. Therefore, propyl acetate was used as the solvent and reaction was heated to higher temperatures (100 °C) to obtain the desired polymer **52**. Finally, the removal of the acetyl function with K_2CO_3 in methanol resulted the desired α-OH-PVP polymer (**53**) in 72% yield.

The synthesized α-OH-PVP polymer (**53**) was characterized by IR spectroscopy. The IR spectrum for the polymer **53** clearly shows the absence of Ac group (absence of CO stretch) and the presence

of OH group. The molecular weight of polymer **53** was found to be 67,425 Da as determined by gel permeation chromatography using TSKgel GMHxl column and THF as eluent.

3.3.2.2 Encapsulation of α-OH-PVP nanocarrier with dsDNA

The encapsulation ability of α-OH-PVP with dsDNA was studied. Clathrin heavy chain (CHC) ds DNA sample (523 base pairs; MW 509,402 Da)) was provided by Dr. Kun Yan Zhu's laboratory and 5% by weight of dsDNA was encapsulated with α-OH-PVP nanocarrier (95% by weight) in water, following the same procedure used for the encapsulation of adenine with chitosan: PEG polymer.

The particle sizes of the α-OH-PVP nanocarriers and encapsulated dsDNA/polymer nanoparticles were measured using atomic force microscopy (AFM) using tapping mode with a high aspect ratio tip. Figure 3.10 shows the representative AFM images of α-OH-PVP nanocarriers and encapsulated α-OH-PVP /dsDNA nanoparticles.

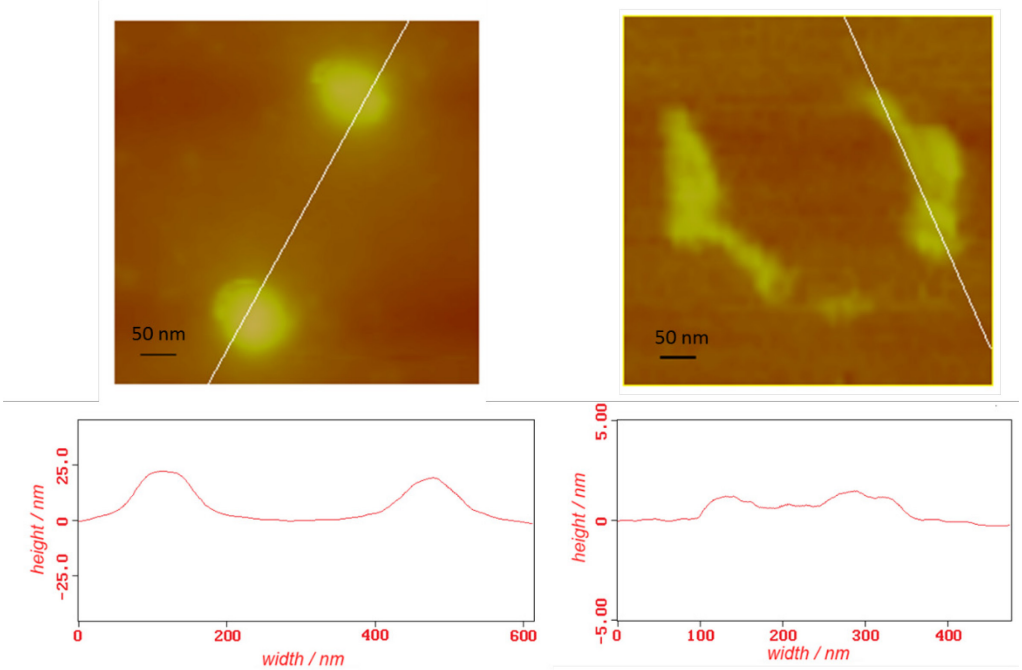

Figure 3.11: Representative AFM images of α-OH-PVP nanocarrier (left panel - top), the width (90 nm) and height (25 nm) (bottom) of the nanocarriers and encapsulated α-OH-PVP /dsDNA nanoparticles (right panel- top), and the width (~250 nm x 40 nm) and height (5 nm) (bottom) of the nanoparticles. Scale bar is 50 nm.

As shown from AFM images in Figure 3.10, the initial shape of the α-OH-PVP nanocarrier is spherical with diameter of 90 nm. However, when it is incorporated with dsDNA, the shape changed to elongated structures and the size is ~250 nm x 40 nm. Since the dsDNA has 523 base pairs and its length is estimated to be ~157 nm, (which is based on the distance ~0.3 nm between two nucleotides in A-form RNA), the AFM images (Figure 3.10, right panel) suggest the dsDNA is wrapped around by α-OH-PVP polymer.

3.3.2.3 Encapsulation of α-OH-PVP nanocarrier with siRNA (18 mers)

Similarly, the incorporation of siRNA (18 mers; MW ~6,120) with α-OH-PVP polymer was carried out by a mixing of siRNA (5% by weight) with α-OH-PVP (95% by weight) in water, and the resulting solution was lyophilized to give white solid. UV spectra of siRNA alone and the nanocarrier incorporated siRNA by α-OH-PVP were taken.

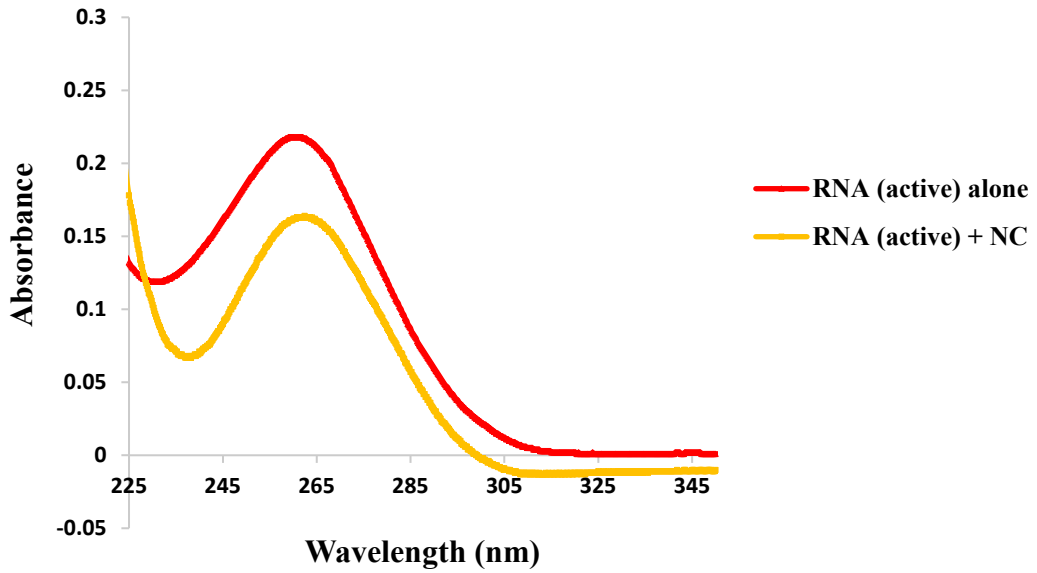

Figure 3.12: UV spectrum for the encapsulation of RNA with α-OH-PVP.

As shown in Figure 3.11, results showed that in the siRNA/α-OH-PVP complex, the UV absorbance is lower than that of siRNA alone, suggesting the possible incorporation of siRNA into nanocarrier.

3.3.3. Analysis of RNAi efficiencies among dsRNA/chitosan: PEG and dsRNA/ α-OH-PVP nanoparticles

Inspired from above preliminary results, testing of RNAi efficiencies for polymers encapsulated with particular dsRNA compared to naked RNA was carried out finally. Dr. Kun Yan Zhu provided two of the gene specific dsRNA molecules that are responsible for the encoding genes of the synthesis of vacuolar (H^+)-ATPase subunit (VhaSFD) protein of WCR. That two dsRNA will be denoted as (1) dsDvSFD (114 base pairs) and dsDvSFD2 (112 base pairs). As a control gene, double stranded green fluorescence protein (dsGFP) was used.

Nanoparticles of dsRNA/chitosan: PEG and dsRNA/ α-OH-PVP were made for each of the three different dsRNA molecules. Briefly, 5% by weight of dsRNA solution in deionized water was mixed with the corresponding amount of chitosan: PEG in 0.18% acetic acid in deionized water or α-OH-PVP (95% by weight) in deionized water, and this mixture was heated to 50 °C and cooled at 4 °C in ice water bath for 1 hour. This solution was lyophilized to give a solid.

The encapsulated dsRNA/chitosan: PEG and dsRNA/ α-OH-PVP nanoparticles were examined for RNAi efficiency by Dr. Young Ho Kim, in Dr. Kun Yan Zhu's laboratory. Briefly, 10 µg of encapsulated dsRNA containing nanoparticles or naked dsRNA was mixed with 30 mg of artificial diet and it was given to two days old total of 10 starved male and female adults separately. They were allowed to eat the diet for 10 hours. Then, they were given the normal artificial diet up to six days. Samples were obtained from each adult after two and six days of feeding and gene expression level was carried out using RT-qPCR. Two replicates were carried out.

Figure 3.12 shows the results for the expression of DvVhaSFD transcripts after feeding with the nanoparticles containing or naked dsRNA diet for 2 days.

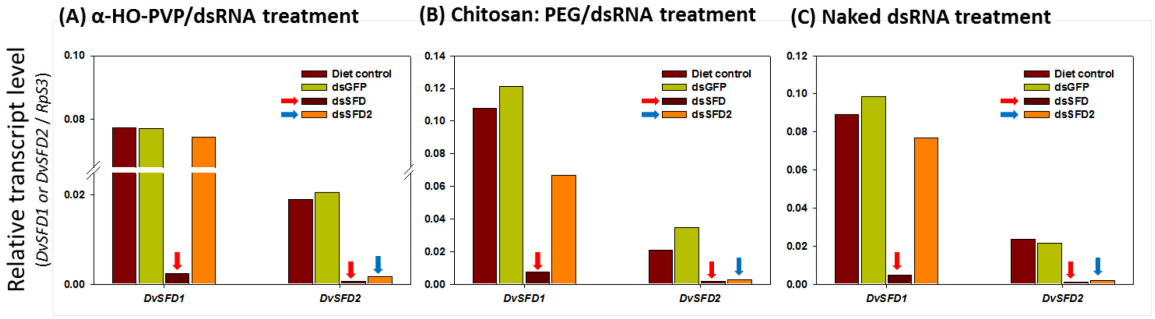

Figure 3.13: Expression of DvVhaSFD transcripts after dsRNA feeding for 2 days.

It can be seen from the above results that, nanoparticles encapsulated with dsSFD, dsSFD2 and naked dsRNA treatments have caused the significant suppression of relative transcript levels of DvSFD1 and DvSFD2 variants compared to controls. Besides, dsSFD alone strongly suppressed the expression of both transcript variants whereas dsSFD2 selectively suppressed the expression of DvSFD2. Moreover, there are no significant differences among α-OH-PVP/dsRNA, chitosan: PEG/dsRNA and naked dsRNA for the relative expression of DvVhaSFD transcripts after dsRNA feeding for 2 days.

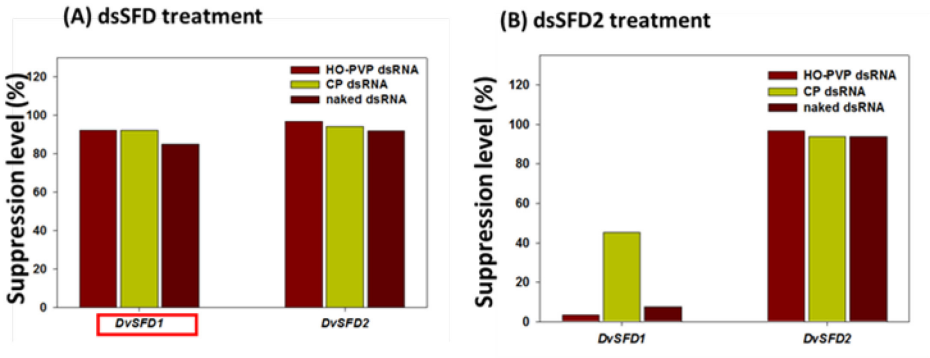

	HO-PVP dsRNA	CP dsRNA	Naked dsRNA
DvSFD1	92.0 %	92.2 %	84.9 %
DVSFD2	96.9 %	94.2 %	91.9 %

	HO-PVP dsRNA	CP dsRNA	Naked dsRNA
DvSFD1	3.3 %	45.3 %	7.6 %
DVSFD2	96.9 %	94.0 %	94.0 %

Figure 3.14: RNAi efficiency after dsRNA feeding for 2 days.

As shown from above data, nanoparticles formulated with dsSFD RNA and naked dsSFD RNA effectively suppress the both DvSFD1 and DvSFD2 target transcripts (92.0 - 96.9%), 2 days after dsRNA feeding. Among the nanoparticles formed with dsSFD2 RNA, chitosan: PEG/dsSFD2 shows a higher suppression (45.3%) of DvSFD1 transcript compared to that of α-OH-PVP and naked dsRNA feeding. Besides, there is an effective suppression of DvSFD2 transcript (94 –

96.9%) from the nanoparticles formed with dsSFD2 RNA and naked dsSFD2 RNA after 2 days of feeding.

Figure 3.14 shows the results for the expression of DvVhaSFD transcripts after feeding with the nanoparticles containing or naked dsRNA diet for 6 days.

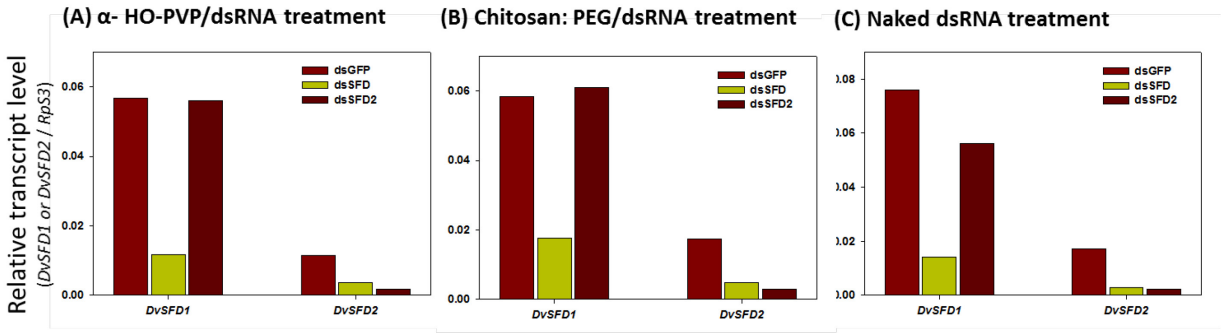

Figure 3.15: Expression of DvVhaSFD transcripts after dsRNA feeding for 6 days.

When comparing the DvVhaSFD transcript after dsRNA feeding for 6 days, it can be still seen that, dsSFD containing nanoparticles and naked dsSFD strongly suppressed the expression of both transcript variants whereas dsSFD2 selectively suppressed the expression of DvSFD2. There is no difference among nanoparticles and naked dsSFD. However, the relative transcript level of both variants seems to be higher compared to that of 2 days suggests that the suppression is gradually decreased after 6 days.

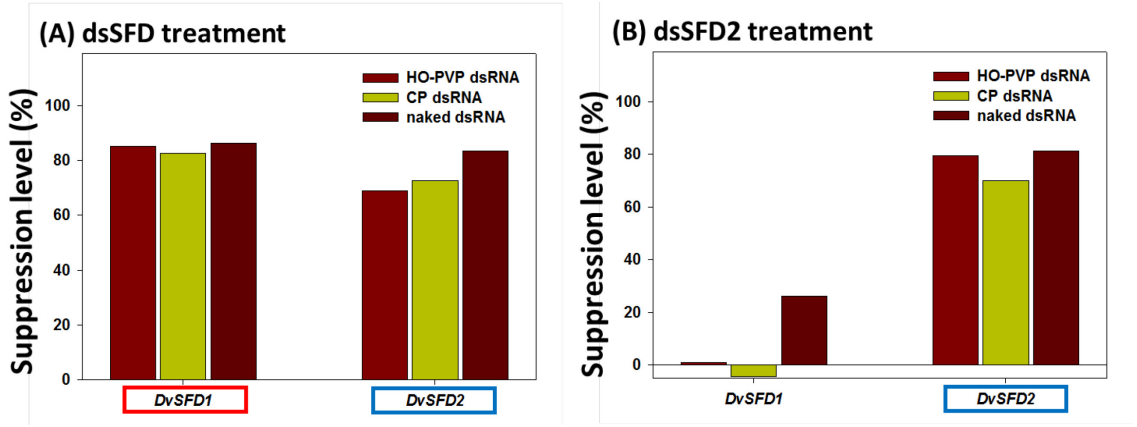

	HO-PVP dsRNA	CP dsRNA	Naked dsRNA
DvSFD1	85.0 %	82.7 %	86.4 %
DVSFD2	68.9 %	72.6 %	83.5 %

	HO-PVP dsRNA	CP dsRNA	Naked dsRNA
DvSFD1	1.1 %	-4.3 %	26.2 %
DVSFD2	79.4 %	70.0 %	81.3 %

Figure 3.16: RNAi efficiency after dsRNA feeding for 6 days.

It can be seen from the Figure 3.15 that, the suppression level of both target transcripts are relatively lower (68.9 – 86.4%) compared to that of 2 days, yet, RNAi efficiency is still can be seen. But, when comparing the results of nanoparticles containing dsSFD with naked dsSFD, it is clearly demonstrating that nanoparticles do not behave stronger than that of naked dsSFD, whereas naked dsSFD treatment seems act on insects better than the nanoparticles. The results implied that the dsRNAs did not form nanoparticles with the nanocarrier.

3.3.4 Future perspectives

Since the above discussed two polymer conjugates are not successful as nanocarriers for gene delivery into WCR, a previously reported chitosan: galactose polymer was synthesized to study

the specific dsRNA delivery into WCR.[31,32] The synthetic scheme for the synthesis of chitosan: galactose polymer is shown in Scheme 3.5.

Scheme 3.5: Synthesis of chitosan: galactose polymer[31,32]

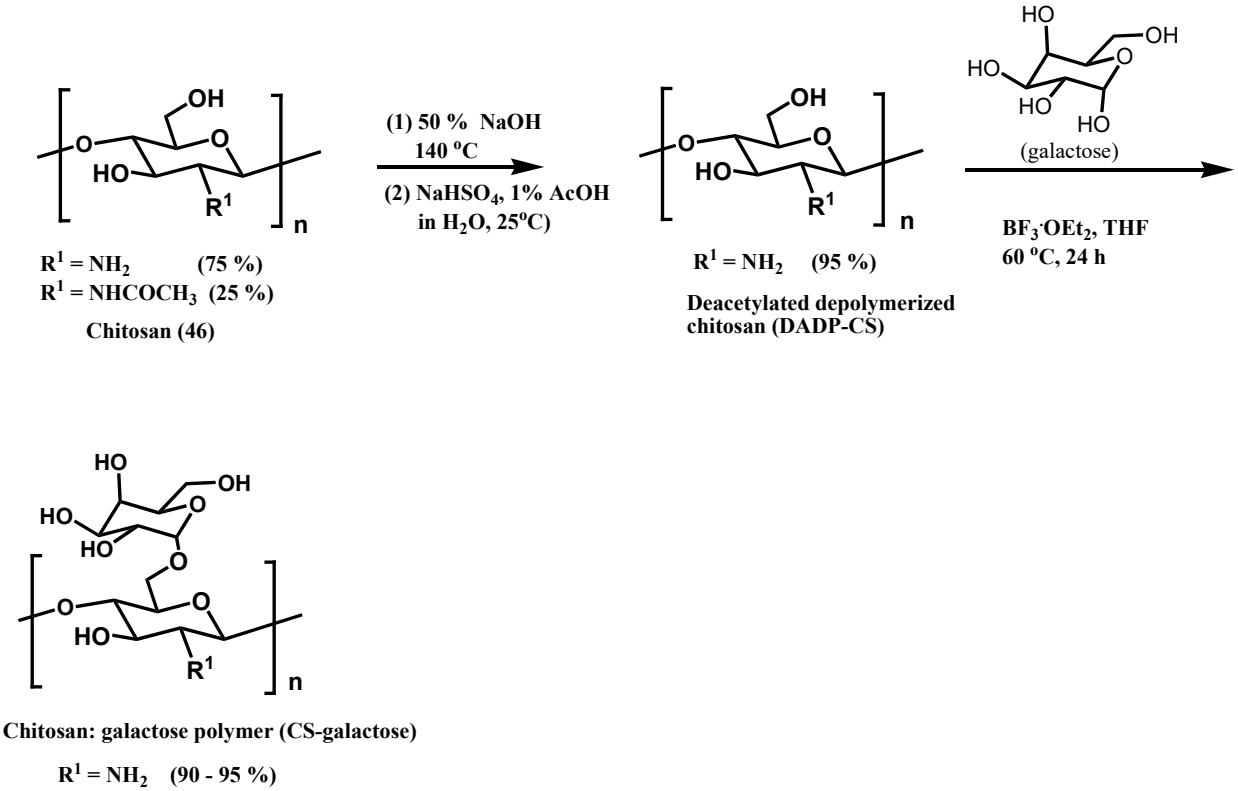

As shown in Scheme 3.5, chitosan: galactose polymer (CS-galactose) was synthesized following a reported method.[31,32] Briefly, commercially available chitosan (**46**) was deacetylated using 50% NaOH followed by depolymerized by adding $NaHSO_4$ into a solution of deacetylated chitosan in 1 % AcOH in water. Finally, the deacetylated depolymerized chitosan (**DADP-CS**) was reacted with galactose and boron trifluoride diethyl etherate ($BF_3{\cdot}OEt_2$) to obtain chitosan: galactose polymer (**CS-galactose**). The synthesized polymer was characterized by proton NMR. In future, this polymer will be tested to identify whether it is a suitable nanocarrier for the delivery of dsRNA into WCR.

3.4 Conclusion

In pursuit of an investigating nanodelivery of specific dsRNA for suppressing the western corn rootworm (WCR, *Diabrotica virgifera virgifera*) genes, two of the novel polymer based nanomaterials have been designed and synthesized by modifying chitosan and PVP as nanocarriers. Chitosan is an Environmental Protection Agency (EPA) approved polymer and it was modified by PEGylating with activated PEG to obtain chitosan: PEG nanocarriers. By PEGylating the chitosan, we believed that it can improve the efficacy and solubility of the chitosan: PEG nanoparticles. In addition, another EPA approved polymer, PVP was modified by hydroxylating to obtain α-OH-PVP nanocarriers. The synthesized polymers were characterized by IR spectroscopy and used for the encapsulation of specific dsRNA molecules, which are important for the formation of an essential protein sub unit of WCR. The results from the RNAi efficacy testing experiments demonstrate that, dsRNA was effective in gene suppression in WCR, however, none of the polymer based nanomaterials show better RNAi efficacy profile than that of naked dsRNA. Therefore, stability testing of the encapsulated nanoparticles were studied and results showed that dsRNA are either dissociate quickly from the nanoparticles or stable nanoparticles are not formed between the nanocarriers and specific dsRNA molecules. In future, novel analogues of chitosan such as chitosan:galactose, and PVP are being designed and developed and will be evaluated for their ability to make nanoparticles with dsRNA.

3.5 Experimental Section

3.5.1 General methods

Nuclear magnetic resonance spectra were obtained from a Varian 400-MHz spectrometer using deuteriochloroform ($CDCl_3$) as the solvent unless otherwise stated and all chemical shifts reported in ppm. Low resolution mass spectra were obtained from an API 2000-triple quadrupole ESI-MS/MS mass spectrometer (from Applied Biosystems). Infrared spectra were taken from a ThermoScientific Nicolet 380 FT-IR instrument. A Hewlett-Packard diode array UV/VIS spectrophotometer was used in the UV measurements. A Nanoscope IIIa scanning probe microscope (Digital Instruments Inc., Santa Barbara, CA, USA) workstation equipped with a multimode head using E-series or J-series piezoceramic scanner (Digital Instruments, Santa Barbara, CA) was used to obtain AFM images. Chemicals were purchased from Fisher Scientific, Aldrich Chemical Co., Chem-Impex International, and VWR.

3.5.1.1 Synthesis of chitosan/PEG (5:1) nanocarrier

Chitosan: PEG polymer (**47**)

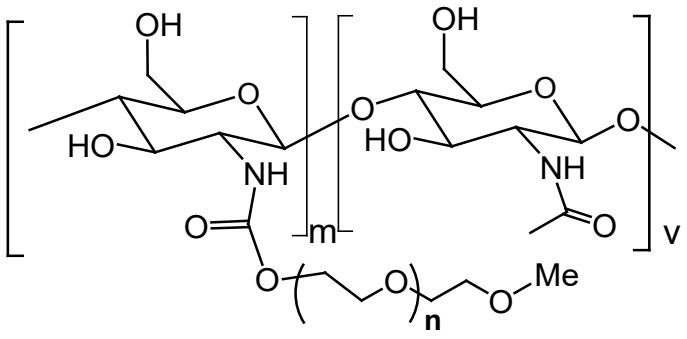

A mixture of 2-(2-methoxyethoxy)ethyl 1H-imidazole-1-carboxylate (**45**) (294 mg, 0.456 mmol) and chitosan (25% N-acetylated) (**46**) (495 mg, 2.28 mmol) were vaccum dried for two hours. It was added 5 ml of dry DMF and the resulting suspension was refluxed at 120 °C for 12 hours under argon atmosphere. 10 mL of diethyl ether was added and the mixture was centrifuged at 10,000 rpm for 10 minutes. Supernatant was removed and residue was added another 10 ml of dry ethyl ether and centrifuged at 10,000 rpm for 10 minutes. Residue was dried under vacuum to obtain chitosan: PEG polymer (**47**) as a brown color powder. The corresponding IR spectrum is shown in Appendix A.

3.5.1.2 Synthesis of α-OH-PVP nanocarrier

Preparation of **MoOPH** (oxodiperoxymolybdlenum(pyridine) (hexamethylphosphorictriamide) has been reported previously.[30] It was prepared as below.

A 20 g of MoO_3 was added to a 500 ml three neck round bottom flask fitted with a magnetic stirrer and it was added 100 mL of 30 % H_2O_2 and stirred vigorously. An oil bath preheated to 40 °C was used to heat the mixture until a mild exothermic reaction was observed. As soon as the internal temperature reached 35 °C, the mixture was stirred at 40 °C for a total of 3.5 hours while maintaining the internal temperature at 35 °C – 40 °C. After 3.5 hours, the reaction mixture was cooled to 20 °C and it was filtered to remove solids. The yellow solution was cooled to 10 °C and HMPA 24.3 mL was added slowly while stirring. The resulting yellow precipitate was collected on a Buchner funnel and recrystallized from methanol to obtain 25 g of yellow crystalline precipitate of $MoO_5.H_2O$.HMPA. Further drying over vacuum desiccator, 0.2 mm Hg of pressure, 24 hours over P_2O_5 resulted MoO_5.HMPA with a 42% yield. A 10 g of anhydrous complex of MoO_5.HMPA was added dry THF 20 mL and it was stirred well until all dissolved. 2.1 mL of

pyridine was added dropwise while keeping the reaction in a 20 °C water bath. The yellow precipitate formed was filtered and washed with a small amount of dry THF followed by 25 mL of dry ether twice. It was dried over vacuum to obtain 4.6 g of MoOPH (94% yield).

3-Hydroxy-1-vinylpyrrolidin-2-one (**49**)

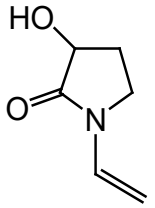

Diisopropylamine (0.825 mL, 5.85 mmol) was added to a solution of dry THF under argon atmosphere and cooled to -78 °C and n-BuLi (4.8 mL, 4.5 mmol) was added dropwise and stirred for 20 minutes at -78 °C. The prepared LDA solution was added dropwise to a solution of 1-Vinyl-2-pyrrollidinone (**48**) (500 mg, 4.49 mmol) in dry THF and stirred at -78 °C for one hour. The prepared enolate of compound **48** was brought to -22 °C and it was added to a suspension of MoOPH (2.92 g, 6.75 mmol) in dry THF at -22 °C. This suspension was turned to a blue-green solution after 15 minutes and the reaction was neutralized by adding 25 mL of saturated sodium sulfite (Na_2SO_3) solution and reaction was warmed to 20 °C. 20 ml of H_2O was added and further stirred for 15 minutes. Organic layer was separated and aqueous layer was extracted three times with ether. Combined organic layers were dried over Na_2SO_4, filtered, concentrated and column chromatographed using a mixture of DCM and methanol (15:1) as an eluent to give 300.0 mg (52% yield) of compound **49** as white solid. ^{1}H NMR δ ppm 1.98 - 2.05 (m, 1 H), 2.38 - 2.67 (m, 1 H), 3.29 - 3.49 (m, 1 H), 3.50 - 3.74 (m, 1 H), 3.75 (br s, 1 H), 4.32 - 4.66 (m, 3 H), 7.06 (br dd, *J* = 16.0, 9.0 Hz, 1 H); ^{13}C NMR ($CDCl_3$), δ 175.14, 129.3, 96.16, 70.32, 41.28, 27.47.

2-Oxo-1-vinylpyrrolidin-3-yl acetate (**50**)

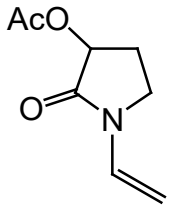

To a solution of 3-hydroxy-1-vinylpyrrolidin-2-one (**49**) (300 mg, 2.36 mmol) in 5 mL dry pyridine was added Ac_2O dropwise. Reaction was stirred at 50 °C – 60 °C overnight under argon atmosphere. Reaction was diluted with 50 ml DCM. It was extracted with 25 mL of H_2O followed by 25 mL of 5 % HCl. Organic layer was dried over Na_2SO_4, filtered, concentrated and column chromatographed using a mixture of hexane and diethyl ether as an eluent to give 344.0 mg (86% yield) of compound **50** as white solid. ^{1}H NMR (400 MHz, CHLOROFORM-*d*) δ ppm 2.03 (br dd, *J*=13.28, 9.37 Hz, 1 H), 2.15 (s, 3 H), 2.66 (s, 1 H), 3.33 - 3.51 (m, 1 H), 3.61 (dd, *J*=9.76, 2.73 Hz, 1 H), 4.42 - 4.64 (m, 2 H), 5.38 (t, *J*=8.40 Hz, 1 H), 7.03 - 7.25 (m, 1 H).

Co-polymer (**51**)

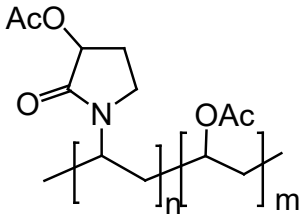

To a solution of 2-oxo-1-vinylpyrrolidin-3-yl acetate (**50**) (25 mg, 0.148 mmol) in 100 µL of dry acetone was added dry vinyl acetate (13 mg, 0.148 mmol) using a micro syringe. To this mixture, catalytic amount of AIBN (0.24 mg, 0.00148 mmol) was added and stirred at 70 °C for 18 hours. The reaction mixture was concentrated and 200 µL of ether was added to the residue. The resulted

white precipitate was washed with 100 µL of ether twice to remove unreacted starting material. The white solid was vacuum dried to obtain copolymer **51** (16 mg) as a white solid (39% yield). ^{1}H NMR (400 MHz, CHLOROFORM-*d*) δ ppm 1.19 (br d, *J*=6.64 Hz), 1.94 - 2.22 (m), 2.55 (br s), 3.45 (br d, *J* = 7.03 Hz), 5.33 (br s).

Polymer (**52**)

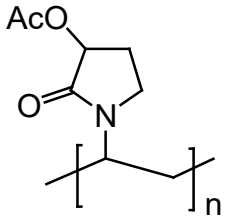

Compound (**50**) (200 mg, 1.18 mmol) and catalytic amount of copolymer **51** (2 mg, 0.0118 mmol) was dried under vacuum and was added dry propyl acetate (100 µL) under argon atmosphere. This mixture was heated to 70 °C and then was added AIBN (3 mg, 0.4 mol %) in 100 µL of dry propyl acetate. The mixture was heated at 100 °C under argon atmosphere for 18 hours. The reaction mixture was concentrated to remove propyl acetate and crude was washed with 100 µL of ether to remove unreacted starting material. The resulted white solid was then put under vacuum to obtain polymer **52** (180 mg) as a white solid (90 % yield). ^{1}H NMR (400 MHz, CHLOROFORM-*d*) δ ppm 1.68 (br s), 1.73 - 1.91 (m), 2.14 (br d, *J* = 7.42 Hz), 2.6 (br s), 3.27 (br s), 5.35 (br s).

Polymer **53**

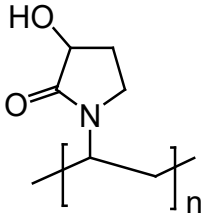

To a solution of compound **52** (100 mg, 0.592 mmol) in 2 ml of methanol was added anhydrous K_2CO_3 (121 mg, 0.88 mmol) slowly and stirred at room temperature for 48 hours. Acetic acid (101 µL in 1 mL deionized water, 1.76 mmol) was added to neutralize the K_2CO_3 and the solution was transferred into 3500 MWCO dialysis tubing using 6 mL deionized water and carried out the dialysis for 18 hours. The resulted solution was lyophilized to obtain polymer **53** (52 mg**)** as a white solid (72% yield). The polymer **53** was characterized by IR spectroscopy and corresponding IR spectrum is attached in Appendix A.

3.5.1.3. Synthesis of chitosan: galactose nanocarrier

Deacetylated depolymerized chitosan (**DADP-CS**)

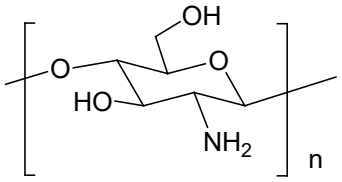

A solution of commercially available chitosan (46) 2 g in 40 mL of 50 % w/v NaOH solution was refluxed at 140 °C in an oil bath for 4 hours.[31] After 4 hours, reaction mixture was cooled to room temperature and was added a large amount of deionized water to remove NaOH. The mixture was filtered and the resulted light brown color solid was dried in the oven at 40 °C overnight to obtain 1 g of deacetylated chitosan. Then to a solution of 1 g of deacetylated chitosan in 100 mL of 1% acetic acid solution was added 0.1 M $NaHSO_4$ (1.51 g of $NaHSO_4$ in 10 mL water) dropwise and stirred for 3 hours at room temperature. Reaction mixture was filtered and the filtrate was added 1N NaOH aqueous solution until the product is precipitated. The precipitate was isolated by

centrifugation it was lyophilized to obtain deacetylated depolymerized chitosan (DADP- CS). The polymer was characterized by IR spectroscopy and the spectrum is attached in Appendix A.

Chitosan: galactose polymer (**CS-galactose**)

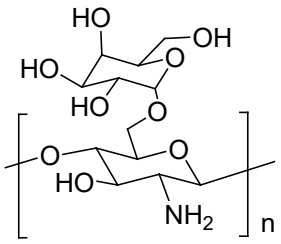

To a solution of **DADP-CS** (30 mg, 0.167 mmol) and galactose (76 mg, 0.42 mmol) in 2 mL dry THF was added 0.02 mL of boron trifluoride diethyletherate ($BF_3.OEt_2$) (0.167 mmol) and the mixture was heated at 60 °C under argon atmosphere for 24 hours. After 24 hours, solvent was removed by rotary evaporation and the mixture was transferred into a 1000 MWCO dialysis tubing using 5 ml deionized water and carried out the dialysis for 18 hours. The resulted solution was lyophilized to obtain chitosan: galactose polymer (**CS-galactose**) (40 mg**)** as a light brown solid (95 % yield). ^{1}H NMR (400 MHz, D_2O) δ ppm 3.3 – 4.0 (br m), 2.95 (br s).

3.5.1.4 General procedure for the formation of chitosan/adenine nanoparticles

A 5% by weight of adenine (MW 135.13 g/mol) in deionized water was added to a solution of chitosan: PEG nanocarrier (95% by weight) in 0.18 % acetic acid in deionized water, and the resulting solution was heated to 50 °C for one minute and then was cooled in 4 °C for one hour. The solution was finally lyophilized to give a solid.

3.5.1.5 General procedure for the formation of chitosan: PEG/dsDNA nanoparticles

A 5% by weight of dsDNA (523 base pairs; MW 509,402 Da) in deionized water was added to a solution of chitosan: PEG nanocarrier (95% by weight) in 0.18 % acetic acid in deionized water, and the resulting solution was heated to 50 °C for one minute and then was cooled in 4 °C for one hour. The solution was finally lyophilized to give a solid.

3.5.1.6 General procedure for the formation of chitosan: PEG/dsRNA nanoparticles

The formation of chitosan: PEG/dsRNA nanoparticles was same as that described in section *3.5.1.4*.

3.5.1.7 General procedure for the formation of α-OH-PVP/dsDNA nanoparticles

A 5% by weight of dsDNA (523 base pairs; MW 509,402 Da) in deionized water was added to a solution of α-OH-PVP nanocarrier (95% by weight) in deionized water, and the resulting solution was heated to 50 °C for one minute and then was cooled in 4 °C for one hour. The solution was finally lyophilized to give a solid.

3.5.1.8 General procedure for the formation of α-OH-PVP/dsRNA nanoparticles

The formation of α-OH-PVP /dsRNA nanoparticles was same as that described in section *3.5.1.4*.

3.5.1.9 Atomic Force Microscopy (AFM) Imaging

AFM was used to examine the nanoparticles using a tapping mode with a high aspect ratio tip. Briefly, 30 μL of the nanoparticle solution in deionized water was placed onto freshly cleaved mica, and dried with air. AFM images on different locations of the mica were then obtained using a Nanoscope IIIa scanning probe microscope (Digital Instruments Inc., Santa Barbara, CA, USA).

3.6 References

1. Kanasty, R.; Dorkin, J. R.; Vegas, A.; Anderson, D., Delivery materials for siRNA therapeutics. *Nature materials* **2013**, *12* (11), 967-977.

2. Williford, J.-M.; Wu, J.; Ren, Y.; Archang, M. M.; Leong, K. W.; Mao, H.-Q., Recent advances in nanoparticle-mediated siRNA delivery. *Annual review of biomedical engineering* **2014**, *16*, 347-370.

3. Katoch, R.; Sethi, A.; Thakur, N.; Murdock, L. L., RNAi for insect control: current perspective and future challenges. *Applied biochemistry and biotechnology* **2013**, *171* (4), 847-873.

4. Price, D. R.; Gatehouse, J. A., RNAi-mediated crop protection against insects. *Trends in biotechnology* **2008**, *26* (7), 393-400.

5. Huvenne, H.; Smagghe, G., Mechanisms of dsRNA uptake in insects and potential of RNAi for pest control: a review. *Journal of insect physiology* **2010**, *56* (3), 227-235.

6. Baum, J. A.; Bogaert, T.; Clinton, W.; Heck, G. R.; Feldmann, P.; Ilagan, O.; Johnson, S.; Plaetinck, G.; Munyikwa, T.; Pleau, M., Control of coleopteran insect pests through RNA interference. *Nature biotechnology* **2007**, *25* (11), 1322-1326.

7. Mao, Y.-B.; Cai, W.-J.; Wang, J.-W.; Hong, G.-J.; Tao, X.-Y.; Wang, L.-J.; Huang, Y.-P.; Chen, X.-Y., Silencing a cotton bollworm P450 monooxygenase gene by plant-mediated RNAi impairs larval tolerance of gossypol. *Nature biotechnology* **2007**, *25* (11), 1307-1313.

8. Kim, Y. H.; Issa, M. S.; Cooper, A. M.; Zhu, K. Y., RNA interference: Applications and advances in insect toxicology and insect pest management. *Pesticide biochemistry and physiology* **2015**, *120*, 109-117.

9. Katoch, R.; Thakur, N., Insect gut nucleases: a challenge for RNA interference mediated insect control strategies. *Int. J. Biochem. Biotechnol.* **2012**, *1* (8), 198-203, 7 pp.

10. Swevers, L.; Smagghe, G., Use of RNAi for control of insect crop pests. In *Arthropod-Plant Interactions*, Springer: **2012**; pp 177-197.

11. Rodrigues, T. B.; Figueira, A., Management of Insect Pest by RNAi—A New Tool for Crop Protection. **2016,** 371-390.

12. Bolhassani, A.; Javanzad, S.; Saleh, T.; Hashemi, M.; Aghasadeghi, M. R.; Sadat, S. M., Polymeric nanoparticles: potent vectors for vaccine delivery targeting cancer and infectious diseases. *Human vaccines & immunotherapeutics* **2014,** *10* (2), 321-332.

13. Pimentel, D., Environmental and economic costs of the application of pesticides primarily in the United States. *Environment, development and sustainability* **2005**, *7* (2), 229-252.

14. Gordon, K. H.; Waterhouse, P. M., RNAi for insect-proof plants. *Nature biotechnology* **2007**, *25* (11), 1231-1232.

15. Whyard, S.; Singh, A. D.; Wong, S., Ingested double-stranded RNAs can act as species-specific insecticides. *Insect biochemistry and molecular biology* **2009**, *39* (11), 824-832.

16. Zhang, H.; Li, H. C.; Miao, X. X., Feasibility, limitation and possible solutions of RNAi-based technology for insect pest control. *Insect science* 2013, *20* (1), 15-30.

17. Fire, A.; Xu, S.; Montgomery, M. K.; Kostas, S. A.; Driver, S. E.; Mello, C. C., Potent and specific genetic interference by double-stranded RNA in Caenorhabditis elegans. *nature* **1998**, *391* (6669), 806-811.

18. Terenius, O.; Papanicolaou, A.; Garbutt, J. S.; Eleftherianos, I.; Huvenne, H.; Kanginakudru, S.; Albrechtsen, M.; An, C.; Aymeric, J.-L.; Barthel, A., RNA interference in

Lepidoptera: an overview of successful and unsuccessful studies and implications for experimental design. *Journal of insect physiology* **2011,** *57* (2), 231-245.

19. Whitehead, K. A.; Langer, R.; Anderson, D. G., Knocking down barriers: advances in siRNA delivery. *Nature reviews Drug discovery* **2009**, *8* (2), 129-138.

20. Khot, L. R.; Sankaran, S.; Maja, J. M.; Ehsani, R.; Schuster, E. W., Applications of nanomaterials in agricultural production and crop protection: a review. *Crop protection* **2012**, *35*, 64-70.

21. Lee, J.-M.; Yoon, T.-J.; Cho, Y.-S., Recent developments in nanoparticle-based siRNA delivery for cancer therapy. *BioMed research international* **2013**, 1-11.

22. Xu, H.; Li, Z.; Si, J., Nanocarriers in gene therapy: a review. *Journal of biomedical nanotechnology* **2014**, *10* (12), 3483-3507.

23. Draz, M. S.; Fang, B. A.; Zhang, P.; Hu, Z.; Gu, S.; Weng, K. C.; Gray, J. W.; Chen, F. F., Nanoparticle-mediated systemic delivery of siRNA for treatment of cancers and viral infections. *Theranostics* **2014**, *4* (9), 872-892.

24. Tamura, A.; Nagasaki, Y., Smart siRNA delivery systems based on polymeric nanoassemblies and nanoparticles. *Nanomedicine* **2010,** *5* (7), 1089-1102.

25. Zhang, X.; Zhang, J.; Zhu, K., Chitosan/double-stranded RNA nanoparticle-mediated RNA interference to silence chitin synthase genes through larval feeding in the African malaria mosquito (Anopheles gambiae). *Insect molecular biology* **2010**, *19* (5), 683-693.

26. http://www.monsanto.com/products/pages/corn-rootworm-backgrounder.aspx

27. Saharan, V.; Mehrotra, A.; Khatik, R.; Rawal, P.; Sharma, S.; Pal, A., Synthesis of chitosan based nanoparticles and their in vitro evaluation against phytopathogenic fungi. *International journal of biological macromolecules* **2013**, *62*, 677-683.

28. dos Santos Silva, M.; Cocenza, D. S.; Grillo, R.; de Melo, N. F. S.; Tonello, P. S.; de Oliveira, L. C.; Cassimiro, D. L.; Rosa, A. H.; Fraceto, L. F., Paraquat-loaded alginate/chitosan nanoparticles: preparation, characterization and soil sorption studies. *Journal of hazardous materials* **2011**, *190* (1), 366-374.

29. Grillo, R.; Pereira, A. E.; Nishisaka, C. S.; de Lima, R.; Oehlke, K.; Greiner, R.; Fraceto, L. F., Chitosan/tripolyphosphate nanoparticles loaded with paraquat herbicide: an environmentally safer alternative for weed control. *Journal of hazardous materials* **2014**, *278*, 163-171.

30. Vedejs, E.; Engler, D.; Telschow, J., Transition-metal peroxide reactions. Synthesis of. alpha.-hydroxycarbonyl compounds from enolates. *The Journal of Organic Chemistry* **1978**, *43* (2), 188-196.

31. Lin, W.J.; Chen, T.D.; Liu, C.W., Synthesis and characterization of lactobionic acid grafted pegylated chitosan and nanoparticle complex application. *Polymer* **2009**, *50* (17), 4166-4174.

32. Lin, W.J.; Hsu, W.Y., Pegylation effect of chitosan based polyplex on DNA transfection. *Carbohydrate polymers*, **2015**. *120*, 7-14.

Chapter 4 - Synthesis of Viral Protease Inhibitors

4.1 Introduction

Infections caused by viruses result severe detrimental effects to human way of life and it has been estimated that approximately 25% of people will be died from an infection.[1] Not only humans, but also other multi cellular organisms on earth get affected from viral infections and therefore create even far more threat to humans.

In principle, antiviral drugs could be designed to target either at viral proteins or host cellular proteins and both approaches have certain advantages and disadvantages.[2] Targeting viral proteins more likely result more specific, less toxic compounds, yet, it can result compounds with a narrow spectrum of activity and likely create a higher chance of virus-drug resistance. Targeting host cellular proteins may afford compounds with a broader spectrum of activity, yet, it can result higher toxicity.[2]

Among the several diseases caused by viruses, gastroenteritis has attracted public attention as it is globally responsible for great morbidity and mortality among all ages. There are about 70,000 hospitalizations and over 800 deaths annually, in the United States, alone.[3] The leading pathogen for the majority of cases of gastroenteritis are noroviruses (NV) and is responsible for ~58% of all food borne illnesses.[3] NV associated gastroenteritis results symptoms such as diarrhea, fever, nausea, vomiting etc and usually last for about three days in healthy adults, however, elderly, and immunocompromised patients experience prolong symptoms. There is no specific medication available for the treatment of NV infections, and therefore discovery of novel anti-norovirus drugs is highly warranted.

In our efforts of discovering potent novel anti-NV compounds, we focused on synthesizing several tripeptidyl analogues by changing the P1, P2, P3 positions and the N-terminal cap (P4) as shown in Figure 4.1.[4,5]

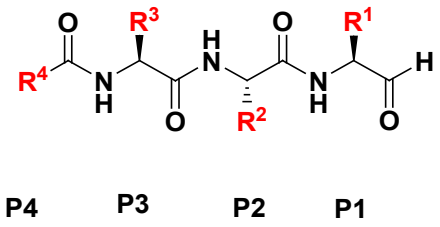

Figure 4.1: Generic tripeptidyl protease inhibitor structure.

In the first part of this chapter, I summarized the work I carried out in the synthesis of novel anti-NV analogues by changing the R^1 and R^4 positions and in the second part, I discussed the work I carried out in the large scale synthesis of known dipeptidyl compound (GC376) for evaluating its efficacy on feline infectious peritonitis (FIP) *in vivo* using cats.

4.2 Background

NVs are non-enveloped, single stranded RNA viruses with a positive sense genome (~7.5 kb) and belongs to the genus *Norovirus* in the family of *Caliciviridae*. RNA genome of NVs have organized into three open reading frames (ORFs). ORF1 encodes a polyprotein of six/seven nonstructural protein products, ORF2 encodes major structural capsid protein VP1 and ORF3 encodes minor structural capsid protein VP2. NV genome is covalently linked to a viral protein called VPg at the 5′end and is polyadenylated at the 3′ end (Figure 4.2).[3]

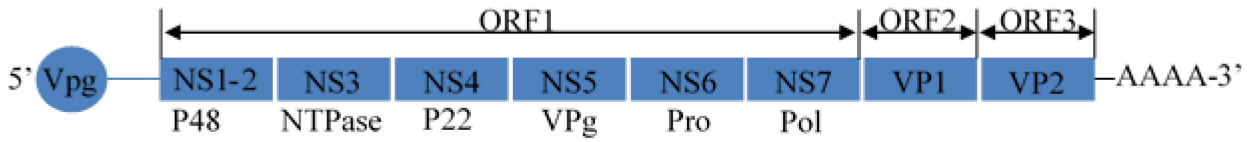

Figure 4.2: Schematic representation of the RNA genome of NVs.

NV outbreaks often occur in semi-closed environments such as hospitals, cruise ships, nursing homes, schools etc and usually difficult to control due to their low infectious dose (17 virus particles), prolong persistence in the environment, and their ability to withstand general sanitary measures used against other microorganisms.[3]

Viruses belongs to the picornavirus-like supercluster, which includes picornaviruses, caliciviruses, and coronaviruses possess important nonstructural enzymes called 3C or 3C-like proteases (3Cpro or 3CLpro, respectively), which contain a typical chymotrypsin-like fold and a catalytic triad (or dyad) with a Cys residue as a nucleophile.[4] These enzymes act as promising targets to focus on drug discovery due to their central roles play on these viruses. 3Cpro or 3CLpro involves in the cleavage of the viral polyprotein into mature or intermediate virus proteins, thus being an essential part in viral replication and propagation.[4] Both 3Cpro or 3CLpro share common characteristics which include, a typical chymotrypsin-like fold; catalytic triad consists of cysteine (Cys), histidine (His), and glutamine (Glu) (or Asp) residues; use a Cys (SH side chain) as the active site nucleophile to cleave the peptide substrate scissile bond and a preference for a Glu or Gln residue at the P1 position on the substrate.[4]

Our efforts to create potent anti-NV compounds primarily targeted on the inhibition of NV 3C-like protease (NV3CLpro).[5] Apart from having the above mentioned features, studies have shown that His30, Glu54 and Cys139 are conserved in all NV3CLpro enzymes and the His30/Cys139 pair work as an acid-base dyad that is essential for protease activity.[6] X ray crystal structures of

the NV3CLpro have been reported.[7] The substrate binding site of NV3CLpro consists of substrate binding pockets (S1, S2, S3…) which have been defined in an order of moving away from the active site toward the bound substrates N-terminus end. When considering about the interactions between the NV3CLpro with natural substrates, it has been found that, the residues Thr134, His157 and Ala16028 in the S1 pocket interact with the P1 glutamine (Gln)/ glutamic acid (Glu) of the substrate.[7] The S2 pocket is hydrophobic in nature and contains residues such as Ile109, Arg112 and Val114 to favor the accommodation of bulky hydrophobic P2 side chains such as Leu and Phe.[7] By designing peptidyl molecules as the inhibitors, we believed that it can mimic the primary substrate of the NV3CLpro to interact well with the enzyme.

Coronaviruses in the family of *Coronaviridae* are another important viruses that infect both animals and humans creating wide range of diseases.[8] Feline coronavirus cause feline infectious peritonitis (FIP), a highly fatal disease among domestic and wild cats and is associated with immune responses and involves depletion of T cells.[8] Groutas and coworkers have discovered a potent dipeptidyl compound (GC376) that targets 3C-like protease (3CLpro) with broad-spectrum activity against various human and animal coronaviruses.[4,9] As a collaboration with that group, I was involved in the gram-scale (15g -20g) synthesis of GC376 to evaluate its therapeutic efficacy as a 3CLpro inhibitor in laboratory cats with FIP.[8]

Therefore, this chapter will discuss the syntheses of tripeptidyl compounds and GC376 as 3CLpro inhibitors in NV and FECV respectively.

4.3 Results and discussion

Previous studies done by Groutas and coworkers were able to discover a potent dipeptidyl compound (GC373) that shows micromolar inhibition (IC_{50} = 1.82 μM, EC_{50} = 2.1 μM) of

NV3CLpro *in vitro* using a fluorescence resonance energy transfer (FRET) enzyme assay and in a NV cell based assay.[4,9-11] GC373 possesses Gln "surrogate" at P1 position which can be recognized by the S1 enzyme pocket, Leu at P2 position that will be recognized by the S2 pocket and a Cbz N-terminal cap. The presence of aldehyde function at C-terminal position can act as the electrophilic site for nucleophilic attack from Cys139. With this knowledge in hand, our initial research efforts focused on synthesizing a new class of NV protease inhibitors using a structure-activity relationship (SAR) approach. As a part of that project, I was involved in testing the effect of the substituents at P1 and N-terminal cap positions on the anti-NV activity. In order to investigate how the nature of P1 affects the anti-NV activity of these compounds, two molecules had been synthesized by changing the substituent at P1 position. We proposed the triazole functionality to mimic Glu/ Gln residue of the natural P1 substrate to investigate how it affects the activity of the synthesized molecules as anti-NV compounds.[12] The 1,2,3-triazole functionality offers a hydrolysis-stable amide replacement of glutamine surrogate, thus believed to have better anti-NV activity.[12,13]

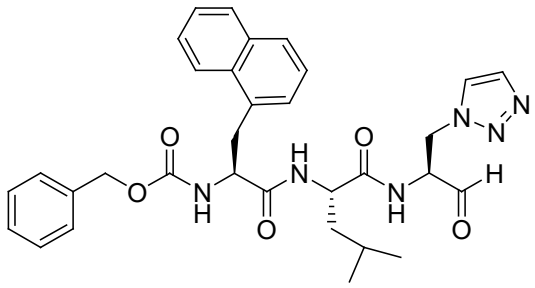

55

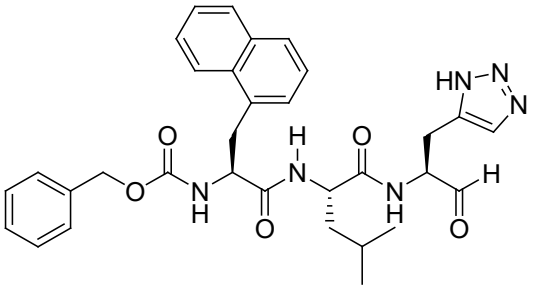

56

Figure 4.3: Synthesized anti-NV compounds for structure activity relationship studies to evaluate the effect of P1 residue.

In order to prepare compounds **55** and **56**, intermediates **62** and **66** need to be prepared first. The synthetic scheme to prepare **62** and **66** is shown in Scheme 4.1.

Scheme 4.1: Syntheses of intermediates 60 and 66

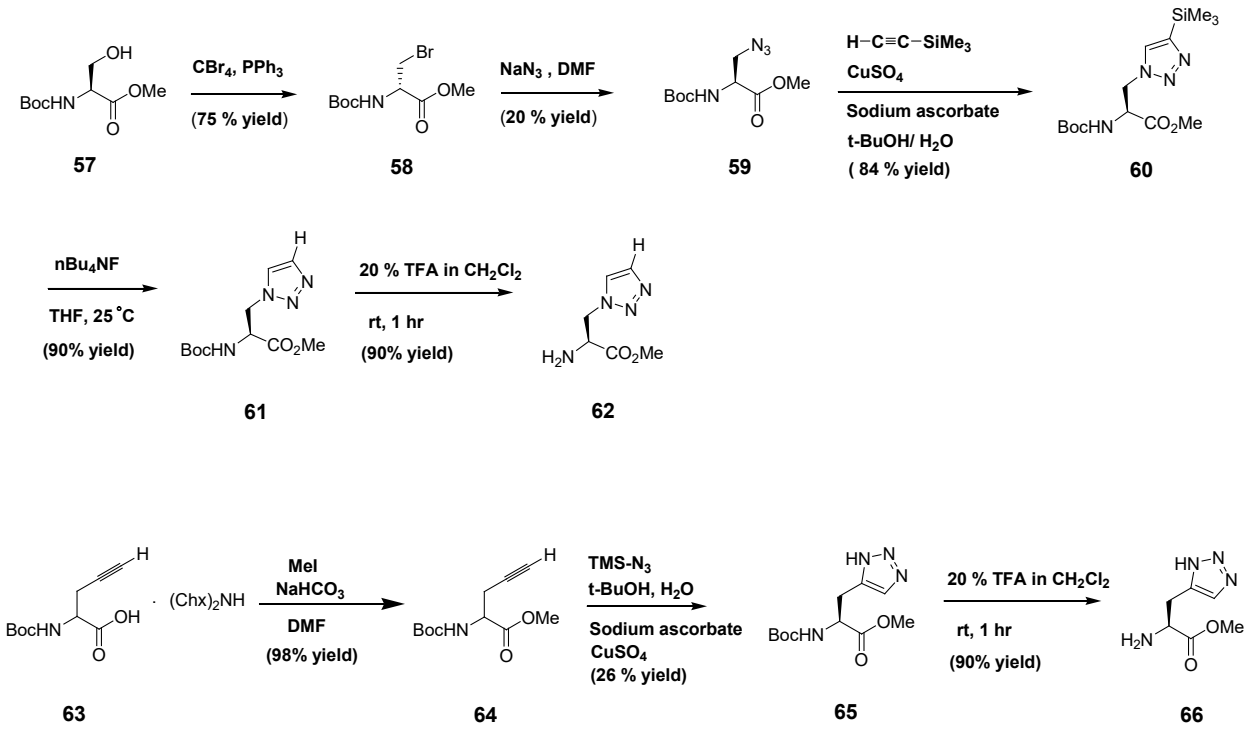

Intermediate **62** was achieved in total of four steps. The replacement of the hydroxyl functionality of *N*-(tert-Butoxycarbonyl)-L-serine methyl ester (**57**) using CBr_4 and triphenyl phosphine (PPh_3) yielded brominated product **58** in 75% yield.[12] The nucleophilic substitution reaction (SN_2) occurred between compound **58** with sodium azide in DMF resulted azide intermediate for the click triazole formation (**59**). However, the yield for this step was significantly low due to the formation of E2 elimination product in 3:1 ratio. Reacting the chiral azide (**59**) with the ethynyltrimethylsilane in the presence of Cu(II) and sodium ascorbate in water/tert-butanol solvent yielded the corresponding 1,2,3-triazole (**60**) in high yields. Subsequent removal of the

trimethylsilyl functionality using nBu_4NF followed by TFA treatment to deprotect the Boc group resulted the target compound (**62**) as the TFA salt.

Intermediate **66** was prepared in total of three steps. Starting with Boc-L-proparglycine dicyclohexylammonium) salt, the carboxylic functionality was converted to methyl ester using methyl iodide under basic conditions. Reaction of trimethylsilyl azide with the compound **64** in the presence of Cu(II) and sodium ascorbate in water/tert-butanol solvent yielded the corresponding triazole (**65**).[13] Subsequent removal of the Boc protecting group resulted the target compound (**66**) as the TFA salt.

Scheme 4.2: Syntheses of compounds 55 and 56

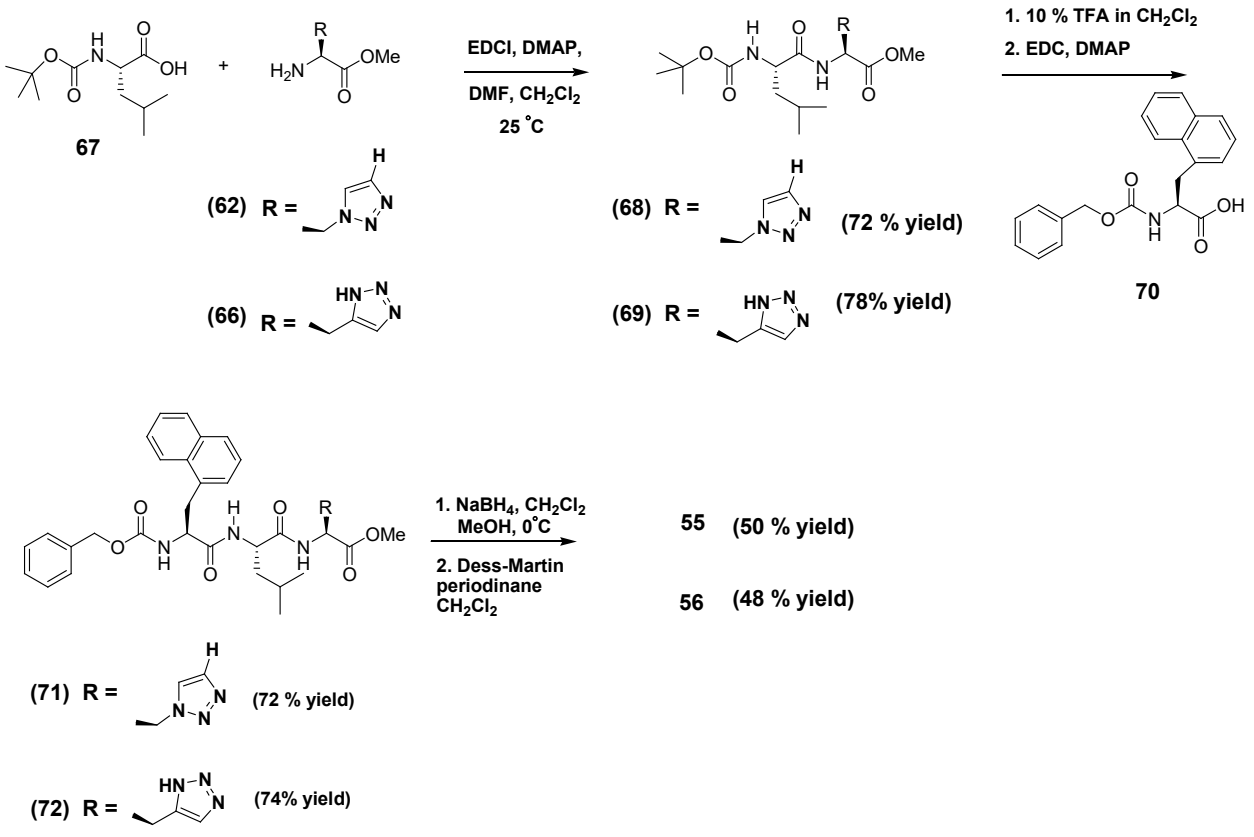

Synthetic scheme for the preparation of compounds **55** and **56** using the intermediates **62** and **66** is shown in Scheme 4.2. Hence, the reaction of **62** and **66** with (S)-N-Boc-leucine (**67**) in the presence of 1-ethyl-3-(3-dimethylaminopropyl)carbodiimide (EDCI) afforded dipeptides **68** and **69** respectively, which upon removal of the Boc group and coupling with (S)-*N*-Cbz-1-napthylalanine gave tripeptides **71** and **72** respectively in good yields. Reduction of the methyl ester function with sodium borohydride followed by oxidation with Dess-Martin periodinane (DMP) furnished corresponding compounds **55** and **56** respectively in moderate yield.

We also studied the involvement of N-terminal cap on the activity of anti-NV compounds. Therefore, Cbz cap was replaced by thiazoles and amino-4-methylcoumarin (AMC) functionalities to evaluate the activity of the newly designed compounds and these compounds were synthesized by me and Dr. Allan Prior.

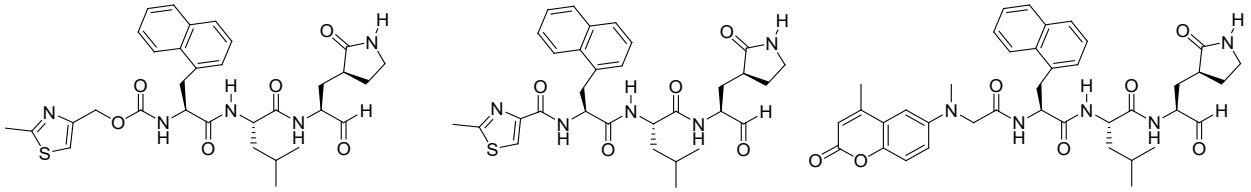

73 **74** **75**

Figure 4.4: Synthesized anti-NV compounds by modifying N-terminal cap.

Synthetic scheme for the preparation of compound **73** is shown in Scheme 4.3.

Scheme 4.3: Synthesis of compound 73

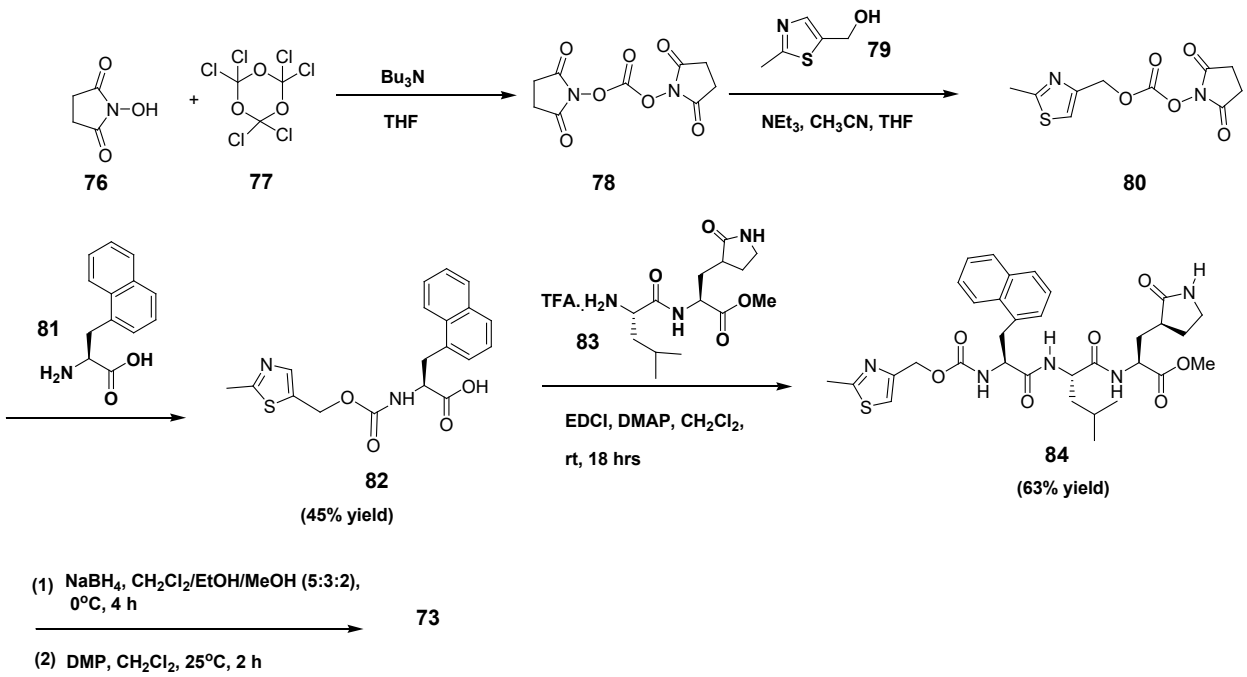

76 77 78 79 80 81 82 83 84 73

(45% yield)

(63% yield)

The reaction of triphosgene (**77**) with *N*-hydroxysuccinamide (**76**) in the presence of tributyl amine and THF as the solvent yielded compound **78**. The reaction of compound **78** with compound **79** in a mixture of CH_3CN and THF followed by the addition of NEt_3 resulted the activated alcohol **80** followed by the addition of compound **81** resulted the compound **82**. The reaction of **82** and **83** in the presence of EDCI afforded compound **84** in 63% yield. Reduction of the methyl ester function with sodium borohydride followed by oxidation with Dess-Martin periodinane (DMP) furnished corresponding compound **73** in moderate yield.

Synthetic scheme for the preparation of compounds **74** and **75** is shown in Scheme 4.4.

Scheme 4.4: Syntheses of compounds 74 and 75

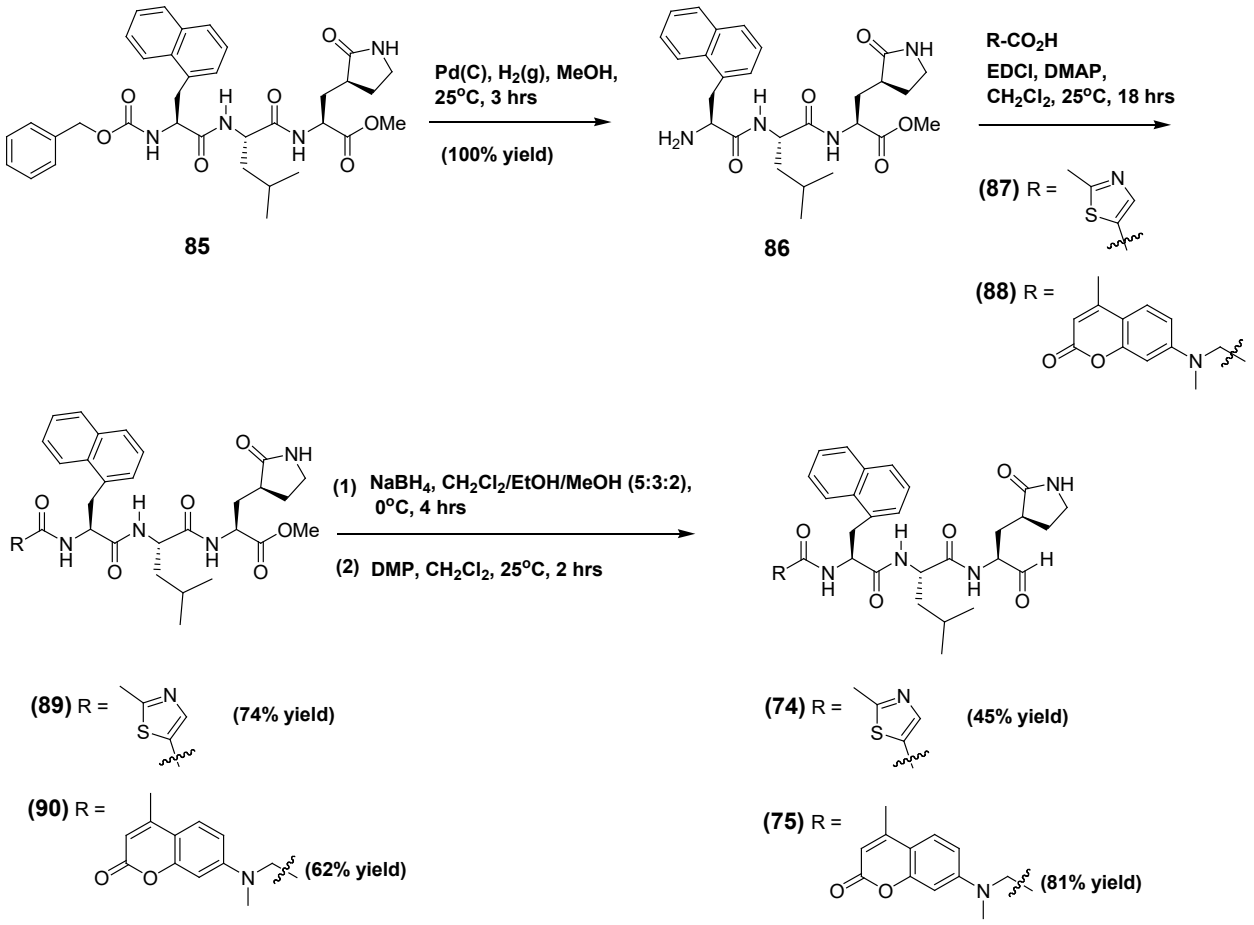

Synthesis of compounds **74** and **75** was achieved as shown in Scheme 4.4. Deprotection of the Cbz group in compound **85** afforded free amine **86**. Coupling of compound **86** with corresponding acid **87** and **88** in the presence of EDCI afforded tripeptidyl ester **89** and **90**. The acid precursor **88** was prepared as shown in Scheme 4.5. Reduction of the methyl ester function of compounds **89** and **90** followed by oxidation with DMP furnished corresponding compounds **74** and **75** in 45% and 81% yields, respectively.

Scheme 4.5: Synthesis of acid precursor 88

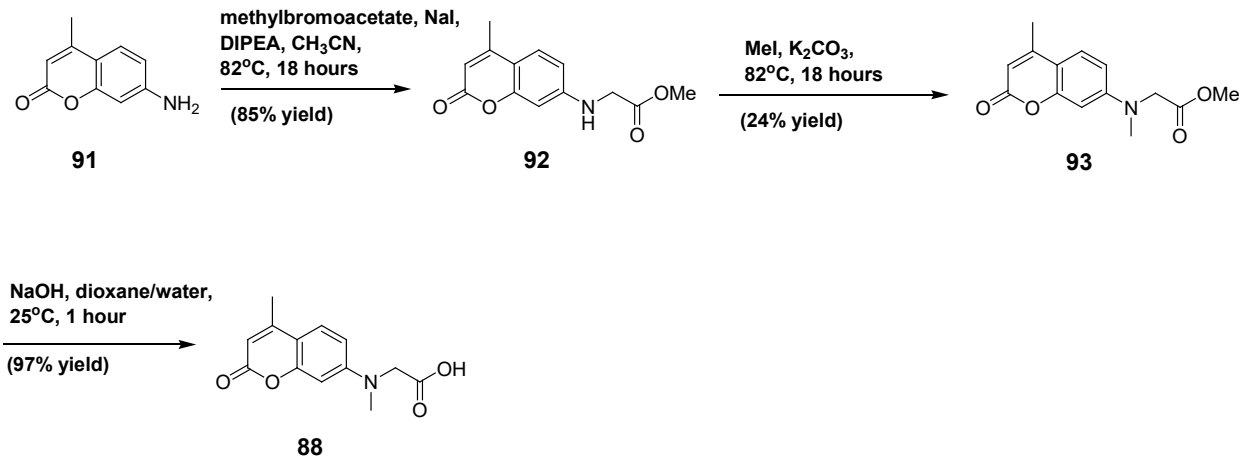

Table 4.1: Activity Data for Compounds 55, 56, 73 - 75 in NV 3CLpro (enzyme) and NV (cell) Assays.

Compound	IC_{50} (Enzyme), µM	EC_{50} (Cell), µM
55	>10	>10
56	>10	>10
73	>10	>10
74	0.5	0.08
75	1.5	2.5

As shown in Table 4.1, compounds **55** and **56** in which the glutamine surrogate had been replaced with traizole functionalities seem not act as inhibitors towards NV 3CLpro. This suggests the importance of having the glutamine surrogate moiety in the P1 position. Since the natural substrate for NV 3CLpro possesses Glu/Gln at the P1 site, it seems that the P1 position of the synthesized compounds need to have glutamine moiety for better NV 3CLpro activity. Among the compounds in which the Cbz N-terminal cap had been replaced, the smaller thiazole cap in compound **74** proved to be better than the compounds **73** and **75.**

4.3.1 Synthesis of GC376

Large scale synthesis (15 g -20 g) of GC376 (discovered by Dr. Groutas's group) was carried out to evaluate its therapeutic efficacy as a 3CLpro inhibitor in laboratory cats with FIP.[8] Synthetic scheme is shown in Scheme 4.6 and 4.7.

Scheme 4.6: Synthesis of glutamine surrogate methyl ester (98)

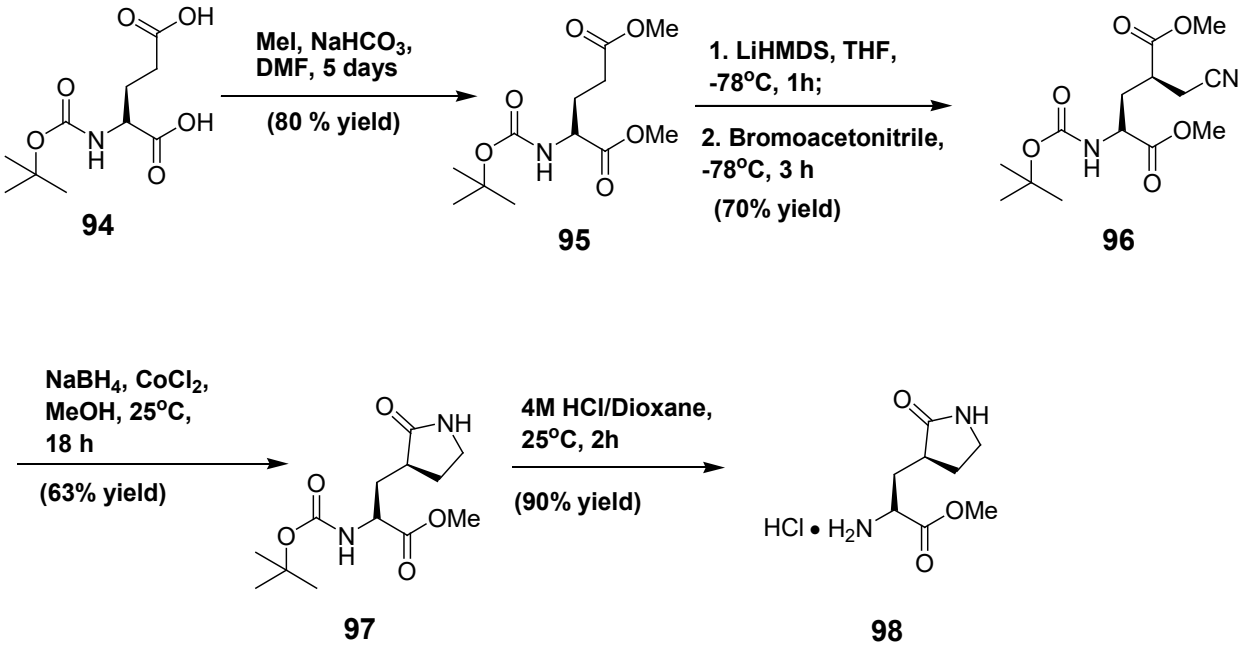

In order to prepare the GC376, first, the glutamine surrogate methyl ester (**98**) was prepared (40-50 g) following a recent literature procedure as shown in Scheme 4.6.[14] In brief, N-Boc glutamic acid (**94**) was treated with methyl iodide and sodium bicarbonate in DMF for 5 days to give N-Boc-glutamic dimethyl ester (**95**). Double deprotonation of **95** using lithium hexamethyldisilazane (LiHMDS) followed by dropwise addition of bromoacetonitrile at -78°C, stirring for 3 hours followed by quenching with acetic acid furnished the alkylated nitrile compound (**96**) with excellent diastereoselectivity, as only one diastereomer (1,3-anti) of **96** was observed from the reaction. The nitrile (**96**) was reduced with sodium borohydride and cobalt(II) chloride in methanol

to give an amine intermediate which undergoes ring closure by an acyl substitution reaction with the side chain ester group to produce the lactam ring as seen in compound **97**. The removal of the Boc group of **97** using 4M HCl in dioxane gave the glutamine surrogate methyl ester (**98**) in good yield.

Scheme 4.7 : Synthesis of GC376

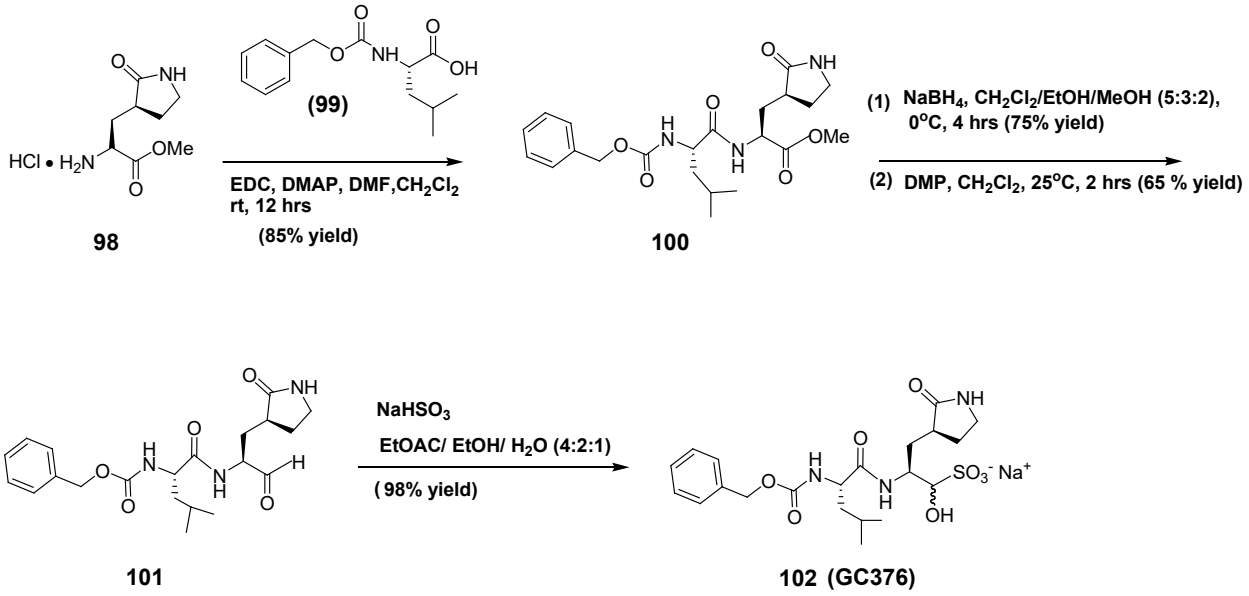

GC376 was prepared following the reported procedure.[4] (S)-N-Cbz-leucine (**99**) which was prepared by reacting L-leucine with the benzylchloroformate under basic conditions in water/dioxane mixture was allowed to react with compound **98** in the presence of 1-ethyl-3-(3-dimethylaminopropyl)carbodiimide (EDCI) to afford dipeptidyl methyl ester (**100**). The reduction of compound **100** using $NaBH_4$ followed by oxidation with DMP resulted the compound **101**, which was then converted to bisulfite adduct (**102**) using sodium bisulfite to afford GC376 in high yield.

4.4 Conclusion

In pursuit of identifying novel tripeptidyl compounds which can inhibit NV3CLpro, the effects of the substituents attached to P1 and N-terminal cap positions on the activity of the molecules were studied by synthesizing various compounds. It can be seen that the presence of glutamine surrogate at P1 position, and the presence of N-terminal Cbz cap are important features for better activity of these molecules. In addition, the work done by Dr. Allan prior on this project, was able to discover a potent tripeptidyl anti-noroviral compound which strongly inhibit NV3CLpro in enzyme and cell based assays with IC_{50} 0.14 μM and EC_{50} 0.04 μM. This compound has an aldehyde warhead, a P1 glutamine surrogate, a P2 leucine, a P3 L-1-napthylalanine and an N-terminal Cbz cap.[5] In addition, this compound also possess strong inhibitory activities against other viral strains in the caliciviridae, picornaviridae, and coronaviridae families especially human rhino virus (HRV) and SARS. Prompted by these encouraging results, further SAR studies are ongoing to improve the activity and bioavailability of the lead compounds.

4.5 Experimental Section

(R)-Methyl 3-bromo-2-(tert-butoxycarbonyl)propanoate / L-N-Boc-β-bromoalanine methyl ester (**58**)

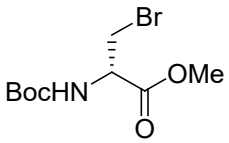

To a solution of N-(tert-butoxycarbonyl)-L-serine methyl ester (**57**) (1.00 g, 4.56 mmol) in 25 ml of dry CH_2Cl_2 was added PPh_3 (1.79g, 6.84 mmol) and carbon tetrabromide (CBr_4) (2.27g, 6.84 mmol) and mixture was stirred at room temperature for 12 hours. Upon addition of diethyl ether, (200 mL) the resulting precipitate was removed by filtration and organic layer was washed with

saturated $NaHCO_3$ (50 mL) followed by brine (50 mL), dried over anhydrous sodium sulfate, and concentrated. The concentrate was column chromatographed on silica gel using a gradient mixture of hexane and ethyl acetate as eluants to give 0.975 g of product **58** (75% yield). ^{1}H NMR (400 MHz, CHLOROFORM-*d*) δ ppm 5.39 (br s, 1 H), 4.76 (br d, *J* = 8.20 Hz, 1 H), 3.81 (s, 3 H), 3.71 (br dd, *J* = 10.54, 3.51 Hz, 2 H), 1.46 (s, 9 H).

(S)-Methyl 3-azido-2-(tert-butoxycarbonyl)propanoate (**59**)

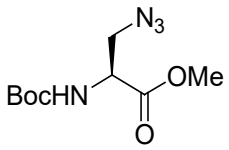

To a solution of compound **58** in dry DMF 5 ml was added NaN_3 and was stirred for 2 hours at room temperature. It was diluted with 5 ml of water and extracted with CH_2Cl_2 (15 mL x 2). The combined organic layers were washed with brine, dried over sodium sulfate, filtered, concentrated and column chromatographed on silica gel using a gradient mixture of hexane and ethyl acetate as eluants to give 17 mg of product **59** (20% yield). ^{1}H NMR (400 MHz, CHLOROFORM-*d*) δ ppm 5.38 (s, 1 H), 4.47 (s, 1H), 3.79 (s, 3 H), 3.72 (br d, J=3.51 Hz, 2 H), 1.45 (s, 9 H).

(S)-Methyl 2-(tert-butoxycarbonyl)-3-(4-(trimethylsilyl)-1H-1,2,3-triazol-1-yl)propanoate (**60**)

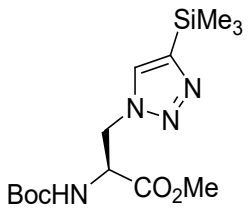

Azide (**59**) (72.8 mg, 0.298 mmol) and 1 equivalent of ethynyltrimethylsilane (29.3 mg, 0.298 mmol) were dissolved in a mixture of 1 mL t-BuOH and 0.5 ml water. With vigorous stirring, sodium ascorbate (5.9 mg, 0.0298 mmol) was added followed by copper sulfate (0.47 mg, 0.00298 mmol) solution in 500 μL water. The mixtures were stirred at room temperature for 24 hours. It was added 30 mL water and extracted with EtOAc. The combined organic layers were washed with brine, dried over sodium sulfate, filtered, concentrated and column chromatographed on silica gel using a gradient mixture of hexane and ethyl acetate as eluants to give 17 mg of product **60** (20% yield). ^{1}H NMR (400 MHz, CHLOROFORM-*d*) δ ppm 7.47 (s, 1 H), 5.38 (s, 1 H), 4.82 (br d, J=4.30 Hz, 3 H), 3.77 (s, 3 H), 1.43 (s, 9 H), 0.31 (s, 9 H).

(S)-Methyl 2-(tert-butoxycarbonyl)-3-(1H-1,2,3-triazol-1-yl)propanoate (**61**)

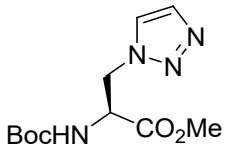

A 35 μL of 1M NBu_4NF was syringed into a solution of compound **60** (8 mg, 0.0234 mmol) in THF. The mixture was stirred at room temperature under argon for one hour. Two drops of acetic acid were added and was concentrated to dryness.

(S)-Methyl 2-amino-3-(1H-1,2,3-triazol-1-yl)propanoate (**62**)

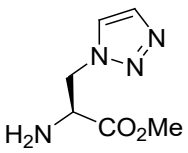

A 20% TFA in CH_2Cl_2 was added to compound **61** (20 mg, 0.074 mmol) in 2 mL CH_2Cl_2. Stirred at room temperature for one hour. It was concentrated to obtain 11.3 mg of compound **62** (90% yield).

(S)-Methyl 2-(tert-butoxycarbonyl)pent-4-ynoate (**64**)

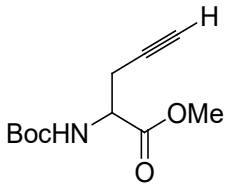

To a solution of compound **63** (189.14 mg, 0.888 mmol) in dry DMF (8 mL) was added $NaHCO_3$ (149.18 mg, 1.776 mmol) followed by MeI (183 µL, 3.552 mmol) and was stirred at room temperature under argon atmosphere for 12 hours. The reaction was diluted with 30 mL water and extracted with EtOAc (75 mL x 3). The combined organic layers were washed with 0.1% HCl followed by H_2O (50 mL x 2), brine, dried over sodium sulfate, filtered, concentrated and column chromatographed on silica gel using a gradient mixture of hexane and EtOAc as eluants to give 198 mg of product **64** (98% yield). ^{1}H NMR (400 MHz, CHLOROFORM-*d*) δ ppm 5.33 (br s, 1H), 4.46 – 4.49 (m, 1H), 3.78 (s, 3 H), 2.64 - 2.81 (m, 2 H), 2.03 -2.04 (m, 1H), 1.45 (m, 9 H).

(S)-Methyl 2-(tert-butoxycarbonyl)-3-(3H-1,2,3-triazol-4-yl)propanoate (**65**)

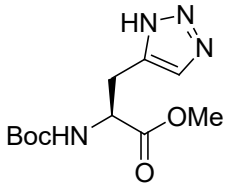

Azido trimethylsilane (328 mg, 2.85 mmol) and 1 equivalent of compound **64** (162 mg, 0.714 mmol) were dissolved in a mixture of 1 mL t-BuOH and 0.5 ml water. With vigorous stirring,

sodium ascorbate (70.69 mg, 0.357 mmol) was added followed by copper sulfate (5.7 mg, 0.036 mmol) solution in 500 µL water. The mixtures were stirred at 65 °C under argon atmosphere for 24 hours. The reaction was diluted with 50 mL water and extracted with EtOAc (100 mL x 3). The combined organic layers were washed with 10% NH_4OH, brine, dried over sodium sulfate, filtered, concentrated and column chromatographed on silica gel using a gradient mixture of hexane and ether as eluants to give 49.4 mg of product **65** (26% yield). ^{1}H NMR (400 MHz, CHLOROFORM-*d*) δ ppm 7.51 (s, 1 H), 5.46 (br d, J=8.20 Hz, 1 H), 4.67 (br s, 1 H), 3.74 (s, 3 H), 3.26 (br s, 2 H), 1.42 (s, 9 H).

(S)-Methyl 2-amino-3-(3H-1,2,3-triazol-4-yl)propanoate (**66**)

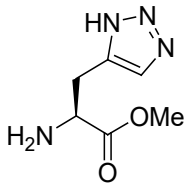

A 20% TFA in CH_2Cl_2 was added to compound **65** (48 mg, 0.178 mmol) in 2 ml CH_2Cl_2. Stirred at room temperature for one hour. It was concentrated to obtain 28 mg of compound **66** (93% yield).

(S)-Methyl-2-((S)-2-(tert-butoxycarbonyl)-4-methylpentanamido)-3-(1H-1,2,3-triazol-1-yl)propanoate (**68**)

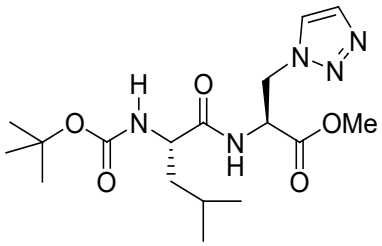

To the amine compound (**62**) (67.7 mg, 0.238 mmol) was added (S)-N-boc-leucine (65.37 mg, 0.262 mmol), EDCI (91.06 mg, 0.477 mmol) and DMAP (72.70 mg, 0.596 mmol) followed by dry CH_2Cl_2 (10 mL), dry DMF (2 mL) and the resulting solution was stirred at 25°C for 18 hours under argon atmosphere. The reaction mixture was partitioned between water (100 mL) and CH_2Cl_2 (10 0 mL), the aqueous layer was acidified to pH = 2 using 2 N HCl, and extracted three times with CH_2Cl_2 (100 mL each). The combined organic layers were dried (anhydrous $MgSO_4$), filtered, and concentrated to yield a solid which was purified by silica gel chromatography using a gradient elution of CH_2Cl_2: MeOH) to yield compound **68**, 70 mg (72% yield) as a white solid. ^{1}H NMR (400 MHz, CHLOROFORM-*d*) δ ppm 7.62 -7.68 (2 H), 7.13 (br s, 1H), 5.05 (br s, 1H), 4.84 – 4.92 (m, 3H), 4.07 (br s, 1 H), 3.77 (s, 3 H), 1.58 - 1.84 (m, 2 H), 1.40 (s, 9 H), 0.85 - 0.98 (m, 6 H).

(S)-Methyl-2-((S)-2-(tert-butoxycarbonyl)-4-methylpentanamido)-3-(3H-1,2,3-triazol-4-yl)propanoate (**69**)

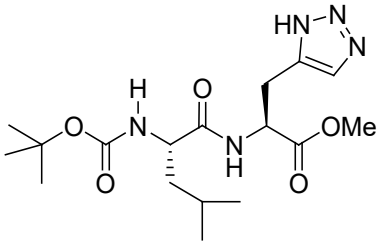

Compound **69** was prepared via the same procedure as that of compound **68** to obtain 70 mg (78% yield) as a white solid. ^{1}H NMR (400 MHz, CHLOROFORM-*d*) δ ppm 7.46 – 7.49 (m, 1H), 7.39 (s, 1 H), 5.24 – 5.27 (m, 1H), 4.91 - 4.97 (m, 1 H), 4.20 (br s, 1H), 3.76 (s, 3 H), 3.27 (br d, J = 5.08 Hz, 2 H), 1.66 (br d, J = 6.64 Hz, 1 H), 1.59 (br dd, J = 13.67, 7.42 Hz, 2 H), 1.43 (s, 9 H), 1.23 - 1.35 (m, 1 H), 0.82 - 0.96 (m, 6 H). ^{13}C NMR ($CDCl_3$), δ 172.98, 171.37, 162.86, 156.33, 80.77, 53.41, 52.87, 51.94, 41.37, 36.76, 31.72, 28.55, 24.87, 22.89,22.28.

(S)-Methyl-2-((S)-2-((S)-2-(benzyloxycarbonyl)-3-(naphthalen-1-yl)propanamido)-4-methylpentanamido)-3-(1H-1,2,3-triazol-1-yl)propanoate (**71**).

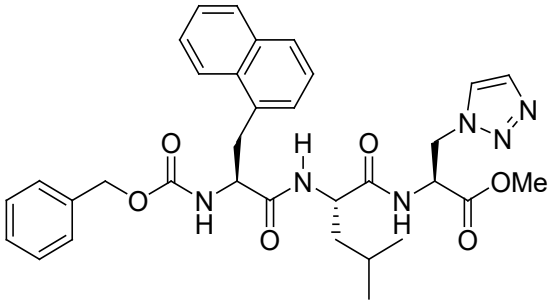

The N-Boc-dipeptide **68** (70 mg, 0.19 mmol) was dissolved in 10% TFA/CH_2Cl_2 (5 mL) and stirred at 25°C for 4 hours. The solvent was removed on the rotary evaporator to yield a sticky oil that was re-dissolved in chloroform followed by removal of the solvent once again on the rotary evaporator to yield a semi-solid material. After sitting under high vacuum for 0.5 hours, a white solid (amine intermediate) was obtained in quantitative yield. To this amine intermediate (90 mg, 0.22 mmol) was added (S)-N-Cbz-1-naphthylalanine (**70**) (77 mg, 0.22 mmol), EDCI (84 mg, 0.44 mmol) and DMAP (54 mg, 0.44 mmol) followed by dry CH_2Cl_2 (15 mL) and the resulting solution was stirred at 25°C for 18 hours under argon atmosphere. The reaction mixture was partitioned between water (100 mL) and CH_2Cl_2 (100 mL), the aqueous layer was acidified to pH = 2 using 2 N HCl, and extracted three times with CH_2Cl_2 (100 mL each). The combined organic layers were dried (anhydrous Na_2SO_4), filtered, and concentrated to yield a solid which was purified by silica gel chromatography using a gradient elution of CH_2Cl_2: MeOH) to yield compound **71**, 114 mg (72% yield) as a white solid. ^{1}H NMR (400 MHz, CHLOROFORM-*d*) δ ppm 0.76 - 0.91 (m, 6 H), 0.91 - 1.11 (m, 1 H), 1.20 - 1.49 (m, 2 H), 3.56 (br d, *J* = 6.64 Hz, 1 H), 3.68 (br dd, *J* = 14.45, 6.64 Hz, 1 H), 3.78 (s, 3 H), 4.16 - 4.42 (m, 1 H), 4.43 - 4.69 (m, 1 H), 4.70

- 4.94 (m, 3 H), 4.94 - 5.18 (m, 2 H), 5.12 (m, 2H), 6.22 (br d, *J* = 6.64 Hz, 1 H), 6.92 (br s, 1 H), 7.26 - 7.41 (m, 6 H), 7.42 - 7.62 (m, 3 H), 7.72 - 7.81 (m, 1 H), 7.81 - 8.00 (m, 2 H), 8.19 (m, 1H).

(S)-Methyl-2-((S)-2-((S)-2-(benzyloxycarbonyl)-3-(naphthalen-1-yl)propanamido)-4-methylpentanamido)-3-(3H-1,2,3-triazol-4-yl)propanoate (**72**)

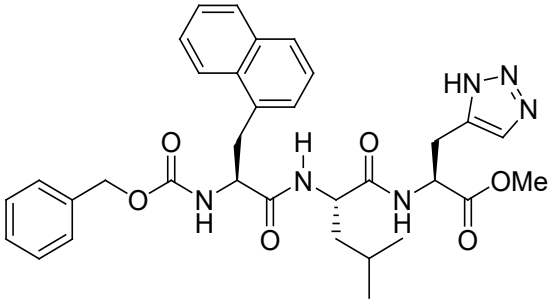

Compound **72** was prepared via the same procedure as that of compound **71** to obtain 74 mg (74% yield) as a white solid. 1H NMR (400 MHz, CHLOROFORM-d) δ ppm 0.66 - 0.93 (m, 1 H), 0.77 (br t, J = 6.05 Hz, 5 H), 1.24 (br s, 1 H), 1.33 - 1.62 (m, 4 H), 1.98 (br s, 1 H), 3.07 - 3.34 (m, 2 H), 3.44 (br s, 1 H), 3.53 - 3.68 (m, 2 H), 3.73 (s, 3 H), 4.42 - 4.61 (m, 1 H), 4.61 - 4.79 (m, 1 H), 4.80 - 5.03 (m, 3 H), 5.77 (br s, 1H), 6.80 - 7.08 (m, 2 H), 7.17 (br s, 2 H), 7.30 - 7.51 (m, 4 H), 7.67 (br d, J = 16.40 Hz, 2 H), 7.73 - 7.88 (m, 1 H), 8.06 (br s, 1 H).

Benzyl-(S)-1-((S)-4-methyl-1-oxo-1-((S)-1-oxo-3-(1H-1,2,3-triazol-1-yl)propan-2-ylamino)pentan-2-ylamino)-3-(naphthalen-1-yl)-1-oxopropan-2-ylcarbamate (**55**)

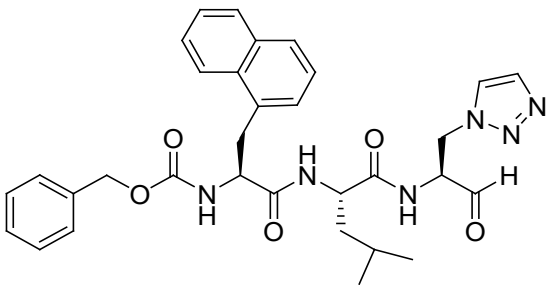

To a solution of ester **72** (53 mg, 0.086 mmol) in CH_2Cl_2/MeOH (1:1) (8 mL) at 0ºC was added $NaBH_4$ (2.81 mg, 0.129 mmol) in small portions over a period of 4 hours. The reaction was quenched with water (0.5 mL) and diluted with 100 mL of CH_2Cl_2. The solution was passed through a short plug of silica gel and the organic material washed thoroughly with 30:1 CH_2Cl_2/MeOH (100 mL). The filtrate was concentrated to yield a solid which was dissolved in distilled CH_2Cl_2 (10 mL) and treated with Dess-Martin periodinane (DMP) for 2 h at 25ºC. The reaction mixture was filtered and the filtrate was concentrated and purified by silica gel chromatography using a gradient solvent elution of 25% acetone/CH_2Cl_2 to 100% acetone. The fractions containing the product were combined and concentrated to give a white solid to which was added $CHCl_3$ (20 mL). After sitting for 10 min the mixture was filtered through a glass frit funnel (fine) and the filtrate was concentrated to provide aldehyde **55** (50% yield) as a white solid. ^{1}H NMR (400 MHz, CHLOROFORM-*d*) δ ppm 0.84 (br t, *J* = 6.44 Hz, 6 H), 3.41 (br dd, *J* = 14.25, 8.40 Hz, 1 H), 3.55 - 3.79 (m, 1 H), 4.37 (br s, 2 H), 4.40 - 4.64 (m, 2 H), 4.65 - 4.88 (m, 2 H), 4.90 - 5.13 (m, 2 H), 5.17 - 5.41 (m, 1 H), 5.30 (s, 1 H), 6.10 - 6.36 (m, 1 H), 7.30 - 7.43 (m, 3 H), 7.45 - 7.70 (m, 3 H), 7.72 - 7.83 (m, 1 H), 7.87 (br d, *J* = 6.64 Hz, 1 H), 8.15 (br d, *J* = 8.20 Hz, 1 H), 9.50 – 9.55 (s, 1H).

Benzyl (S)-1-((S)-4-methyl-1-oxo-1-((S)-1-oxo-3-(3H-1,2,3-triazol-4-yl)propan-2-ylamino)pentan-2-ylamino)-3-(naphthalen-1-yl)-1-oxopropan-2-ylcarbamate (**56**)

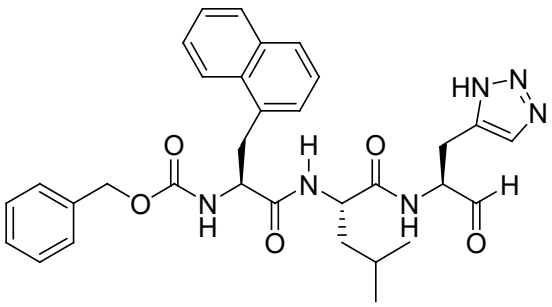

Compound **56** was prepared via the same procedure as that of compound **55** to obtain 5.3 mg (48% yield) as a white solid. ^{1}H NMR (400 MHz, CHLOROFORM-d) δ ppm 0.84 (br t, J = 6.44 Hz, 6 H), 3.41 (br dd, J = 14.25, 8.40 Hz, 1 H), 3.55 - 3.79 (m, 1 H), 4.37 (br s, 2 H), 4.40 - 4.64 (m, 2 H), 4.65 - 4.88 (m, 2 H), 4.90 - 5.13 (m, 2 H), 5.17 - 5.41 (m, 1 H), 5.30 (s, 1 H), 6.10 - 6.36 (m, 1 H), 7.30 - 7.43 (m, 3 H), 7.45 - 7.70 (m, 3 H), 7.72 - 7.83 (m, 1 H), 7.87 (br d, J = 6.64 Hz, 1 H), 8.25 (br d, J = 8.20 Hz, 1 H), 9.50 (s, 1H).

Compound **78**

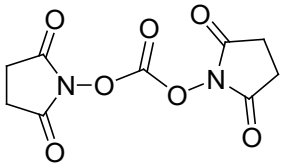

To a mixture of triphogene (**77**) (1.4572 g, 4.9 mmol) and N-hydroxysuccinamide (**76**) (2.82 g, 24.55 mmol) in THF (20 mL) at 0°C was added tributylamine (5.43 g, 29.4 mmol) dropwise. The resulting mixture was stirred at room temperature under argon atmosphere for six hours. The white solid formed was separated via filtration and was washed with cold THF and dried under vaccum to obtain 1.93 g of compound **78**.

Compound **80**

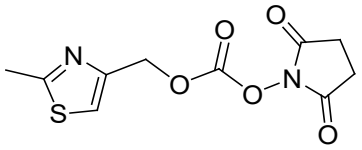

To compound **79** (120 mg, 0.93 mmol) in a mixture of CH3CN (3 ml) and THF (10 mL) was added compound **78** (150 mg, 0.93 mmol) and trimethylamine (0.4 g, 0.5 mL) and was stirred at

room temperature for five hours. The resulting compound **80** was used in next step without further purification.

(S)-2-(((2-Methylthiazol-5-yl)methoxy)carbonyl)-3-(naphthalen-1-yl)propanoic acid (**82**)

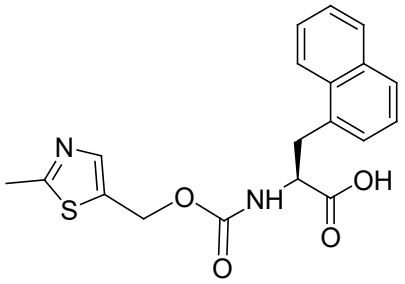

To compound **81** (0.158 g, 0.73 mmol) in 3 mL THF was added NEt_3 until it gets basic. This mixture was transferred into the solution of activated alcohol (**80**) and was stirred for 36 hours until precipitate is disappeared. The reaction was added 15 mL water and it was acidified to pH = 5-6. It was extracted with CH_2Cl_2 (100 mL x 3). The combined organic layers were dried (anhydrous Na_2SO_4), filtered, and concentrated to yield a solid which was purified by silica gel chromatography using a gradient elution of CH_2Cl_2: MeOH to yield compound **82**, 154 mg (45% yield) as a white solid. ^{1}H NMR (400 MHz, CHLOROFORM-*d*) δ ppm 2.61 (br s, 3 H), 3.36 (br s, 1 H), 3.74 (br s, 1 H), 4.77 (br s, 1 H), 5.05 (br s, 2 H), 5.41 (br s, 1 H), 7.43 (br s, 4 H), 7.70 (br s, 1 H), 7.80 (br s, 1 H), 8.06 (br s, 1 H).

(S)-Methyl-2-((S)-4-methyl-2-((S)-2-(((2-methylthiazol-4-yl)methoxy)carbonyl)-3-(naphthalen-1-yl)propanamido)pentanamido)-3-((S)-2-oxopyrrolidin-3-yl)propanoate (**84**)

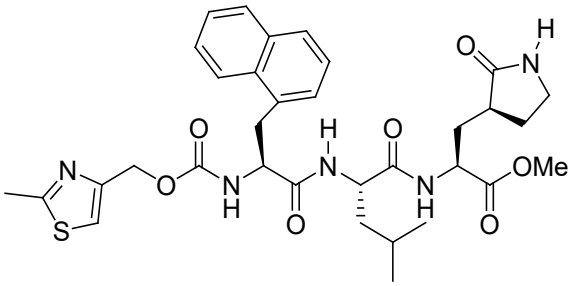

To the amine intermediate **83** (25 mg, 0.062 mmol) was added compound **82** (23 mg, 0.062 mmol), EDCI (24 mg, 0.124 mmol) and DMAP (15 mg, 0.124 mmol) followed by dry CH_2Cl_2 (8 mL) and the resulting solution was stirred at 25ºC for 18 hours under argon atmosphere. The reaction mixture was partitioned between water (100 mL) and CH_2Cl_2 (100 mL), the aqueous layer was extracted three times with CH_2Cl_2 (100 mL each). The combined organic layers were dried (anhydrous Na_2SO_4), filtered, and concentrated to yield a solid which was purified by silica gel chromatography using a gradient elution of CH_2Cl_2: MeOH) to yield compound **84**, 25 mg (72% yield) as a white solid. ^{1}H NMR (400 MHz, CHLOROFORM-*d*) δ ppm 0.90 (d, *J*=6.25 Hz, 6 H), 1.46 (br d, *J*=13.67 Hz, 1 H), 1.53 - 1.72 (m, 2 H), 1.76 - 1.95 (m, 2 H), 2.09 - 2.21 (m, 1 H), 2.31 - 2.46 (m, 2 H), 2.67 (s, 3 H), 3.18 - 3.39 (m, 2 H), 3.44 (br d, *J* = 7.42 Hz, 1 H), 3.64 (br d, *J* = 14.84 Hz, 1 H), 3.72 (s, 3 H), 4.45 (br s, 1 H), 4.51 - 4.64 (m, 2 H), 5.11 (br s, 2 H), 5.55 (br d, *J* = 7.42 Hz, 1 H), 6.43 (br s, 1 H), 6.86 (br d, *J* = 8.59 Hz, 1 H), 7.27 - 7.37 (m, 2 H), 7.43 - 7.55 (m, 3 H), 7.73 (br d, *J* = 6.64 Hz, 1 H), 7.81 - 7.86 (m, 1 H), 7.95 (br d, *J* = 5.86 Hz, 1 H), 8.13 (br d, *J* = 7.03 Hz, 1 H).

(2-Methylthiazol-4-yl)methyl (S)-1-((S)-4-methyl-1-oxo-1-((S)-1-oxo-3-((S)-2-oxopyrrolidin-3-yl)propan-2-ylamino)pentan-2-ylamino)-3-(naphthalen-1-yl)-1-oxopropan-2-ylcarbamate (**73**)

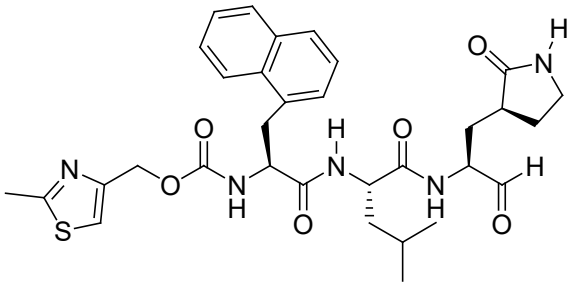

To a solution of ester **84** (25 mg, 0.038 mmol) in CH_2Cl_2/EtOH/MeOH (5:3:2) (6 mL) at 0°C was added $NaBH_4$ (11.61 mg, 0.307 mmol) in small portions over a period of 4 hours. The reaction was quenched with water (0.5 mL) and diluted with 50 mL of CH_2Cl_2. The solution was passed through a short plug of silica gel and the organic material washed thoroughly with 30:1 CH_2Cl_2/MeOH (50 mL). The filtrate was concentrated to yield a solid which was dissolved in distilled CH_2Cl_2 (10 mL) and treated with Dess-Martin periodinane (DMP) (18 mg, 0.043 mmol) for 2 h at 25°C. The reaction mixture was filtered and the filtrate was concentrated and purified by silica gel chromatography using a gradient solvent elution of 25% acetone/CH_2Cl_2 to 100% acetone. The fractions containing the product were combined and concentrated to give a white solid to which was added $CHCl_3$ (20 mL). After sitting for 10 min the mixture was filtered through a glass frit funnel (fine) and the filtrate was concentrated to provide aldehyde **73** (50% yield) as a white solid. ^{1}H NMR (400 MHz, CHLOROFORM-*d*) δ ppm 0.89 (br d, *J* = 5.86 Hz, 6 H), 1.13 - 1.34 (m, 2 H), 1.38 - 1.63 (m, 2 H), 2.02 (br d, *J* = 12.50 Hz, 1 H), 2.36 (br s, 3 H), 2.67 (s, 3 H), 3.11 - 3.37 (m, 3 H), 3.47 (br d, *J* = 8.98 Hz, 1 H), 3.54 - 3.83 (m, 2 H), 4.22 (br s, 1 H), 4.37 - 4.66 (m, 3 H), 5.13 (br s, 2 H), 5.48 (br s, 1 H), 5.98 (br s, 1 H), 6.67 – 6.68 (m, 1H), 7.29 - 7.39 (m, 1 H), 7.39 - 7.60 (m, 3 H), 7.62 - 7.78 (m, 1 H), 7.83 (br d, *J* = 7.81 Hz, 1 H), 8.14 (br s, 1 H) 9.41 (s, 1H).

2-[2-(2-Amino-3-naphthalen-1-yl-propionylamino)-4-methyl-pentanoylamino]-3-(2-oxopyrrolidin-3-yl)-propionic acid methyl ester (**86**)

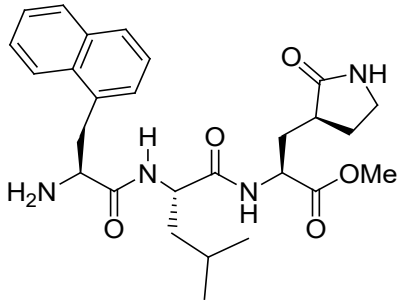

Palladium (on carbon) (10 mg) was added to a solution of **85** (0.16 mmol) in MeOH (2 mL) and the flask was flushed with hydrogen gas (1 atm). The reaction was stirred for 3 h at 25°C. The reaction was filtered through a layer of celite and the filtrate was concentrated to yield compound 86 (80 mg, 100%) as a white solid. ^{1}H NMR δ 8.22 (d, J = 7.81 Hz, 1H), 8.17 (d, J = 5.86 Hz, 1H), 7.87 (d, J = 7.42 Hz, 1H), 7.78 (d, J = 8.20 Hz, 1H), 7.47 - 7.57 (m, 2H), 7.31 - 7.44 (m, 3H), 6.34 - 6.61 (m, 1H), 4.68 - 4.75 (m, 1H), 4.34 - 4.44 (m, 1H), 3.92 - 4.00 (dd, J = 2.73, 11.15 Hz, 1H), 3.82 (dd, J = 2.73, 10.15 Hz, 1H), 3.72 (s, 3H), 3.24 - 3.39 (m, 2H), 2.85 (dd, J = 10.35, 13.86 Hz, 1H), 2.30 - 2.44 (m, 2H), 2.14 - 2.26 (m, 1H), 1.68 - 1.92 (m, 4H), 1.54 - 1.63 (m, 1H), 0.91 - 1.03 (m, 6H); ^{13}C NMR δ 179.8, 174.8, 173.2, 134.2, 134.2, 132.0, 129.0, 127.9, 127.6, 126.4, 126.0, 125.5, 124.0, 55.9, 52.5, 51.8, 51.1, 42.2, 40.7, 38.7, 38.6, 32.9, 28.3, 24.9, 23.1, 22.3.

2-(4-Methyl-2-{2-[(2-methyl-thiazole-5-carbonyl)-amino]-3-naphthalen-1-ylpropionylamino}-pentanoylamino)-3-(2-oxo-pyrrolidin-3-yl)-propionic acid methyl ester (**89**)

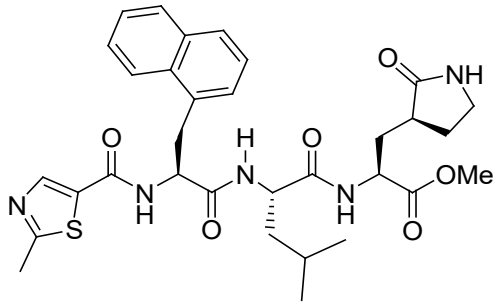

To a mixture of compound **86** (53 mg, 5.59 mmol), compound **87** (5.59 mmol), 1-ethyl-3-(3-dimethylaminopropyl)carbodiimide (EDCI) (10.2 mmol), and 4-(dimethylamino)pyridine (DMAP) (10.2 mmol) under argon was added dry DMF (10 mL). The solution was stirred at 25ºC and dry CH_2Cl_2 (25 mL) was added, and the resulting solution was stirred for 18 h. The reaction was partitioned between water (100 mL) and CH_2Cl_2 (100 mL). The pH of the aqueous layer was adjusted to 3 using 2N HCl. The organic layer was removed, and the aqueous layer was extracted twice with CH_2Cl_2 (100 mL each). The combined organic layers were dried (anhydrous $MgSO_4$), filtered and concentrated to yield a sticky solid which was purified by silica gel chromatography (30:1 CH_2Cl_2: MeOH) to yield compound **89**, 37 mg (74% yield) as a white solid. ^{1}H NMR δ 8.17 (d, J = 8.20 Hz, 1H), 7.92 (d, J = 7.42 Hz, 1H), 7.83 (s, 1H), 7.79 (d, J = 7.81 Hz, 1H), 7.70 (d, J = 7.81 Hz, 1H), 7.27 - 7.51 (m, 6H), 6.59 (br. s., 1H), 4.98 - 5.05 (m, 1H), 4.48 - 4.58 (m, 2H), 3.72 (s, 3H), 3.59 - 3.63 (m, 2H), 3.21 - 3.32 (m, 2H), 2.60 (s, 3H), 2.33 - 2.44 (m, 1H), 2.10 - 2.20 (m, 1H), 1.96 (br. s., 1H), 1.84 - 1.92 (m, 1H), 1.76 - 1.83 (m, 1H), 1.62 - 1.71 (m, 1H), 1.53 - 1.61 (m, 1H), 1.42 - 1.50 (m, 1H), 0.85 (d, J = 6.25 Hz, 6H); ^{13}C NMR δ 180.0, 172.5, 172.3, 171.3, 170.7, 160.9, 143.5, 134.1, 133.8, 132.8, 132.2, 129.1, 128.1, 127.8, 126.7, 126.0, 125.6, 123.7, 54.7, 52.6, 52.5, 51.5, 41.7, 40.8, 38.7, 35.0, 33.6, 29.9, 28.4, 24.9, 23.0, 22.2, 19.6; MS, m/z 644.2 $(M+Na)^+$.

2-[4-Methyl-2-(2-{2-[methyl-(4-methyl-2-oxo-2H-chromen-7-yl)-amino]-acetylamino}-3-naphthalen-1-yl-propionylamino)-pentanoylamino]-3-(2-oxo-pyrrolidin-3-yl)-propionic acid methyl ester (**90**)

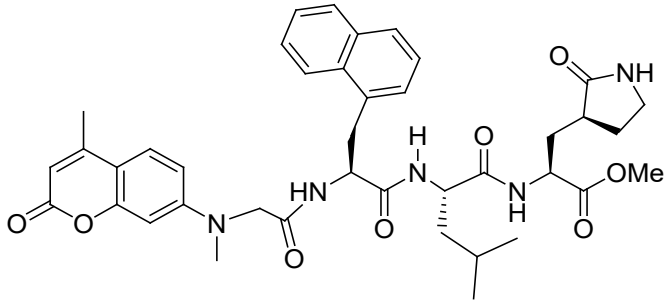

Compound **90** was prepared via the same procedure as that of compound **89** to obtain 36 mg (62 % yield) as a yellow solid. ^{1}H NMR δ 8.06 (d, J = 7.01 Hz, 1H), 7.94 (d, J = 7.03 Hz, 1H), 7.76 (dd, J = 2.93, 6.44 Hz, 1H), 7.60 - 7.64 (m, 1H), 7.41 - 7.48 (m, 2H), 7.17 - 7.25 (m, 3H), 7.06 (d, J = 8.20 Hz, 1H), 6.78 (d, J = 7.03 Hz, 1H), 6.37 (d, J = 2.34 Hz, 1H), 6.30 (dd, J = 2.34, 8.98 Hz, 1H), 6.27 (s, 1H), 6.04 (s, 1H), 4.76 - 4.84 (m, 1H), 4.47 - 4.60 (m, 2H), 3.86 - 3.92 (m, 2H), 3.72 (s, 3H), 3.63 (dd, J = 5.86, 14.45 Hz, 1H), 3.38 (dd, J = 8.98, 14.45 Hz, 1H), 3.27 - 3.33 (m, 2H), 2.76 (s, 3H), 2.36 - 2.47 (m, 1H), 2.34 (s, 3H), 2.09 - 2.19 (m, 1H), 1.85 - 1.93 (m, 1H), 1.76 - 1.85 (m, 1H), 1.66 - 1.75 (m, 1H), 1.53 - 1.63 (m, 1H), 1.39 - 1.48 (m, 1H), 0.90 (d, J = 6.25 Hz, 6H); ^{13}C NMR δ 180.0, 172.4, 172.3, 170.8, 170.2, 161.8, 155.5, 152.8, 151.6, 134.0, 132.5, 132.2, 129.1, 128.1, 127.7, 126.7, 126.0, 125.8, 125.4, 123.5, 111.4, 110.8, 109.1, 99.5, 57.5, 54.4, 52.6, 52.2, 51.7, 41.8, 40.7, 39.6, 38.7, 34.2, 33.3, 28.7, 25.0, 23.2, 22.2, 18.7; MS, m/z 748.2 $(M+Na)^{+}$.

2-Methyl-thiazole-5-carboxylic acid (1-{1-[1-formyl-2-(2-oxo-pyrrolidin-3-yl)ethylcarbamoyl]-3-methyl-butylcarbamoyl}-2-naphthalen-1-yl-ethyl)-amide (**74**)

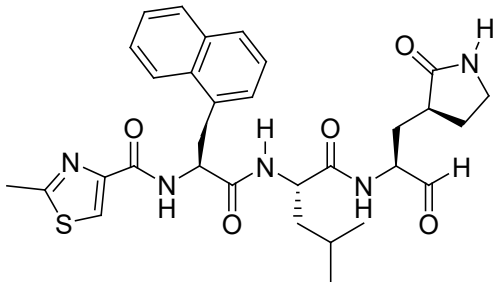

Compound **74** was prepared via the same procedure as that of compound **73** to obtain 30 mg (45 % yield) as a white solid. ^{1}H NMR δ 9.42 (s, 1H), 8.25 (d, J = 8.59 Hz, 1H), 8.17 (d, J = 5.86 Hz, 1H), 7.80 - 7.85 (m, 1H), 7.73 (d, J = 8.20 Hz, 1H), 7.51 - 7.57 (m, 1H), 7.45 - 7.51 (m, 1H), 7.32 - 7.43 (m, 3H), 6.96 (d, J = 7.03 Hz, 1H), 6.84 (d, J = 7.81 Hz, 1H), 5.89 (br. s., 1H), 4.97 - 5.05 (m, 1H), 4.46 - 4.54 (m, 1H), 4.20 - 4.27 (m, 1H), 3.62 - 3.67 (m, 2H), 3.25 - 3.40 (m, 2H), 2.66 (s, 3H), 2.32 - 2.41 (m, 1H), 1.60 - 1.94 (m, 5H), 1.39 - 1.56 (m, 2H), 0.81 - 0.90 (m, 6H); ^{13}C NMR δ 200.1, 180.1, 173.0, 170.9, 161.0, 143.7, 135.9, 134.2, 133.5, 132.7, 132.3, 129.2, 128.3, 128.1, 126.8, 126.1, 125.7, 123.9, 58.3, 54.9, 52.5, 41.5, 40.8, 38.7, 35.1, 30.0, 29.2, 25.0, 23.1, 22.0, 19.8; MS, m/z 614.4 $(M+Na)^{+}$.

4-Methyl-2-(2-{2-[methyl-(4-methyl-2-oxo-2H-chromen-7-yl)-amino]-acetylamino}-3naphthalen-1-yl-propionylamino)-pentanoic acid [1-formyl-2-(2-oxo-pyrrolidin-3-yl)ethyl]-amide (**75**)

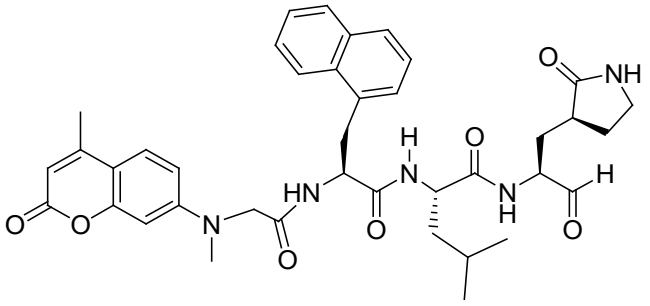

Compound **75** was prepared via the same procedure as that of compound **73** to obtain 27 mg (81 % yield) as a white solid. ^{1}H NMR δ (major isomer) 9.48 (s, 1H), 8.30 - 8.38 (m, 1H), 8.10 (d, J = 8.98 Hz, 1H), 7.83 - 7.93 (m, 1H), 7.76 (d, J = 8.59 Hz, 1H), 7.62 (d, J = 8.98 Hz, 1H), 7.42 - 7.51 (m, 2H), 7.18 - 7.29 (m, 4H), 6.81 (d, J = 8.59 Hz, 1H), 6.70 (d, J = 6.25 Hz, 1H), 6.42 (s, 1H), 6.33 (br. s., 1H), 6.07 (s, 1H), 5.80 - 5.86 (m, 1H), 4.75 - 4.83 (m, 1H), 4.54 - 4.62 (m, 1H), 4.45 - 4.53 (m, 1H), 4.26 - 4.35 (m, 1H), 3.85 - 3.89 (m, 2H), 3.65 - 3.75 (m, 2H), 3.29 - 3.38 (m, 2H), 2.72 (s, 3H), 2.36 (s, 3H), 1.37 - 1.93 (m, 6H), 0.88 - 0.93 (m, 6H); MS, m/z 718.3 $(M+Na)^+$.

(4-Methyl-2-oxo-2H-chromen-7-ylamino)-acetic acid methyl ester (**92**)

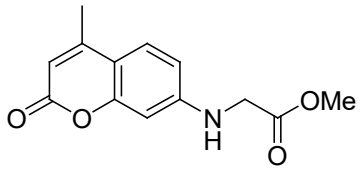

A solution containing 7-amino-4-methylcoumarin **91** (0.57 mmol), NaI (0.57 mmol), methylbromoacetate (0.63 mmol) and DIPEA (0.63 mmol) in dry acetonitrile (6 mL) was heated at 82ºC for 18 h. The reaction was filtered and the filtrate was concentrated to give an oil that was purified by silica gel column chromatography (15:1 CH_2Cl_2: MeOH) to afford compound **92** (120 mg, 85%) as a yellow solid. ^{1}H NMR δ 7.39 (d, J = 8.98 Hz, 1H), 6.56 (dd, J = 2.34, 8.98 Hz, 1H), 6.42 (d, J = 2.34 Hz, 1H), 6.02 (s, 1H), 4.78 - 4.84 (m, 1H), 3.97 (d, J = 5.08 Hz, 2H), 3.82 (s, 3H), 2.35 (s, 3H); ^{13}C NMR δ 170.8, 161.9, 156.0, 153.0, 150.3, 125.9, 111.6, 110.8, 110.4, 98.7, 52.8, 45.1, 18.8; MS, m/z 270.1 $(M+Na)^+$.

[Methyl-(4-methyl-2-oxo-2H-chromen-7-yl)-amino]-acetic acid methyl ester (**93**)

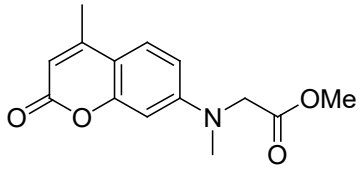

Methyl iodide (0.73 mmol) and K_2CO_3 (0.98 mmol) were added to a solution of **92** (0.49 mmol) in dry acetonitrile (5 mL) and refluxed at 82ºC for 18 hours. The reaction was filtered and partitioned between CH_2Cl_2 (20 mL) and water (20 mL). The organic layer was removed and the aqueous layer was extracted with CH_2Cl_2 (20 mL x 3), the combined organic layers were dried ($MgSO_4$), filtered and concentrated to give a yellow oil that was purified by silica gel chromatography (15:1 CH_2Cl_2: MeOH) to yield compound **93** (31 mg, 24%) as a yellow solid. ^{1}H NMR δ 7.43 (d, J = 8.83 Hz, 1H), 6.61 (dd, J = 2.54, 8.83 Hz, 1H), 6.53 (d, J = 2.54 Hz, 1H), 6.02 (s, 1H), 4.15 (s, 2H), 3.76 (s, 3H), 3.15 (s, 3H); ^{13}C NMR δ 170.6, 162.0, 155.8, 152.9, 151.9, 125.7, 110.9, 110.3, 109.0, 99.1, 54.2, 52.5, 39.9, 18.7; MS, m/z 284.0 $(M+Na)^+$.

[Methyl-(4-methyl-2-oxo-2H-chromen-7-yl)-amino]-acetic acid (**88**)

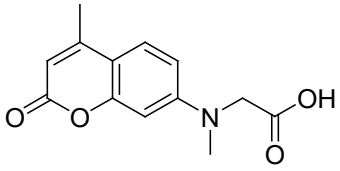

The ester **93** (0.08 mmol) was dissolved in 1:1 dioxane:water (1 mL) and treated with 2N NaOH (0.12 mL). After stirring at 25ºC for 1 hour, the reaction was partitioned between water (20 mL) and CH_2Cl_2 (20 mL) then acidified to pH 2 using aq. HCl. The aqueous layer was extracted with CH_2Cl_2 (15 mL x 3), the combined CH_2Cl_2 layers were dried (Na_2SO_4), filtered and concentrated to yield compound **88** (20 mg, 100%) as a yellow solid. ^{1}H NMR δ 8.58 (br. s., 1H), 7.42 (d, J = 8.98 Hz, 1H), 6.62 (d, J = 8.98 Hz, 1H), 6.51 (s, 1H), 6.01 (s, 1H), 4.16 (s, 2H), 3.13 (s, 3H), 2.34

(s, 3H); ^{13}C NMR δ 174.4, 162.7, 155.6, 153.5, 151.9, 125.8, 110.9, 110.0, 109.2, 99.0, 61.4, 39.9, 18.7; MS, m/z 270.0 $(M+Na)^+$.

The syntheses of compounds **94** – **102** (syntheses procedures for glutamine surrogate and GC376) have been reported previously and they were prepared following the reported procedures.[4,14]

4.6 References

1. Beutler, B.; Eidenschenk, C.; Crozat, K.; Imler, J.-L.; Takeuchi, O.; Hoffmann, J. A.; Akira, S., Genetic analysis of resistance to viral infection. *Nature Reviews Immunology* **2007,** *7* (10), 753-766.

2. De Clercq, E., Strategies in the design of antiviral drugs. *Nature Reviews Drug Discovery* **2002,** *1* (1), 13-25.

3. Rocha-Pereira, J.; Nascimento, M. S. J., Targeting Norovirus: Strategies for the Discovery of new antiviral Drugs. *InTech* **2012,** *7*, 121-150.

4. Kim, Y.; Lovell, S.; Tiew, K.-C.; Mandadapu, S. R.; Alliston, K. R.; Battaile, K. P.; Groutas, W. C.; Chang, K.-O., Broad-spectrum antivirals against 3C or 3C-like proteases of picornaviruses, noroviruses, and coronaviruses. *Journal of virology* **2012,** *86* (21), 11754-11762.

5. Prior, A. M.; Kim, Y.; Weerasekara, S.; Moroze, M.; Alliston, K. R.; Uy, R. A. Z.; Groutas, W. C.; Chang, K.-O.; Hua, D. H., Design, synthesis, and bioevaluation of viral 3C and 3C-like protease inhibitors. *Bioorganic & medicinal chemistry letters* **2013,** *23* (23), 6317-6320.

6. Nakamura, K.; Someya, Y.; Kumasaka, T.; Ueno, G.; Yamamoto, M.; Sato, T.; Takeda, N.; Miyamura, T.; Tanaka, N., A norovirus protease structure provides insights into active and substrate binding site integrity. *Journal of virology* **2005,** *79* (21), 13685-13693.

7. Takahashi, D.; Hiromasa, Y.; Kim, Y.; Anbanandam, A.; Yao, X.; Chang, K. O.; Prakash, O., Structural and dynamics characterization of norovirus protease. *Protein Science* **2013,** *22* (3), 347-357.

8. Kim, Y.; Liu, H.; Kankanamalage, A. C. G.; Weerasekara, S.; Hua, D. H.; Groutas, W. C.; Chang, K.-O.; Pedersen, N. C., Correction: Reversal of the Progression of Fatal Coronavirus Infection in Cats by a Broad-Spectrum Coronavirus Protease Inhibitor. *PLoS Pathog* **2016,** *12* (5), e1005650.

9. Tiew, K.-C.; He, G.; Aravapalli, S.; Mandadapu, S. R.; Gunnam, M. R.; Alliston, K. R.; Lushington, G. H.; Kim, Y.; Chang, K.-O.; Groutas, W. C., Design, synthesis, and evaluation of inhibitors of Norwalk virus 3C protease. *Bioorganic & medicinal chemistry letters* **2011,** *21* (18), 5315-5319.

10. Chang, K.-O.; Takahashi, D.; Prakash, O.; Kim, Y., Characterization and inhibition of norovirus proteases of genogroups I and II using a fluorescence resonance energy transfer assay. *Virology* **2012,** *423* (2), 125-133.

11. Chang, K.-O.; Sosnovtsev, S. V.; Belliot, G.; King, A. D.; Green, K. Y., Stable expression of a Norwalk virus RNA replicon in a human hepatoma cell line. *Virology* **2006,** *353* (2), 463-473.

12. Battenberg, O. A.; Nodwell, M. B.; Sieber, S. A., Evaluation of α-pyrones and pyrimidones as photoaffinity probes for affinity-based protein profiling. *The Journal of organic chemistry* **2011,** *76* (15), 6075-6087.

13. Gajewski, M.; Seaver, B.; Esslinger, C. S., Design, synthesis, and biological activity of novel triazole amino acids used to probe binding interactions between ligand and neutral amino acid transport protein SN1. *Bioorganic & medicinal chemistry letters* **2007,** *17* (15), 4163-4166.

14. Mou, K.; Xu, B.; Ma, C.; Yang, X.; Zou, X.; Lü, Y.; Xu, P., Novel CADD-based peptidyl vinyl ester derivatives as potential proteasome inhibitors. *Bioorganic & medicinal chemistry letters* **2008,** *18* (6), 2198-2202.

Appendix A - ^{1}H NMR, ^{13}C NMR, and IR

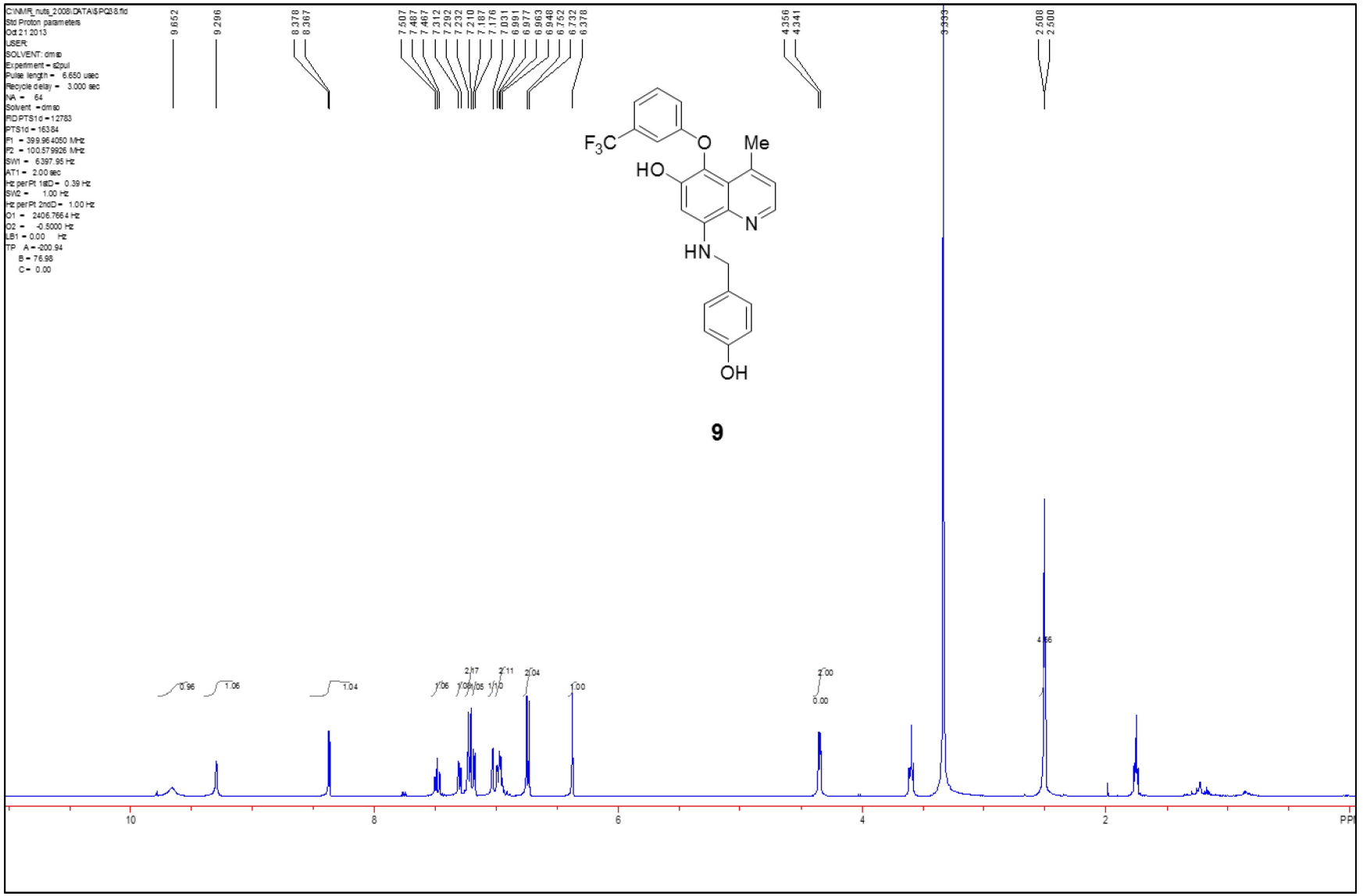

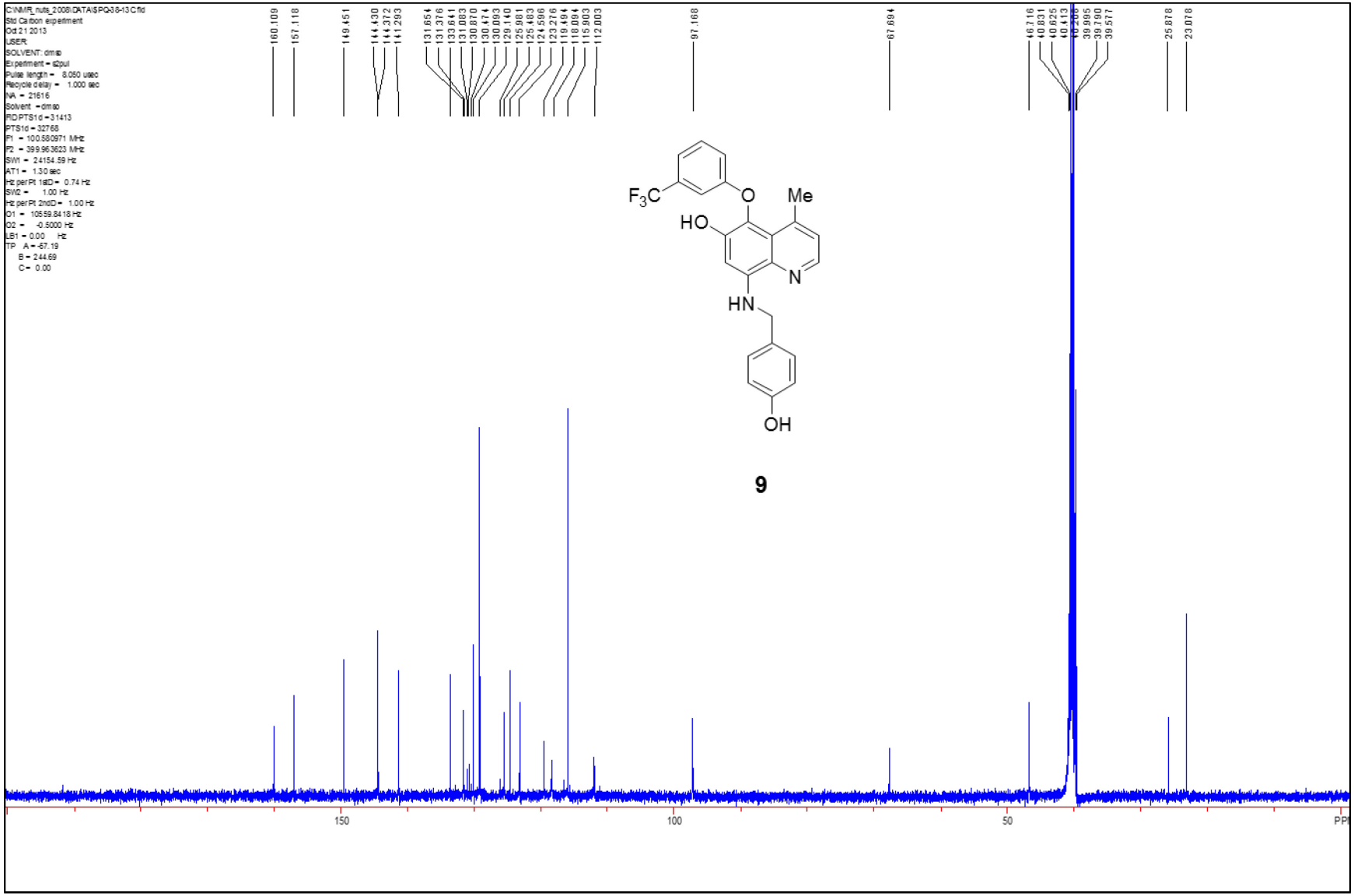
C:\NMR_nuts_2008\DATA\SPQI-38-13C.fid
Std Carbon experiment
Oct 21 2013
USER:
SOLVENT: dmso
Experiment = s2pul
Pulse length = 8.050 usec
Recycle delay = 1.000 sec
NA = 21616
Solvent = dmso
FIDPTS1d = 31413
PTS1d = 32768
F1 = 100.580971 MHz
F2 = 399.963623 MHz
SW1 = 24154.59 Hz
AT1 = 1.30 sec
Hz per Pt 1stD = 0.74 Hz
SW2 = 1.00 Hz
Hz per Pt 2ndD = 1.00 Hz
O1 = 10559.8418 Hz
O2 = -0.5000 Hz
LB1 = 0.00 Hz
TP A = -67.19
B = 244.69
C = 0.00
160.109
157.118
149.451
144.430
144.372
141.293
131.654
131.376
133.641
131.083
130.870
130.474
130.093
129.140
125.981
125.483
124.596
123.276
119.494
118.094
115.903
112.003
97.168
67.694
46.716
40.831
40.625
40.413
40.206
39.995
39.790
39.577
25.878
23.078
F3C
O
Me
HO
N
HN
OH
9
150
100
50
PPM

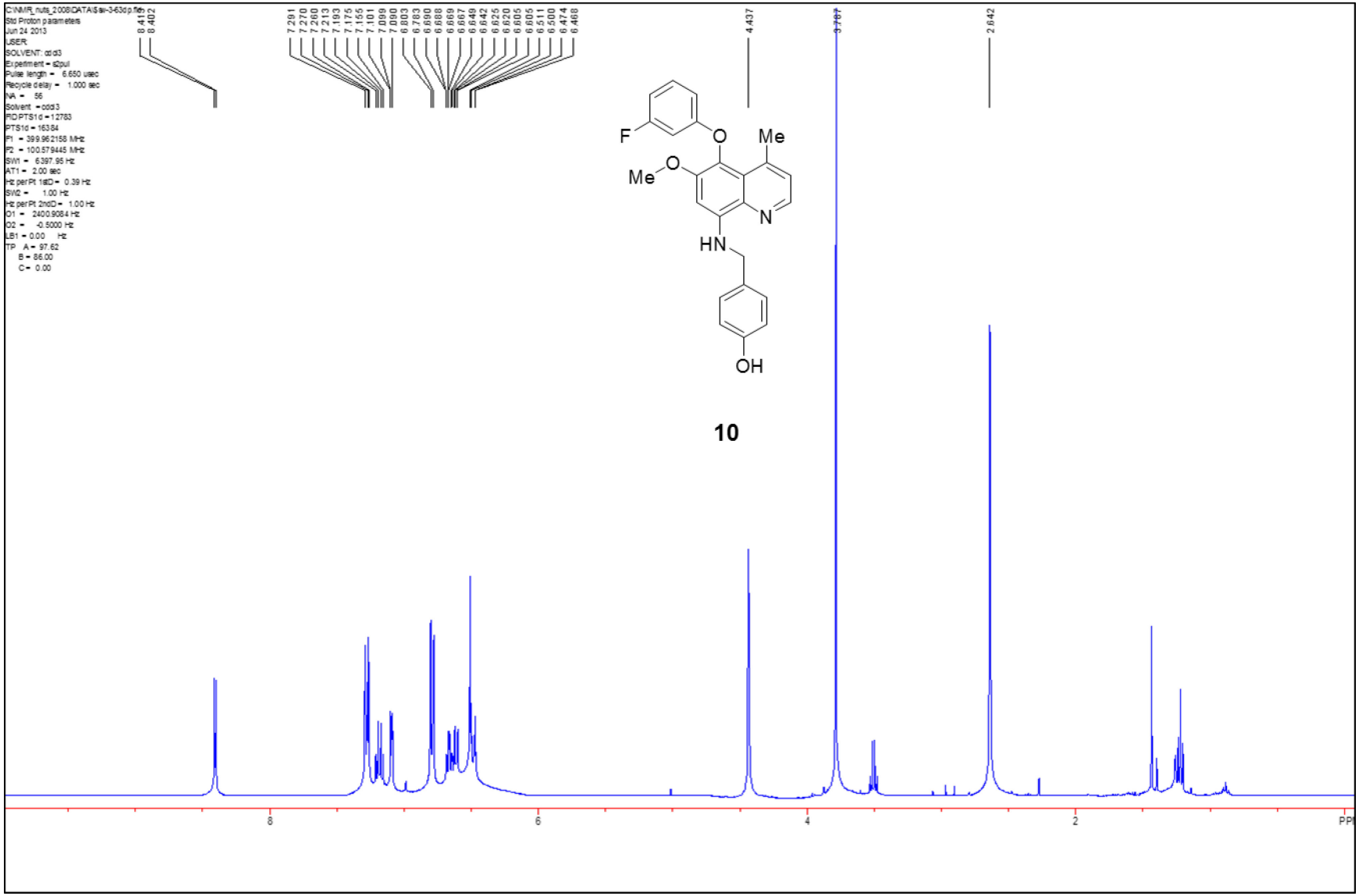
8.419
8.402
7.291
7.270
7.260
7.213
7.193
7.175
7.155
7.101
7.099
7.090
6.803
6.783
6.690
6.688
6.669
6.667
6.649
6.642
6.625
6.620
6.605
6.605
6.511
6.500
6.474
6.468
4.437
3.767
2.642
F
O
Me
Me
O
N
HN
OH
10
8
6
4
2
PPM

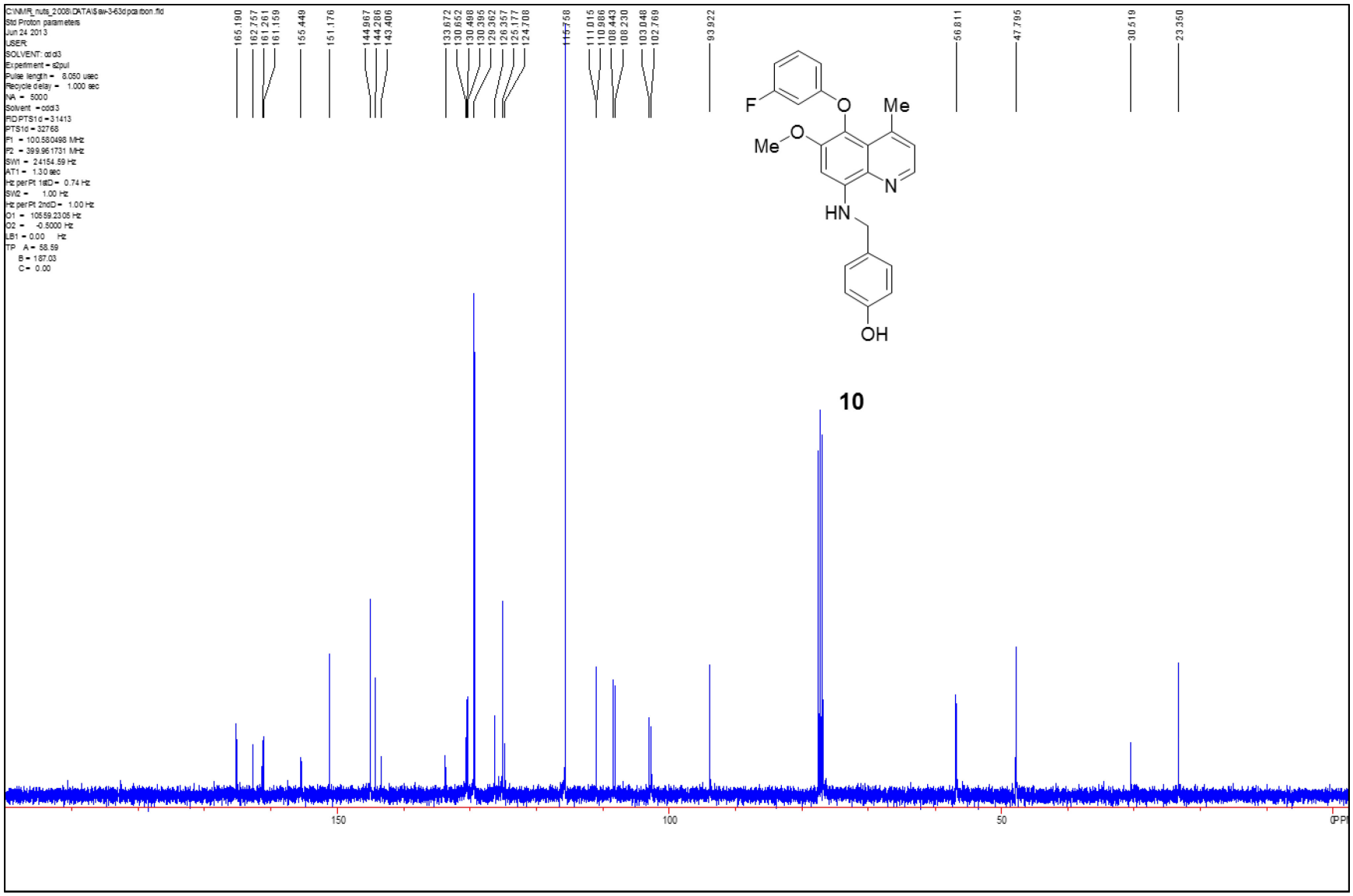
C:\NMR_nuts_2008\DATA\Saw-3-63d pcarbon.fid
Std Proton parameters
Jun 24 2013
USER:
SOLVENT: cdcl3
Experiment = s2pul
Pulse length = 8.050 usec
Recycle delay = 1.000 sec
NA = 5000
Solvent = cdcl3
FIDPTS1d = 31413
PTS1d = 32768
P1 = 100.580498 MHz
P2 = 399.961731 MHz
SW1 = 24154.59 Hz
AT1 = 1.30 sec
Hz per Pt 1stD = 0.74 Hz
SW2 = 1.00 Hz
Hz per Pt 2ndD = 1.00 Hz
O1 = 10559.2305 Hz
O2 = -0.5000 Hz
LB1 = 0.00 Hz
TP A = 58.59
B = 187.03
C = 0.00
165.190
162.757
161.261
161.159
155.449
151.176
144.967
144.266
143.406
133.672
130.652
130.498
130.395
129.362
126.357
125.177
124.708
115.758
111.015
110.986
108.443
108.230
103.048
102.769
93.922
56.811
47.795
30.519
23.350
F
O
Me
O
Me
N
HN
OH
10
150
100
50
0

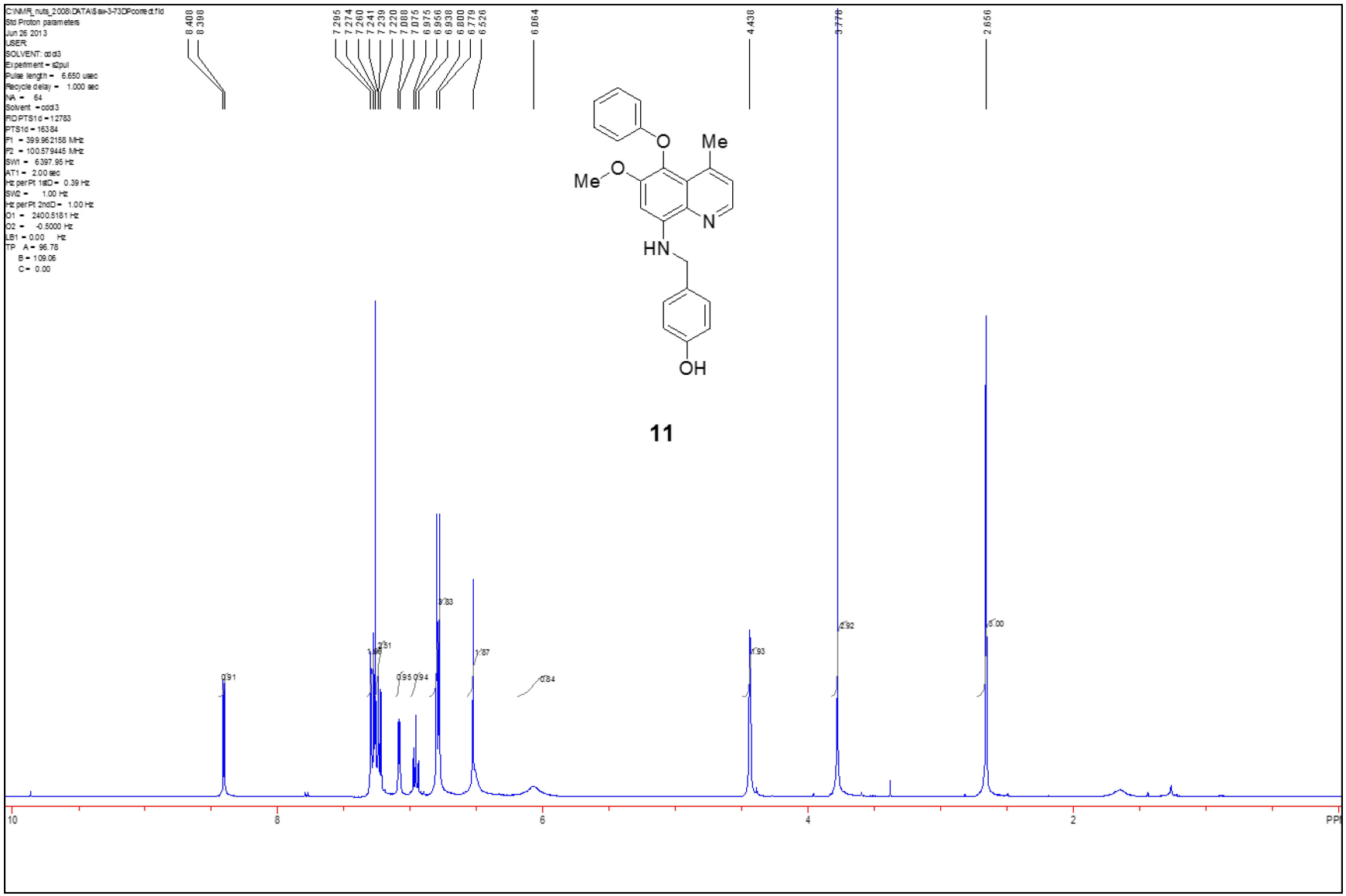
8.408
8.398
7.295
7.274
7.260
7.241
7.239
7.220
7.088
7.075
6.975
6.956
6.938
6.800
6.779
6.526
6.064
4.438
3.778
2.656
O
Me
Me
O
N
HN
OH
11
0.91
2.31
0.95
0.94
3.83
1.87
0.84
1.93
2.92
6.00
10
8
6
4
2
PPM

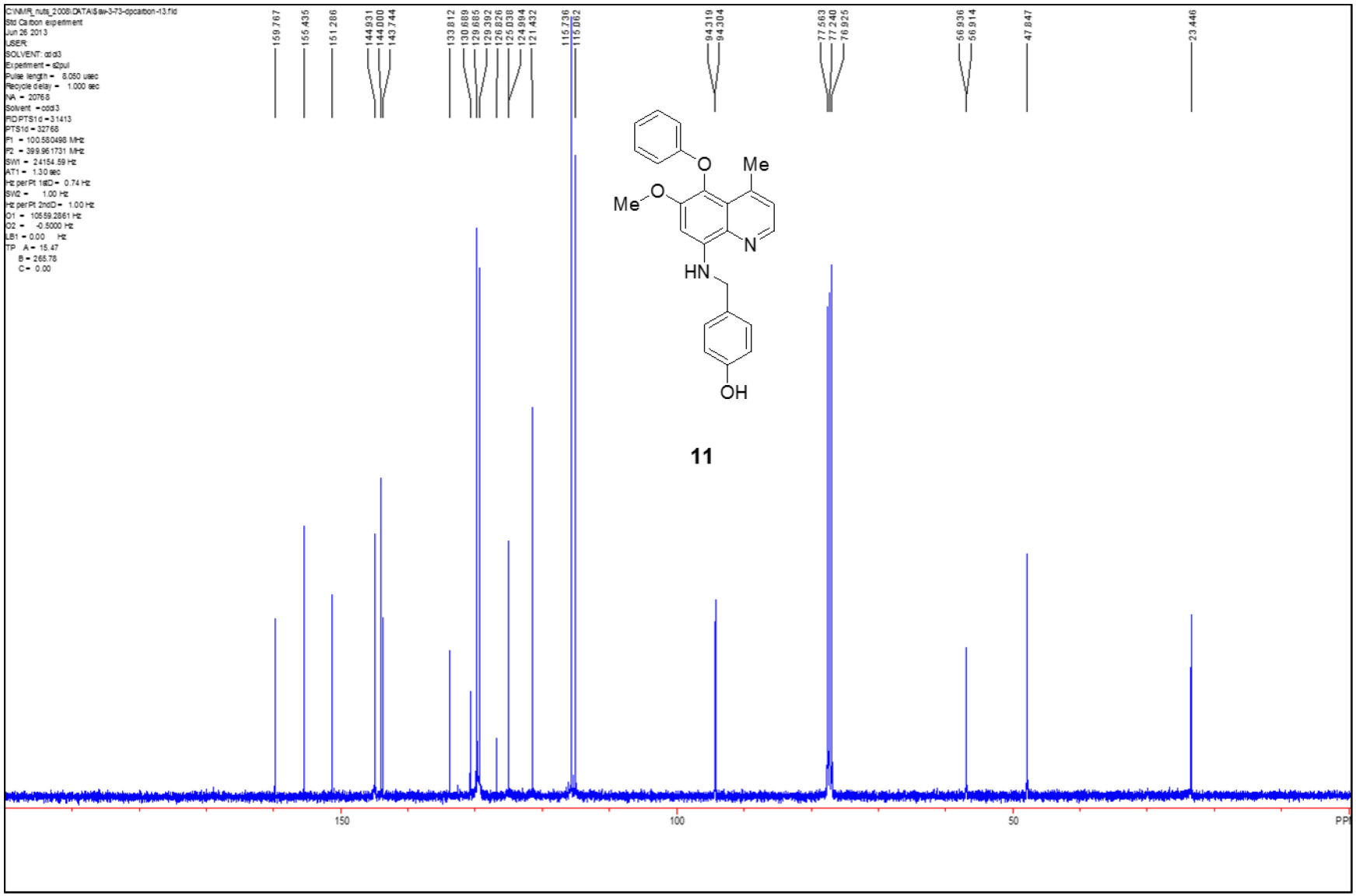
159.767
155.435
151.286
144.931
144.000
143.744
133.812
130.689
129.685
129.392
126.826
125.038
124.994
121.432
115.736
115.062
94.319
94.304
77.563
77.240
76.925
56.936
56.914
47.847
23.446
O
Me
Me
O
N
HN
OH
11
150
100
50

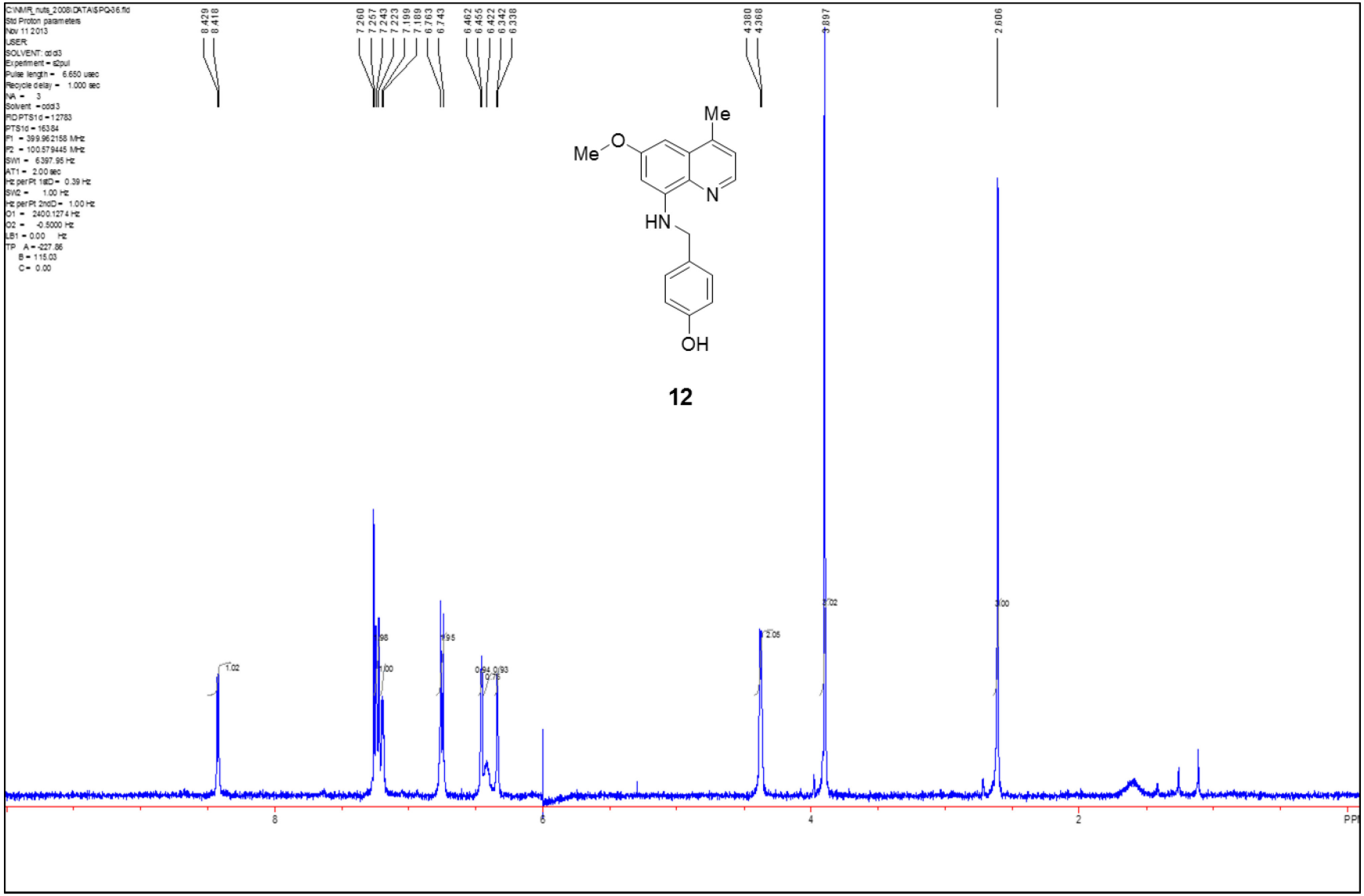
8.429
8.418
7.260
7.257
7.243
7.223
7.199
7.189
6.763
6.743
6.462
6.455
6.422
6.342
6.338
4.380
4.368
3.897
2.606
Me
Me
O
N
HN
OH
12
1.02
2.05
2.02
3.00
8
6
4
2
PPM

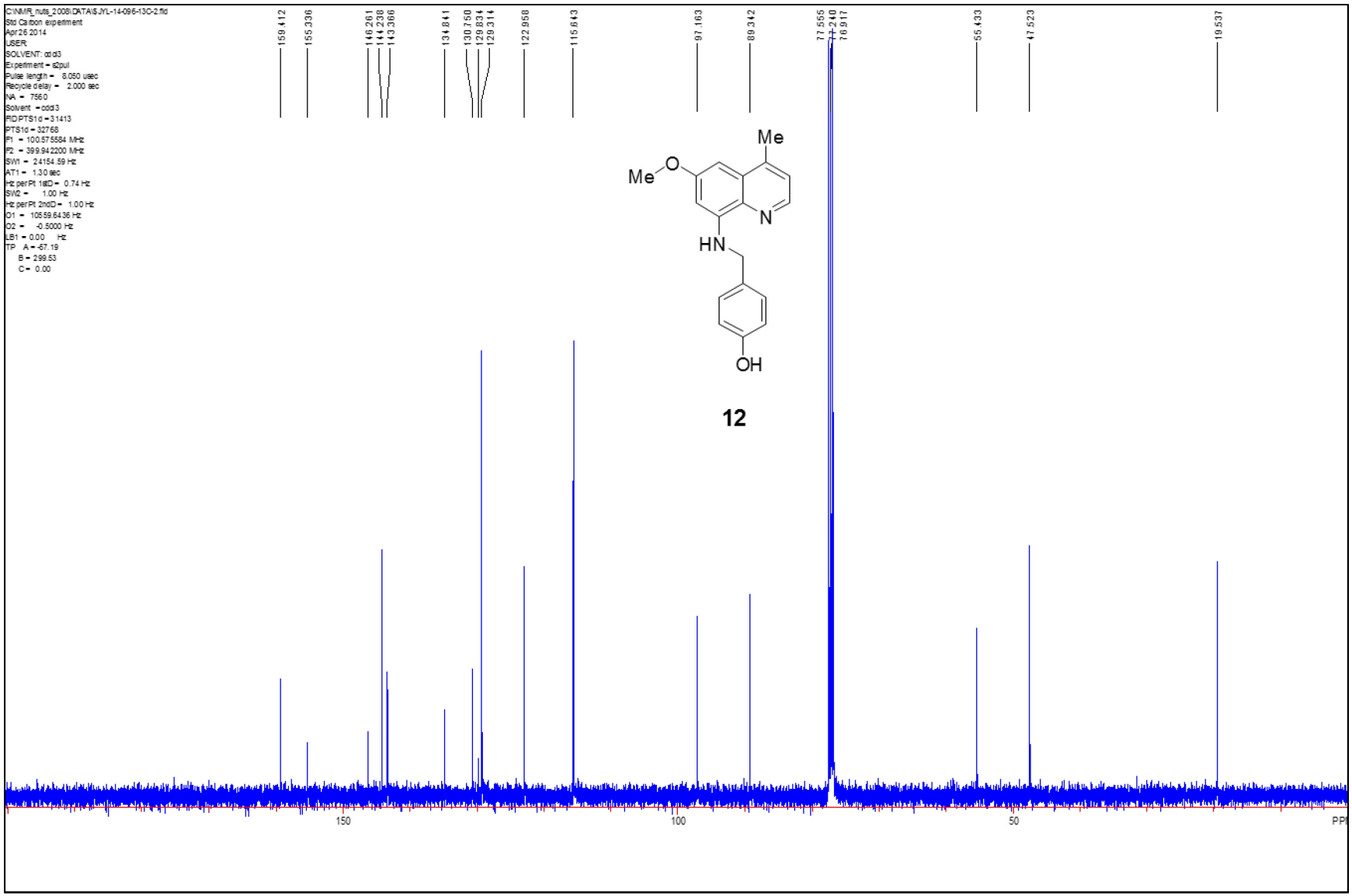
C:\NMR_nuts_2008\DATA\SJYL-14-096-13C-2.fid
Std Carbon experiment
Apr 26 2014
USER:
SOLVENT: cdcl3
Experiment = s2pul
Pulse length = 8.050 usec
Recycle delay = 2.000 sec
NA = 7560
Solvent = cdcl3
FIDPTS1d = 31413
PTS1d = 32768
P1 = 100.575584 MHz
P2 = 399.942200 MHz
SW1 = 24154.59 Hz
AT1 = 1.30 sec
Hz per Pt 1stD = 0.74 Hz
SW2 = 1.00 Hz
Hz per Pt 2ndD = 1.00 Hz
O1 = 10559.6436 Hz
O2 = -0.5000 Hz
LB1 = 0.00 Hz
TP A = -67.19
B = 299.53
C = 0.00
159.412
155.336
146.261
144.238
143.366
134.841
130.750
129.834
129.314
122.958
115.643
97.163
89.342
77.555
77.240
76.917
55.433
47.523
19.537
Me
O
Me
N
HN
OH
12
150
100
50
PPM

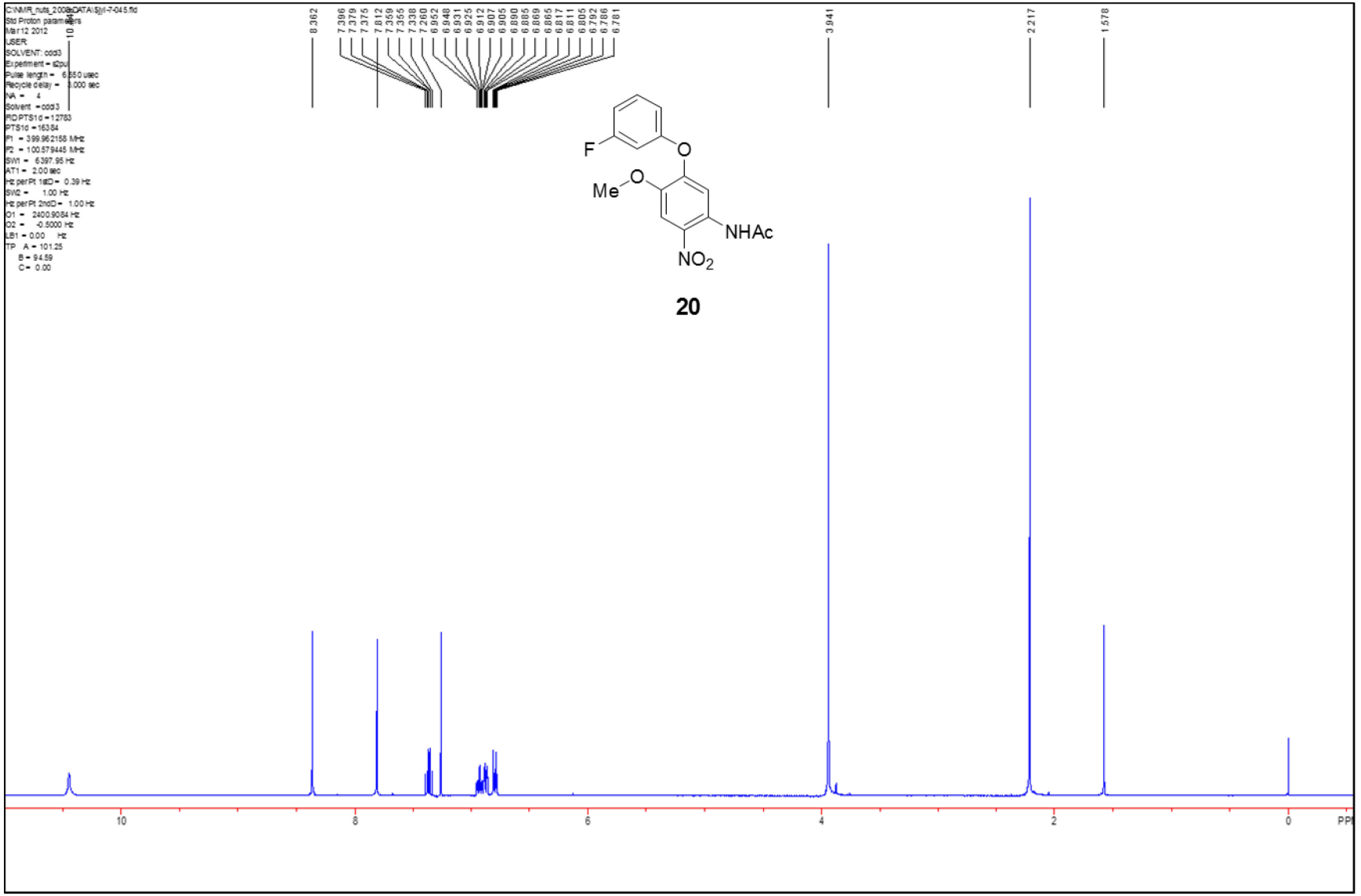
8.362
7.396
7.379
7.375
7.812
7.359
7.355
7.338
7.290
6.952
6.948
6.931
6.925
6.912
6.907
6.905
6.890
6.885
6.869
6.865
6.817
6.811
6.805
6.792
6.786
6.781
3.941
2.217
1.578
F
O
Me
O
NHAc
NO2
20
10
8
6
4
2
0
PPM

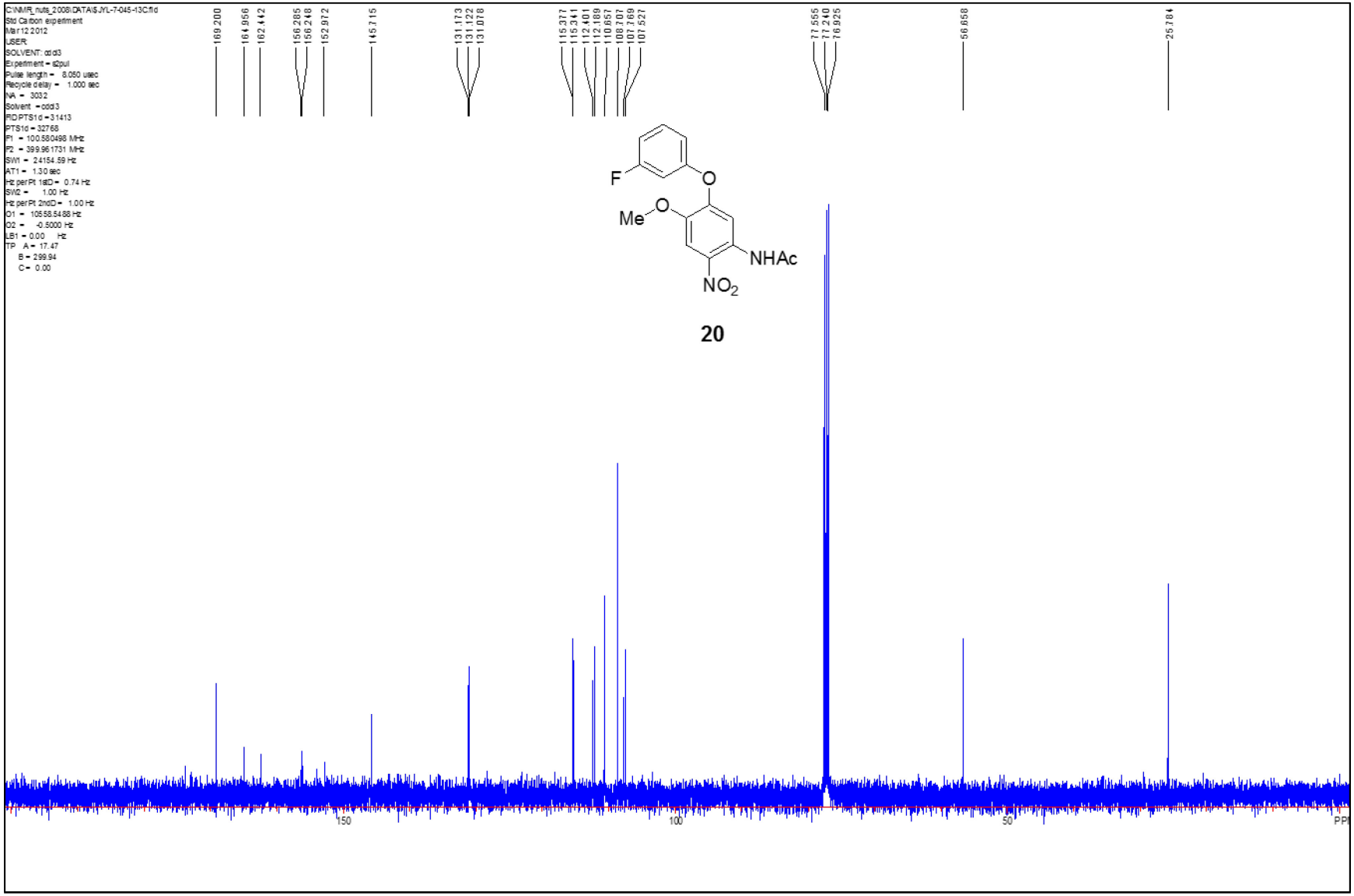
C:\NMR_nuts_2008\DATA\SJYL-7-045-13C.fid
Std Carbon experiment
Mar12 2012
USER
SOLVENT: cdcl3
Experiment = s2pul
Pulse length = 8.050 usec
Recycle delay = 1.000 sec
NA = 3032
Solvent = cdcl3
FIDPTS1d = 31413
PTS1d = 32768
P1 = 100.580498 MHz
P2 = 399.961731 MHz
SW1 = 24154.59 Hz
AT1 = 1.30 sec
Hz perPt 1stD = 0.74 Hz
SW2 = 1.00 Hz
Hz perPt 2ndD = 1.00 Hz
O1 = 10558.5488 Hz
O2 = -0.5000 Hz
LB1 = 0.00 Hz
TP A = 17.47
B = 299.94
C = 0.00
169.200
164.956
162.442
156.285
156.248
152.972
145.715
131.173
131.122
131.078
115.317
115.341
112.401
112.189
110.657
108.707
107.769
107.527
77.555
77.240
76.925
56.658
25.784
F
O
Me
O
NHAc
NO2
20
150
100
50
PPM

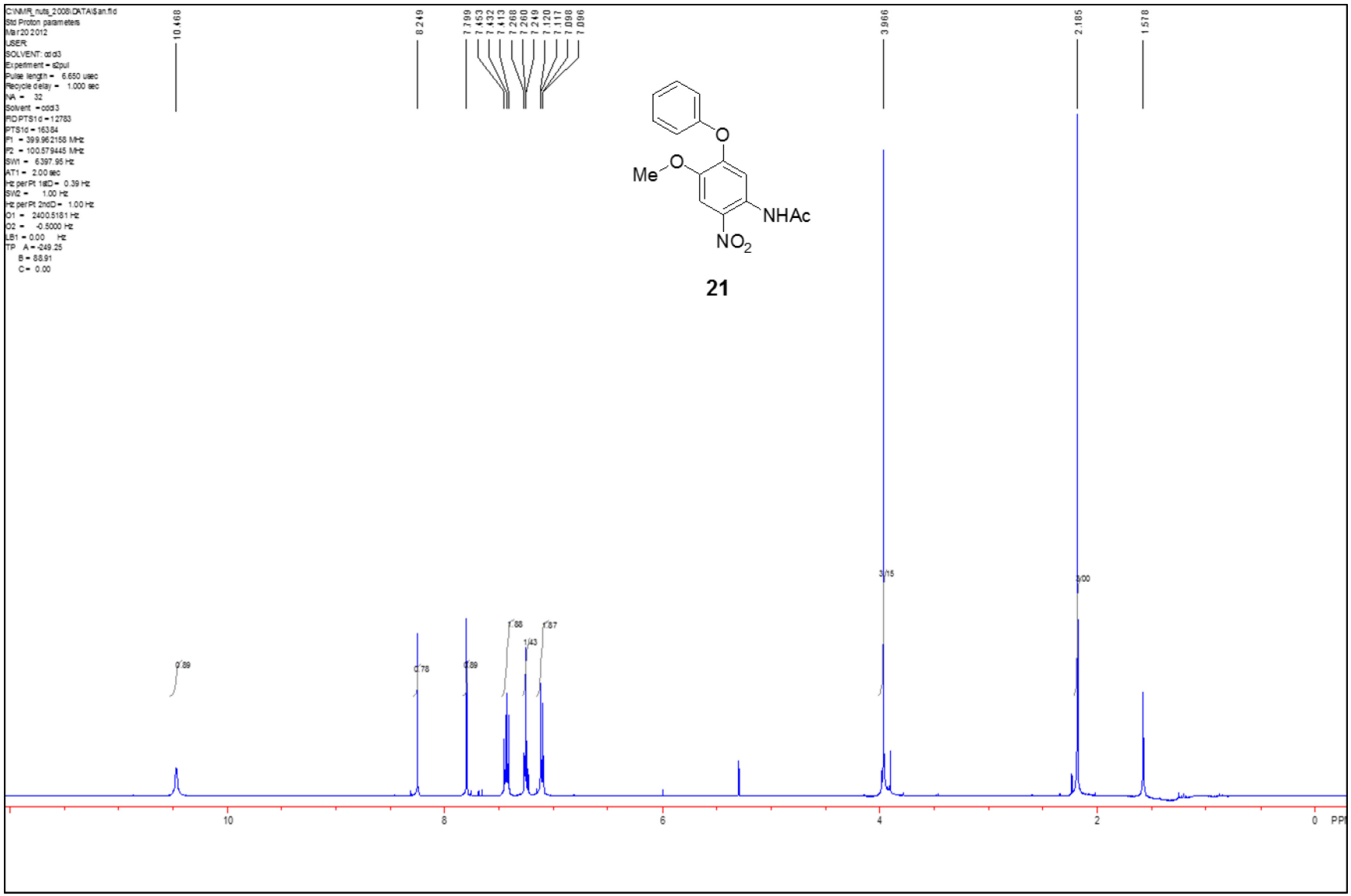
10.468
8.249
7.799
7.453
7.432
7.413
7.268
7.260
7.249
7.120
7.117
7.098
7.096
3.966
2.185
1.578
Me
O
O
NHAc
NO2
21
0.89
0.78
0.89
1.88
1.87
1.43
3.15
6.00
10
8
6
4
2
0
PPM

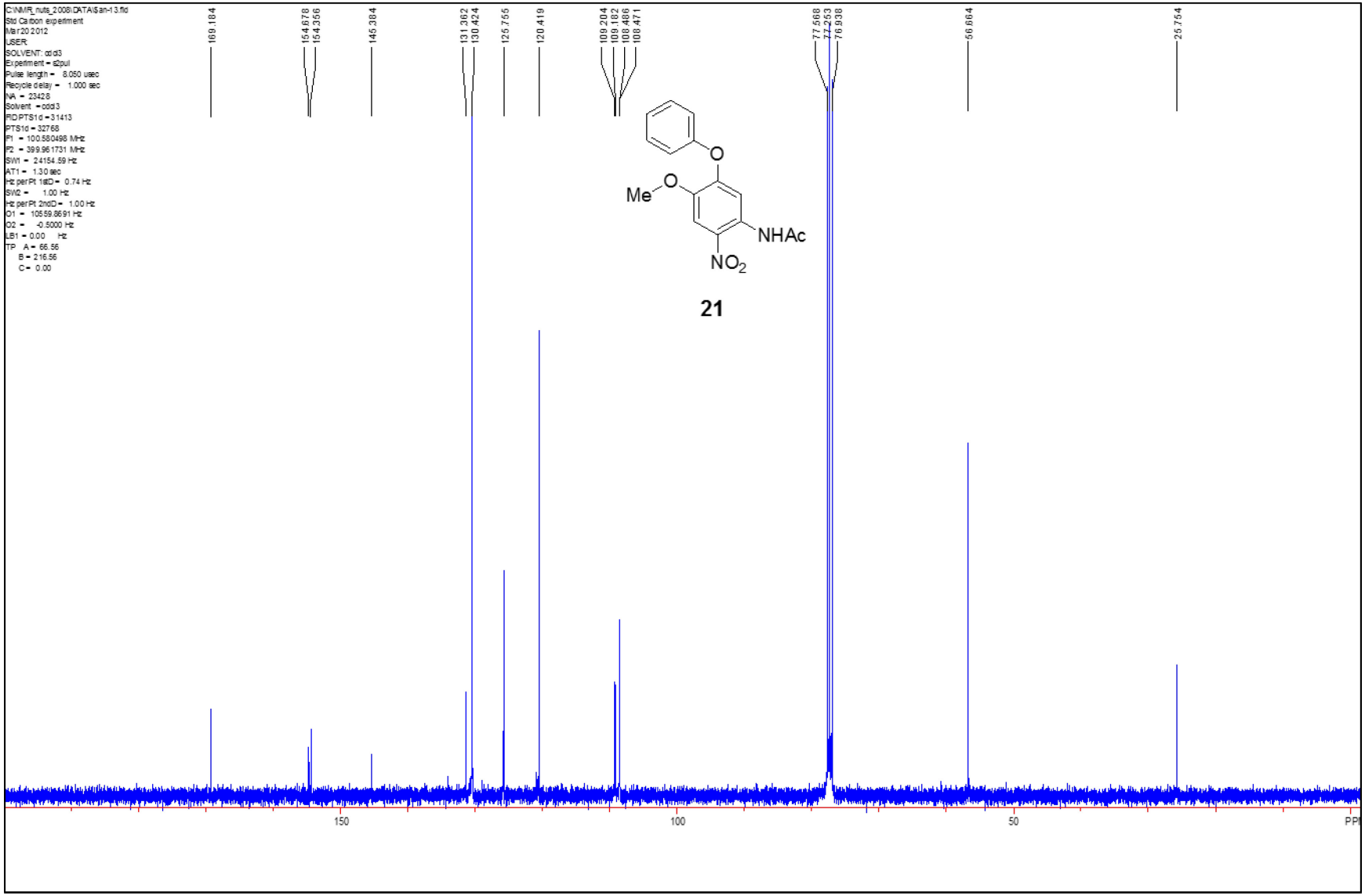
C:\NMR_nuts_2008\DATA\San-13.fid
Std Carbon experiment
Mar 20 2012
USER
SOLVENT: cdcl3
Experiment = s2pul
Pulse length = 8.050 usec
Recycle delay = 1.000 sec
NA = 2342.8
Solvent = cdcl3
FIDRES = 0.31413
PTS1d = 32768
P1 = 100.580498 MHz
P2 = 399.961731 MHz
SW1 = 24154.59 Hz
AT1 = 1.30 sec
Hz per Pt 1stD = 0.74 Hz
SW2 = 1.00 Hz
Hz per Pt 2ndD = 1.00 Hz
O1 = 10559.8691 Hz
O2 = -0.5000 Hz
LB1 = 0.00 Hz
TP A = 66.56
B = 216.56
C = 0.00
169.184
154.678
154.356
145.384
131.362
130.424
125.755
120.419
109.204
109.182
108.486
108.471
77.568
77.253
76.938
56.664
25.754
Me
O
O
NHAc
NO2
21
150
100
50
PPM

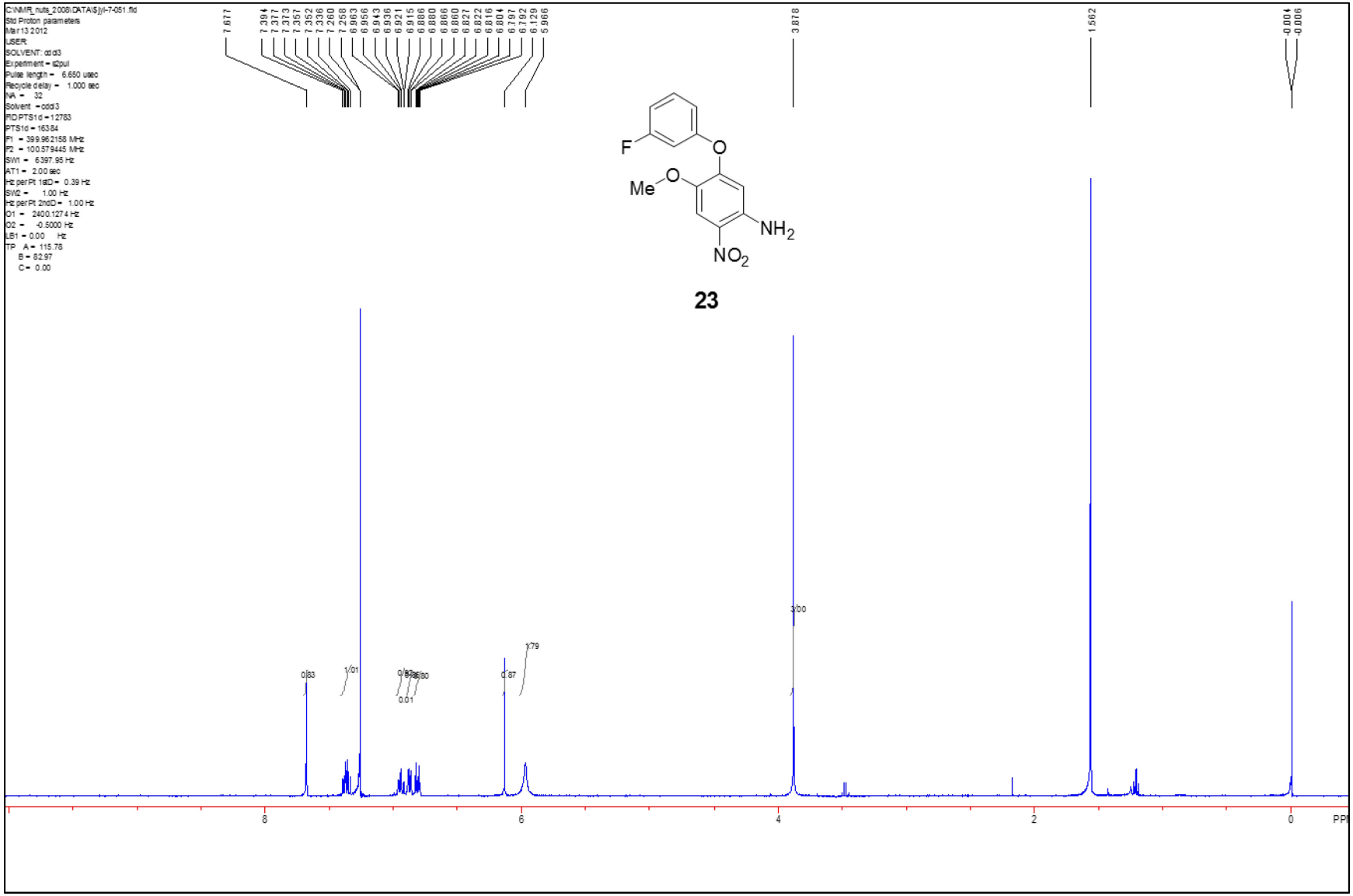
F
O
Me
O
NH2
NO2
23

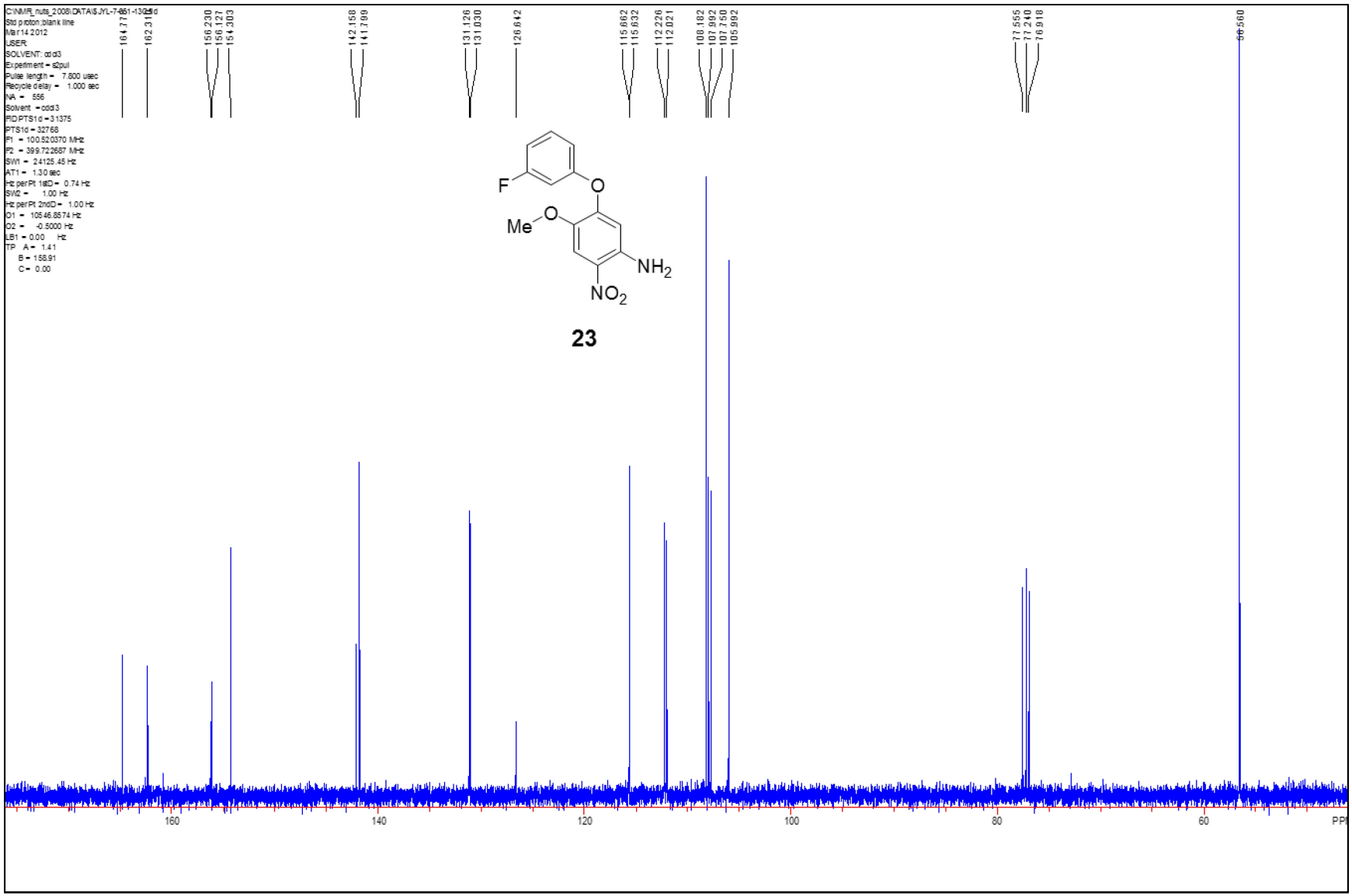
C:\NMR_nuts_2008\DATA\SJYL-7-661-13C-1d
Std proton.blank line
Mar 14 2012
USER:
SOLVENT: cdcl3
Experiment = s2pul
Pulse length = 7.800 usec
Recycle delay = 1.000 sec
NA = 556
Solvent = cdcl3
FIDPTS1d = 31375
PTS1d = 32768
F1 = 100.520370 MHz
F2 = 399.722687 MHz
SW1 = 24125.45 Hz
AT1 = 1.30 sec
Hz per Pt 1stD = 0.74 Hz
SW2 = 1.00 Hz
Hz per Pt 2ndD = 1.00 Hz
O1 = 10546.8574 Hz
O2 = -0.5000 Hz
LB1 = 0.00 Hz
TP A = 1.41
B = 158.91
C = 0.00
164.771
162.316
156.230
156.127
154.303
142.158
141.799
131.126
131.030
126.642
115.662
115.632
112.226
112.021
108.182
107.992
107.750
105.992
77.555
77.240
76.918
56.560
F
O
Me
O
NH2
NO2
23
160
140
120
100
80
60
PPM

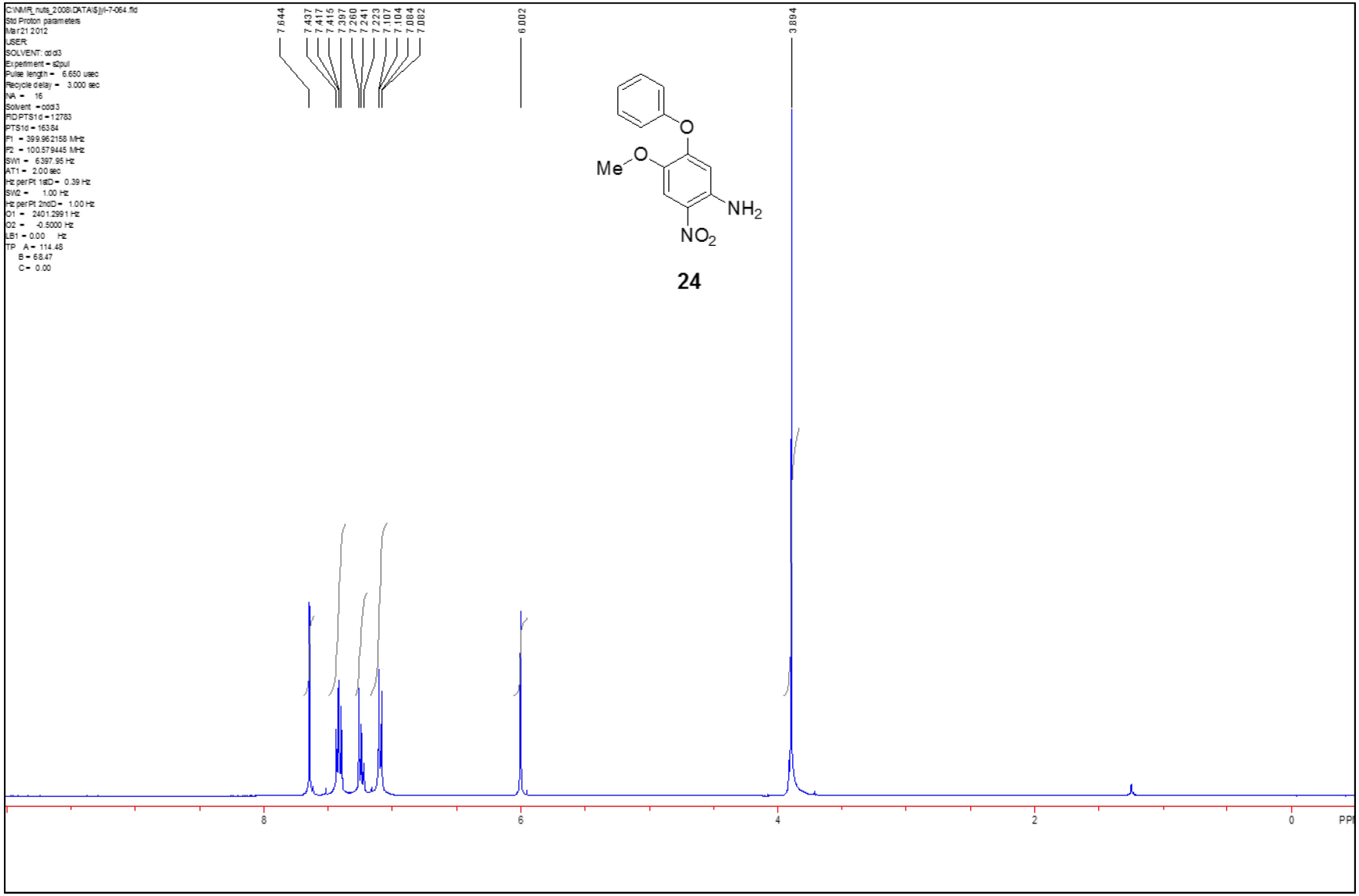
C:\NMR_nuts_2008\DATA\SJ\jl-7-064.fid
Std Proton parameters
Mar 21 2012
USER
SOLVENT: cdcl3
Experiment = s2pul
Pulse length = 6.650 usec
Recycle delay = 3.000 sec
NA = 16
Solvent = cdcl3
FIDPTS1d = 1.2783
PTS1d = 16384
P1 = 399.96158 MHz
P2 = 100.579445 MHz
SW1 = 6397.95 Hz
AT1 = 2.00 sec
Hz per Pt 1stD = 0.39 Hz
SW2 = 1.00 Hz
Hz per Pt 2ndD = 1.00 Hz
O1 = 2401.2991 Hz
O2 = -0.5000 Hz
LB1 = 0.00 Hz
TP A = 114.48
B = 68.47
C = 0.00
7.644
7.437
7.417
7.415
7.397
7.260
7.241
7.223
7.107
7.104
7.084
7.082
6.002
3.894
Me
O
O
NH2
NO2
24
8
6
4
2
0
PPM

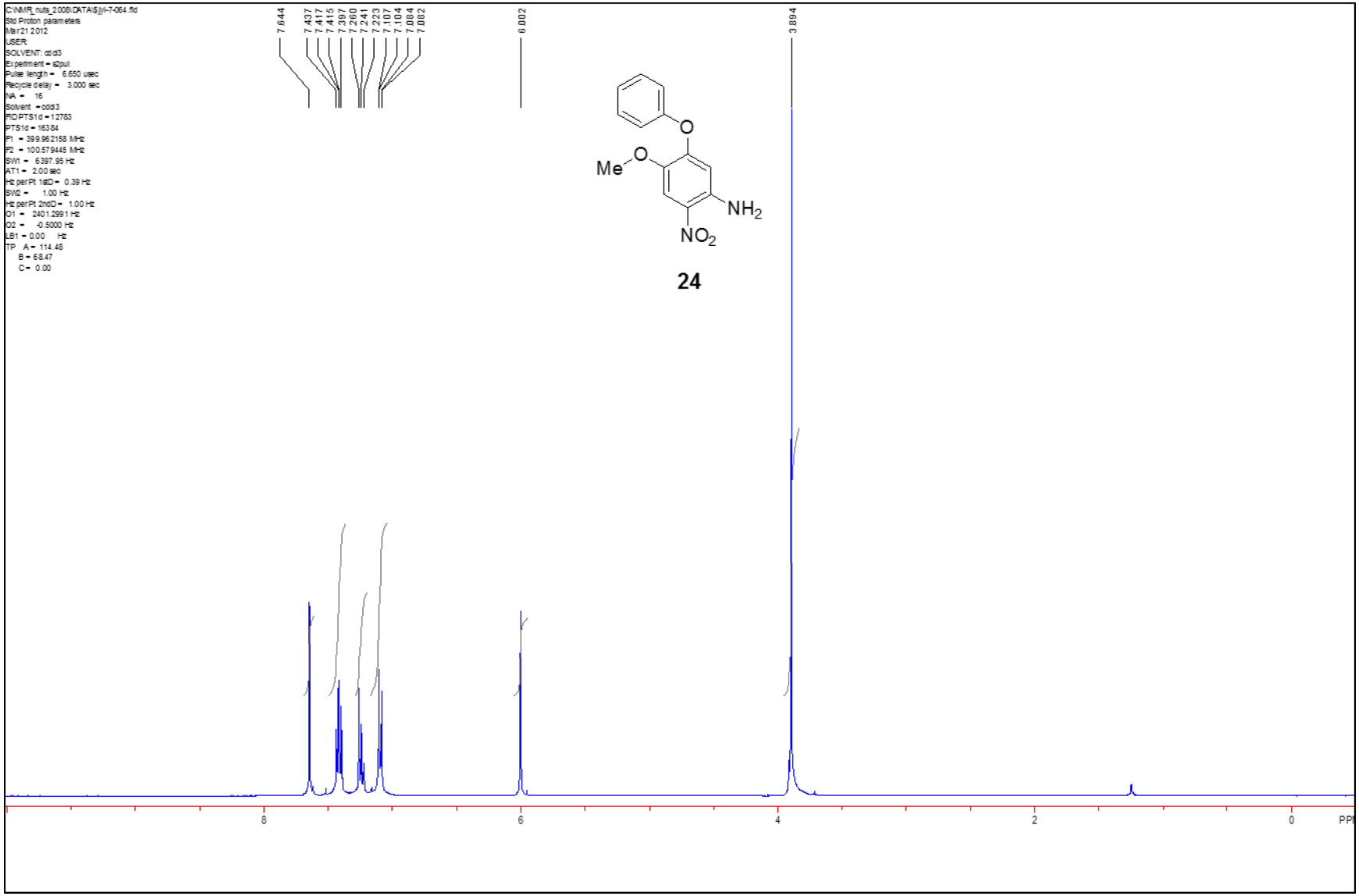
C:\NMR_nuts_2008\DATA\SJ\jl-7-064.fid
Std Proton parameters
Mar 21 2012
USER
SOLVENT: cdcl3
Experiment = s2pul
Pulse length = 6.650 usec
Recycle delay = 3.000 sec
NA = 16
Solvent = cdcl3
FIDPTS1d = 1.2783
PTS1d = 16384
P1 = 399.96158 MHz
P2 = 100.579445 MHz
SW1 = 6397.95 Hz
AT1 = 2.00 sec
Hz per Pt 1stD = 0.39 Hz
SW2 = 1.00 Hz
Hz per Pt 2ndD = 1.00 Hz
O1 = 2401.2991 Hz
O2 = -0.5000 Hz
LB1 = 0.00 Hz
TP A = 114.48
B = 68.47
C = 0.00
7.644
7.437
7.417
7.415
7.397
7.260
7.241
7.223
7.107
7.104
7.084
7.082
6.002
3.894
Me
O
O
NH2
NO2
24
8
6
4
2
0
PPM

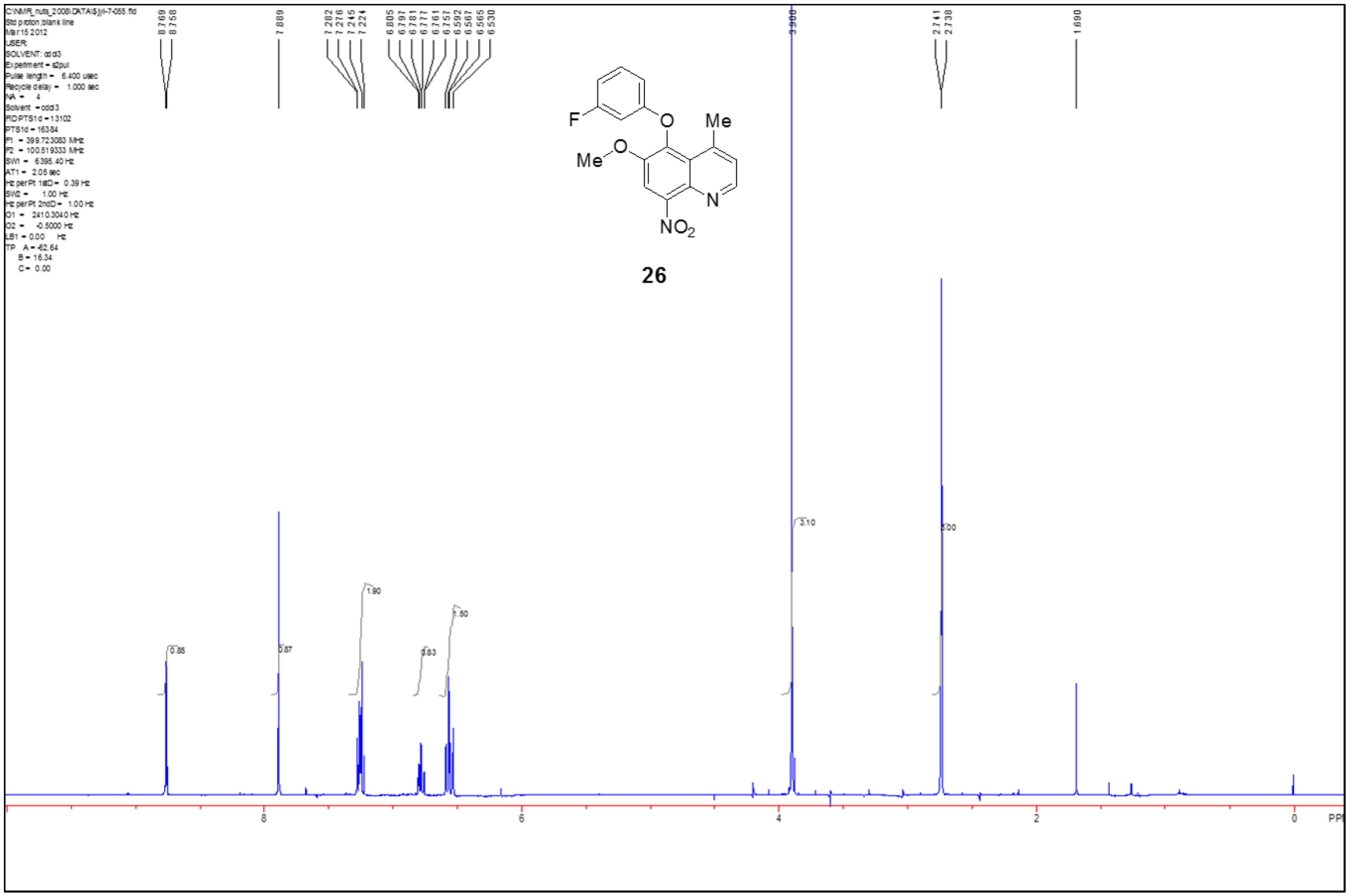
8.769
8.758
7.889
7.282
7.216
7.245
7.224
6.805
6.797
6.781
6.777
6.761
6.757
6.592
6.567
6.565
6.530
3.990
2.741
2.738
1.690
F
O
Me
Me
O
N
NO2
26
0.85
0.87
1.90
0.83
1.50
3.10
3.00
8
6
4
2
0
PPM

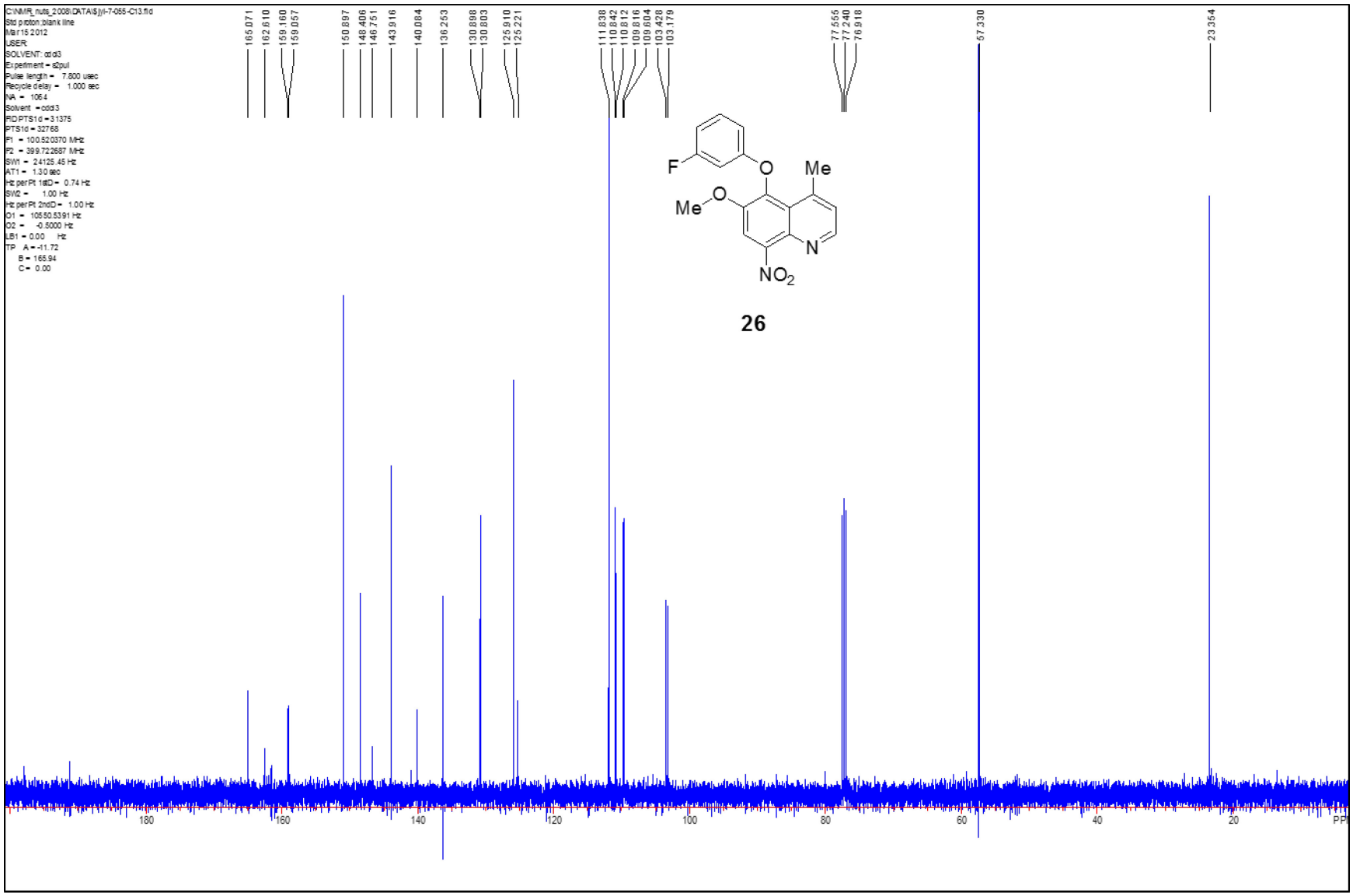
C:\NMR_nuts_2008\DATA\SJ\I-7-055-C13.fid
Std proton.blank line
Mar 15 2012
USER
SOLVENT: cdcl3
Experiment = s2pul
Pulse length = 7.800 usec
Recycle delay = 1.000 sec
NA = 1064
Solvent = cdcl3
FIDPTS1d = 31375
PTS1d = 32768
P1 = 100.520370 MHz
P2 = 399.722687 MHz
SW1 = 24125.45 Hz
AT1 = 1.30 sec
Hz per Pt 1stD = 0.74 Hz
SW2 = 1.00 Hz
Hz per Pt 2ndD = 1.00 Hz
O1 = 10550.5391 Hz
O2 = -0.5000 Hz
LB1 = 0.00 Hz
TP A = -11.72
B = 165.94
C = 0.00
165.071
162.610
159.160
159.057
150.897
148.406
146.751
143.916
140.084
136.253
130.898
130.803
125.910
125.221
111.838
110.842
110.812
109.816
109.604
103.428
103.179
77.555
77.240
76.918
67.330
23.354
F
O
Me
Me
O
N
NO2
26
180
160
140
120
100
80
60
40
20
PPM

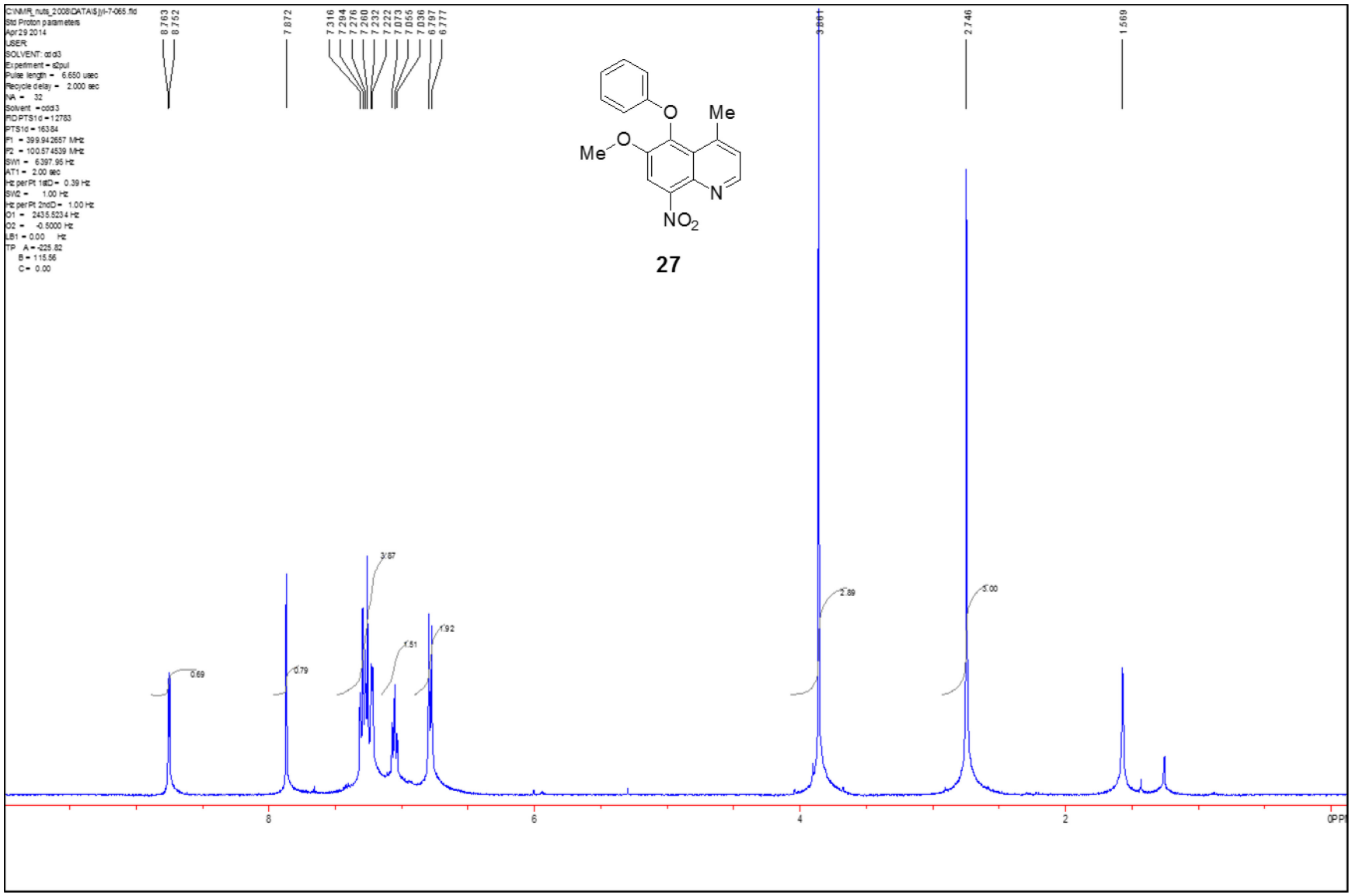
8.763
8.752
7.872
7.316
7.294
7.276
7.260
7.232
7.222
7.073
7.056
7.036
6.797
6.777
3.881
2.746
1.569
O
Me
O
Me
N
NO2
27
0.69
0.79
3.87
1.51
1.92
2.89
3.00
8
6
4
2
0PPM

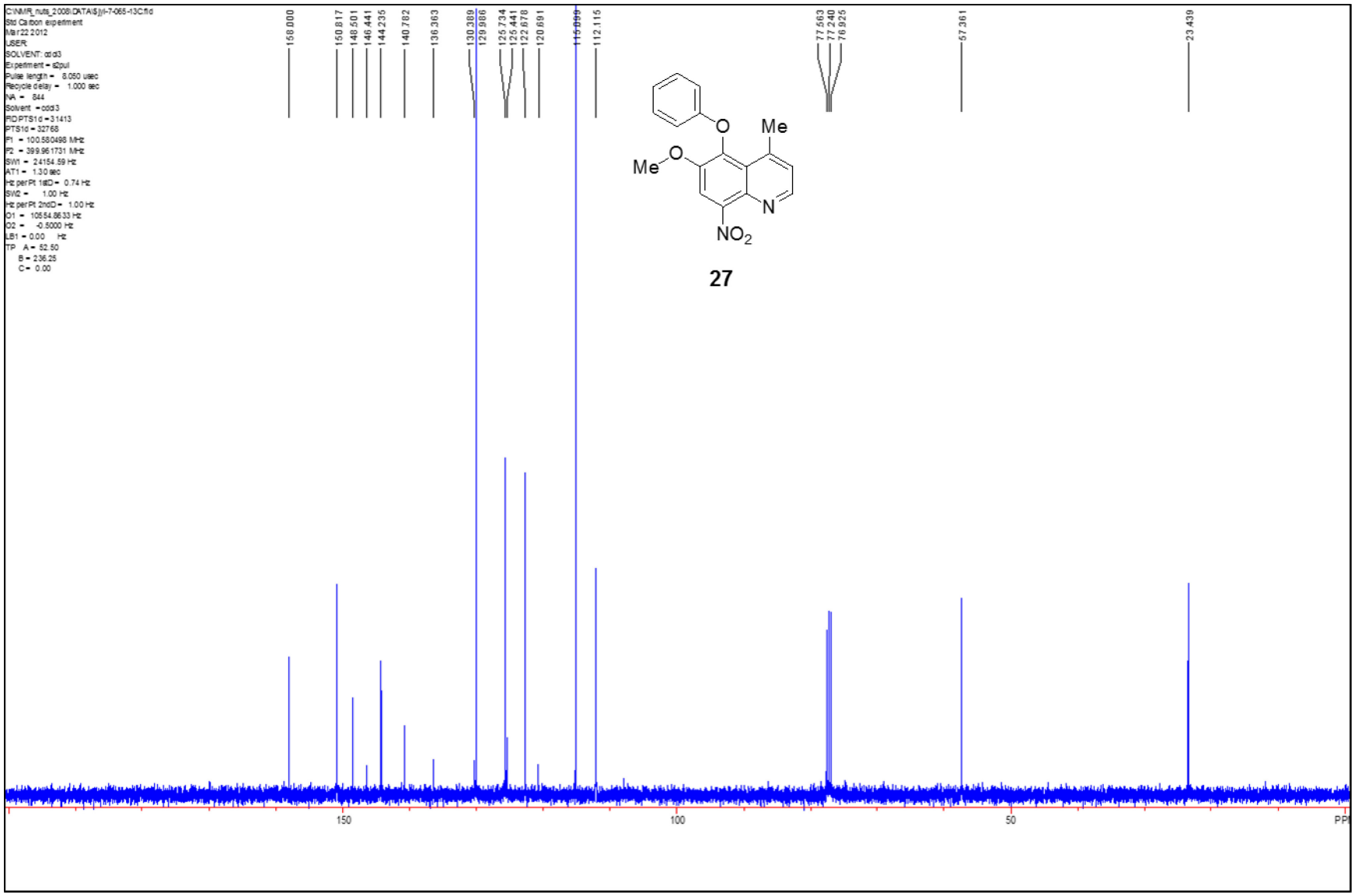
C:\NMR_nuts_2008\DATA\SJ\jl-7-065-13C.fid
Std Carbon experiment
Mar 22 2012
USER:
SOLVENT: cdcl3
Experiment = s2pul
Pulse length = 8.050 usec
Recycle delay = 1.000 sec
NA = 844
Solvent = cdcl3
FIDPTS1d = 31413
PTS1d = 32768
P1 = 100.580498 MHz
P2 = 399.961731 MHz
SW1 = 24154.59 Hz
AT1 = 1.30 sec
Hz per Pt 1stD = 0.74 Hz
SW2 = 1.00 Hz
Hz per Pt 2ndD = 1.00 Hz
O1 = 10554.8633 Hz
O2 = -0.5000 Hz
LB1 = 0.00 Hz
TP A = 52.50
B = 236.25
C = 0.00
158.000
150.817
148.501
146.441
144.235
140.782
136.363
130.389
129.986
125.734
125.441
122.678
120.691
116.099
112.115
77.563
77.240
76.925
57.361
23.439
O
Me
Me
O
N
NO2
27
150
100
50
PPM

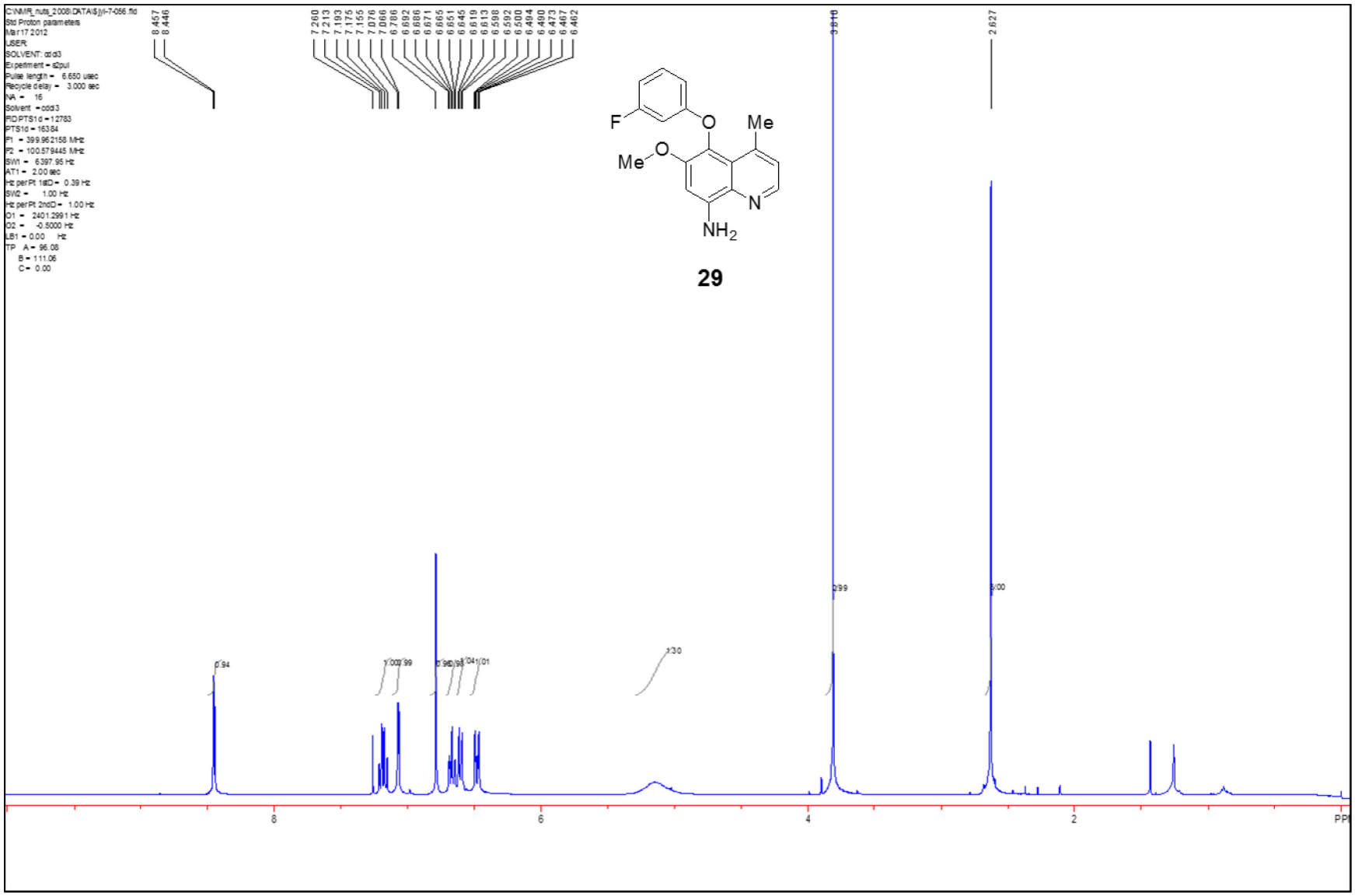
8.457
8.446
7.260
7.213
7.193
7.175
7.155
7.076
7.066
6.786
6.692
6.686
6.671
6.665
6.651
6.645
6.619
6.613
6.598
6.592
6.500
6.494
6.490
6.473
6.467
6.462
3.910
2.627
F
O
Me
Me
O
N
NH2
29
0.94
1.00
0.99
0.96
0.98
1.04
1.01
1.30
2.99
3.00
8
6
4
2
PPM

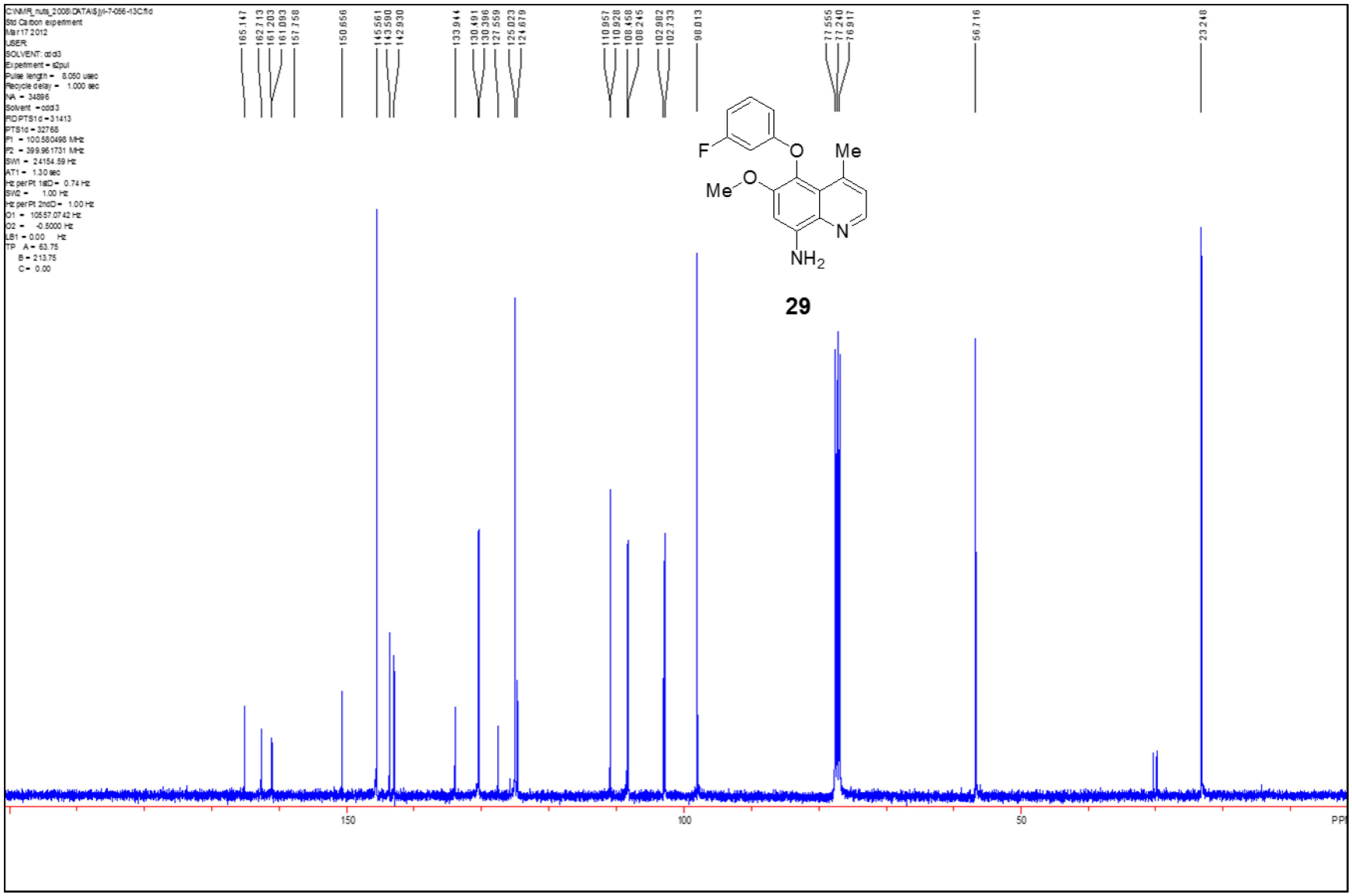
C:\NMR_nuts_2008\DATA\SJ\jl-7-056-13C.fid
Std Carbon experiment
Mar17 2012
USER
SOLVENT: cdcl3
Experiment = s2pul
Pulse length = 8.050 usec
Recycle delay = 1.000 sec
NA = 34896
Solvent = cdcl3
FIDPTS1d = 31413
PTS1d = 32768
P1 = 100.580498 MHz
P2 = 399.961731 MHz
SW1 = 24154.59 Hz
AT1 = 1.30 sec
Hz perPt 1stD = 0.74 Hz
SW2 = 1.00 Hz
Hz perPt 2ndD = 1.00 Hz
O1 = 10557.07 42 Hz
O2 = -0.5000 Hz
LB1 = 0.00 Hz
TP A = 63.75
B = 213.75
C = 0.00
165.147
162.713
161.203
161.093
157.758
150.656
145.561
143.590
142.930
133.944
130.491
130.396
127.559
125.023
124.679
110.957
110.928
108.458
108.245
102.982
102.733
98.013
77.555
77.240
76.917
56.716
23.248
F
O
Me
Me
O
N
NH2
29
150
100
50
PPM

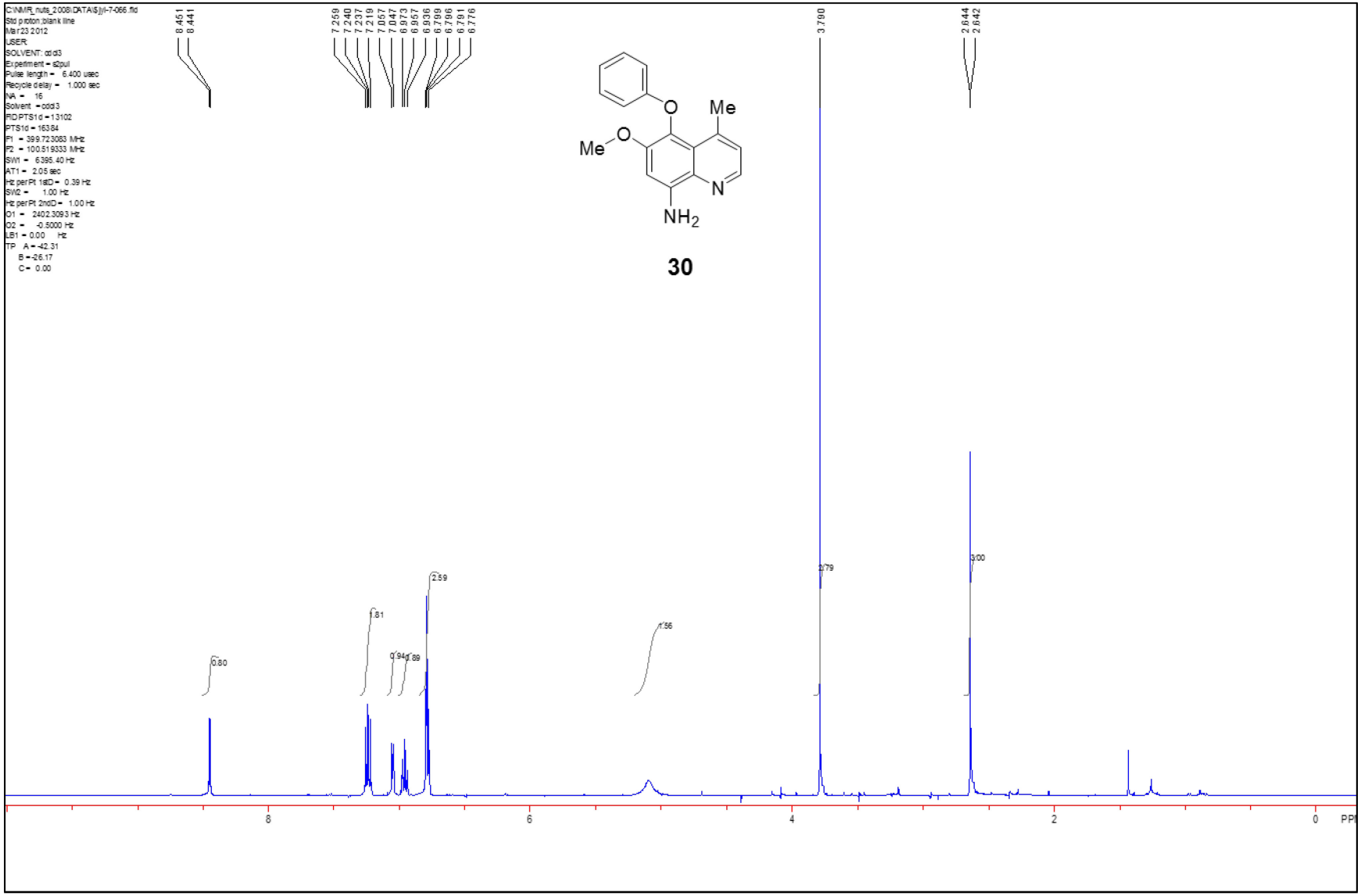
8.451
8.441
7.259
7.240
7.237
7.219
7.057
7.047
6.973
6.957
6.936
6.799
6.796
6.791
6.776
3.790
2.644
2.642
Me
O
Me
O
N
NH2
30
0.60
1.81
0.94
0.89
2.59
1.56
3.79
3.00
8
6
4
2
0
PPM

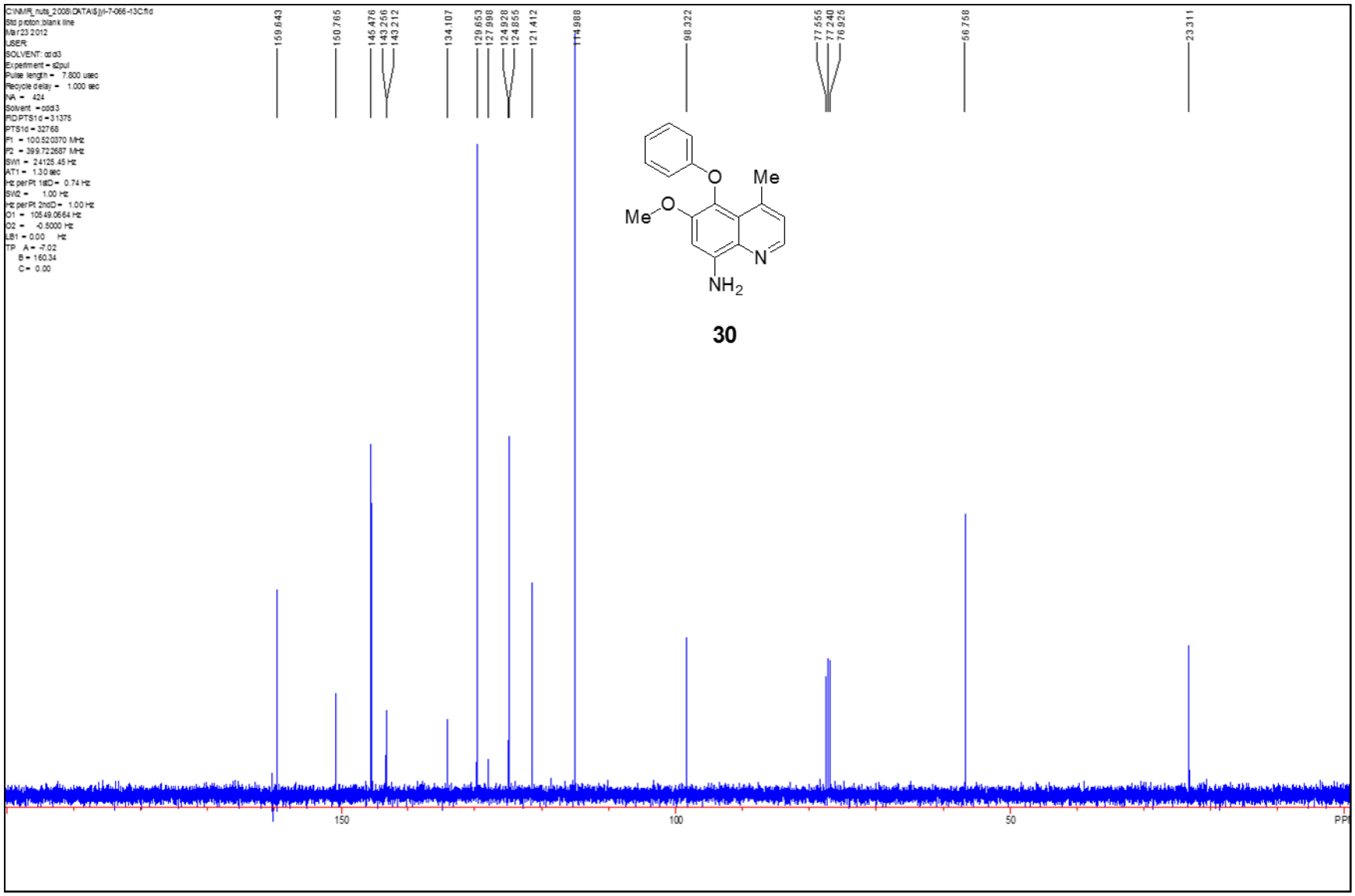
159.643
150.765
145.476
143.256
143.212
134.107
129.653
127.998
124.928
124.855
121.412
114.988
98.322
77.555
77.240
76.925
56.758
23.311
Me
O
Me
O
N
NH2
30
150
100
50

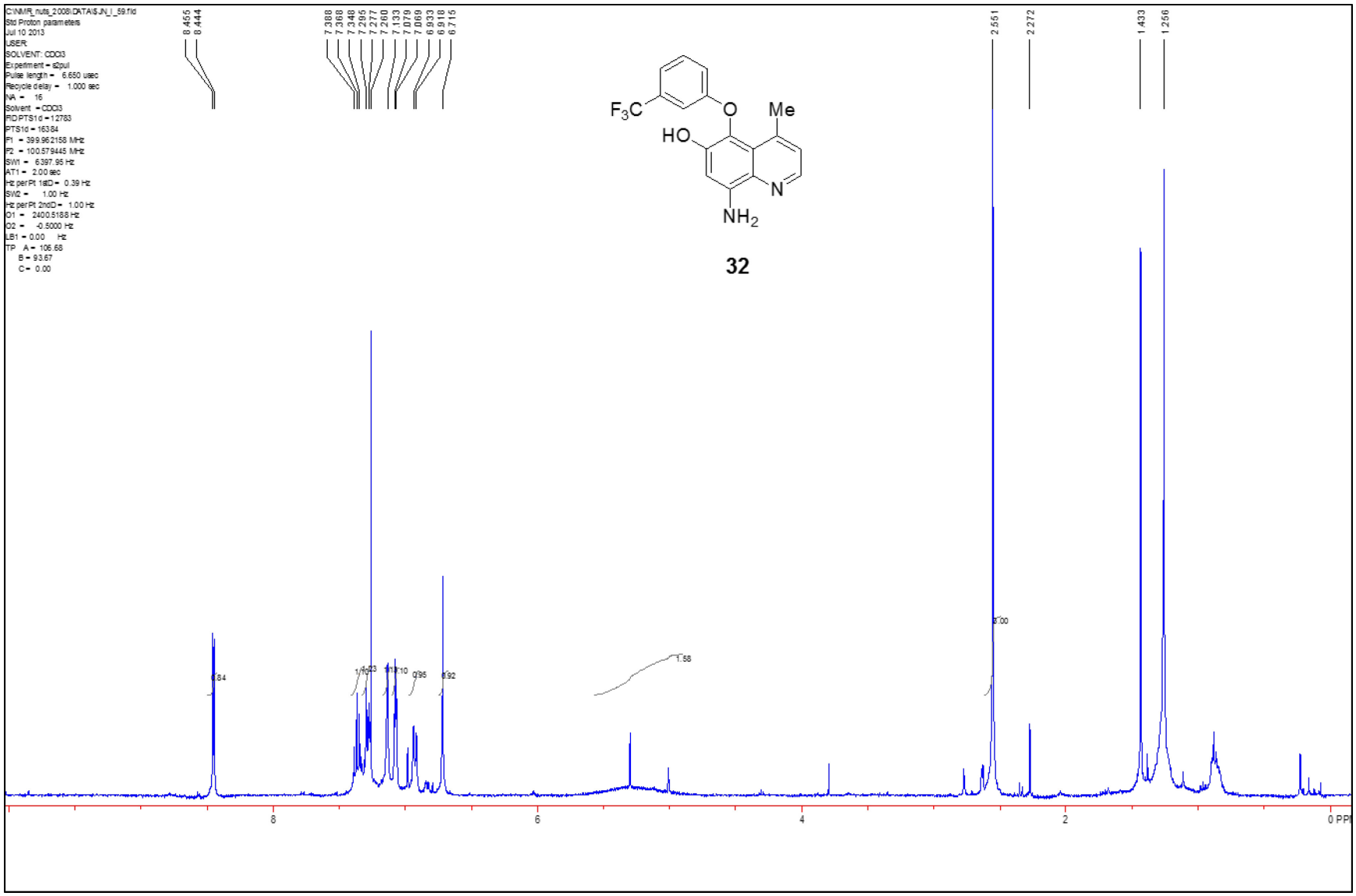
C:\NMR_nuts_2008\DATA\S-JN-I_59.fid
Std Proton parameters
Jul 10 2013
USER
SOLVENT: CDCl3
Experiment = s2pul
Pulse length = 6.650 usec
Recycle delay = 1.000 sec
NA = 16
Solvent = CDCl3
FIDRES = 1.2783
PTS1d = 16384
F1 = 399.96218 MHz
F2 = 100.57944 MHz
SW1 = 6397.95 Hz
AT1 = 2.00 sec
Hz per Pt 1stD = 0.39 Hz
SW2 = 1.00 Hz
Hz per Pt 2ndD = 1.00 Hz
O1 = 2400.5188 Hz
O2 = -0.5000 Hz
LB1 = 0.00 Hz
TP A = 106.68
B = 93.67
C = 0.00
8.455
8.444
7.388
7.368
7.348
7.295
7.277
7.260
7.133
7.079
7.069
6.933
6.918
6.715
2.551
2.272
1.433
1.256
F3C
O
Me
HO
N
NH2
32
0.84
1.03
1.10
0.95
0.92
1.58
9.00
8
6
4
2
0 PPM

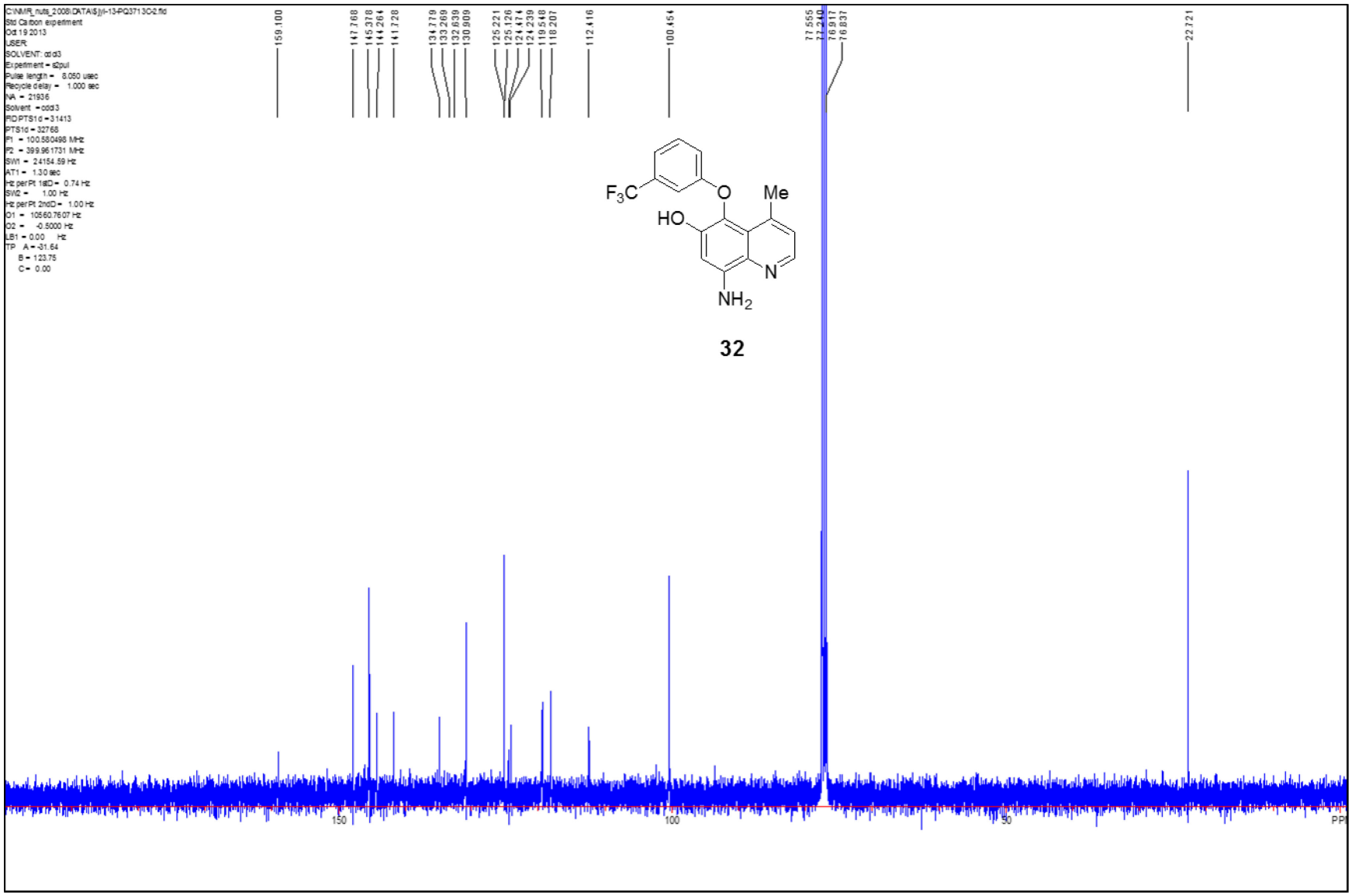
159.100
147.768
145.378
144.264
141.728
134.779
133.269
132.639
130.909
125.221
125.126
124.474
124.239
119.548
118.207
112.416
100.454
77.555
77.240
76.917
76.837
22.721
F3C
O
Me
HO
N
NH2
32
150
100
50
PPM

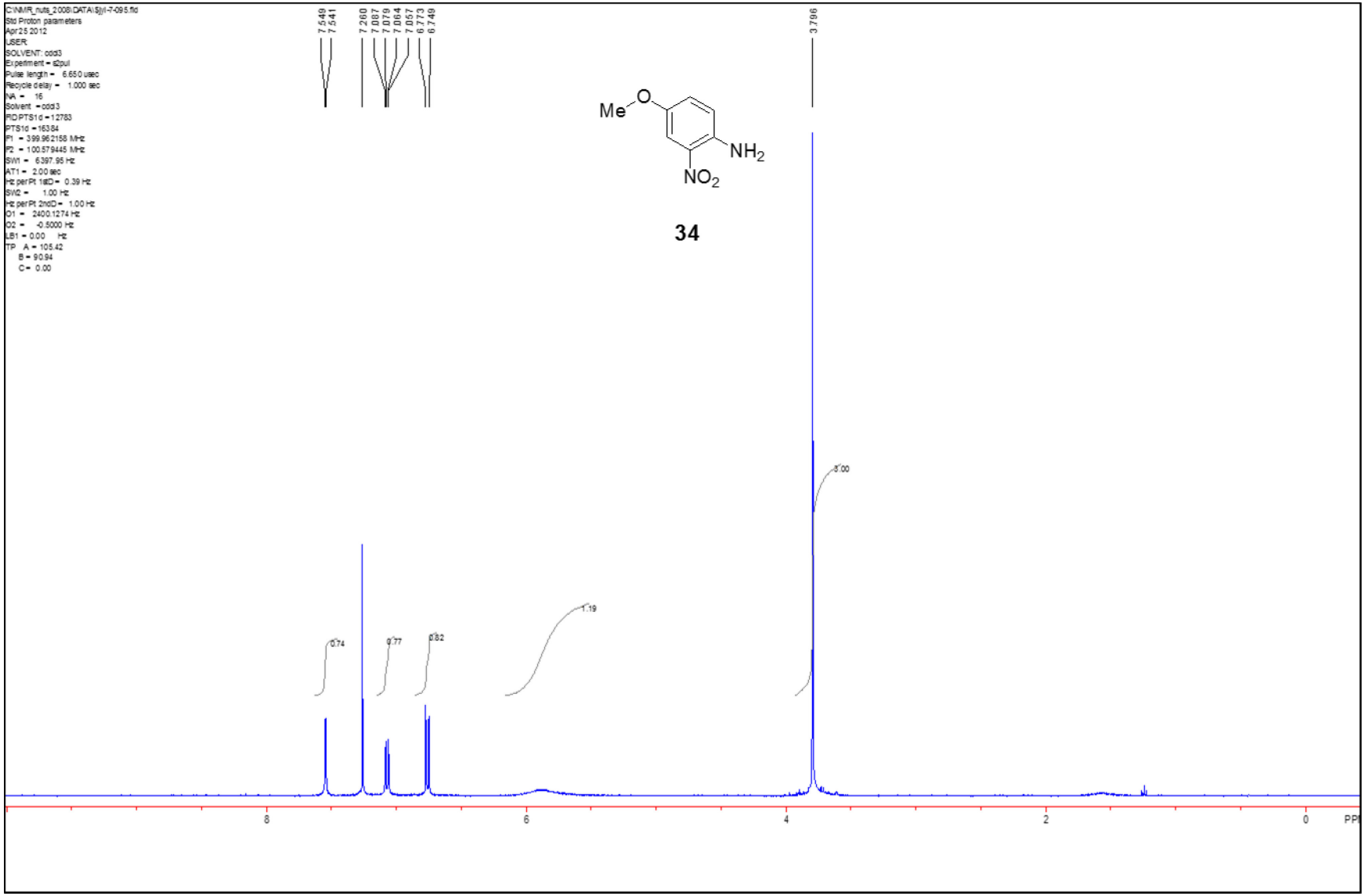
7.549
7.541
7.260
7.087
7.079
7.064
7.057
6.773
6.749
3.796
Me
O
NH2
NO2
34
0.74
0.77
0.82
1.19
3.00
8
6
4
2
0
PPM

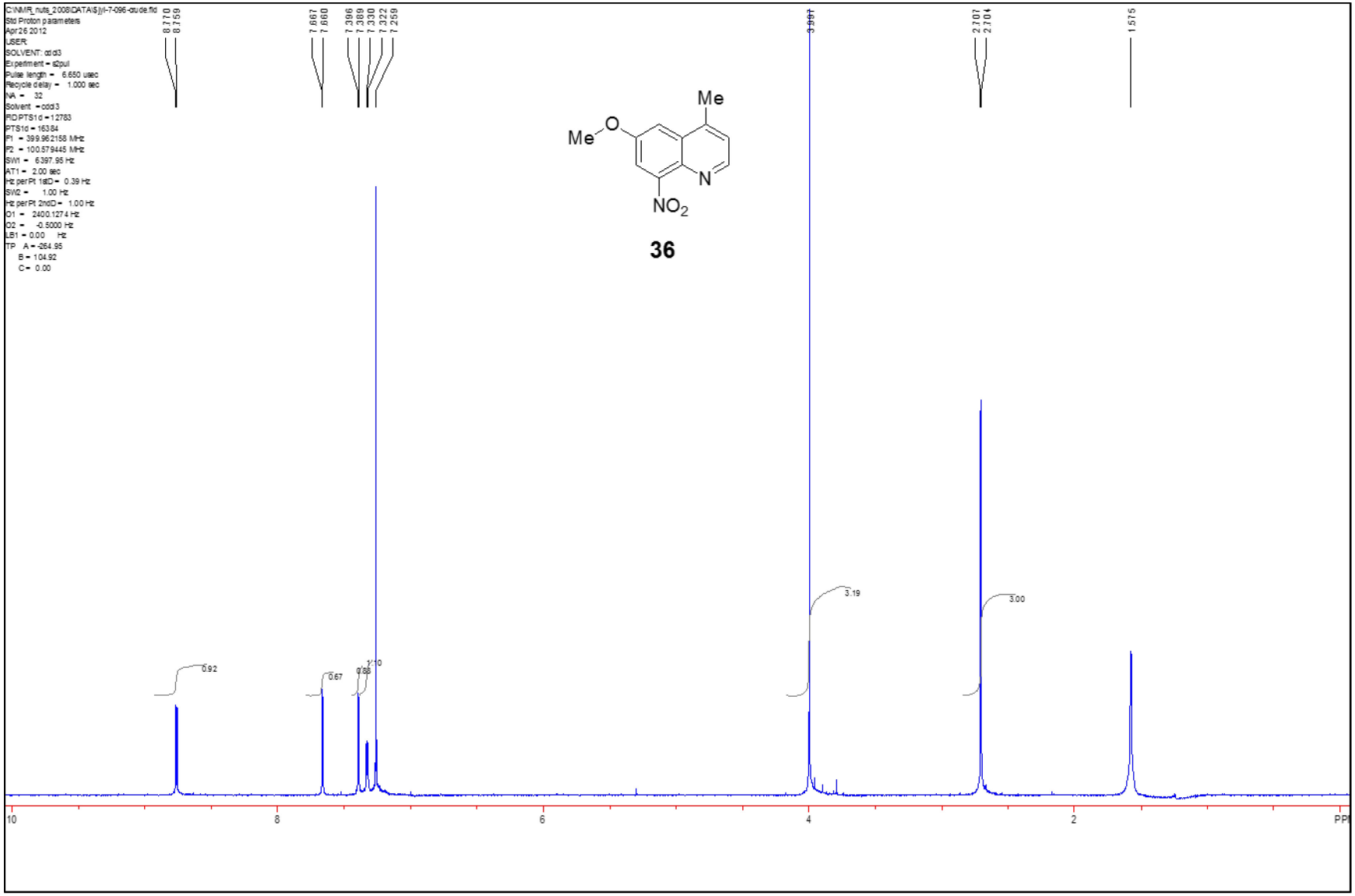
Me
O
Me
N
NO2
36
8.770
8.759
7.667
7.660
7.396
7.389
7.330
7.322
7.259
3.997
2.707
2.704
1.575
0.92
0.67
0.66
1.10
3.19
3.00
10
8
6
4
2
PPM

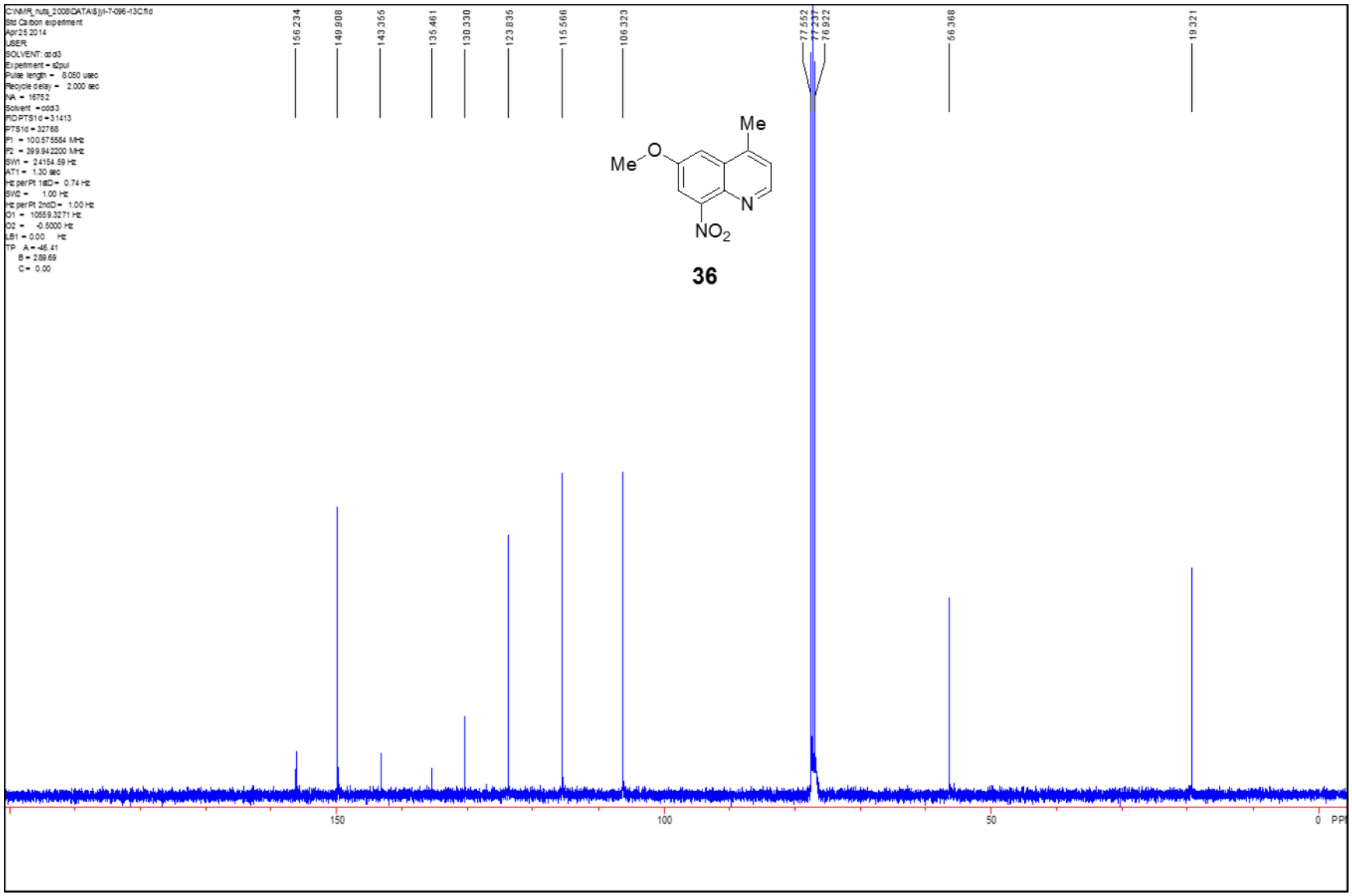
156.234
149.908
143.355
135.461
130.330
123.835
115.566
106.323
77.552
77.237
76.922
56.368
19.321
Me
O
Me
N
NO2
36
150
100
50
0 PPM

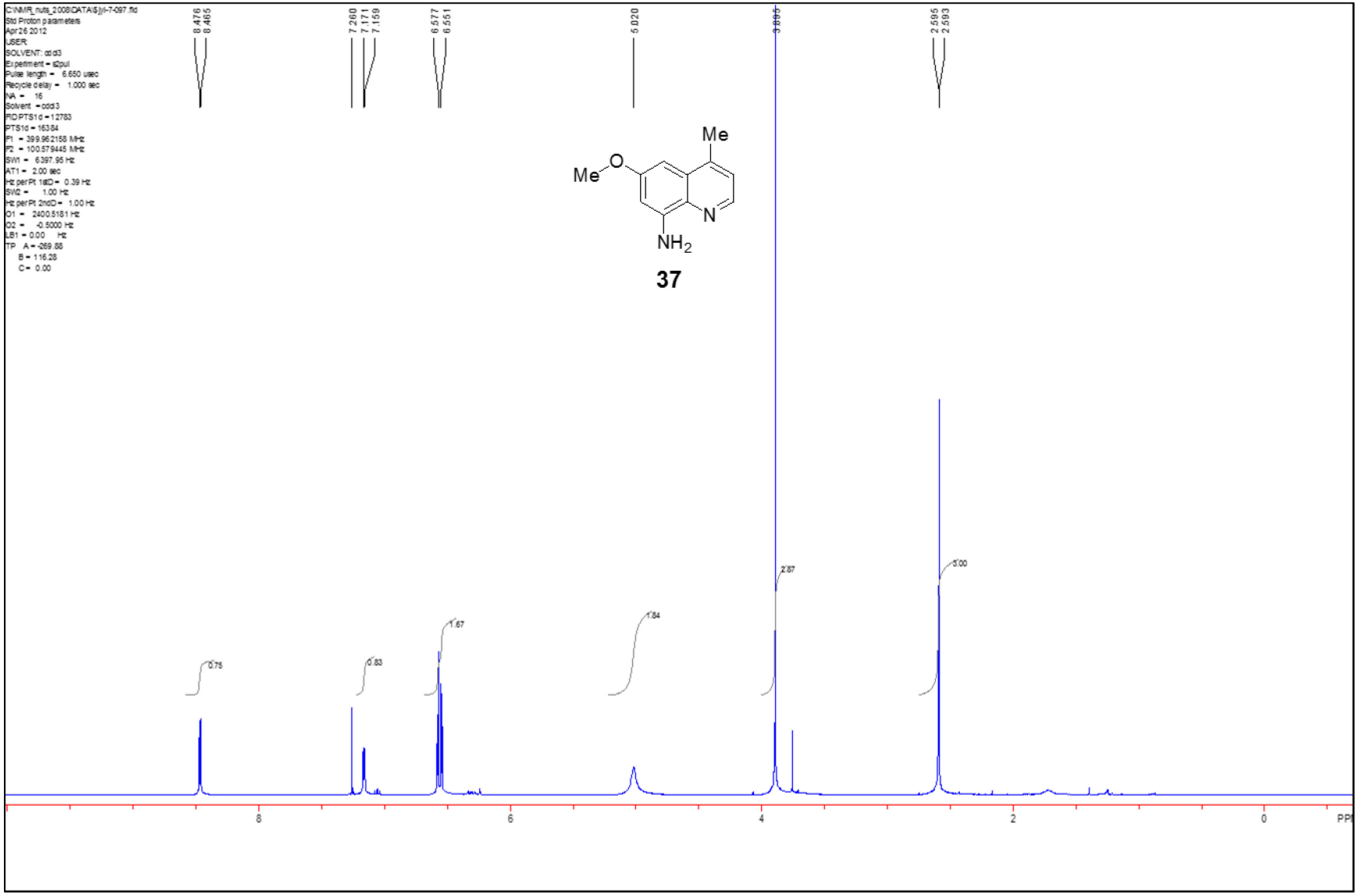
8.476
8.465
7.260
7.171
7.159
6.577
6.551
5.020
3.885
2.595
2.593
Me
Me
O
N
NH2
37
0.75
0.83
1.67
1.84
2.87
3.00
8
6
4
2
0
PPM

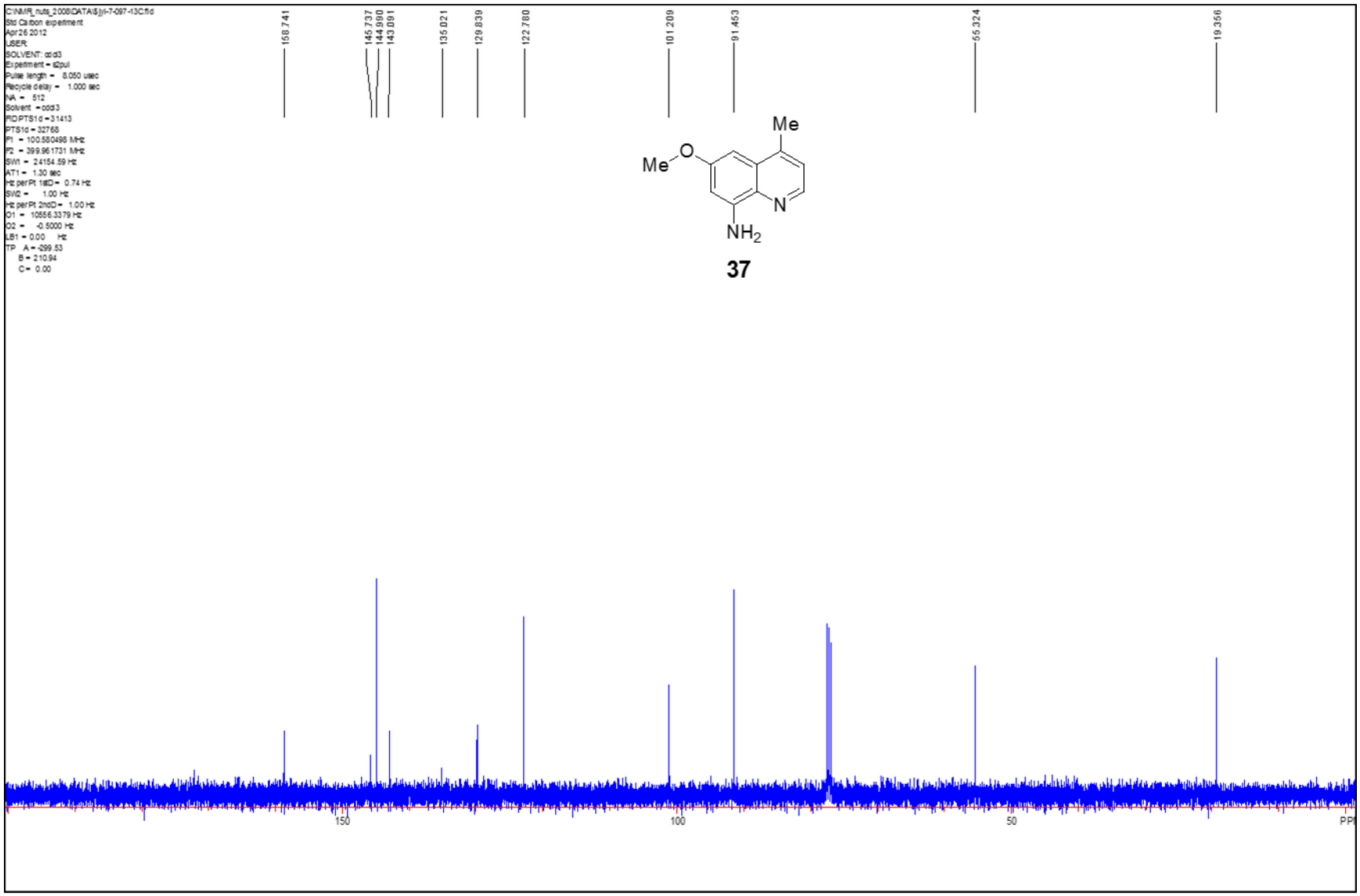
158.741
145.737
144.990
143.091
135.921
129.839
122.780
101.209
91.453
55.324
19.356
Me
Me
O
N
NH2
37
150
100
50

Compound 47 IR

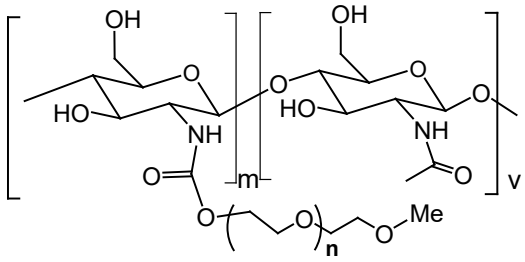

47

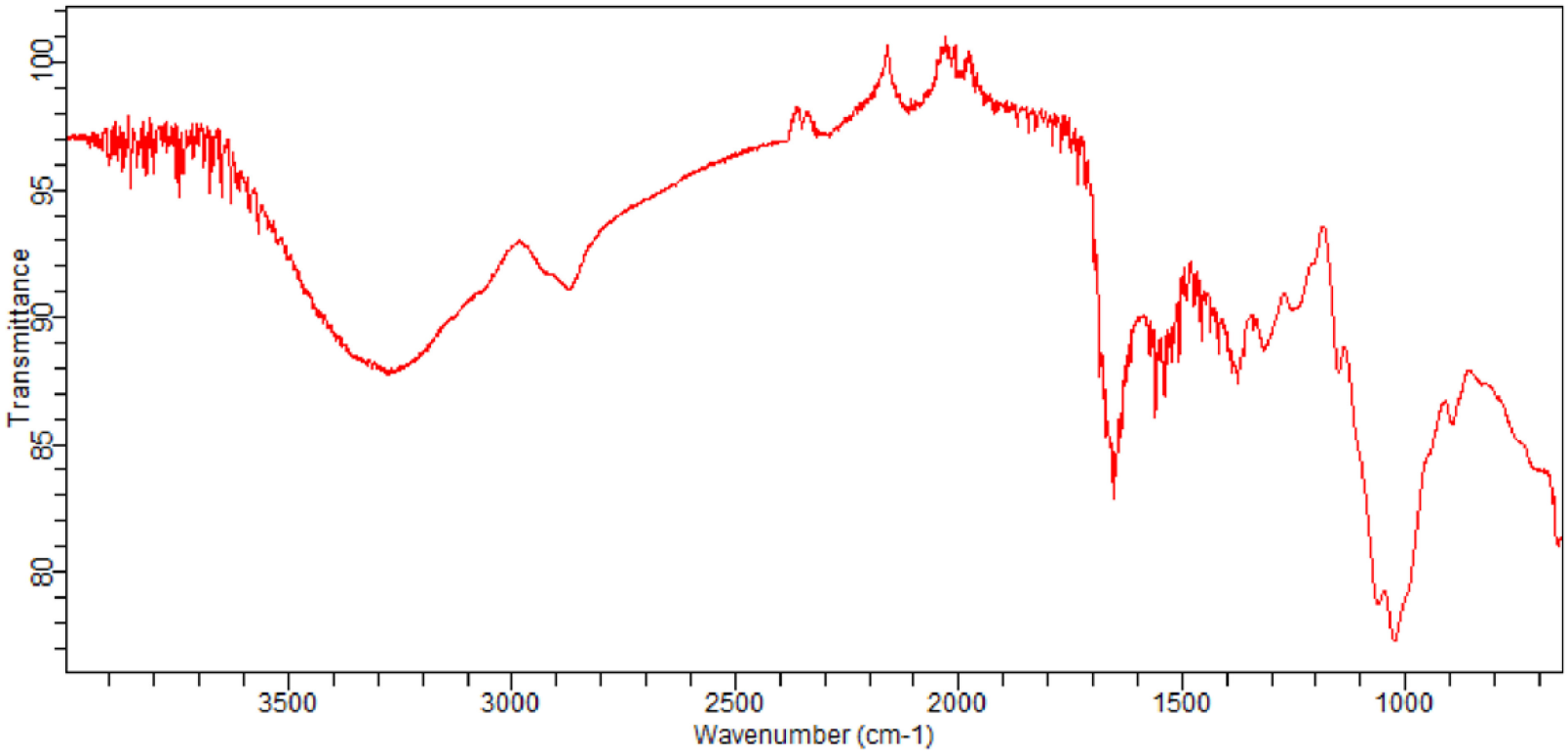

sw-9-86dp

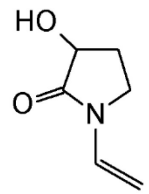
HO
O
N

49

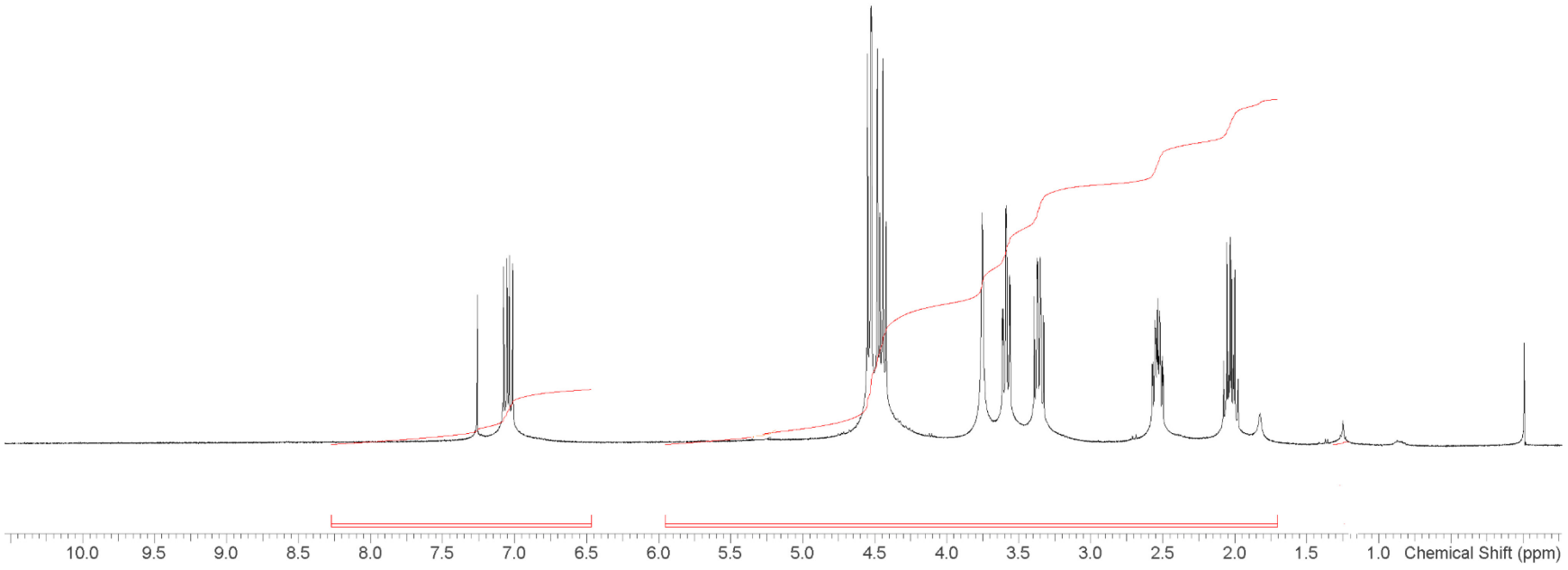
10.0
9.5
9.0
8.5
8.0
7.5
7.0
6.5
6.0
5.5
5.0
4.5
4.0
3.5
3.0
2.5
2.0
1.5
1.0
Chemical Shift (ppm)

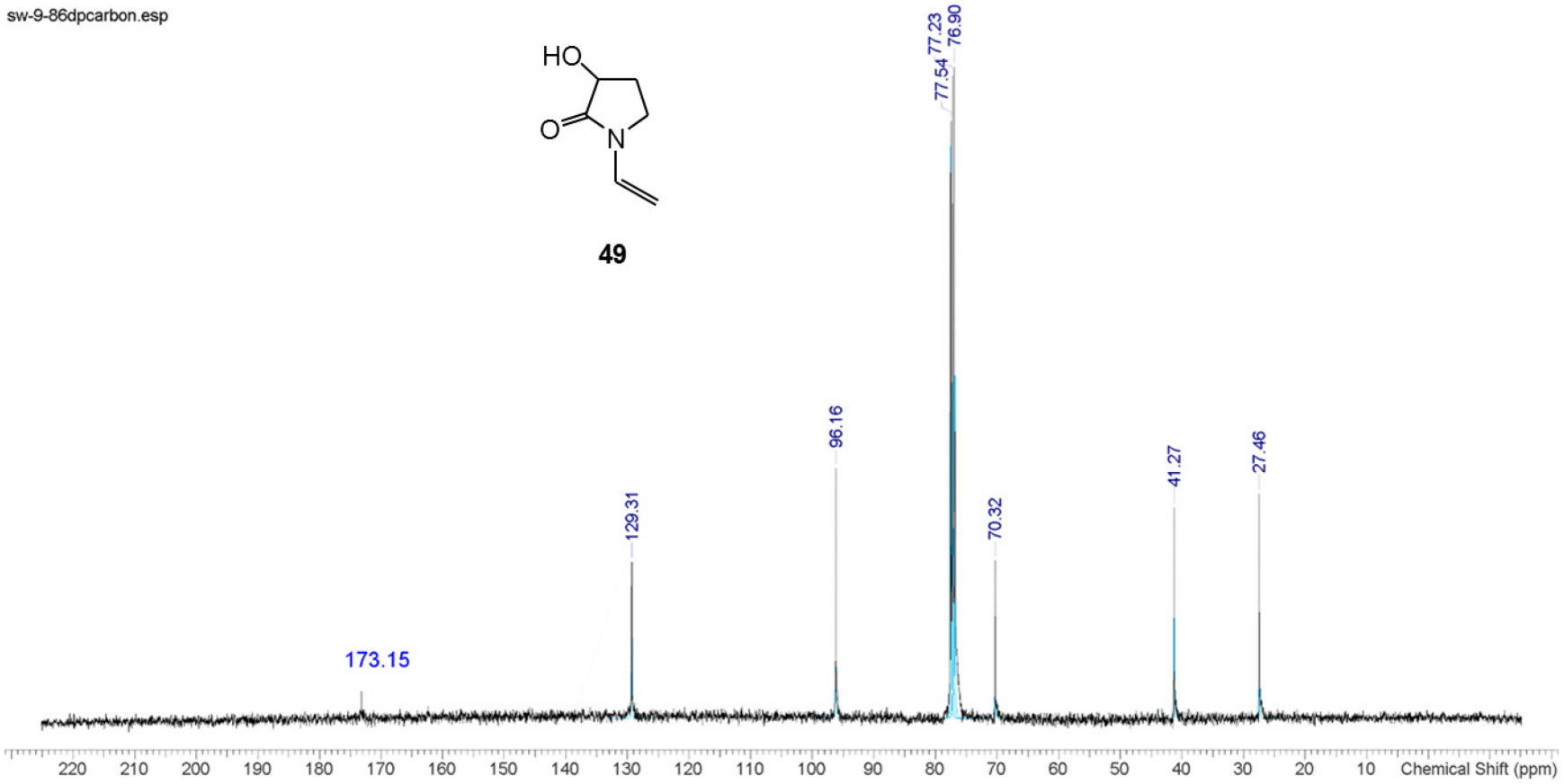
sw-9-86dpcarbon.esp
HO
O
N
49
77.23
76.90
77.54
96.16
129.31
70.32
41.27
27.46
173.15
220 210 200 190 180 170 160 150 140 130 120 110 100 90 80 70 60 50 40 30 20 10 Chemical Shift (ppm)

sw-10-14frac6.esp

50

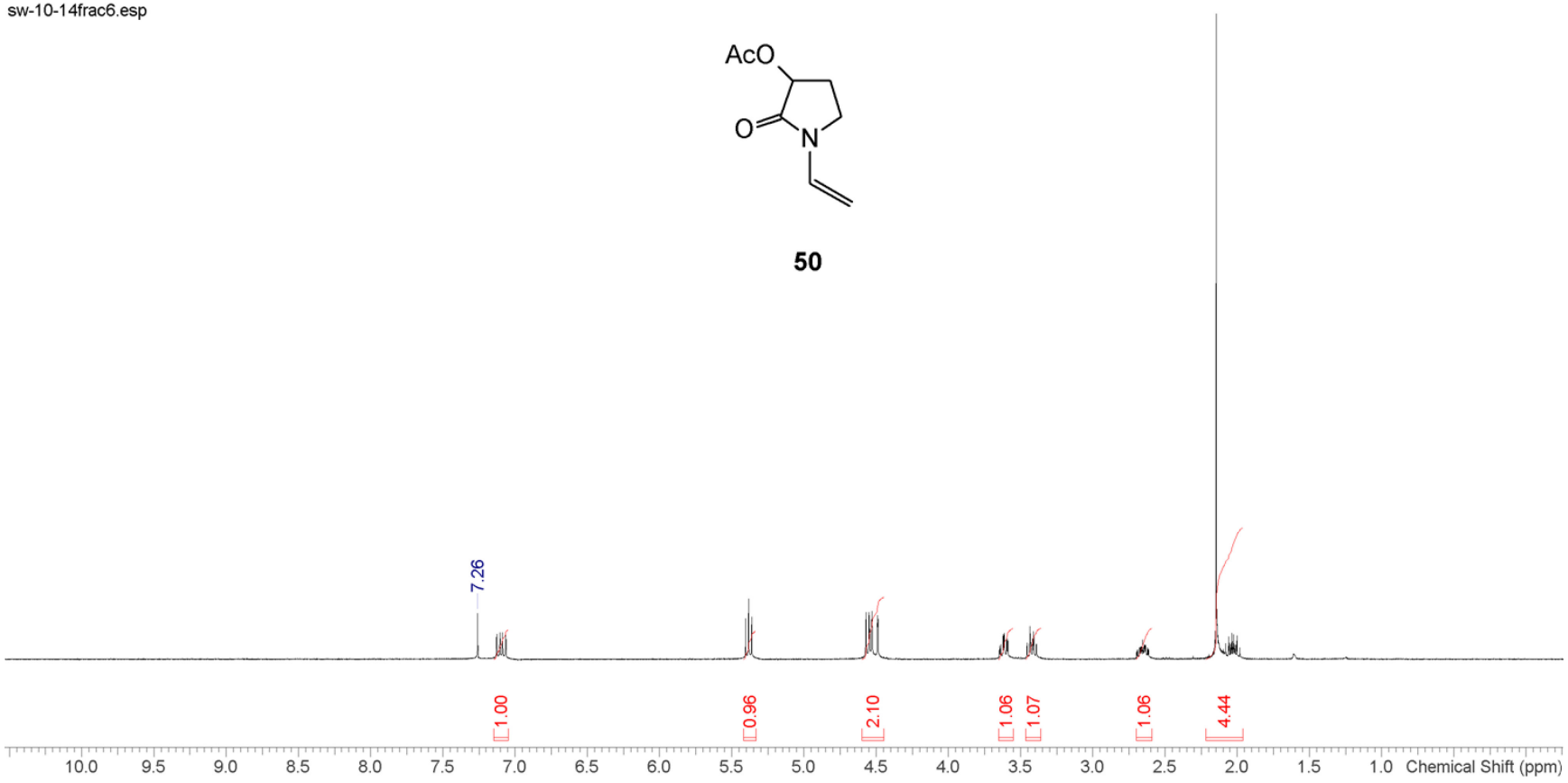

sw-9-120-reaction2-crude

51

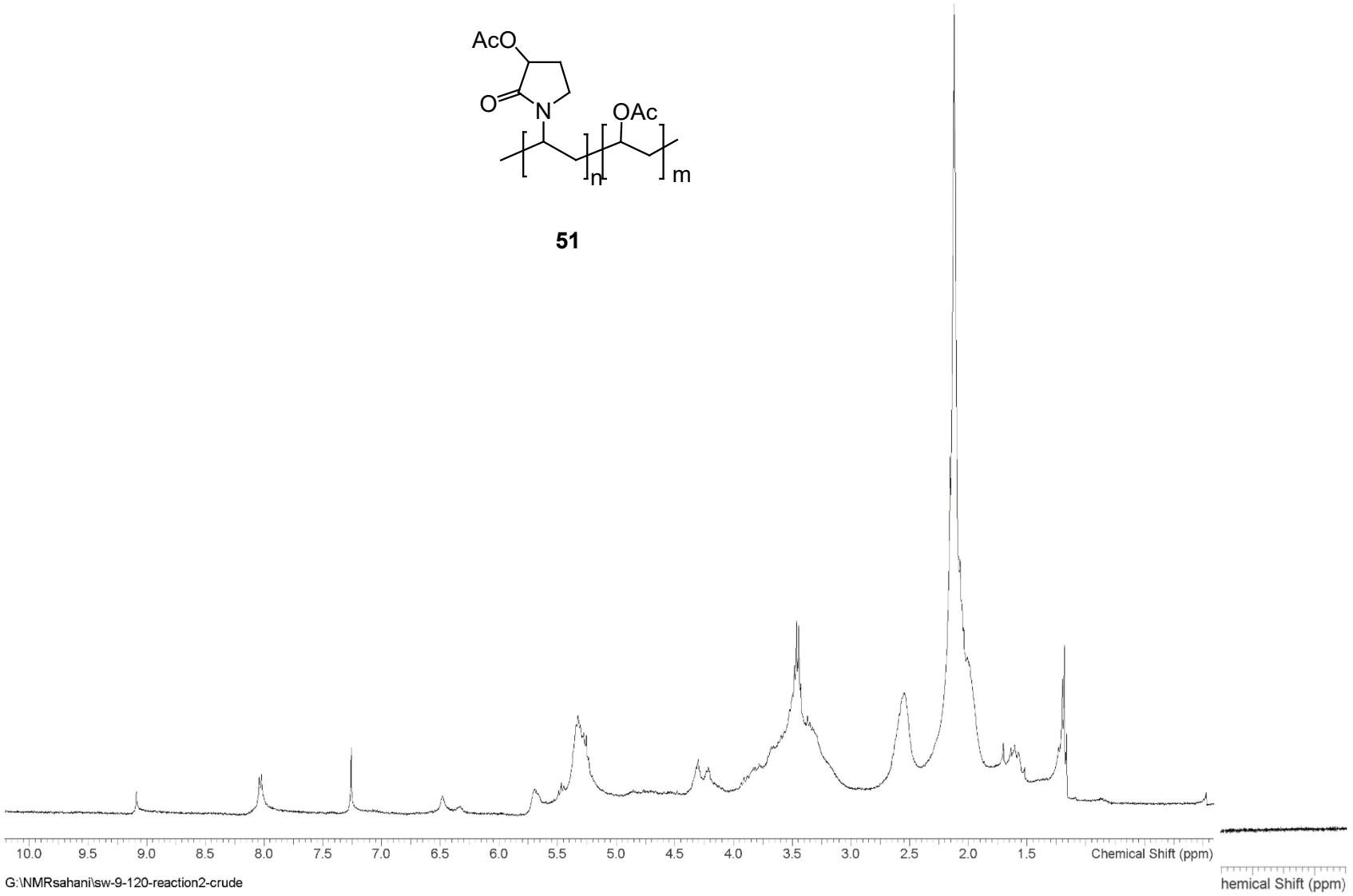

sw-10-15crude.esp

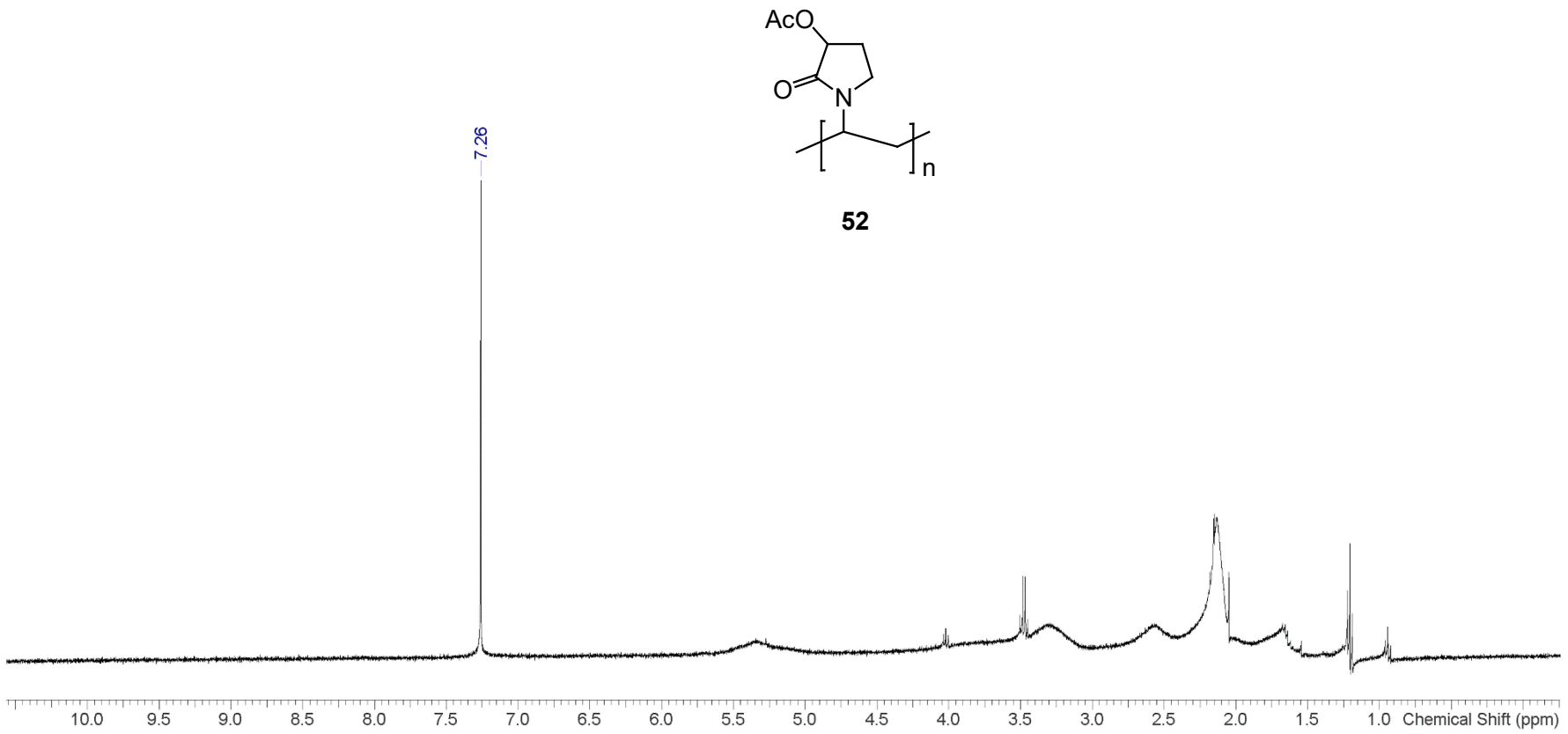

52

Compound 52 IR

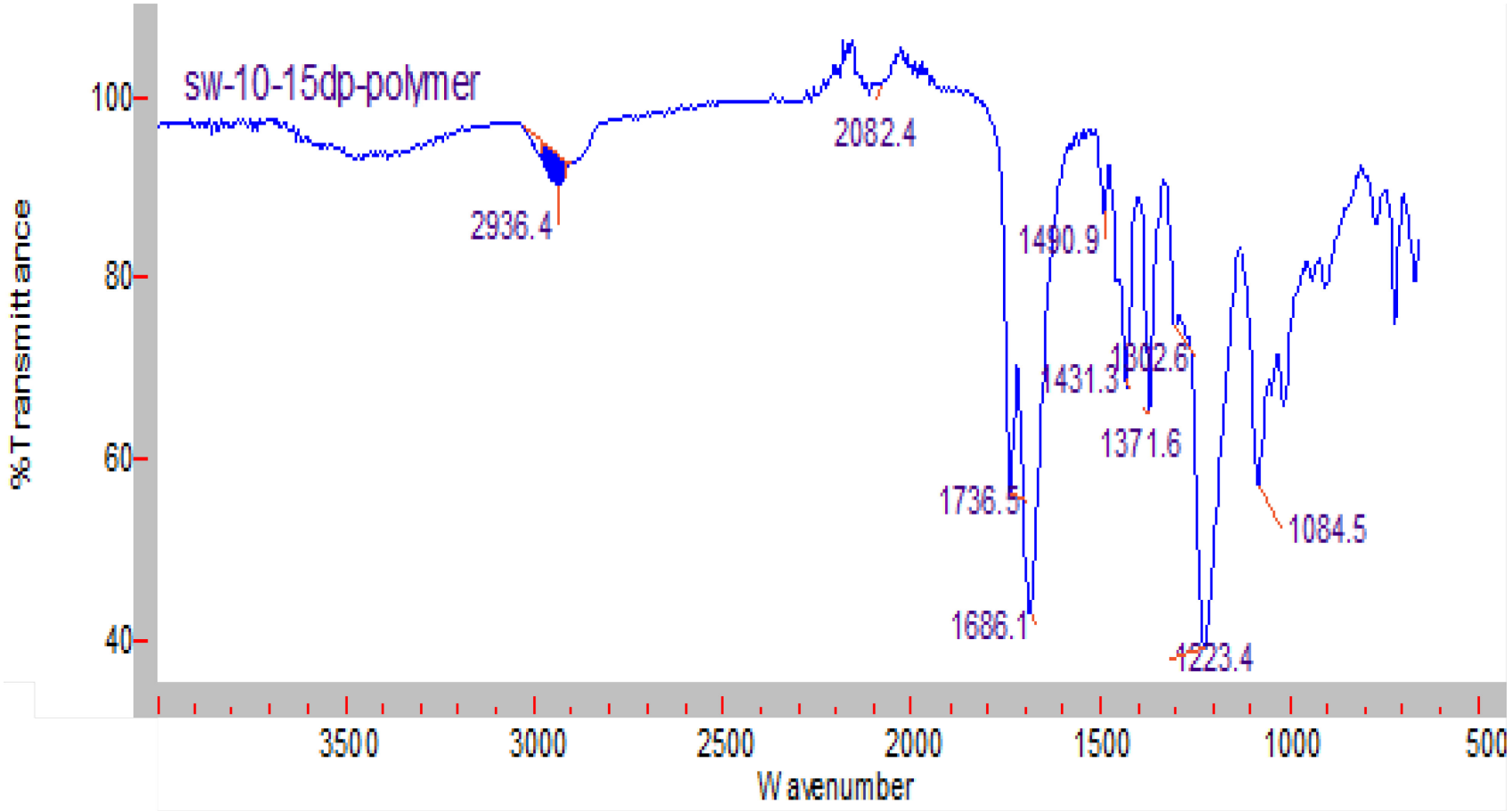

Compound 53 IR

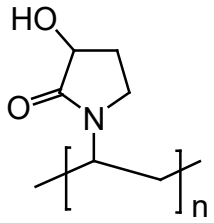

53

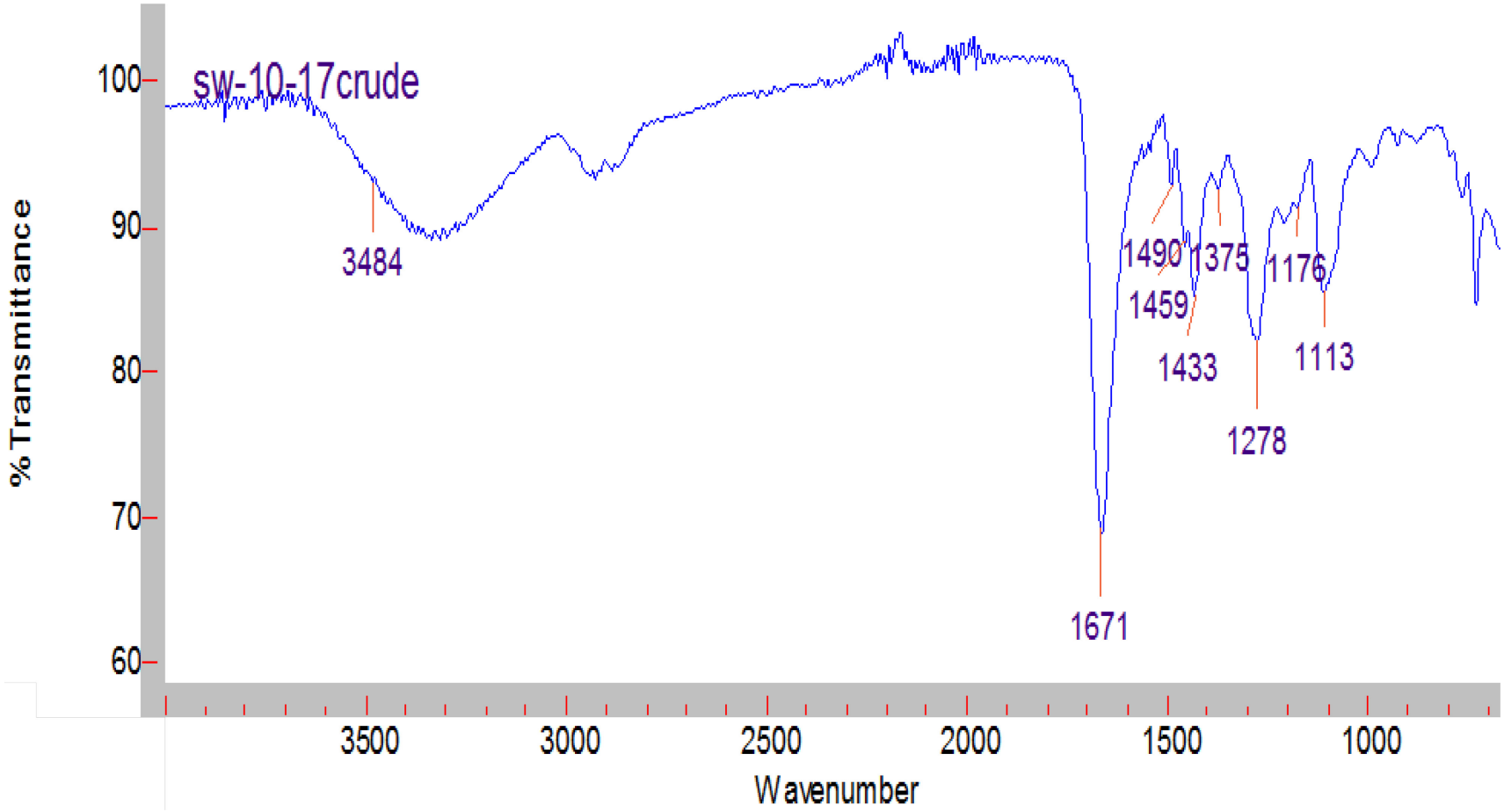

Deacetylated depolymerized chitosan (DADP-CS)

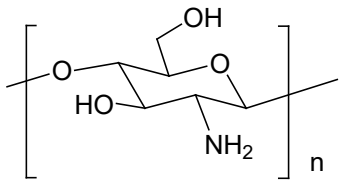

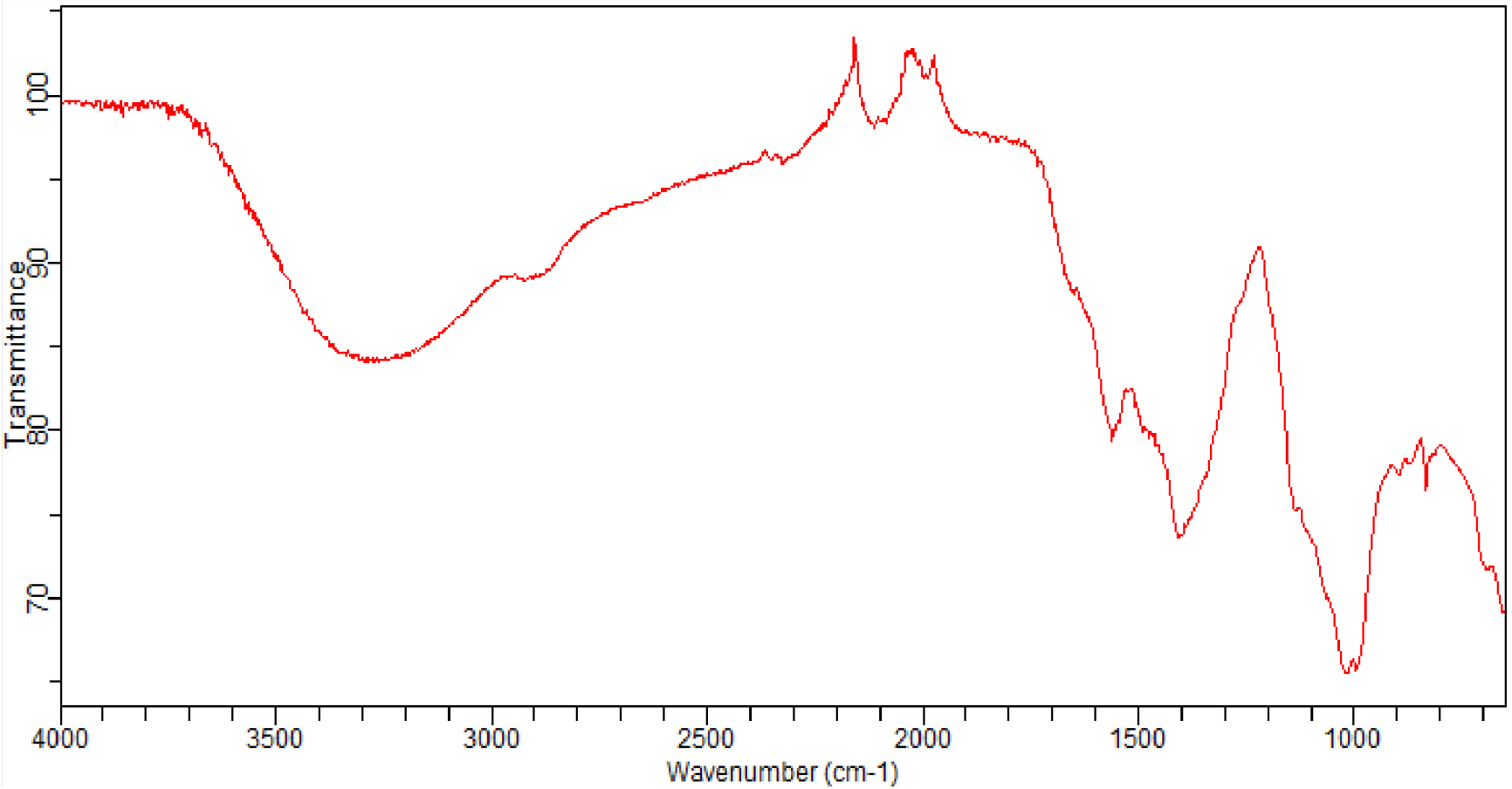

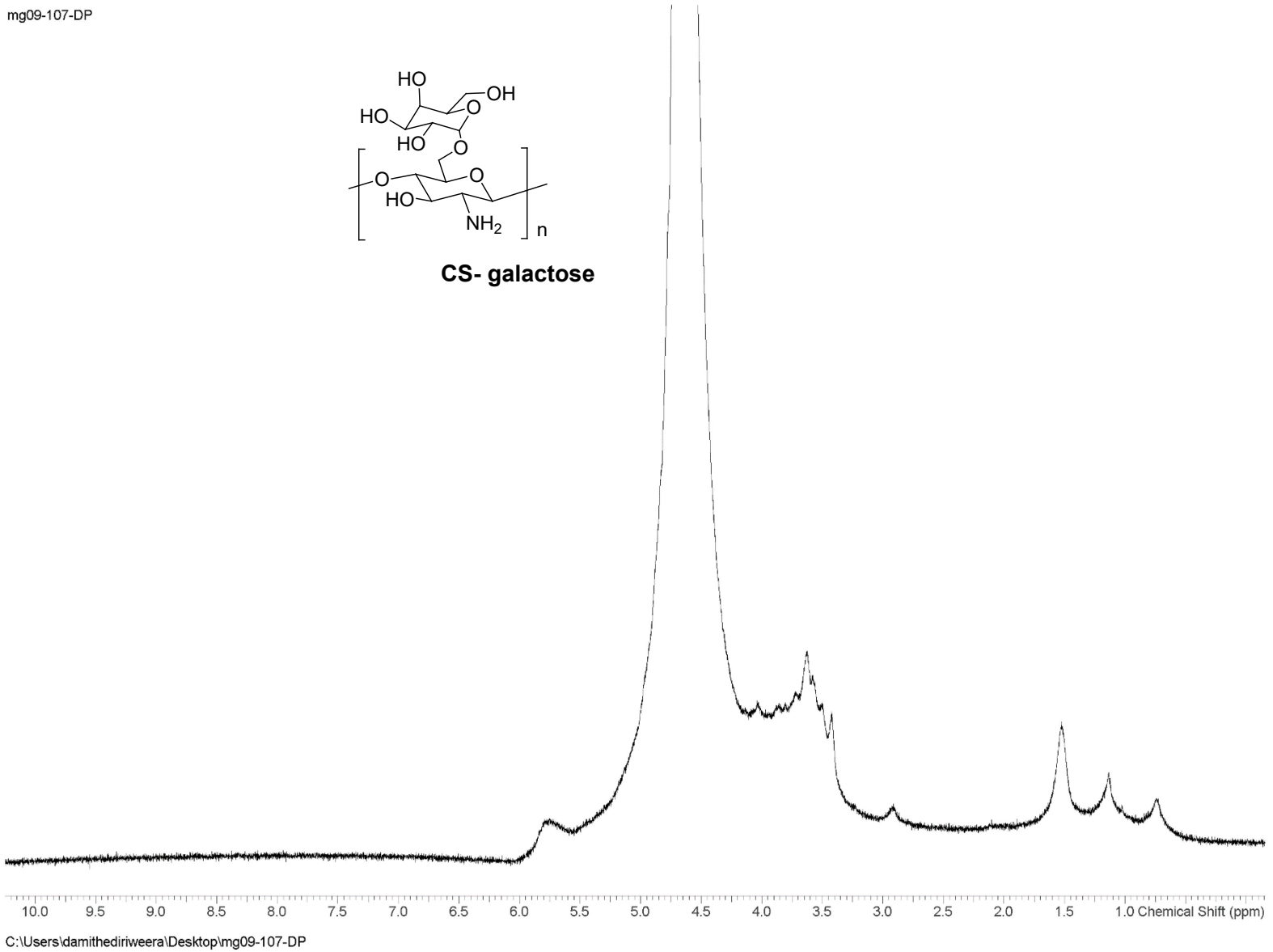
mg09-107-DP
HO
OH
HO
O
HO
O
O
O
HO
NH2
n
CS- galactose
10.0 9.5 9.0 8.5 8.0 7.5 7.0 6.5 6.0 5.5 5.0 4.5 4.0 3.5 3.0 2.5 2.0 1.5 1.0 Chemical Shift (ppm)
C:\Users\damithediriweera\Desktop\mg09-107-DP

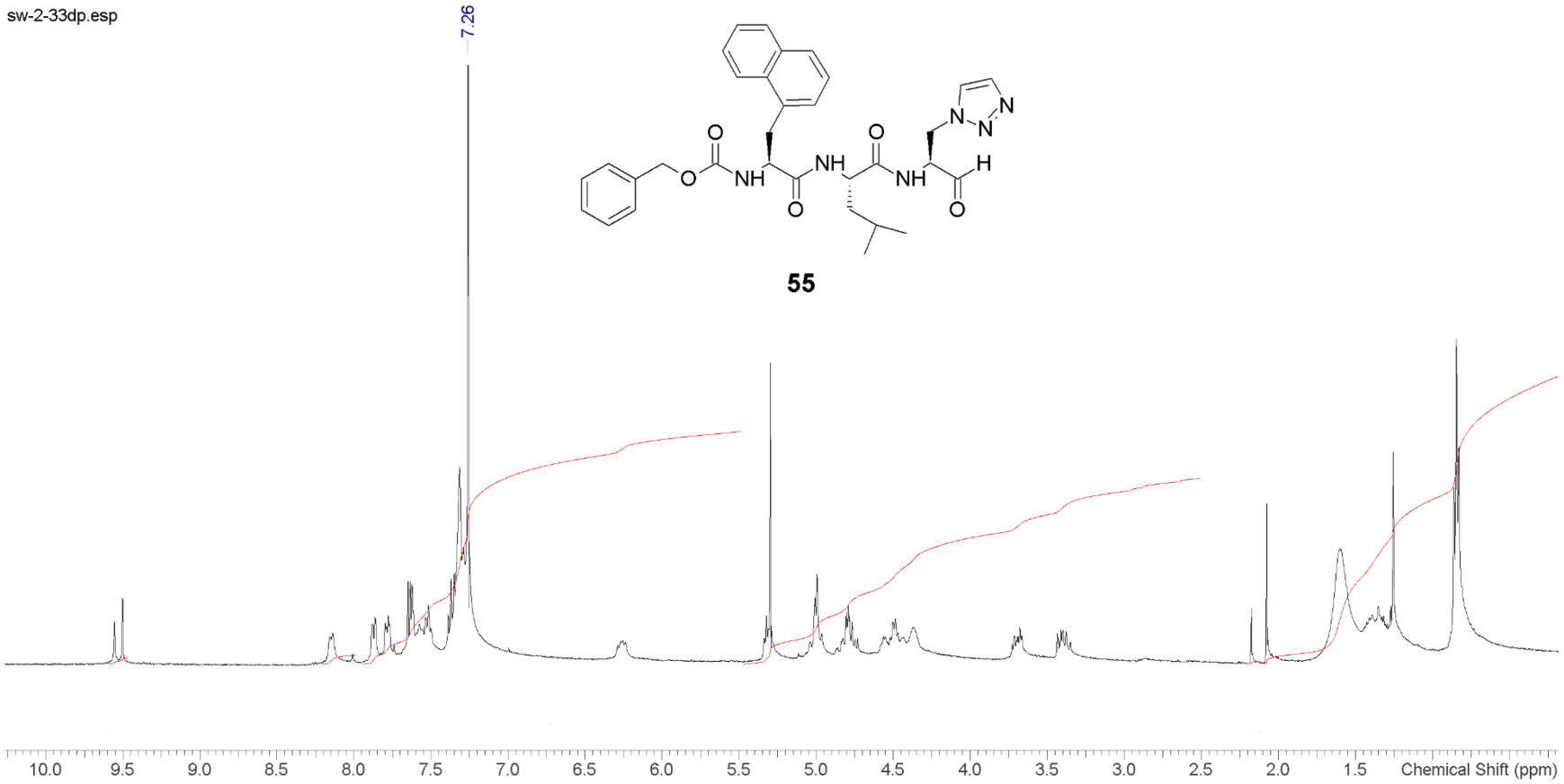
sw-2-33dp.esp
7.26
O
O
NH
O
NH
O
NH
H
O
N
N
N
55
10.0
9.5
9.0
8.5
8.0
7.5
7.0
6.5
6.0
5.5
5.0
4.5
4.0
3.5
3.0
2.5
2.0
1.5
Chemical Shift (ppm)

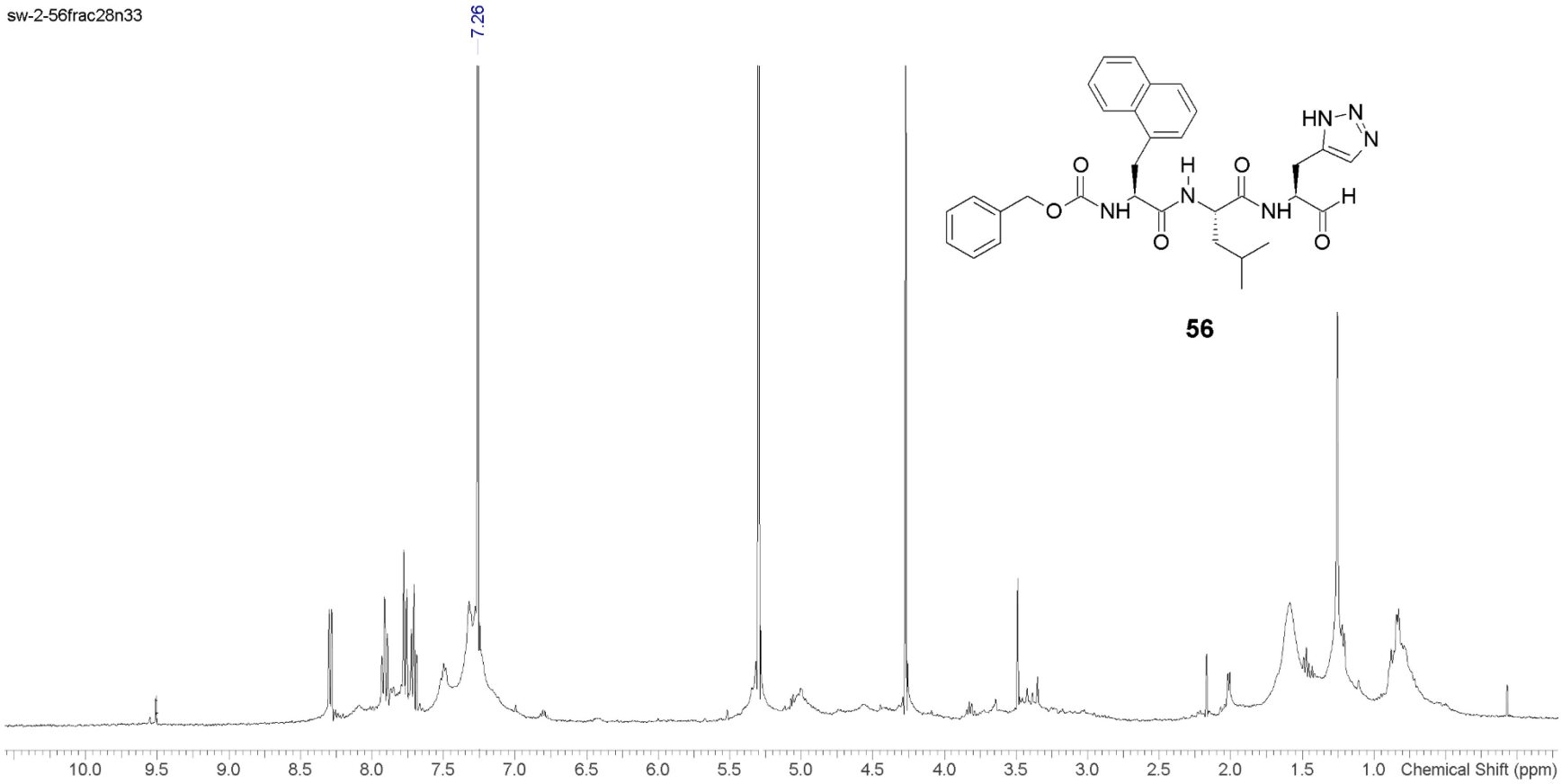
sw-2-56frac28n33
7.26
HN
N
N
O
O
H
O
O
NH
N
NH
H
O
O
56
10.0
9.5
9.0
8.5
8.0
7.5
7.0
6.5
6.0
5.5
5.0
4.5
4.0
3.5
3.0
2.5
2.0
1.5
1.0
Chemical Shift (ppm)

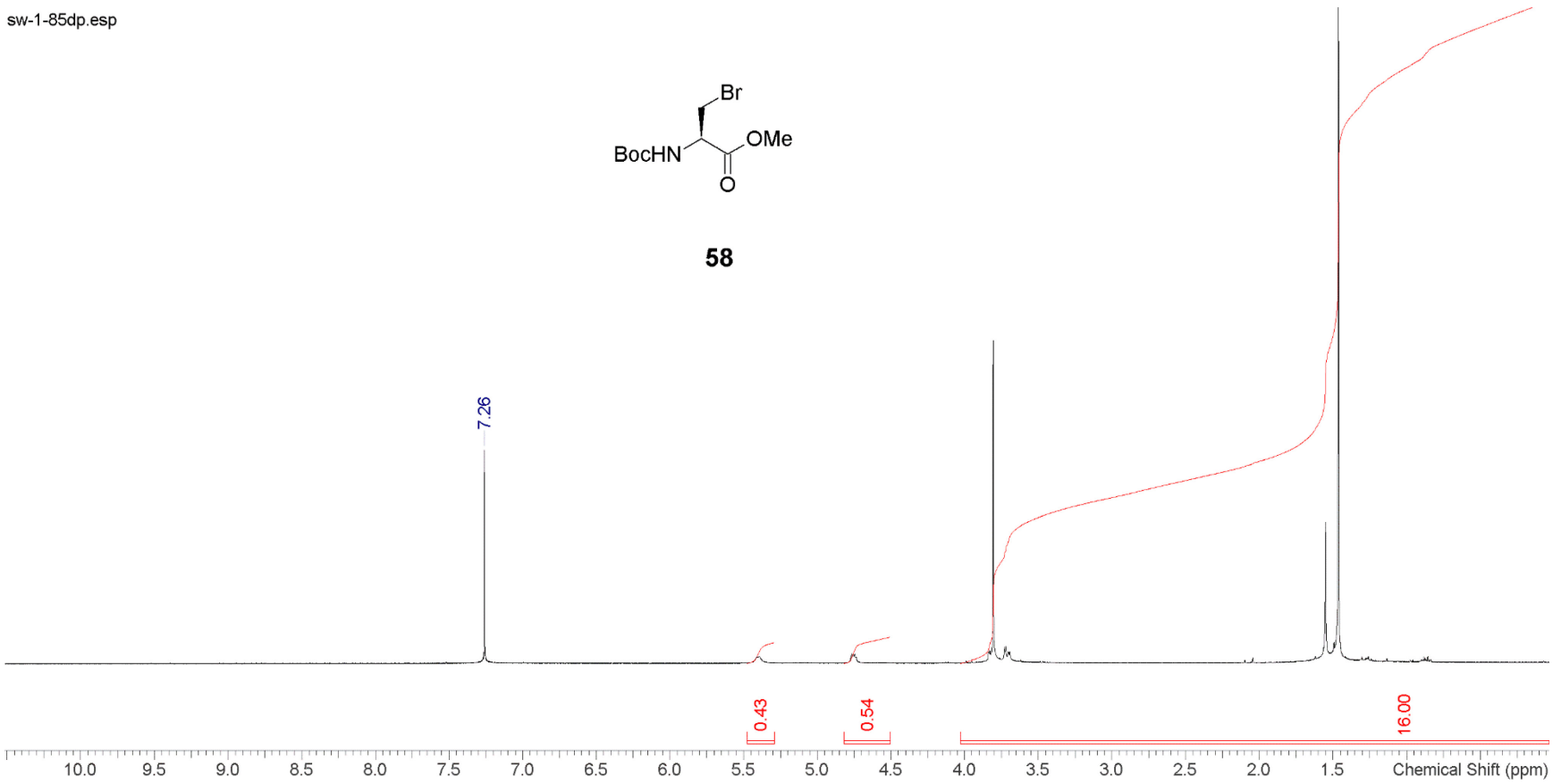
sw-1-85dp.esp
Br
BocHN
OMe
O
58
7.26
0.43
0.54
16.00
10.0
9.5
9.0
8.5
8.0
7.5
7.0
6.5
6.0
5.5
5.0
4.5
4.0
3.5
3.0
2.5
2.0
1.5
Chemical Shift (ppm)

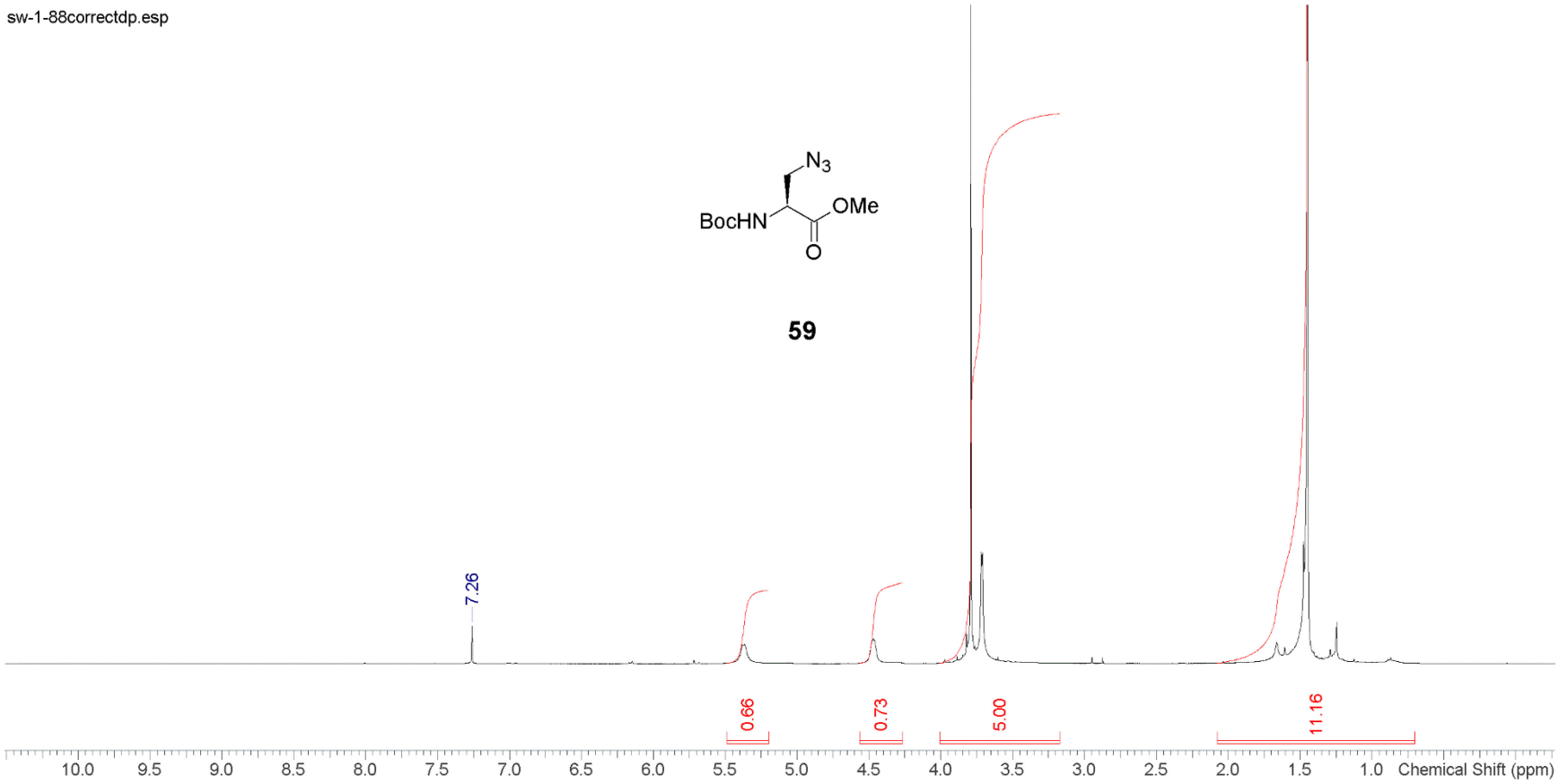
sw-1-88correctdp.esp
N3
BocHN
OMe
O
59
7.26
0.66
0.73
5.00
11.16
10.0
9.5
9.0
8.5
8.0
7.5
7.0
6.5
6.0
5.5
5.0
4.5
4.0
3.5
3.0
2.5
2.0
1.5
1.0
Chemical Shift (ppm)

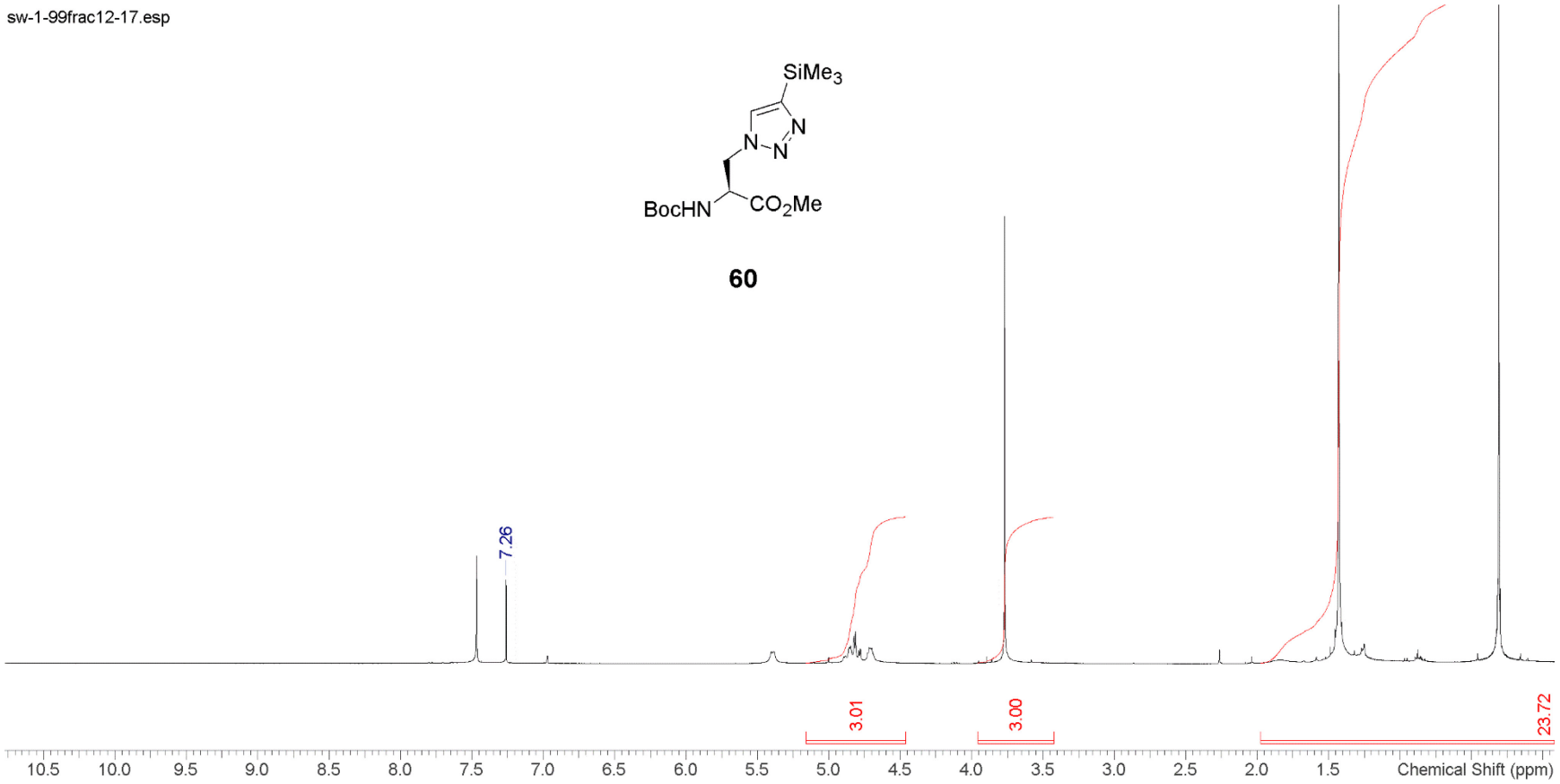
sw-1-99frac12-17.esp
SiMe3
N
N
N
BocHN
CO2Me
60
7.26
3.01
3.00
23.72
10.5
10.0
9.5
9.0
8.5
8.0
7.5
7.0
6.5
6.0
5.5
5.0
4.5
4.0
3.5
3.0
2.5
2.0
1.5
Chemical Shift (ppm)

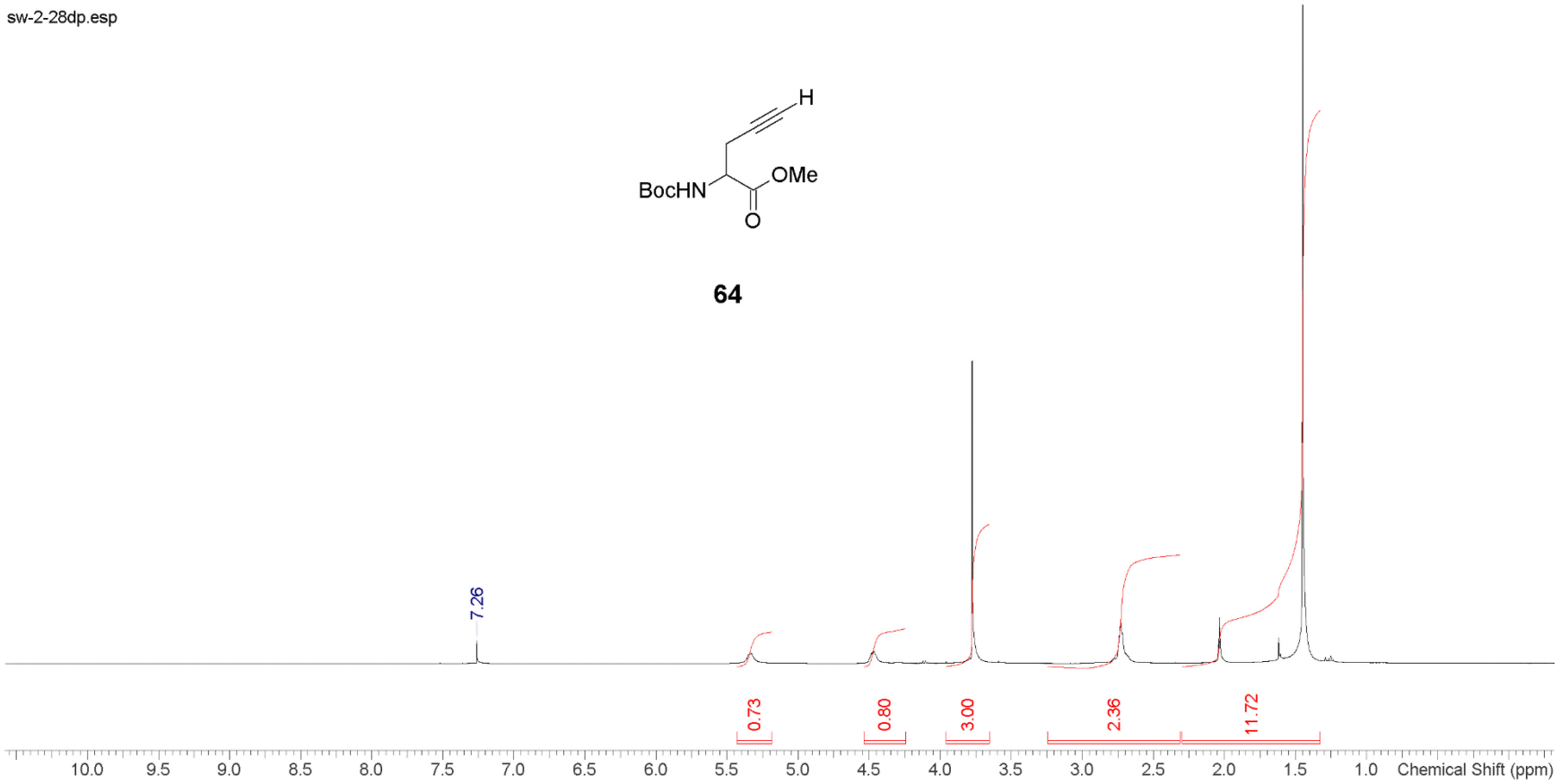
sw-2-28dp.esp
H
BocHN
OMe
O
64
7.26
0.73
0.80
3.00
2.36
11.72
10.0
9.5
9.0
8.5
8.0
7.5
7.0
6.5
6.0
5.5
5.0
4.5
4.0
3.5
3.0
2.5
2.0
1.5
1.0
Chemical Shift (ppm)

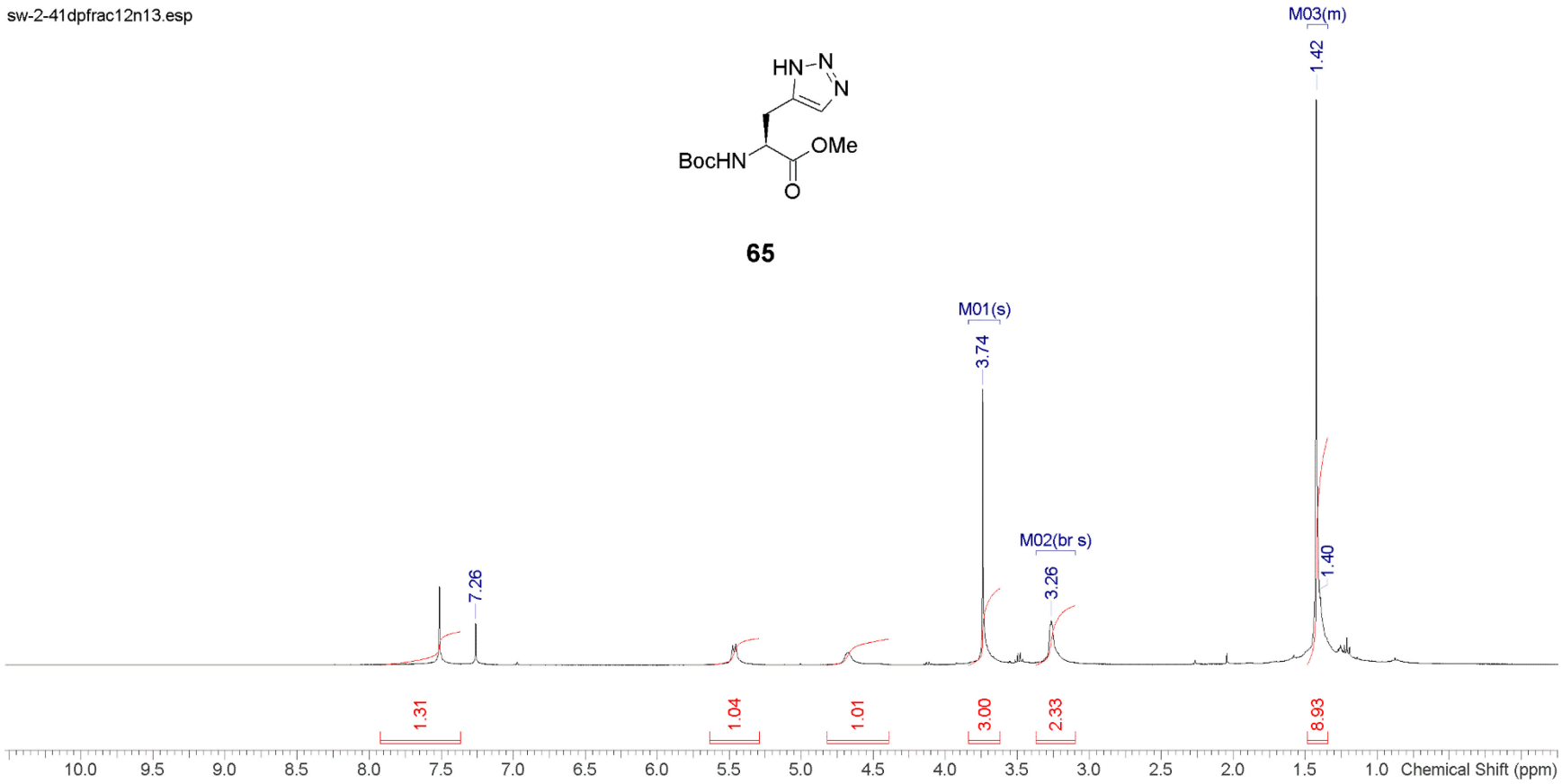
sw-2-41dpfrac12n13.esp
HN
N
N
BocHN
OMe
O
65
M03(m)
1.42
M01(s)
3.74
M02(br s)
3.26
7.26
1.40
1.31
1.04
1.01
3.00
2.33
8.93
10.0
9.5
9.0
8.5
8.0
7.5
7.0
6.5
6.0
5.5
5.0
4.5
4.0
3.5
3.0
2.5
2.0
1.5
1.0
Chemical Shift (ppm)

sw-2-41RepeatDP

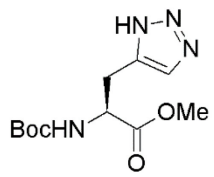

65

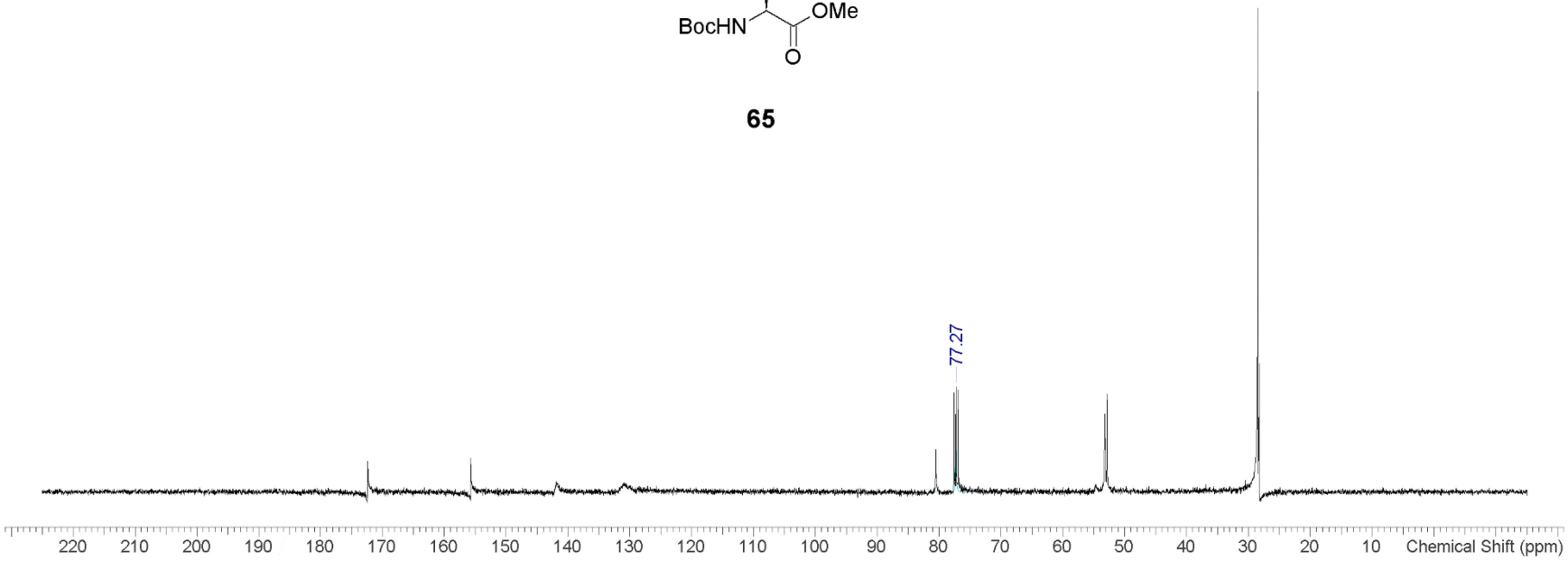

sw-1-112dp.esp

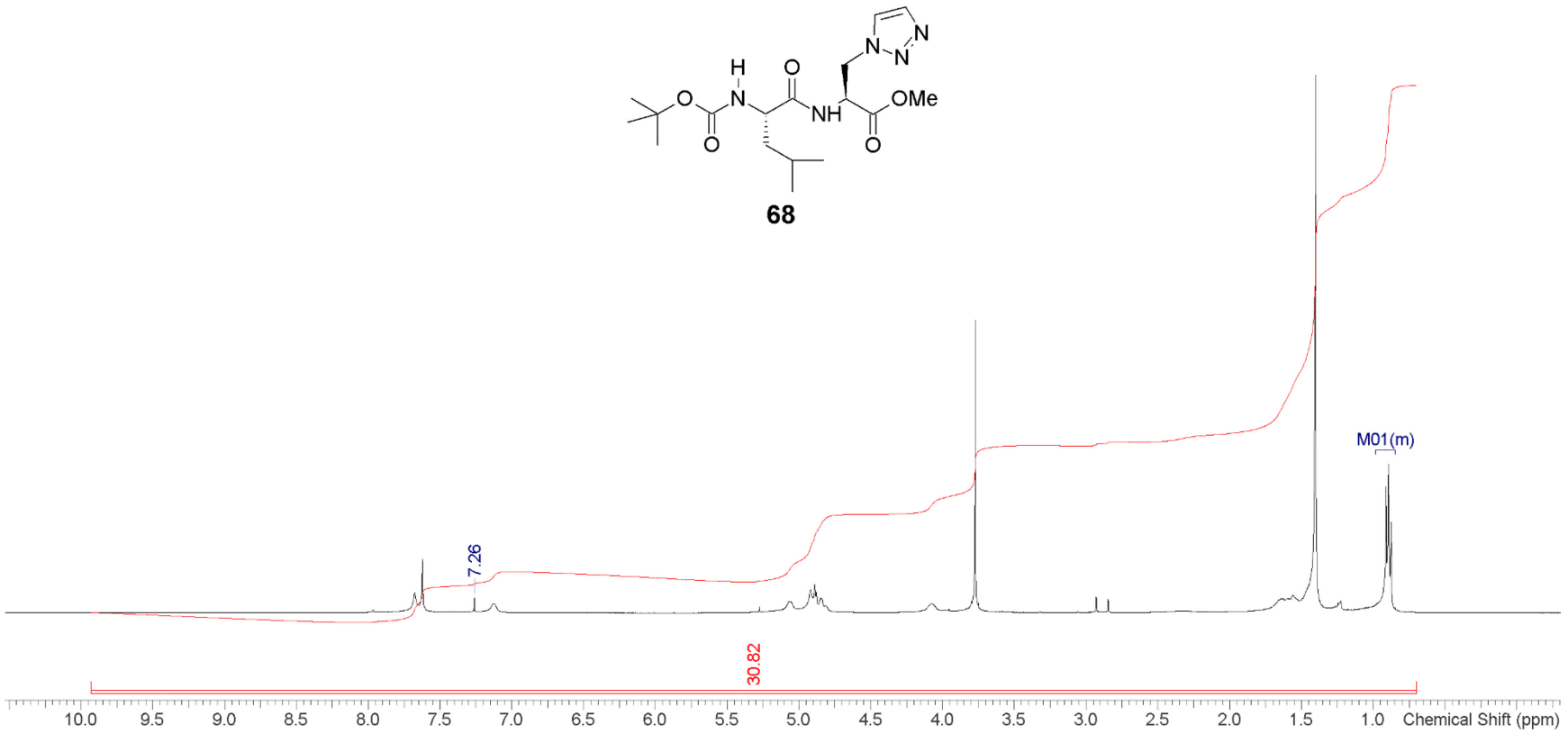

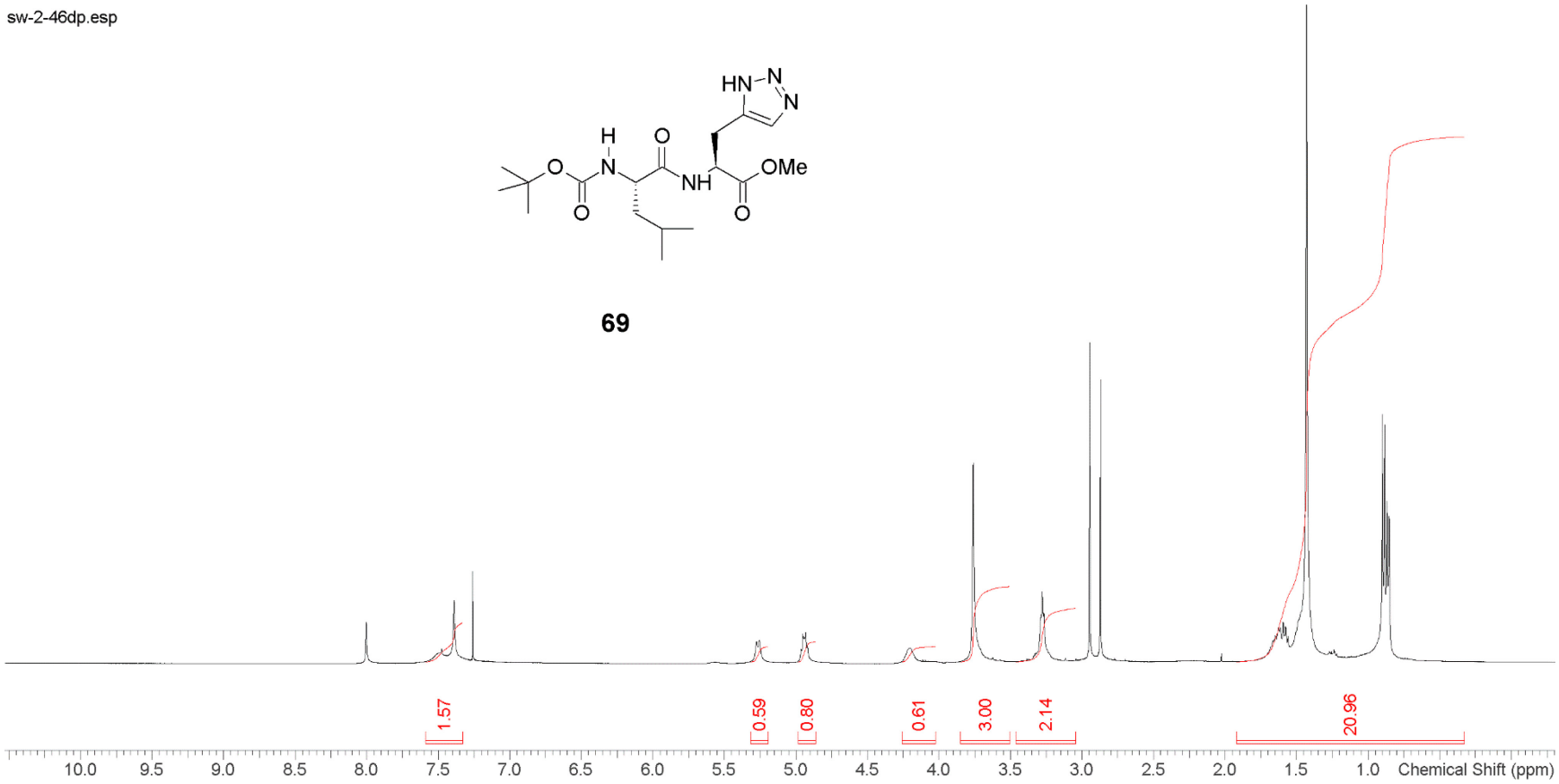
sw-2-46dp.esp
HN
N
N
H
O
N
O
O
NH
OMe
O
69
1.57
0.59
0.80
0.61
3.00
2.14
20.96
10.0
9.5
9.0
8.5
8.0
7.5
7.0
6.5
6.0
5.5
5.0
4.5
4.0
3.5
3.0
2.5
2.0
1.5
1.0
Chemical Shift (ppm)

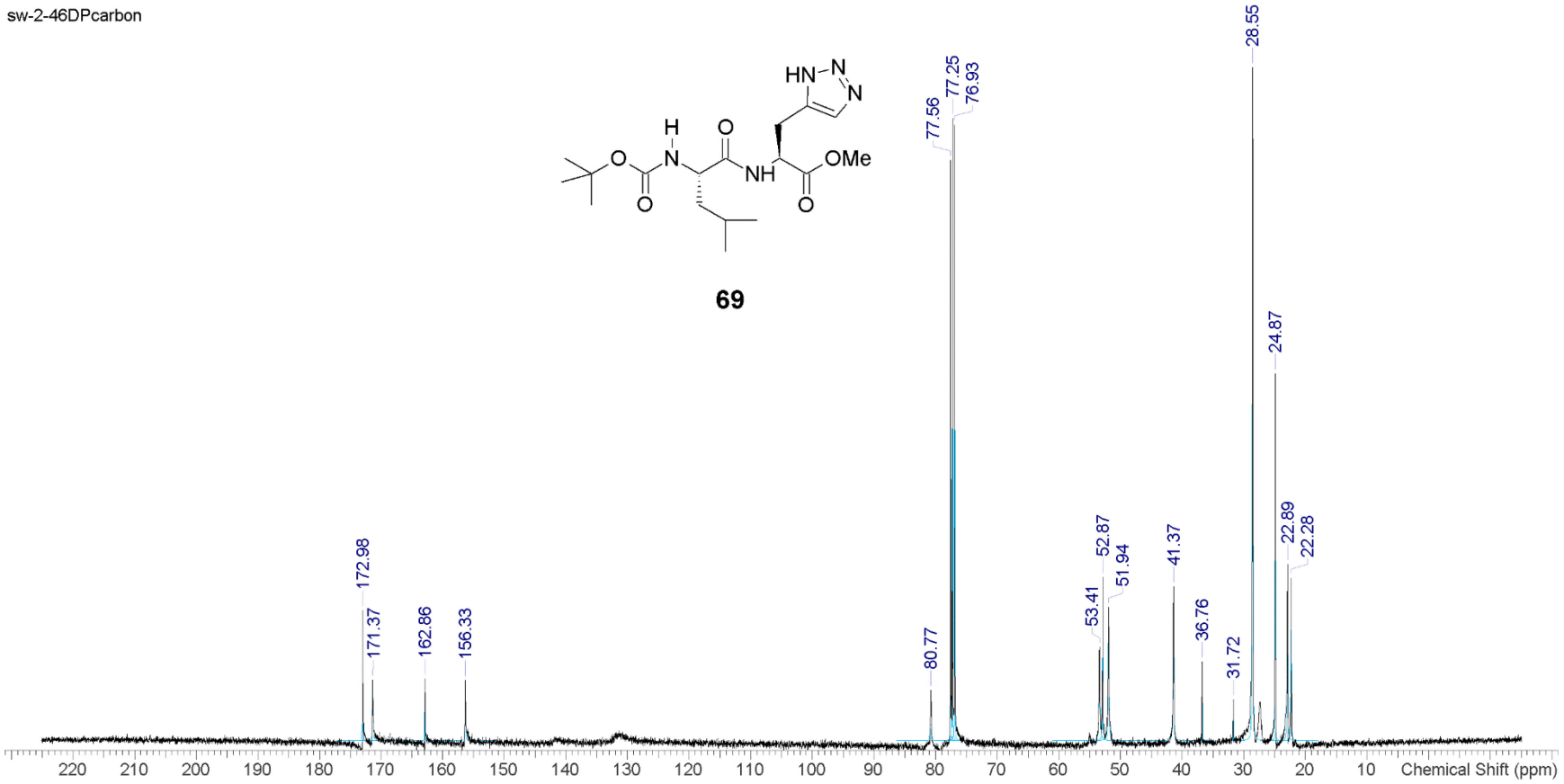
sw-2-46DPcarbon
HN
N
N
H
N
O
O
NH
OMe
O
O
69
172.98
171.37
162.86
156.33
80.77
77.56
77.25
76.93
53.41
52.87
51.94
41.37
36.76
31.72
28.55
24.87
22.89
22.28
220 210 200 190 180 170 160 150 140 130 120 110 100 90 80 70 60 50 40 30 20 10 Chemical Shift (ppm)

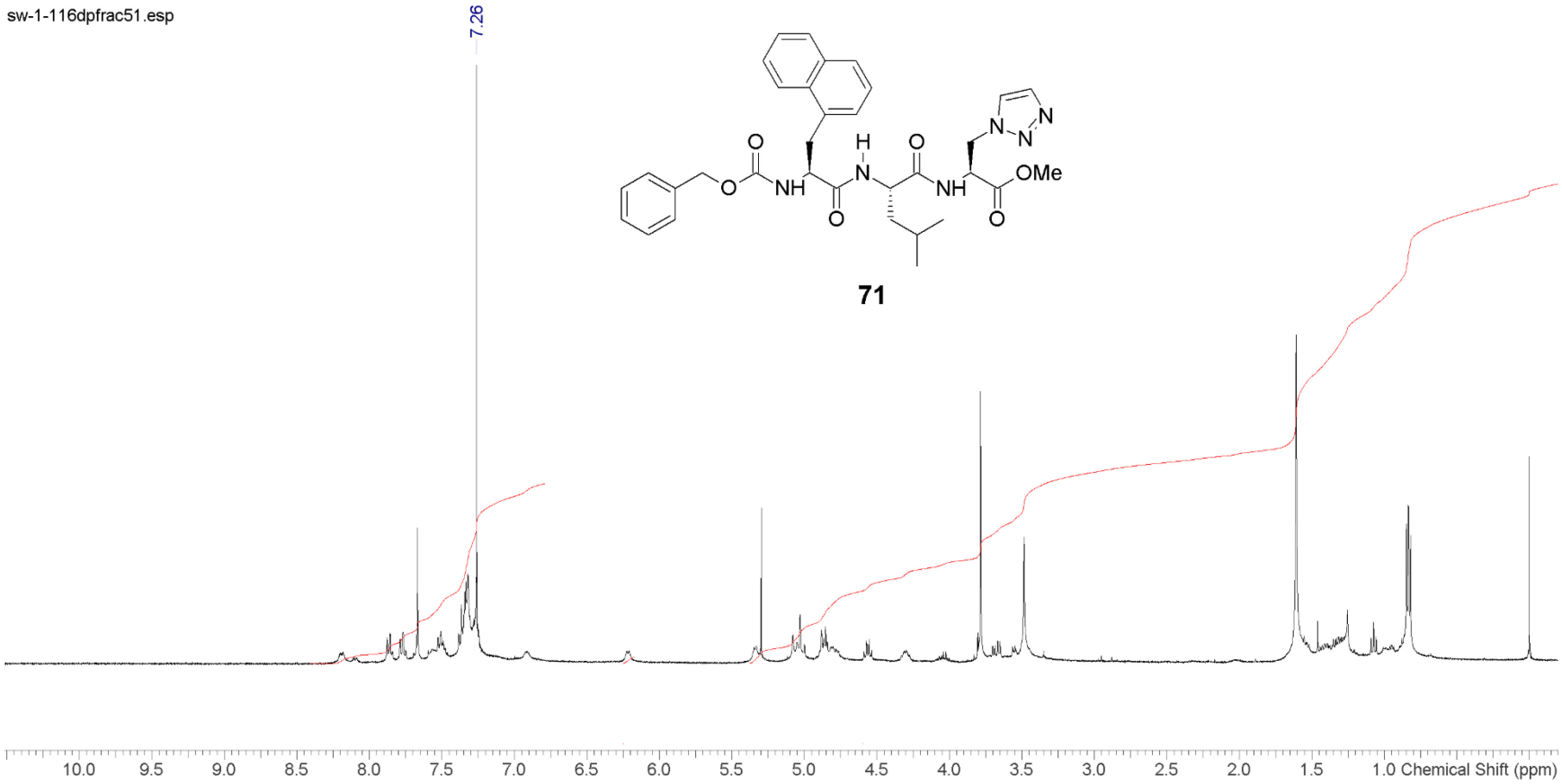
sw-1-116dpfrac51.esp
7.26
O
O
NH
H
N
O
O
NH
N
N
N
OMe
O
10.0
9.5
9.0
8.5
8.0
7.5
7.0
6.5
6.0
5.5
5.0
4.5
4.0
3.5
3.0
2.5
2.0
1.5
1.0 Chemical Shift (ppm)

71

sw-2-50dp.esp

72

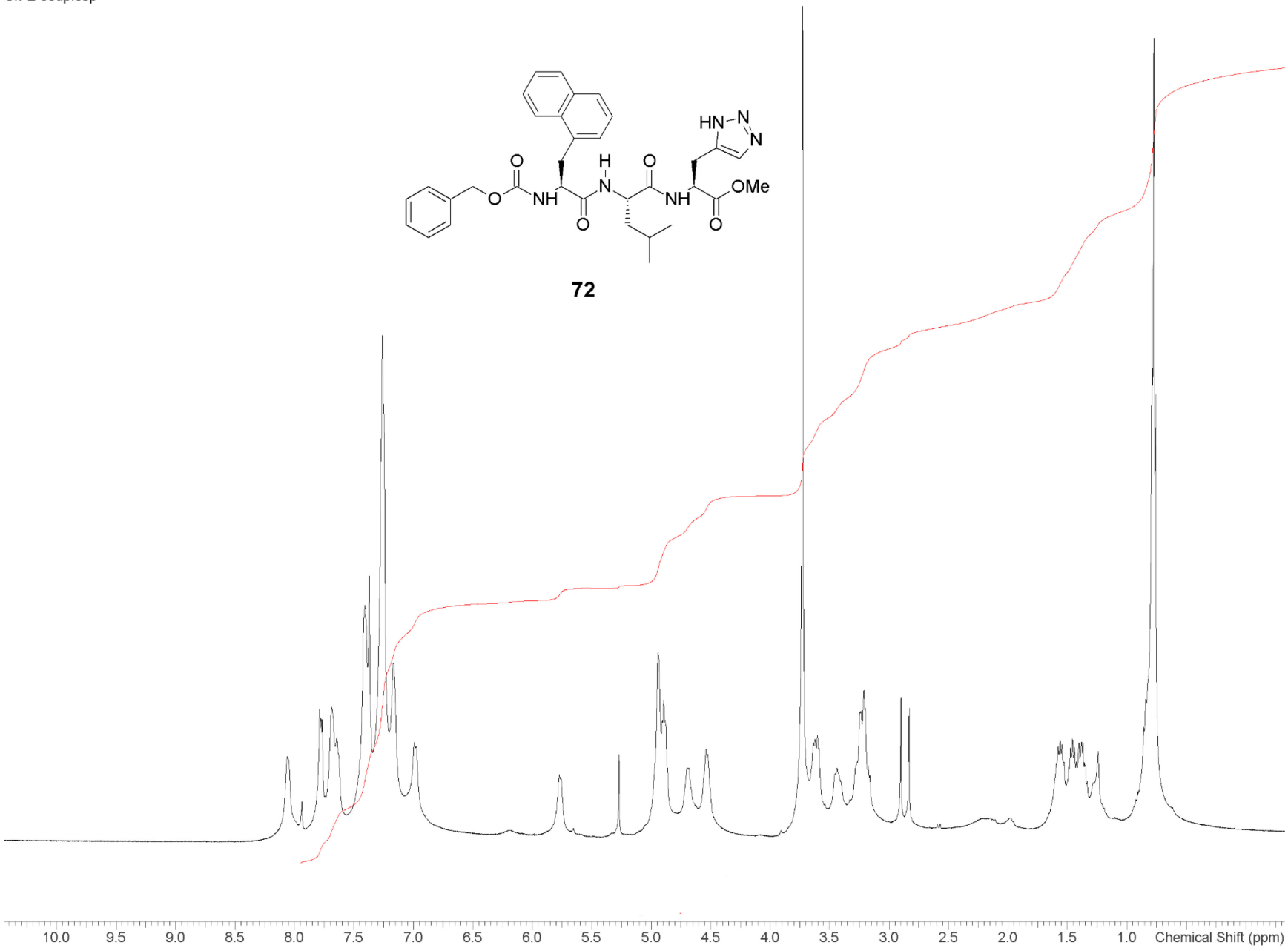

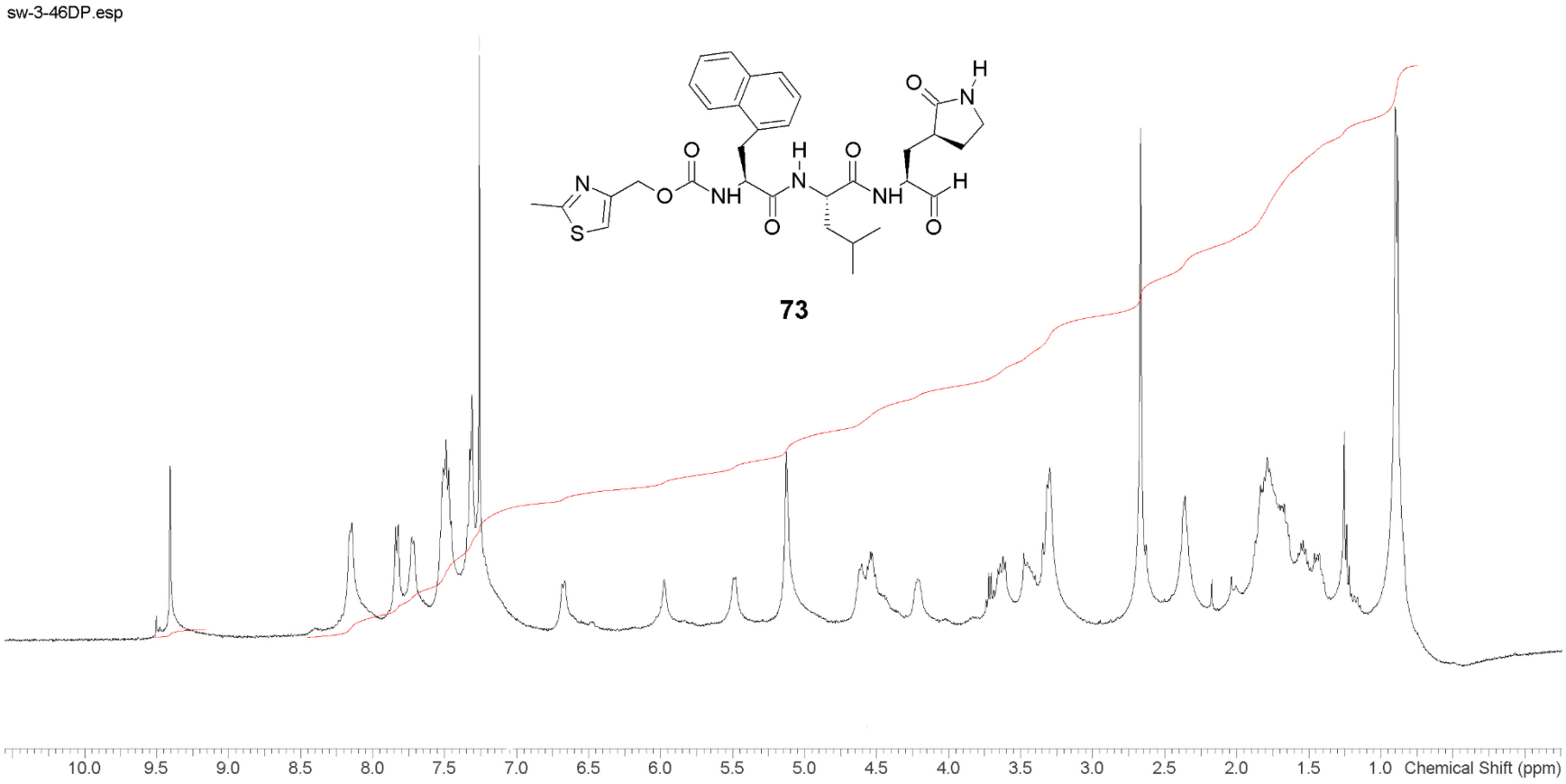
sw-3-46DP.esp
10.0
9.5
9.0
8.5
8.0
7.5
7.0
6.5
6.0
5.5
5.0
4.5
4.0
3.5
3.0
2.5
2.0
1.5
1.0
Chemical Shift (ppm)

73

AP16-37-FR20

74

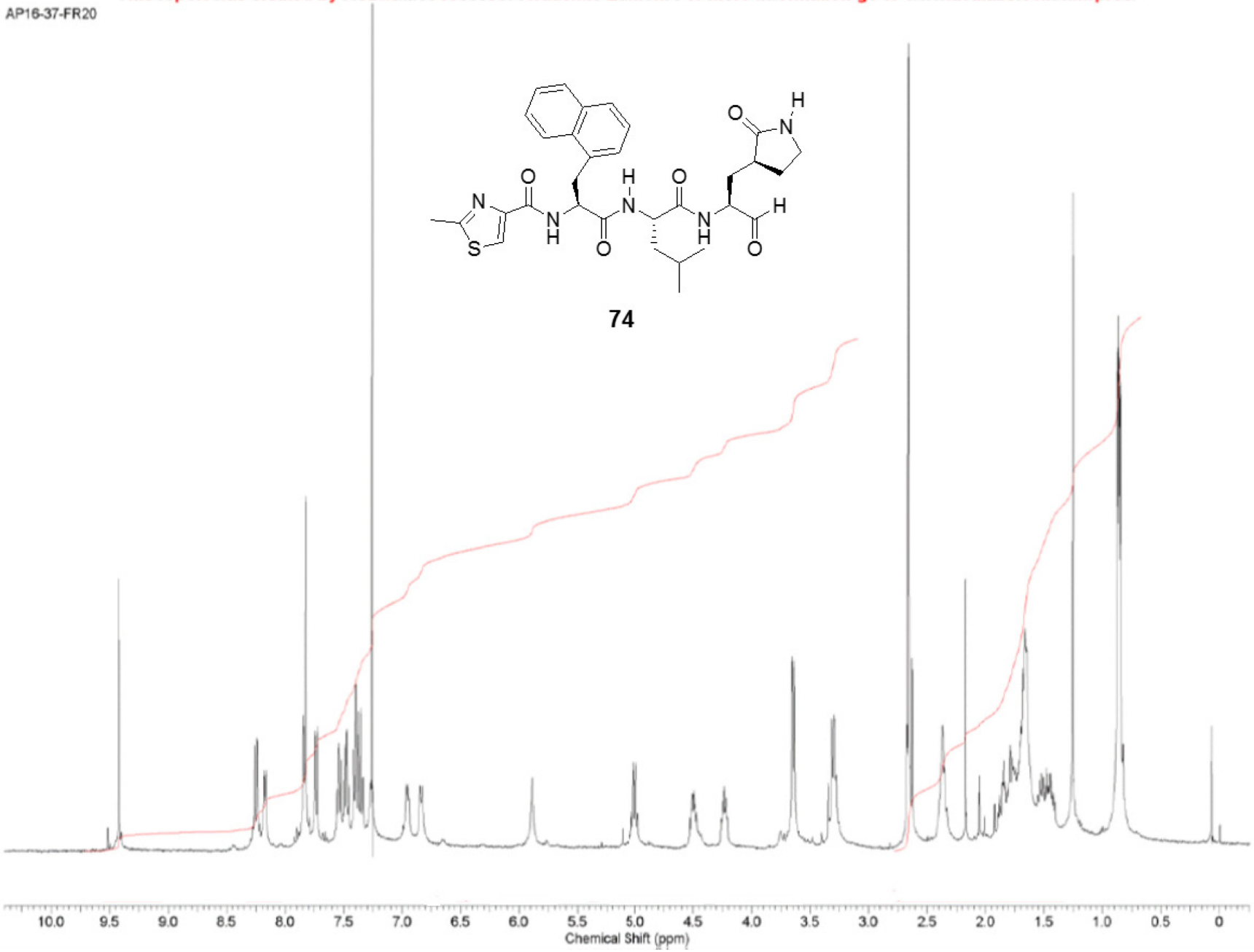

AP16-37-FR20-13C

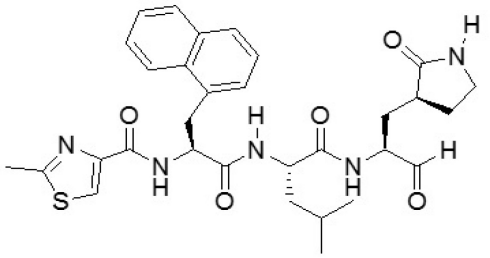

74

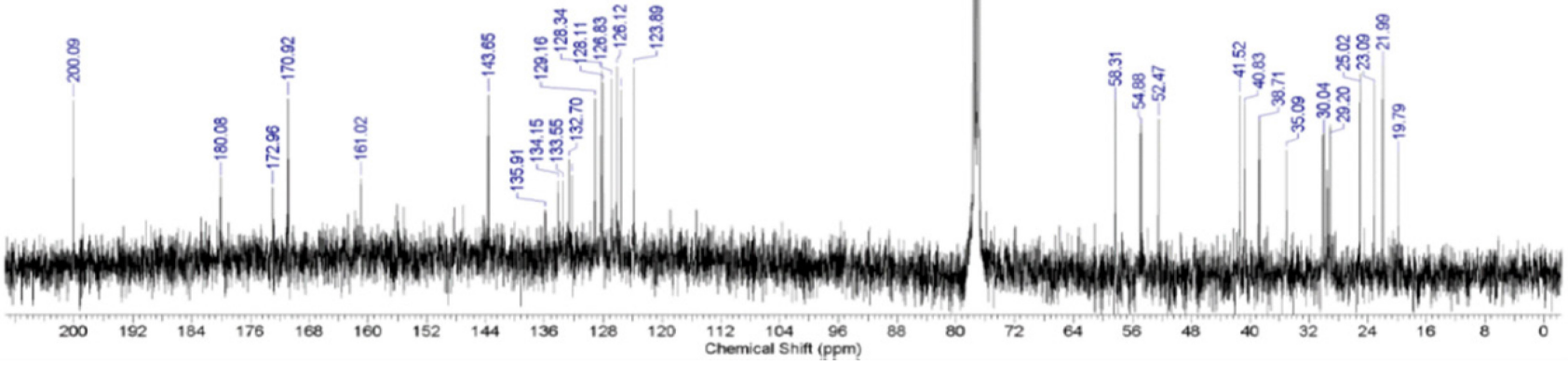

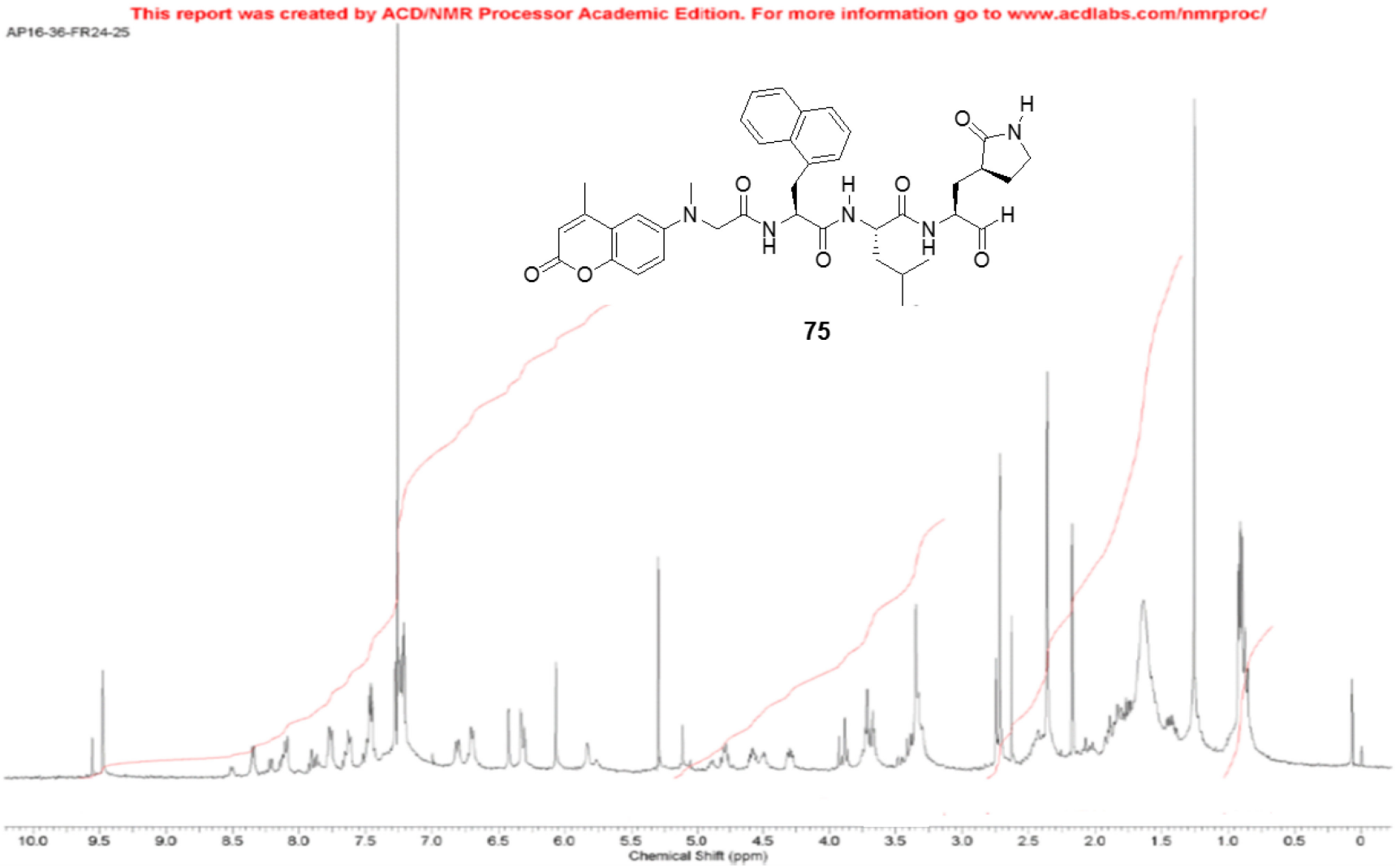
This report was created by ACD/NMR Processor Academic Edition. For more information go to www.acdlabs.com/nmrproc/
AP16-36-FR24-25
10.0
9.5
9.0
8.5
8.0
7.5
7.0
6.5
6.0
5.5
5.0
4.5
4.0
3.5
3.0
2.5
2.0
1.5
1.0
0.5
0
Chemical Shift (ppm)

75

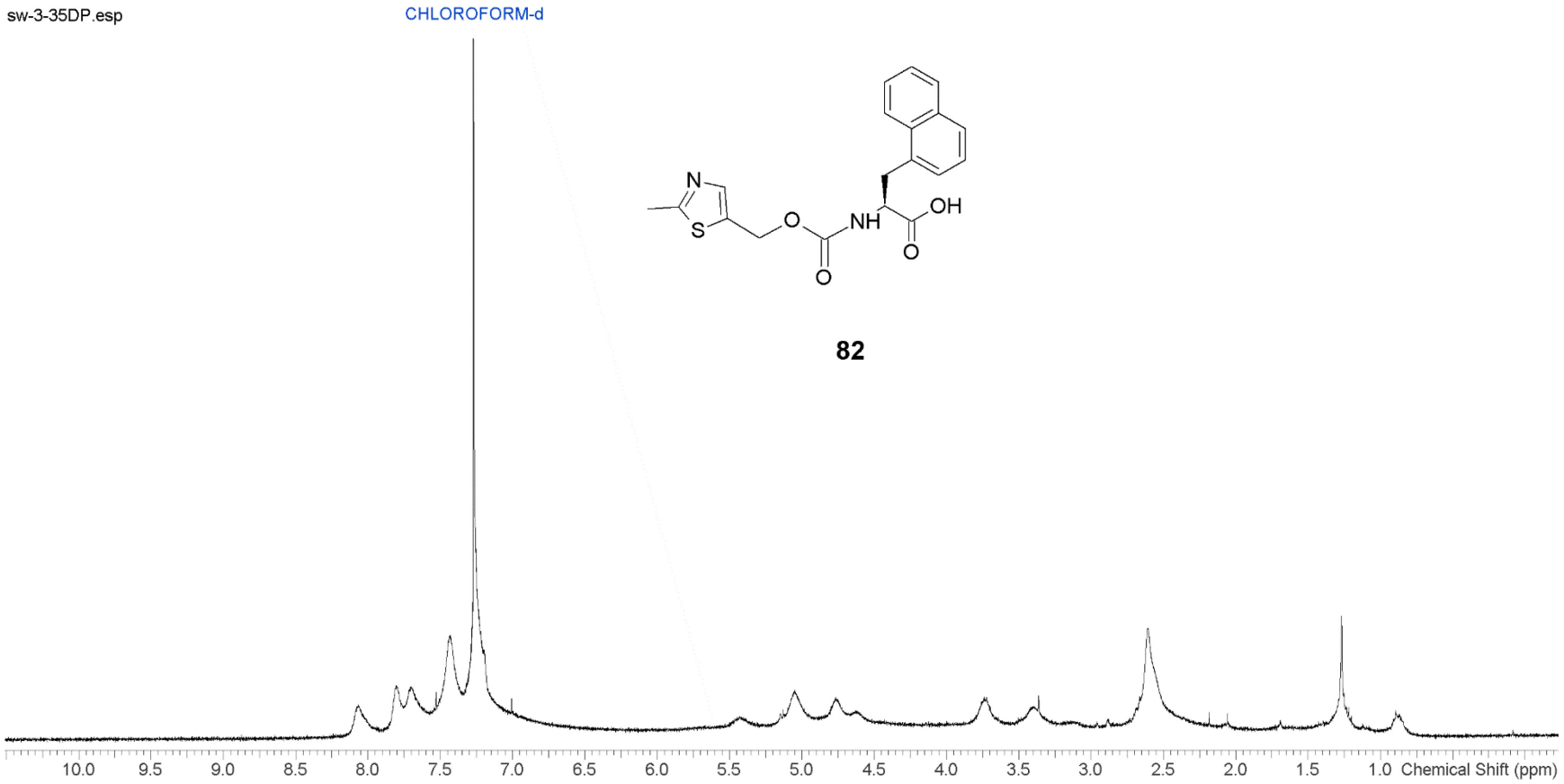
sw-3-35DP.esp
CHLOROFORM-d
N
S
O
NH
OH
O
O
10.0
9.5
9.0
8.5
8.0
7.5
7.0
6.5
6.0
5.5
5.0
4.5
4.0
3.5
3.0
2.5
2.0
1.5
1.0
Chemical Shift (ppm)

82

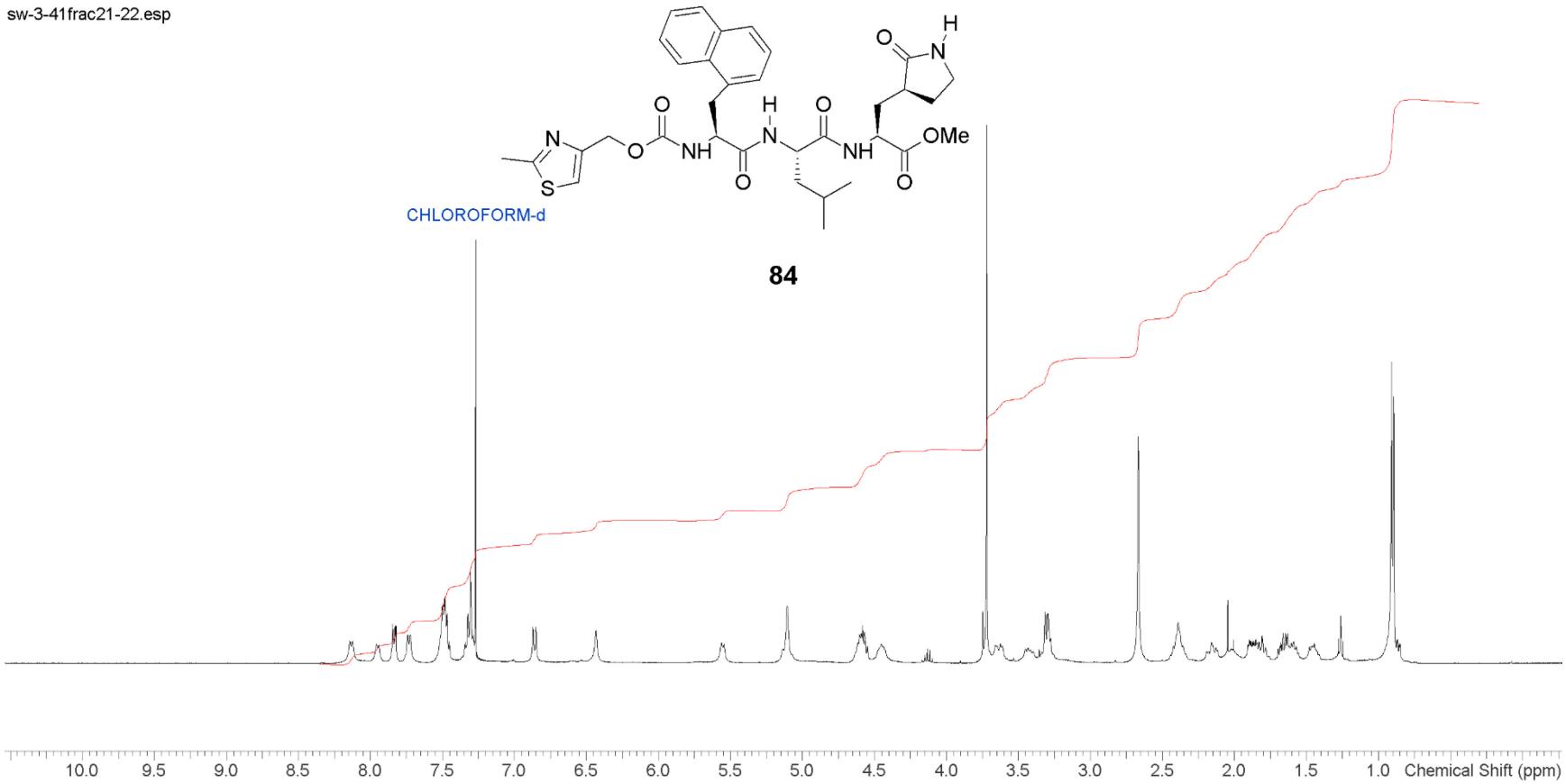
sw-3-41frac21-22.esp
CHLOROFORM-d
84
10.0
9.5
9.0
8.5
8.0
7.5
7.0
6.5
6.0
5.5
5.0
4.5
4.0
3.5
3.0
2.5
2.0
1.5
1.0
Chemical Shift (ppm)

AP16-29-CRUDE

86

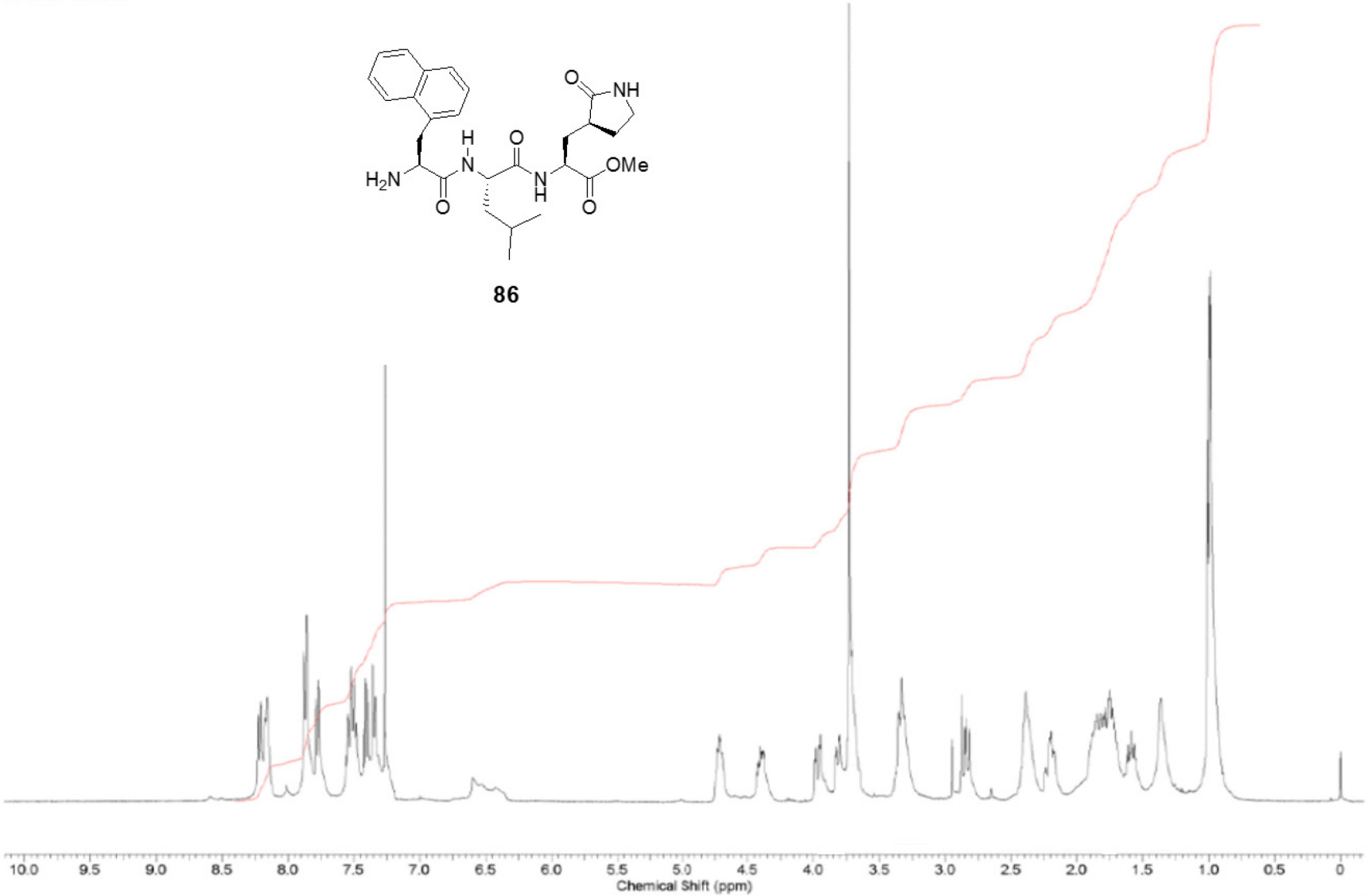

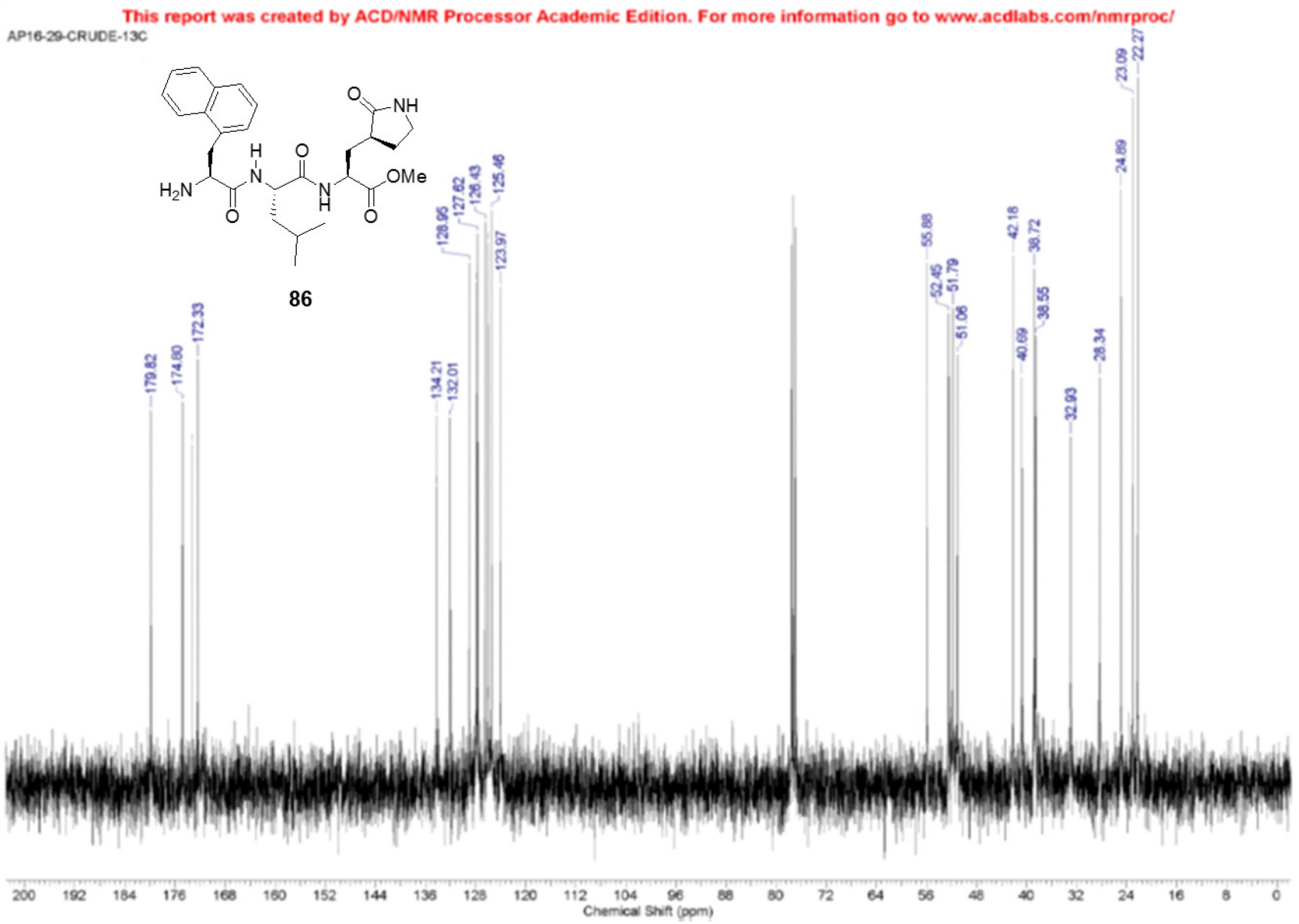
This report was created by ACD/NMR Processor Academic Edition. For more information go to www.acdlabs.com/nmrproc/
AP16-29-CRUDE-13C
86
179.82
174.60
172.33
134.21
132.01
128.95
127.62
126.43
125.46
123.97
55.88
52.45
51.79
51.06
42.18
40.69
38.72
38.55
32.93
28.34
24.89
23.09
22.27
200 192 184 176 168 160 152 144 136 128 120 112 104 96 88 80 72 64 56 48 40 32 24 16 8 0
Chemical Shift (ppm)

AP16-30-CRUDE

88

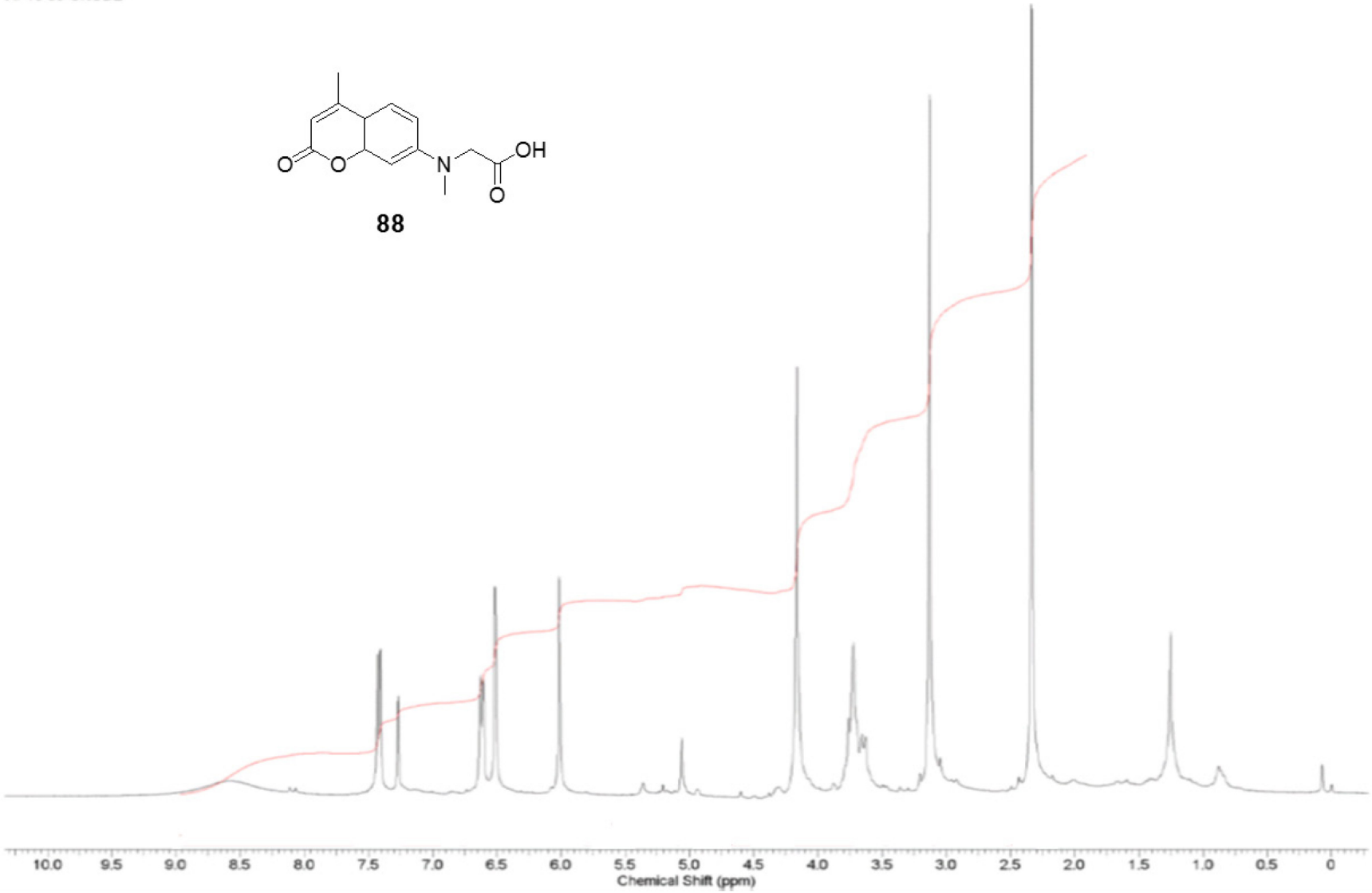

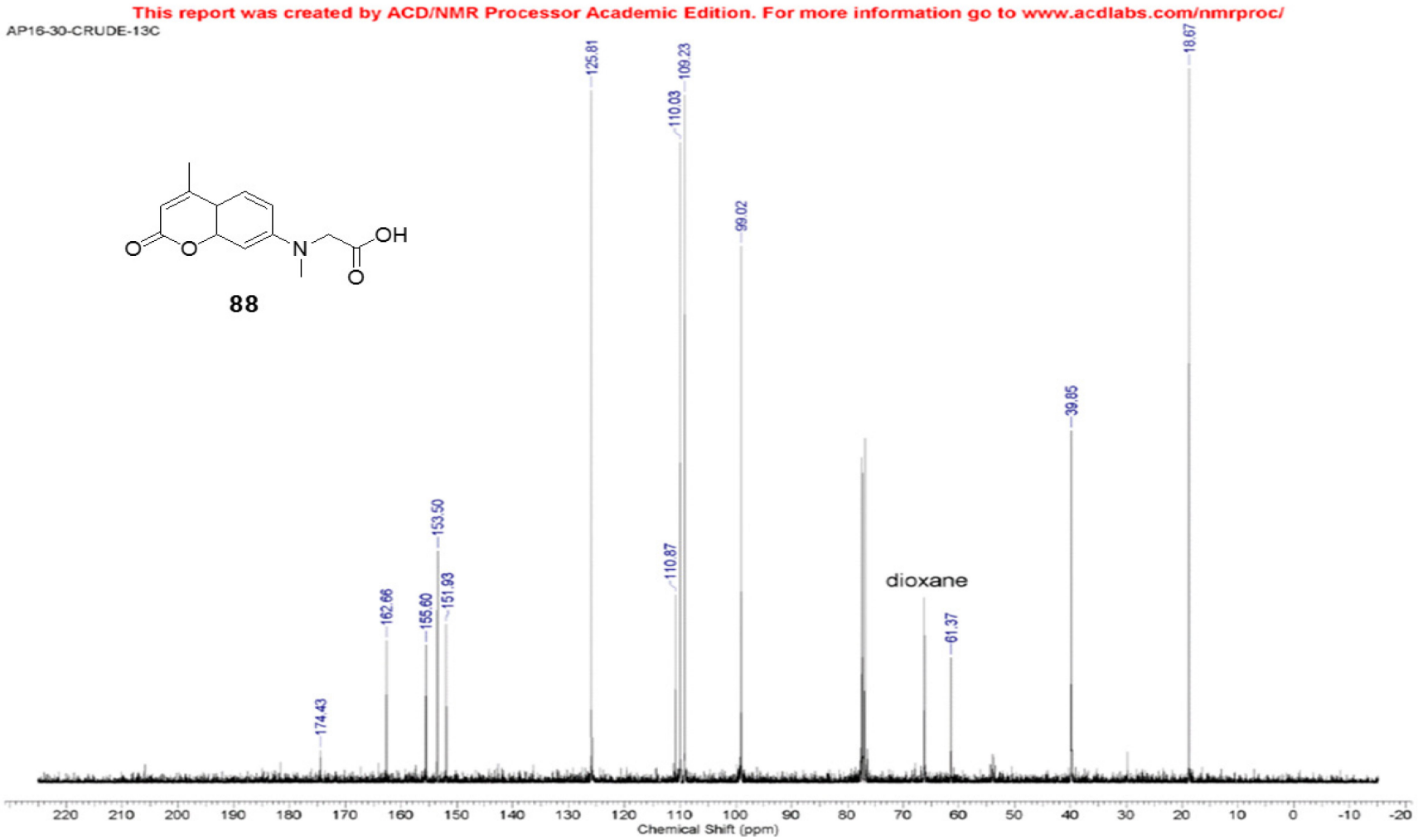
This report was created by ACD/NMR Processor Academic Edition. For more information go to www.acdlabs.com/nmrproc/
AP16-30-CRUDE-13C
125.81
109.23
110.03
99.02
18.67
39.85
153.50
110.87
162.66
155.60
151.93
dioxane
61.37
174.43
O
O
N
OH
O
88
220 210 200 190 180 170 160 150 140 130 120 110 100 90 80 70 60 50 40 30 20 10 0 -10 -20
Chemical Shift (ppm)

AP16-31-FR28-30

89

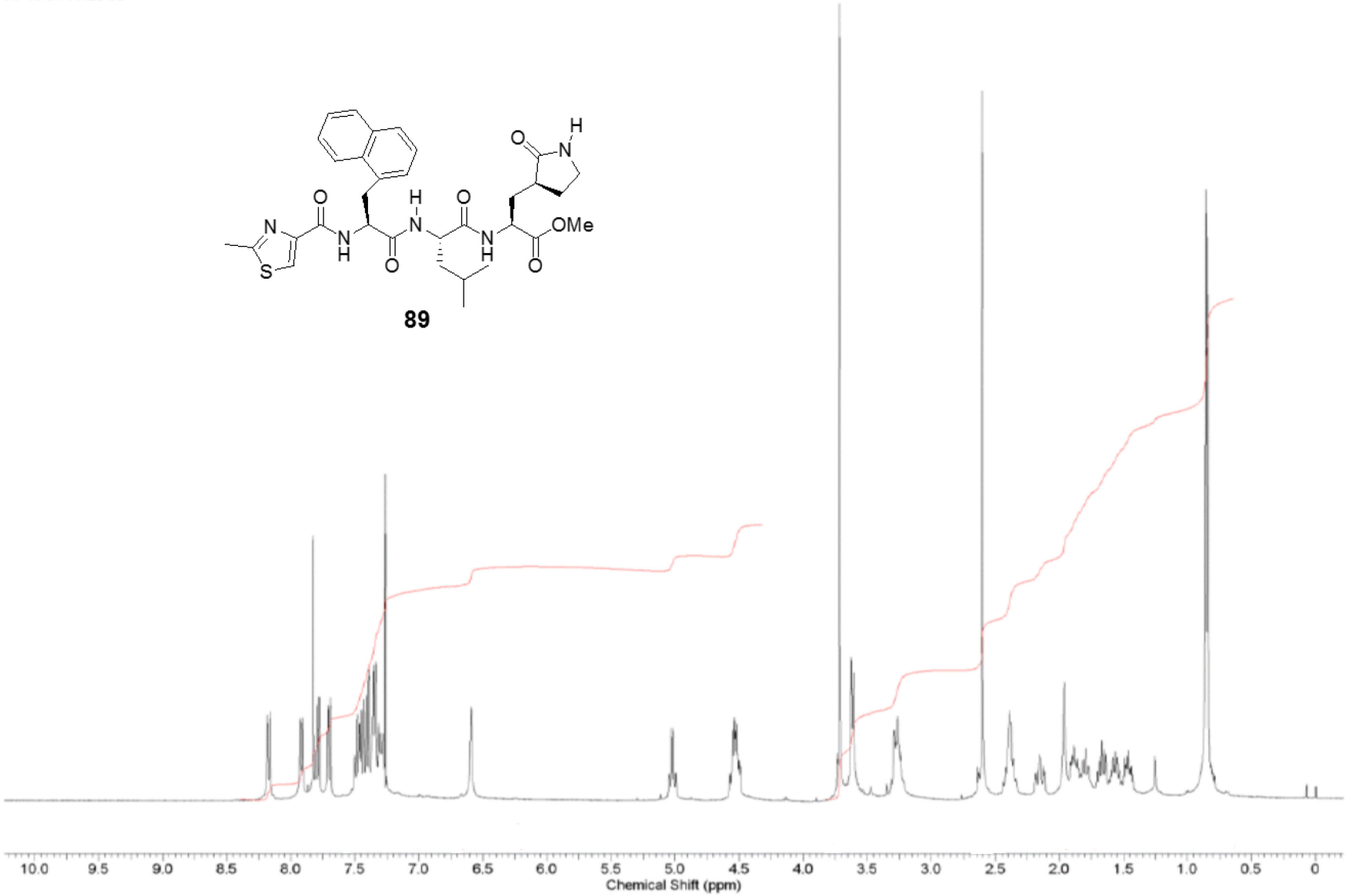

AP16-31-FR23-35-13C

89

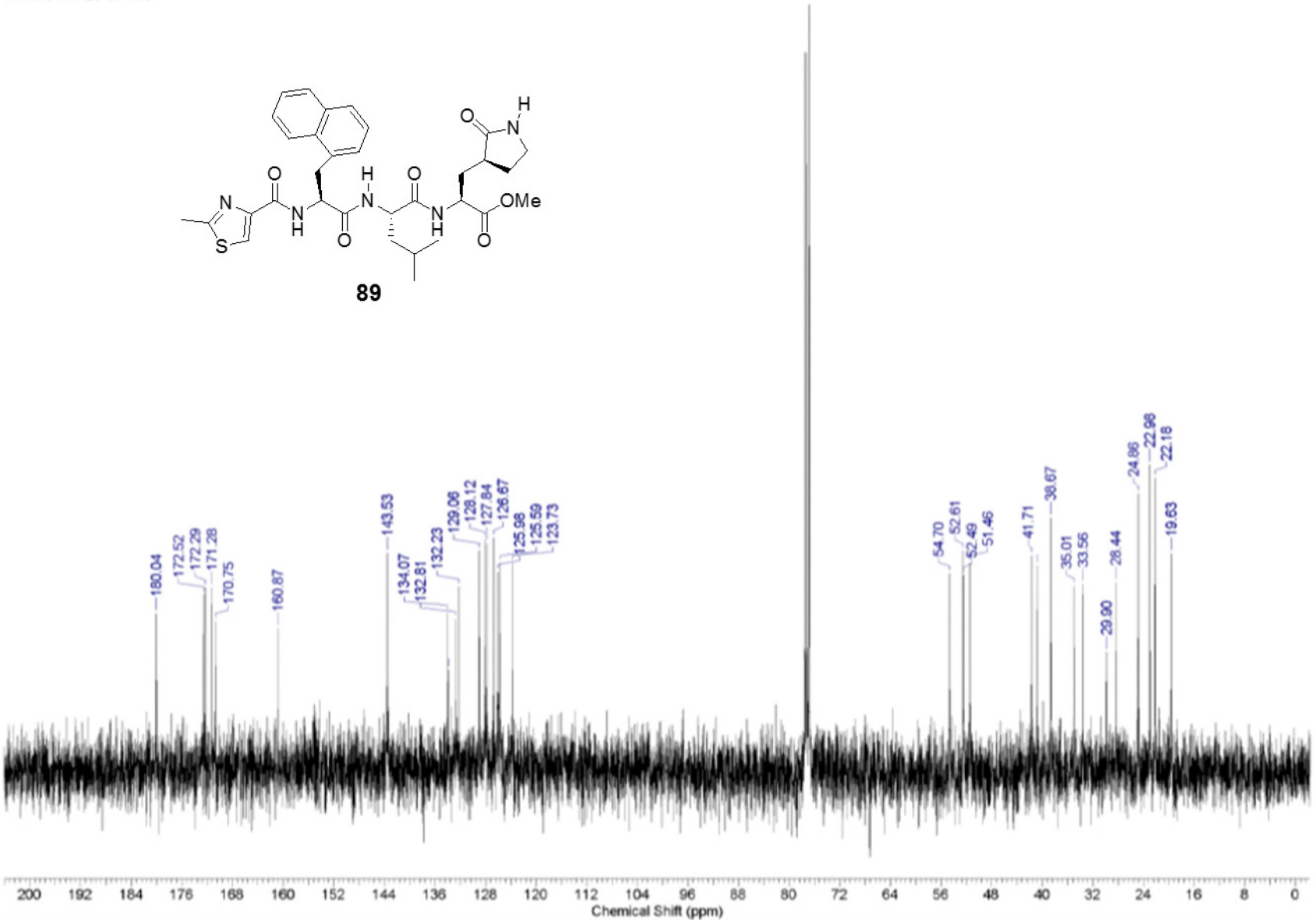

AP16-33-FR47

90

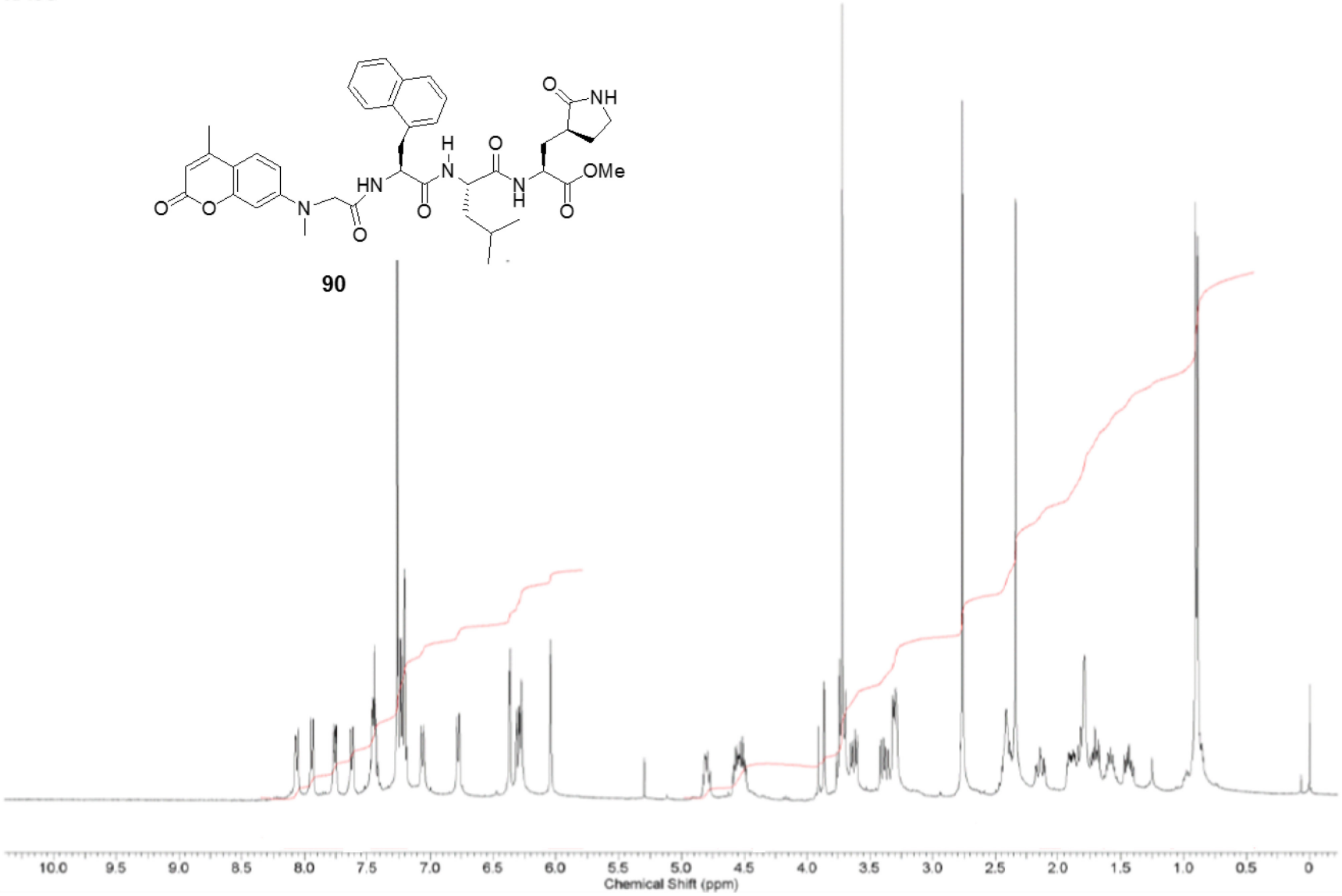

AP16-33-FR47-C13

90

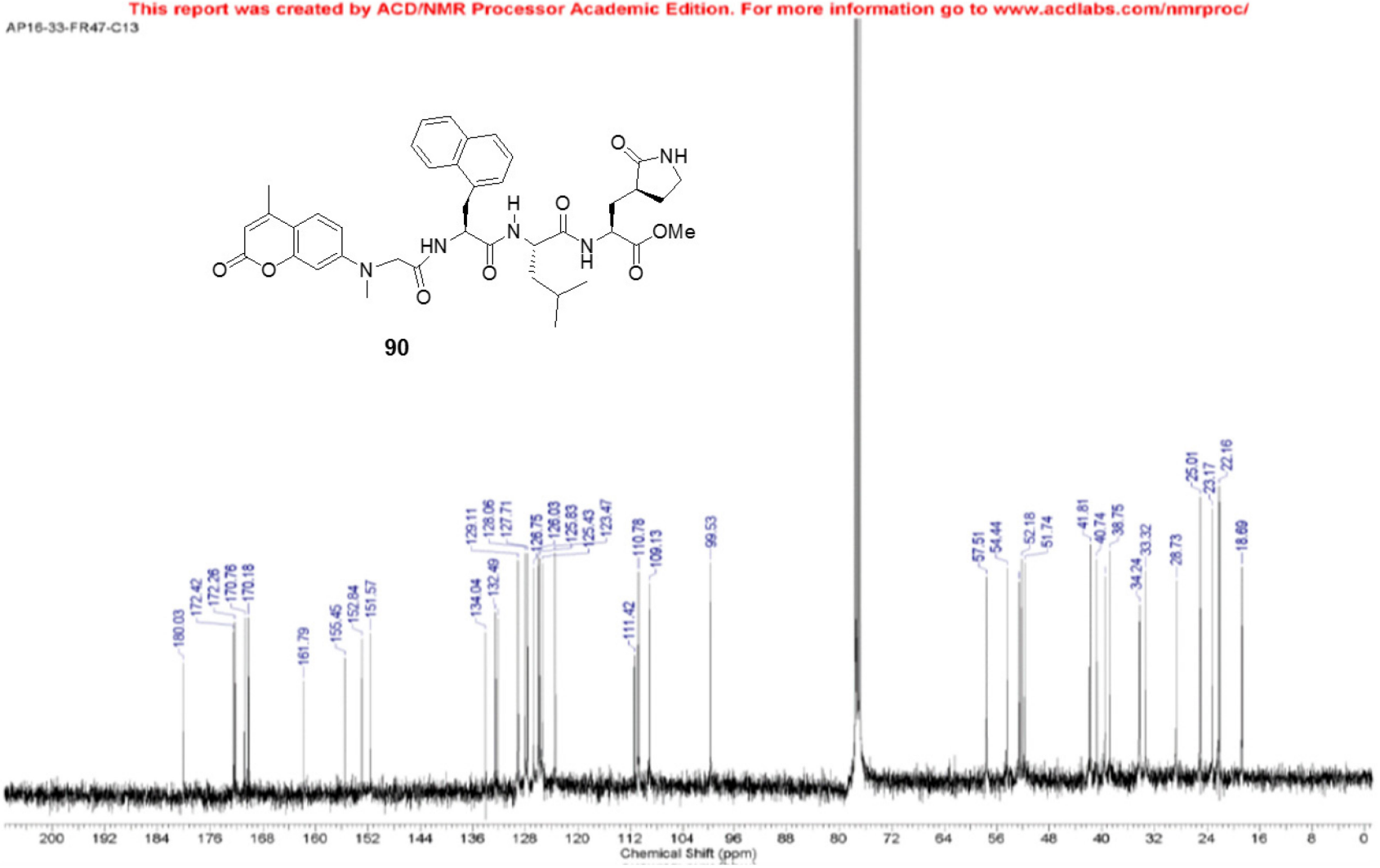

AP16-23-FR3

92

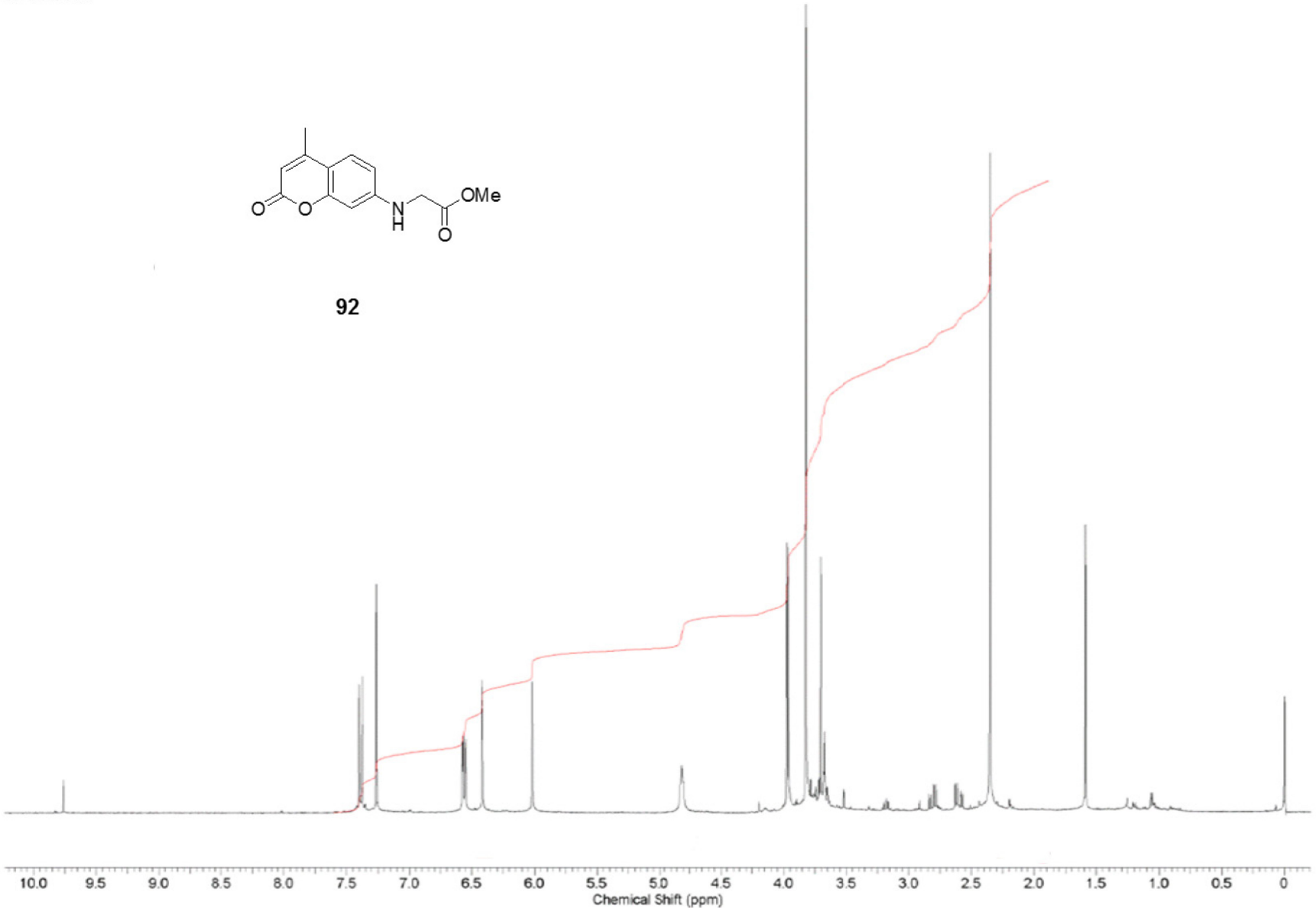

AP16-23-FR3-13C

92

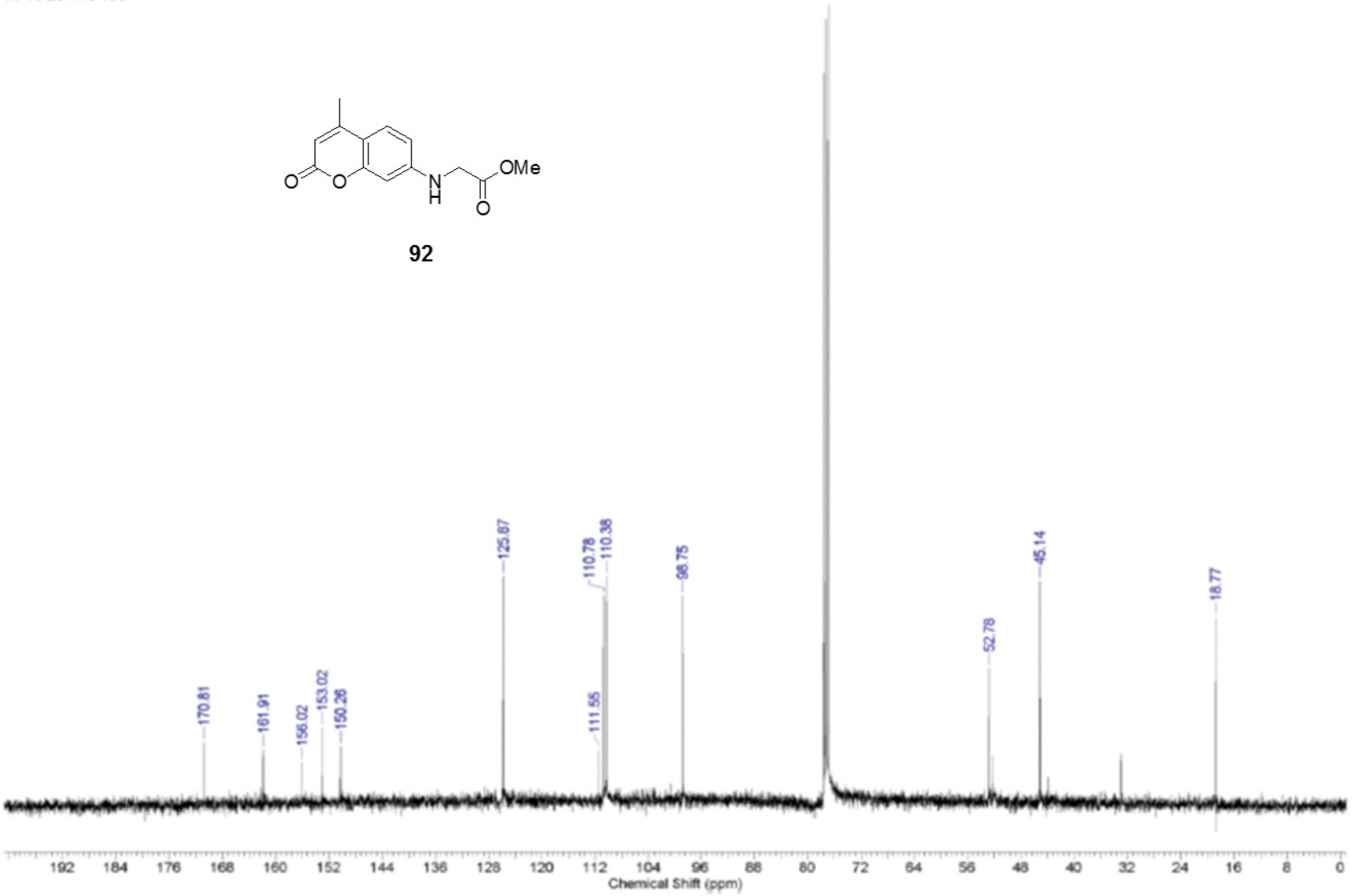

AP16-24-FR25

93

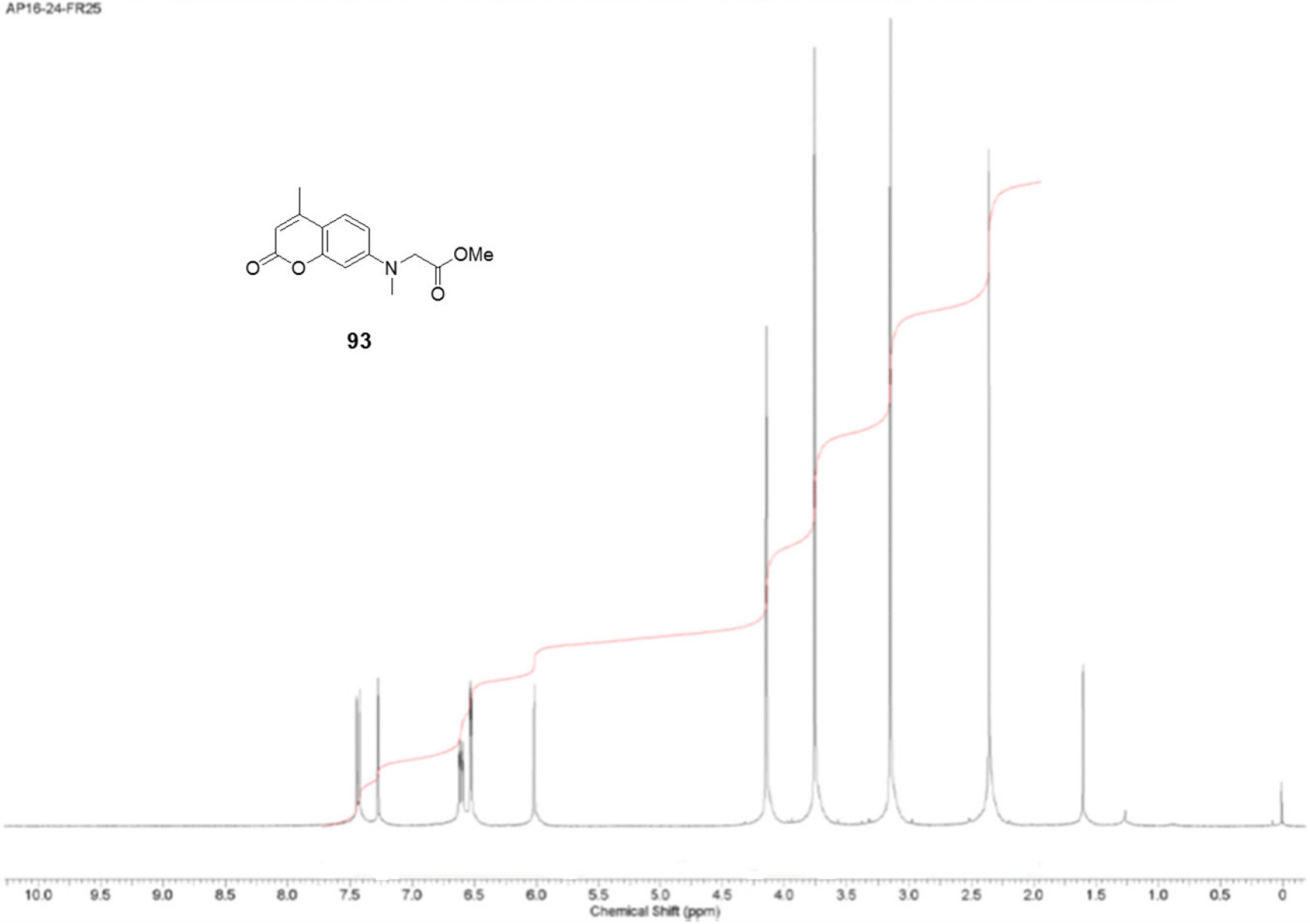

AP16-24-FR25-13C

93